DOI: 10.5281/zenodo.15064568

CURRENT APPROACHES IN ENGINEERING SCIENCES

EDITORS
Prof. Aydın Ruşen, Ph.D.
Assist. Prof. Abdulkadir Dilber, Ph.D.

Current Approaches in Engineering Sciences

EDITORS

Prof. Aydın Ruşen, Ph.D.

Assist. Prof. Abdülkadir Dilber, Ph.D.

Publisher
Platanus Publishing®

Editor in Chief
Prof. Aydın Ruşen, Ph.D. & Assist. Prof. Abdülkadir Dilber, Ph.D.

Cover & Interior Design
Platanus Publishing®

Editorial Coordinator
Arzu Betül Çuhacıoğlu

The First Edition
March, 2025

Publisher's Certificate No
45813

ISBN
978-625-6634-79-4

Platanus Publishing®
Address: Natoyolu Cad. Fahri Korutürk Mah. 157/B, 06480, Mamak, Ankara, Turkey.
Phone: +90 312 390 1 118
web: www.platanuskitap.com
e-mail: platanuskitap@gmail.com

PLATANUS PUBLISHING®

CONTENST

CHAPTER 1

Sustainable Nanotechnology Solutions: Activated Carbon from Bio-Waste for Effective Wastewater Treatment

Yasemin Ozliman[1],[2] & Fikret Muge Alptekin[3] & Melih Soner Celiktas[4]

[1] Ph.D. Candidate, Ege University Solar Energy Institute, Izmir, Turkey, ORCID:0000-0002-0503-7932
[2] Izmir Bakircay University, Izmir, Turkey
[3] Ph.D., University of Brescia, Department of Mechanical and Intdustrial Engineering, Brescia, Italy, Orcid: 0000-0003-2980-5403
[4] Prof. Dr., Ege University, Solar Energy Institute, Izmir, Turkey, Orcid: 0000-0003-2980-5403

1. Introduction

Access to clean, healthy water has developed into a major international concern in the twenty-first century (Feisal et al., 2024). National security concerns currently exist, and water security has started to take on the same economic and political urgency as the energy crises of the previous century. Adding to this, the world's population growth will make the water shortage issue worse (Hijab et al., 2021). Another reason for water scarcity is water pollution (Saleh, 2024). The expression "water pollution" refers to the introduction of elements, compounds, chemicals, organisms, and/or pathogens into surface or groundwater because of human and natural activity, changing the physical, chemical, and biological components of water resources (Akar et al., 2022; Akhtar et al., 2021; Teğin et al., 2024). Development of chemical, metallurgical, and associated sectors has resulted in increasing levels of water contamination during manufacturing processes, which creates serious risks to public health and restricts social and economic advancement (Adnan et al., 2024; Mohd Faizal et al., 2023; Piwowarska et al., 2024). These organizations release large amounts of complex wastewater that contains a significant amount of chloride ions, organic compounds, heavy metals, and dyes (Abewaa et al., 2024; Onyutha et al., 2024; Su et al., 2022). In particular, a lot of concentrate has been paid to concern about the possible risks associated with organic contaminants and heavy metals in industrial effluent (Duan et al., 2024). $ZnCl_2$ is a heavy metal that, while essential for organisms and important for aquatic physiological processes, poses significant risks and detrimental effects on the environment and human health when its concentration exceeds acceptable limits (Yılmaz & Tugrul, 2022). Zinc toxicity has been documented in various fish species, affecting enzyme activities, cell structures, and metabolic processes. In fish, Zn exposure during early life stages (ELS) can lead to significant physiological and biochemical changes, such as alterations in chorion structure, enzyme inhibition, and developmental toxicity. Zinc toxicity is influenced by water properties like temperature, pH, and salinity (Pagano et al., 2017). Zinc chloride, while essential for cellular life, can be highly cytotoxic at certain concentrations and exposure times, affecting respiration, growth, and various microbial activities (Babich & Stotzky, 1978).

Dyes released into wastewater without being removed are another serious contaminant. Discharging colored wastewater into water bodies from many companies, including paper, textile (Khan et al., 2024), food, cosmetics, and pharmaceuticals, has detrimental ecological effects and hazardous repercussions (Ardila-Leal et al., 2021; Inbaraj et al., 2022; Liyanaarachchi et al., 2023). Methylene blue (MB) is one of the toxic dyes that have an adverse impact on

human health and environment (Teweldebrihan et al., 2024). Due to its chemical stability, MB is challenging to remove from industrial effluents using traditional wastewater treatment methods. Therefore, MB-saturated wastewater must be treated before discharge to prevent contamination. Research is ongoing to improve the removal of contaminants of emerging concern, such as MB, from industrial effluents (Dimbo et al., 2024; Takele et al., 2023).

Reverse osmosis (Sun et al., 2024), ion exchange (Buhani et al., 2021), and adsorption (Macchi et al., 2021) are just a few of the treatment technologies that have been the subject of several studies aimed at creating cost-effective water treatment methods for removing these pollutants from wastewater (Qalyoubi et al., 2021). Among them, adsorption has the potential to be a very successful treatment for both removing chloride contaminants and eliminating dye effluent (Dutta et al., 2021; Valli Nachiyar et al., 2023). The equilibrium separation method known as adsorption has proven effective in water decontamination because of its minimal initial costs, flexibility in structure, simplicity of use, and sensitivity to hazardous compounds (Rathi & Kumar, 2021). Additionally, this method doesn't result in any hazardous byproducts. Studies have demonstrated that adsorption is a promising method for removing pollutants (Kumar et al., 2023). Because of this, adsorption has become a popular, cost-effective, and environmentally friendly alternative method for treating wastewater in recent years (Krstić et al., 2018; Qasem et al., 2021). The surface-active sites that result from the adsorbent's functional groups determine how well an adsorbent bond with substances (Dharmapriya et al., 2021). For various pollutants, a variety of adsorbent materials, including natural materials, biological biomasses, and nanomaterials, have been shown to be effective adsorbents (Satyam & Patra, 2024; Sheraz et al., 2024). Since carbon-based adsorbents have such remarkable physical and chemical properties, they are frequently adaptable for treatment (Burdová et al., 2024; Moreno-Piraján & Giraldo, 2012; Pavithra et al., 2024). Producing economically and environmentally friendly porous carbons from renewable biomass sources gives us an achievable route for use in the future (Alptekin & Celiktas, 2022). The most efficient method for converting biomass into value-added products is thermochemical conversion. The porous carbons are one of those valuable items that have received a lot of attention because of their widespread use in important application areas (Ma et al., 2022).

Among these carbon precursors, pellets from forest waste and pomace from olive waste are quite common. This is mainly a result of both the large production of olives and the high waste from forest lands (A. K. Duman et al., 2020). However, in the Mediterranean region, olive trees (Olea europaea L.) are

centuries-old and typical crop (Fraga et al., 2020). With over 11 million hectares of olive trees worldwide, olives are a significant revenue crop for many nations. Turkey ranks fourth in the world with a 7.2% contribution to olive output (Nampeera et al., 2024; Ochando-Pulido & Martinez-Ferez, 2017; Tunalıoglu, 2023). The global output of olive pomace is around 2 million tons per year, while Turkey creates approximately 650.000 tons of olive pomace from olive oil manufacturing per year (A. K. Duman et al., 2020).

In the framework of the circular economy, academics are interested in olive pomace, which makes up 80% of the material used in the production of olive oil. Numerous research demonstrates that olive pulp is not only recyclable but also a valuable substance (Sismanoglu et al., 2023). Furthermore, solid waste can be burned to generate heat or electricity, or they can be heat-treated to create activated carbon, which can be used to remove harmful materials from water (Boufi, 2017). Likewise, forest residues, as cheap and abundant feedstock, can replace current fossil-energy sources, helping to reduce greenhouse gas emissions and improve energy security (Balcioglu et al., 2023).

This study presents a novel evaluation of activated carbons derived from waste olive pomace and pellets for water treatment. Unlike previous research, it specifically compares these two underutilized materials for their efficiency in adsorbing $ZnCl_2$ and methylene blue from aqueous solutions. The study introduces new insights into the relationship between surface area and adsorption capacity, utilizing Langmuir and Freundlich models alongside pseudo second-order kinetics. The high adsorption capacities, particularly for methylene blue with olive pomace-derived AC, highlight the potential of these bio-based materials as sustainable solutions for wastewater treatment and contribute to the circular economy by repurposing agricultural and forest waste.

2. Experimental section

2.1. Materials & Chemicals

Olive pomace was obtained from Taris Olive and Olive Oil Agricultural Sales Cooperatives Unions located in Akhisar, Manisa, Turkey. Pellet was obtained from Serpellet Biomass and Natural Gas Industry Trade. Inc. MB dye with the molecular formula of $C_{16}H_{18}C_lN_3S$ and molar mass of 319.86 g mol^{-1} was purchased from “Interlab”. $ZnCl_2$ molar mass of 136.30 g mol^{-1} was purchased from “Tekkim”. HCl (37% v/v) was obtained from Sigma-Aldrich.

2.2. Activated carbon preparation

Olive pomace and pellet were activated with $ZnCl_2$ at a ratio of 1:4 and carbonized in a fixed bed reactor at 722ºC and with N_2 flow 5ml min^{-1}. The details of the procedure for preparation of activated AC olive pomace and AC Pellet have been described in the previous study (Alptekin et al., 2023).

2.3. Preparation of stock solutions

A stock solution 1000 ppm of MB dye and 1000 ppm $ZnCl_2$ were prepared with deionized (DI) water, and the working solutions were diluted with DI water using the stock solution. Other agents used were all analytical grade and all solutions were prepared with DI water. The chemical resistance of DI water was measured as 18 MΩ cm. Additionally, the following tools were used in the study: a digital pH meter (AZ Instrument, Taiwan, 86505), a digital electronic balance (ISOLAB, I.602.31.002, Germany), an MCL incubator (Mikrotest, MCI120), a UV/VIS spectrometer (Analytikjena, Model: Specord S600).

Solutions with different initial concentrations were prepared by diluting the stock solutions in appropriate proportions. These concentrations were determined as 100 ppm, 150 ppm, 200 ppm, 250 ppm, 300 ppm and 350 ppm for $ZnCl_2$ and MB, respectively. DI water was used when preparing stock solutions.

2.4. $ZnCl_2$ and Methylene blue batch adsorption experiments

The batch adsorption method was employed to remove $ZnCl_2$ and MB from wastewater. Synthetic solutions of $ZnCl_2$ and MB were prepared for the process. Adsorption experiments were conducted in 250 mL Erlenmeyer flasks, each containing 100 mL of $ZnCl_2$ or MB solutions with initial concentrations ranging from 100 to 350 mg L^{-1}. A 100 mg sample of each activated carbon (AC) was added to the flasks, which were stirred at 150 rpm in an MCL incubator at room temperature. For equilibrium studies, experiments were carried out for 1 day to provide equilibrium was reached. The concentrations of $ZnCl_2$ and MB in the prepared solutions were measured using a UV-Visible (UV-Vis) spectrophotometer. The samples' $ZnCl_2$ and MB dye concentration after adsorption was measured using a UV–Vis spectrophotometer at its wavelength (λ) of 664 nm. Because, according to the UV Lambert Beer Law, there is a linear relationship between the concentration of a solution and the absorption values at a certain wavelength (Freha et al., 2024).

The residual concentration was measured with a UV–Vis spectrophotometer, and the equilibrium adsorption capacity (mg/g) was determined as follows:

$$q_e=\frac{(Co-Ce)V}{m} \quad (1)$$

The equation includes C_o is the initial pollutant concentration (mg L^{-1}), C_e is equilibrium concentration (mg L^{-1}), V is solution volume (L), and m is adsorbent mass (g) (Mohd Faizal et al., 2023).

2.5. Adsorption kinetics

The Equation (2) was used to calculate qt (mg g^{-1}), the amount of $ZnCl_2$ and MB adsorbed into the adsorbent at a specific time (min) (Masudur Rhaman et al., 2022).

$$q_t=\frac{(Co-Ct)V}{m} \quad (2)$$

where the adsorbate concentration at time t, is represented by C_t (mg L^{-1}). Both pseudo-first order and pseudo-second order models were used for analyzing the kinetic data. The model that is pseudo-first order is explained by;

$$qt = qe(1 - \exp(-k1t)) \quad (3)$$

where k_1 is the pseudo-first-order model's rate constant, (min^{-1}). Based on this model, the equilibrium capacity and the capacity at time, *t*, determine the linear forces that drives the adsorption rate, and the adsorbent mass, pH, temperature, and initial solute concentration all affect the rate constant, k_1 (Basharat et al., 2021; Basu et al., 2018).

The following is the pseudo-second order;

$$Qt = \frac{k2Qe2t}{1+k2Qet} \quad (4)$$

where the pseudo-second-order model's rate constant is indicated by k_2 (g mg.min^{-1}) (Zhang et al., 2023).

2.6. Adsorption Isotherms

The Freundlich or Langmuir models provide a useful explanation for almost all of adsorption data. The Langmuir isotherm, which is used to explain adsorption phenomena, is based on the idea that monolayer sorption, which causes adsorption on a uniform surface, takes place in the absence of interactions between adsorbed molecules. Here is the linearized Langmuir equation (Langmuir, 1918).

$$\frac{Ce}{qe} = \frac{1}{Qb} + \frac{Ce}{Q} \quad (5)$$

The variable Q represents the maximum amount of adsorption with complete monolayer coverage on the adsorbent surface (mg g^{-1}), whereas b (KL) denotes the Langmuir constant, which is associated with the adsorption energy (L mg^{-1}). The linear plot of Ce/qe against Ce can be used to find constants Q and b by calculating its slope and intercept.

A dimensionless constant separation factor (R_L) defined by the relationship can be used to express the key characteristics of the Langmuir isotherm (Ogunmodede et al., 2015):

$$RL = \frac{1}{1+KLCo} \quad (6)$$

where KL (L mg^{-1}) is the Langmuir constant associated with the energy of adsorption and C_0 (mg L^{-1}) is an initial concentration. The shape of the isotherms can be classified as adverse (R_L >1), linear (R_L = 1), suitable (0 < R_L <1), or irreversible (R_L = 0) based on the value of R_L.

Freundlich proposed the Freundlich isotherm condition in 1906, and it became the primary model suggested for sorption measurements. It might be used for non-ideal sorption on heterogeneous surfaces as well as multi-facet sorption. Eq. (7) gives the mathematical expression for the Freundlich isotherm (Agarwala & Mulky, 2023).

$$\ln(qe) = \ln(Kf) + \frac{1}{n}\ln(Ce) \quad (7)$$

Where Kf is the sorption capacity and 1/n are the sorption intensity (1/n). The sorption power (1/n) indicates the ideality and limit of the adsorbent/adsorbate framework. Plotting ln(qe) vs ln(Ce) results in a straight line with an inclination of 1/n and a block of ln(Kf) (Areej et al., 2024).

2.7. Characterization of Activated Carbon

Scanning electron microscopy (SEM) was used to examine the surface morphology of ACs. Prior to imaging, they were gold-stuppered and mounted on a metal stub using double-sided adhesive carbon tape. ACs micrographs were examined at an accelerating voltage of 30 kV using a SEM system (LEO 1430 VP). Furthermore, the mapping of the elements was done using a SEM.

The generated carbon's BET (Brunauer-Emmett-Teller) surface area was measured using N_2 adsorption-desorption isotherms at -196°C (Micromeritics Gemini VII 2390t). The total pore volume (V_{total}) was calculated using nitrogen adsorption data gathered at a relative pressure of P/P_o = 0.995. The samples were

investigated by X-ray diffraction (XRD, Ultima IV, Rigaku, Tokyo, Japan). XRD measurements were taken at room temperature with a step of 10° in a range of 3–90°. The surface functional groups of samples were determined using a Fourier transform infrared spectrophotometer (Agilent, Cary 630 Perkin Elmer FTIR spectrometer) with a wavelength range of 600-4000 cm^{-1}, 32 scans s^{-1}, and a spectral resolution of 4 cm^{-1}.

3. Results and Discussion

3.1. Characterization Results of Activated Carbons

The textural properties and characteristics of activated carbons obtained from pellet and olive pomace are shown in Table 1. AC_{pellet} exhibited a greater surface area of 1,511.8 ($m^2 g^{-1}$) and total pore volume of 1.13 ($cm^3 g^{-1}$) followed by $AC_{olive\ pomace}$ with 1,019.9 ($m^2 g^{-1}$) and 0.91 ($cm^3 g^{-1}$), respectively. The amount of Zn^{+2} ion that acts as dehydration agents and operation temperature significantly affect the surface area and pore structure of activated carbon (Chen et al., 2017). In this investigation, activated carbons with elevated surface area were synthesized in contrast to the methodology employed by Faizal et al., wherein $ZnCl_2$ served as the chemical activator and the resultant activated carbon was generated at 550°C (Mohd Faizal et al., 2023). Even when using the same activating agent, impregnation ratio, and carbonization conditions, activated carbons can exhibit varying surface areas and pore distributions. This variability is due to the differences in the raw materials and their inherent properties (Gayathiri et al., 2022).

Table 1 The textural properties of activated carbons; pellet and olive pomace.

Sample	S_{BET} (m^2g^{-1})	V_T (cm^3g^{-1})	S_{mic} (m^2g^{-1})	V_{mic} (cm^3g^{-1})	S_{meso} (m^2g^{-1})	V_{meso} (cm^3g^{-1})	D_{av} (nm)
AC_{pellet}	1,511.8	1.13	0	0	1,511.8	1.13	3.4
$AC_{olive\ pomace}$	1,019.9	0.91	184.6	0.08	835.3	0.73	3.9

Fig 1. shows N_2 adsorption-desorption isotherms and pore size distribution of the activated carbons. Based on the the International Union of Pure and Applied Chemistry (IUPAC) physiosorption isotherm classifications, two activated carbons showed Type IV isotherm that is associated with mesoporous adsorbents. The desorption branch of AC_{pellet} exhibited the type H2 hysteresis loop, characteristic of certain ordered mesoporous materials, while $AC_{olive\ pomace}$ displayed the type H4 hysteresis loop, indicative of micro-mesoporous carbons (Thommes et al., 2015).

Hysteresis loops are explained by many kinds of theories. The H2 hysteresis observed for AC_{pellet} is due to porous structures were network effects influence desorption. The presence of mesopores is compatible with H2 hysteresis loop. The adsorption branch of H4 hysteresis loop is based on type I and II isotherms. $AC_{olive\ pomace}$ is more suited for H4 hysteresis theory because of its low mesopore ratio (Bläker et al., 2019).

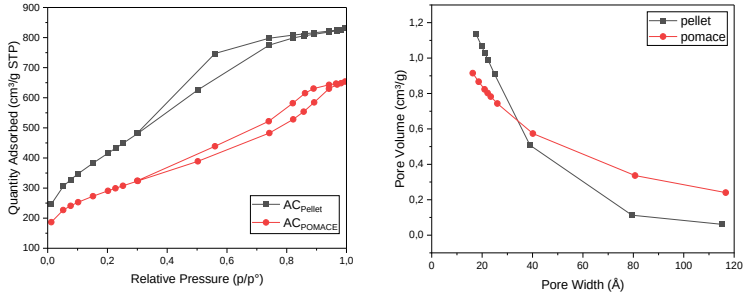

a b

Fig. 1. a) N_2 adsorption-desorption isotherms of the activated carbons, b) pore size distribution of activated carbons.

Pore size distribution is a crucial property of adsorbents, as variations in pore size impact the adsorption capacity for molecules of varying sizes and shapes. This characteristic is also a key factor in choosing carbon adsorbents for specific applications (Gao et al., 2013).

$AC_{olive\ pomace}$ showed microporous structure that mostly cumulated on 2 nm while pellet exhibited mesoporous structure that concentrated between 2-8 nm. The length of a methylene blue molecule is reported to be 13.82 Å (Macedo et al., 2006) - 14.47 Å (Dotto et al., 2015) with a width of around 9.5 Å. Micro size nature of MB resulted in adsorbed in $AC_{olive\ pomace}$.

Fig. 2. exhibits the SEM images of activated carbons at various magnifications. Fig.2 a) and b) shows that pellet activated carbon have a highly porous structure. The pellet exhibited a sponge structure that has plenty of holes. The pores are irregularly distributed and of different sizes. This structure shows that activated carbon has a large surface area. This suggests that there might be a large adsorption capability. Fig. 2.b) was taken at a higher magnification (1000x) and smaller pores can be seen more clearly. The pores are irregular and different sizes. The presence of mesopores indicates that many kinds of molecules can be adsorbed by activated carbon (Brasquet et al., 2000). Fig 2.c) and d) shows that olive pomace exhibited micro-mesoporous structure while mesopores are more

visible. A larger number of mesopores can be seen in the figure. There are large, prominent gaps on the surface. When the surface morphology is analyzed, there are many places with cracks and the irregular pore shape (Tansel & Nagarajan, 2004). Besides the surface area, the areas of micropores and mesopores are crucial. Specifically, meso- and micropores in activated carbon enhance the adsorption of larger molecules. An increase in mesopores with average pore diameters of 2–10 nm results in a larger surface area for the activated carbon (Ozcan et al., 2024). Hence, it seems that AC derived from olive pomace that has micro- mesoporous structure shows better adsorption potential.

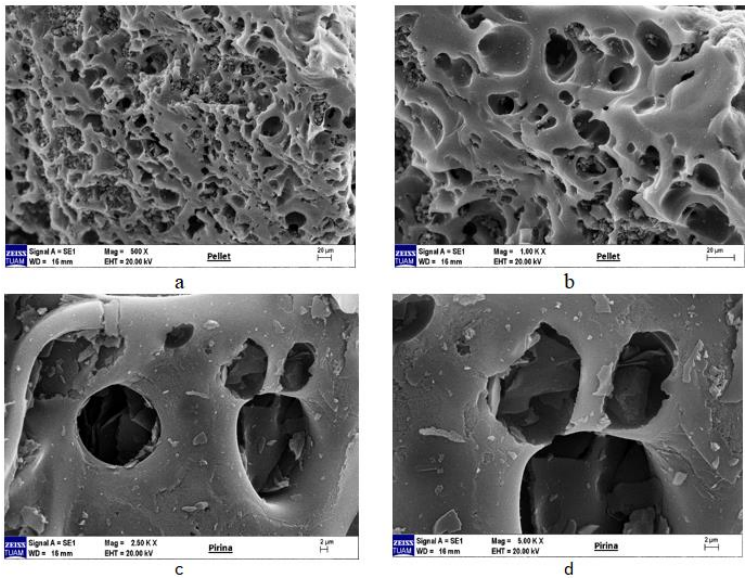

Fig. 2. SEM images of the activated carbons derived from pellet and olive pomace, respectively.

X-ray diffraction analyzes of the synthesized materials were carried out with an XRD, Ultima IV, Rigaku, Tokyo, Japan device. Using X-ray analysis, the mineralogy composition of the studied samples was ascertained. Fig. 3. displays the X-ray diffraction patterns of the raw materials pellet and pomace. Two activated carbons showed amorphous structure. However, the pomace sample has one diffraction peak around 50° and the pellet sample has another small diffraction peak around 38°. Similar results were reported by Alptekin et al. (Alptekin et al., 2023). Thermal and chemical activation of new activated carbon typically disrupts its crystalline structure. Amorphous materials usually exhibit greater surface acidity and a larger specific surface area, which enhances the interaction between the adsorbent and the substrate, leading to increased adsorption (Fito et al., 2023).

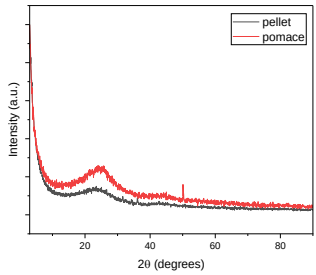

Fig. 3. X-ray diffraction (XRD) profile of ACs.

FT-IR spectra of adsorbent materials are necessary to identify the functional groups on its surface that affect its efficiency or capacity for removing specific pollutants (Zaidi et al., 2023). The 4000-600 cm-1 FTIR spectra of the activated carbons produced from pellet and olive pomace is exhibited in Fig. 4.

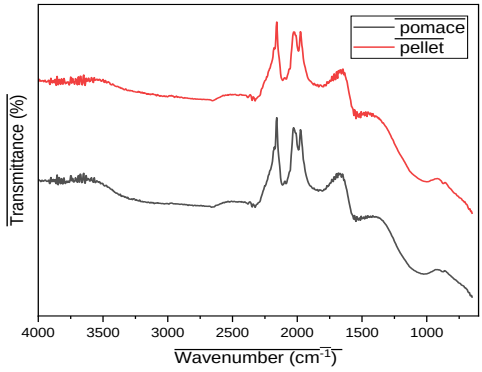

Fig. 4. Fourier transform infrared (FTIR) spectra of olive pomace and pellet before adsorption.

Both activated carbons showed similar functional group. The activated carbons exhibited bands associated with the bending of the C-H aromatic structure in the range 750-850 cm^{-1}. The C-O stretching in alcohol was seen at 1080 cm^{-1} (Shahrokhi-Shahraki et al., 2021). In the range of (1650-1500 cm-1), the activated carbons showed bands related with a stretch of C=O and aromatic structure. At 1800-1900 cm^{-1} and 2000-1900 cm^{-1}, they showed bands associated with a stretch of C=O and C=C=C, respectively (G. Duman, 2021; Kiełbasa et al., 2022; LibreTexts Chemistry, n.d.). The vibration band observed between 2950 and 3000 cm^{-1}, which corresponds to the stretching of CH and CH_2 groups, confirms the presence of cellulose and hemicellulose. The vibration bands at 3400 and 3414 cm^{-1} are attributed to the presence of hydroxyl groups, which contain O-H bonds (Monica & Anbalagan, 2024). The chemical activation and heat

treatment used to produce activated carbon significantly altered the structure and functional groups of the precursors, resulting in activated carbons rich in hydroxyl and carboxyl groups. Key elements such as oxygen, nitrogen, and hydrogen play crucial roles on the AC surface due to their bonding capabilities with other elements (Ukanwa et al., 2019). The findings suggest these functional groups are well-suited for creating durable activated carbons, offering a sustainable method for removing organic pollutants (Sugumaran et al., 2012; Wang et al., 2021).

3.2. Results of Adsorption isotherms

Adsorption is a useful technique for getting rid of damaging substances and colors from wastewater (Agarwala & Mulky, 2023). Solid-liquid adsorption systems are commonly described by the Freundlich and Langmuir isotherm models (Sayed et al., 2024). Table 2 displays the values of the maximum adsorption quantity (q_m), correlation coefficient (R^2), and other characteristics for each isotherm. The Langmuir isotherm claims that adsorption happens on a homogenous surface with sites that have equal energy and are equally accessible for adsorption (Siddiqui et al., 2019; Vargas et al., 2011). The maximum adsorption quantity of $ZnCl_2$ was obtained by AC_{pellet} as 142.85 mg g^{-1}, while 147.05 mg g^{-1} was achieved by $AC_{olive\ pomace}$. For MB, the maximum adsorption quantity of 181.82 mg g^{-1} was obtained by $AC_{olive\ pomace}$.

Table 2. Adsorption isotherm parameters for MB and $ZnCl_2$ adsorption onto ACs

Isotherm Model	Parameter	*Pellet AC*		*Olive pomace AC*	
		$ZnCl_2$	**MB**	**$ZnCl_2$**	**MB**
Langmuir	**qm (mg g^{-1})**	142.85	43.29	147.05	181.82
	KL (L mg^{-1})	0.249	-1.862	0.189	0.67
	Adj. R^2	0.834	0.959	0.609	0.983
	R_L	0.027	-0.0126	0.035	0.008
	Parameter	*Pellet AC*		*Olive pomace AC*	
		$ZnCl_2$	**MB**	**$ZnCl_2$**	**MB**
Freundlich	**K_f (L g^{-1})**	39.03	105.05	83.83	79.51
	n_F	2.55	2.28	13.38	3.33
	Adj. R^2	0.671	0.703	0.009	0.469

A mathematical model that can be applied to heterogeneous systems involving interactions between the molecules which are adsorbed is the Freundlich isotherm. It is possible to determine if the adsorption is linear (nF = 1), a chemical process (nF < 1), or a favorable physical process (nF > 1) using the nF parameter, also referred to as the heterogeneity factor. On the other hand, 1/nF > 1 and 1/nF < 1 represent cooperative adsorption and a normal Langmuir isotherm, respectively (Vargas et al., 2011). Among the isotherms, MB adsorption by

$AC_{olive\ pomace}$ showed the highest the value of R^2 of 0.983. The adsorption behavior of $AC_{olive\ pomace}$ for MB is a great match with the Langmuir model.

Figure 5 shows the separation parameter (R_L), which is a significant parameter of the Langmuir isotherm. The RL value in the Langmuir isotherm reflects the affinity of an adsorbent for an adsorbate. It helps determine the strength of the adsorbent, with a lower RL value indicating better performance in adsorbing the adsorbate from the solution (Branch & Branch, 2024). For all three materials, the R_L values indicate that the adsorption is most favorable at lower concentrations (100 mg and 150 mg). As the concentration increases to 200 mg and above, the adsorption process becomes linear, indicating that the adsorbent's capacity may be reaching equilibrium. At lower concentrations (100 mg and 150 mg), Olive Pomace-$ZnCl_2$ shows the most favorable adsorption process, as indicated by the lowest R_L values.

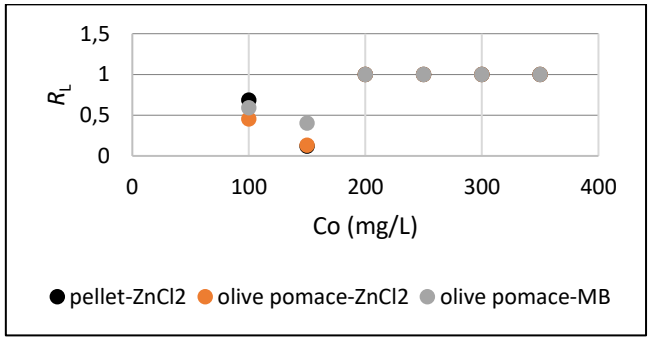

Fig. 5. Langmuir separation factor.

3.3. Results of Adsorption kinetics

To create an equation that can be used to compare various adsorbents under various operating situations as well as to build and optimize an operating method, the equilibrium data of the adsorption process is crucial. An equilibrium process and a rate process can be used to mathematically characterize the adsorption process, which is a mass transfer operation. The concentration of the metal ions bound to the adsorbent and those dissolved in the aqueous phase are in balance (GÖK, 2017).

In adsorption research, equilibrium isotherms and kinetic modeling are essential because they offer experimental design for the ideal possible adsorption (Osagie et al., 2021). Adsorption kinetics are studied to reduce water pollution, relying on the interaction between adsorbate and adsorbent and system conditions. The mechanism and reaction rate are crucial for assessing adsorption

processes. The solute uptake rate, determined by kinetic analysis, dictates the residence time for the adsorption reaction. In liquid-solid adsorption systems, efforts have been made to develop an ideal kinetic model for adsorption on solid surfaces (Ho, 2004; Kavitha & Namasivayam, 2007; M.R. et al., 2009; Shahwan, 2015).

The first-order rate equation for the kinetics of solid-liquid phase adsorption was put forth by Lagergren in 1898. In this model, the adsorption rate is determined by the adsorption capacity, making it one of the earliest approaches to adsorption analysis. Equation 8 provides the pseudo-first order kinetic model equation (S., 1898).

$$Dq_t/dt = k_1(qe - qt) \quad (8)$$

Here, the pseudo-first order rate constant for the kinetic model is denoted by k_1^{-1} (min), and the adsorption capacities at equilibrium and time t, respectively, are represented by qe and qt (mg/g). Equation 9's linear equation form is achieved when this equation is integrated using the boundary conditions q= 0 at t = 0 and q= t at t = t.

$$\ln (q_e - qt) = \ln (qe) - k_1 t \quad (9)$$

Equation 9 may be used to get the value of qe from the shift of the t graph plotted against ln (q_e - q_t) using experimental data, and the value of k1 from the slope of the line (Kobya et al., 2002; Qiu et al., 2009).

Pseudo-second order kinetic model

According to the pseudo-second-order kinetic model, the solute's rate of adsorption is proportionate to the adsorbent's accessible regions. As a result, the repulsive force (qe - qt) is proportional to the number of accessible active regions on the adsorbent, and the reaction rate is related to the amount of solute on the adsorbent surface. The pseudo second order kinetic model's curvilinear form is displayed in Equation 10 (Serpil Edebali., 2019).

$$Dq_t/dt = k_2 (q_e - q_t)^2 \quad (10)$$

Here, the pseudo-second order rate constant for the kinetic model is denoted by k_2 (g mg.min^{-1}), and the adsorption capacities at equilibrium and time t, respectively, are represented by qe and qt (mg/g). The linear equation form found in Equation 11 is derived when this equation is integrated using the boundary conditions q= 0 at t = 0 and q= t at t = t.

$$t/q_t = 1/ k_2 q_e^2 + 1/q_e t \quad (11)$$

Equation 11 can be used to build a t graph against t/qt using experimental data. From this graph, the value of k_2 can be inferred from its shift, and the value of q_e can be found from the line's slope (Kobya et al., 2002; William Kajjumba et al., 2019). The identified kinetic model (eq (5)) was used to match experimental adsorption kinetic data in this study. The results given in Table 3 and Table 4 for $ZnCl_2$ and MB, respectively. Both $ZnCl_2$ and MB, pseudo-second order kinetic model is best-fit kinetic model for both AC_{pellet} and $AC_{olive\ pomace}$ at higher concentration (R^2=0.997-0.999).

Table 3. The kinetic parameters for ZnCl2 adsorption by the ACs.

Pellet AC						
Initial Concentration (ppm) $ZnCl_2$	**Pseudo-first order**			**Pseudo-second order**		
	k_1 (1 min^{-1})	**q_e (g g^{-1})**	**R^2**	**k_2 (L mg-min^{-1})**	**q_e (g g^{-1})**	**R^2**
250	-0.00235	0.917	0.699	-0.028	243.9	0.997
300	-0.00014	1.115	0.775	0.109	303.03	0.999
350	-0.00016	1.073	0.809	0.084	344.83	0.999
Olive pomace AC						
Initial Concentration (ppm) $ZnCl_2$	**Pseudo-first order**			**Pseudo-second order**		
	k_1 (1 min^{-1})	**q_e (g g^{-1})**	**R^2**	**k_2 (L mg-min^{-1})**	**q_e (g g^{-1})**	**R^2**
250	-0.00005	1.391	0.042	-0.0088	243.9	0.999
300	-0.00005	1.391	0.042	0.0578	294.11	0.999
350	-0.00005	1.391	0.042	0.1682	344.83	1

Adsorbent dose = 100 mg/L; contact time = 20 min–100 min.

Fig. 6. shows the kinetic parameters obtained for $ZnCl_2$ and MB adsorption on ACs. The presence of active functional groups specific to methylene blue (MB), a larger surface area conducive to MB adsorption, and increased pore volume and size are some factors that effect on q_e value. The initial phase of adsorption involves MB diffusing through the macropores and mesopores in biochar and activated carbons, while the subsequent phase involves diffusion through the micropores (Sutar & Jadhav, 2024). Even if at higher concentration, $AC_{olive\ pomace}$ showed the highest q_e value of 322.58 mg g^{-1} due to its micro-mesoporous structure.

Table 4. The kinetic models for MB dye adsorption by the ACs

Pellet AC						
Initial Concentration (ppm) MB	**Pseudo-first order**			**Pseudo-second order**		
	k_1 (1 min^{-1})	**q_e (g g^{-1})**	**R^2**	**k_2 (L mg-min^{-1})**	**q_e (g g^{-1})**	**R^2**
250	-0.0024	0.927	0.724	0.0053	243.9	0.999
300	-0.00001	1.115	0.776	0.0014	294.12	0.994
350	-0.00018	1.012	0.773	0.0113	313.48	0.994
Olive pomace AC						
Initial Concentration (ppm) MB	**Pseudo-first order**			**Pseudo-second order**		
	k_1 (1 min^{-1})	**q_e (g g^{-1})**	**R^2**	**k_2 (L mg-min^{-1})**	**q_e (g g^{-1})**	**R^2**
250	-0.00006	0.718	0.428	0.0098	238.1	0.998
300	-0.00005	1.391	0.428	0.0013	294.12	0.997
350	-0.00005	1.391	0.428	0.0022	322.58	0.995

Adsorbent dose = 100 mg/L; contact time = 20 min–100 min.

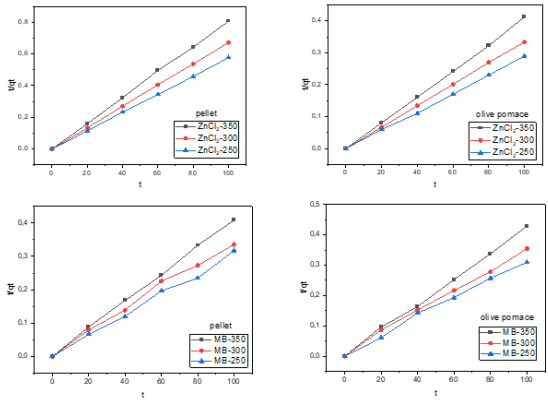

Fig. 6. The fitted pseudo-second-order kinetic model for a) $ZnCl_2$-pellet, b) $ZnCl_2$- olive pomace, c)MB-pellet, d)MB-olive pomace.

4.Conclusion

The activated carbon derived from olive pomace is an effective adsorbent for removal of both methylene blue and $ZnCl_2$ from aqueous solution while activated carbon derived from pellet is favorable for removing of $ZnCl_2$. The adsorption was highly dependent on contact time and initial concentration. The kinetic data indicated that the process follows the Langmuir isotherm, and the reaction rate is described by pseudo-second order kinetics. The maximum adsorption capacity of $AC_{olive\ pomace}$ and AC_{pellet} for $ZnCl_2$ were found to be 147.05 and 142.85 mg g^{-1}, respectively. $AC_{olive\ pomace}$ showed the maximum adsorption capacity of 181.82 mg g^{-1} for methylene blue. Results showed that the physical and chemical characteristics of ACs have a crucial effect on adsorption performance.

According to BET tests, ACs have a surface area that is similar to other types of AC but a much higher micropore volume, suggesting that it could be an effective adsorbent. Hence, $AC_{\text{olive pomace}}$ that has micro and mesoporous structure exhibited good adsorbent behavior both $ZnCl_2$ and methylene blue.

Acknowledgement

Authors would like to express their gratitude to Prof. Dr. Jale Yanik, Prof. Dr. Nurdan Büyükkamacı, Assoc. Prof. Dr. Hasan Sarptaş and Dilvin Çebi for their contributions to work.

Funding

This work is supported by Ege University Scientific Research Projects Coordination Unit, under project number: FOA-2020-22138.

References

Abewaa, M., Arka, A., Haddis, T., Mengistu, A., Takele, T., Adino, E., Abay, Y., Bekele, N., Andualem, G., & Girmay, H. (2024). Hexavalent chromium adsorption from aqueous solution utilizing activated carbon developed from Rumex abyssinicus. *Results in Engineering*, *22*(March), 102274. https://doi.org/10.1016/j.rineng.2024.102274

Adnan, M., Xiao, B., Ali, M. U., Xiao, P., Zhao, P., Wang, H., & Bibi, S. (2024). Heavy metals pollution from smelting activities: A threat to soil and groundwater. *Ecotoxicology and Environmental Safety*, *274*, 116189. https://doi.org/10.1016/J.ECOENV.2024.116189

Agarwala, R., & Mulky, L. (2023). Adsorption of Dyes from Wastewater: A Comprehensive Review. *ChemBioEng Reviews*, *10*(3), 326–335. https://doi.org/10.1002/CBEN.202200011

Akar, T., Uzunel Can, Ü. G., Celik, S., Sayin, F., & Tunali Akar, S. (2022). A hybrid biocomposite of Thamnidium elegans/olive pomace/chitosan for efficient bioremoval of toxic copper. *International Journal of Biological Macromolecules*, *221*, 865–873. https://doi.org/10.1016/J.IJBIOMAC.2022.08.207

Akhtar, N., Syakir Ishak, M. I., Bhawani, S. A., & Umar, K. (2021). Various Natural and Anthropogenic Factors Responsible for Water Quality Degradation: A Review. *Water 2021, Vol. 13, Page 2660*, *13*(19), 2660. https://doi.org/10.3390/W13192660

Alptekin, F. M., & Celiktas, M. S. (2022). Review on Catalytic Biomass Gasification for Hydrogen Production as a Sustainable Energy Form and Social, Technological, Economic, Environmental, and Political Analysis of Catalysts. *ACS Omega*, *7*(29), 24918–24941. https://doi.org/10.1021/ACSOMEGA.2C01538/ASSET/IMAGES/LARGE/AO2C01538_0002.JPEG

Alptekin, F. M., Dunford, N. T., & Celiktas, M. S. (2023). Miscanthus-Derived Energy Storage System Material Production. *ACS Omega*, *8*(9), 8779–8790. https://doi.org/10.1021/ACSOMEGA.3C00024/ASSET/IMAGES/LARGE/AO3C00024_0009.JPEG

Ardila-Leal, L. D., Poutou-Piñales, R. A., Pedroza-Rodríguez, A. M., & Quevedo-Hidalgo, B. E. (2021). A Brief History of Colour, the Environmental Impact of Synthetic Dyes and Removal by Using Laccases. *Molecules*, *26*(13). https://doi.org/10.3390/MOLECULES26133813

Areej, I., Raza, S., Abid, A., Ali, S., Qureshi, A. K., Shaaque, U., Roy, R., Iqbal, R., & Al-Onazi, W. A. (2024). *Fabrication of New Hyper-Cross-linked polymer*

for Efficient Heavy metal Adsorption from Industrial Wastewater. https://doi.org/10.21203/RS.3.RS-3834099/V1

Babich, H., & Stotzky, G. (1978). Toxicity of zinc to fungi, bacteria, and coliphages: Influence of chloride ions. *Applied and Environmental Microbiology*, *36*(6), 906–914. https://doi.org/10.1128/aem.36.6.906-914.1978

Balcioglu, G., Jeswani, H. K., & Azapagic, A. (2023). Energy from forest residues in Turkey: An environmental and economic life cycle assessment of different technologies. *Science of the Total Environment*, *874*, 162316. https://doi.org/10.1016/j.scitotenv.2023.162316

Basharat, S., Rehman, R., & Mitu, L. (2021). Adsorptive Separation of Brilliant Green Dye from Water by Tartaric Acid-Treated Holarrhena antidysenterica and Citrullus colocynthis Biowaste. *Journal of Chemistry*, *2021*(1), 6636181. https://doi.org/10.1155/2021/6636181

Basu, S., Ghosh, G., & Saha, S. (2018). Adsorption characteristics of phosphoric acid induced activation of bio-carbon: Equilibrium, kinetics, thermodynamics and batch adsorber design. *Process Safety and Environmental Protection*, *117*, 125–142. https://doi.org/10.1016/J.PSEP.2018.04.015

Bläker, C., Muthmann, J., Pasel, C., & Bathen, D. (2019). Characterization of Activated Carbon Adsorbents – State of the Art and Novel Approaches. *ChemBioEng Reviews*, *6*(4), 119–138. https://doi.org/10.1002/CBEN.201900008

Boufi, S. (2017). Biocomposites from olive-stone flour: A step forward in the valorization of the solid waste from the olive-oil industry. *Lignocellulosic Fibre and Biomass-Based Composite Materials: Processing, Properties and Applications*, 387–408. https://doi.org/10.1016/B978-0-08-100959-8.00018-4

Branch, A., & Branch, A. (2024). *Evaluating the Efficiency of Two-Parameter Adsorption Isotherm Models in the Adsorption of Methylene Blue*. *43*(4), 1533–1549.

Brasquet, C., Rousseau, B., Estrade-Szwarckopf, H., & Le Cloirec, P. (2000). Observation of activated carbon fibres with SEM and AFM correlation with adsorption data in aqueous solution. *Carbon*, *38*(3), 407–422. https://doi.org/10.1016/S0008-6223(99)00120-7

Buhani, Wijayanti, T. A., Suharso, Sumadi, & Ansori, M. (2021). Application of modified green algae Nannochloropsis sp. as adsorbent in the simultaneous adsorption of Methylene Blue and Cu(II) cations in solution. *Sustainable Environment Research*, *31*(1), 1–12. https://doi.org/10.1186/S42834-021-00090-Y/FIGURES/12

Burdová, H., Brázová, V., Kwoczynski, Z., Snow, J., Trögl, J., & Kříženecká, S. (2024). Miscanthus x giganteus biochar: Effective adsorption of pharmaceuticals from model solution and hospital wastewater. *Journal of Cleaner Production*, 142545. https://doi.org/10.1016/J.JCLEPRO.2024.142545

Chen, R., Li, L., Liu, Z., Lu, M., Wang, C., Li, H., Ma, W., & Wang, S. (2017). Preparation and characterization of activated carbons from tobacco stem by chemical activation. *Journal of the Air and Waste Management Association*, *67*(6), 713–724. https://doi.org/10.1080/10962247.2017.1280560

Dharmapriya, T. N., Li, D. Y., Chung, Y. C., & Huang, P. J. (2021). Green Synthesis of Reusable Adsorbents for the Removal of Heavy Metal Ions. *ACS Omega*, *6*(45), 30478. https://doi.org/10.1021/ACSOMEGA.1C03879

Dimbo, D., Abewaa, M., Adino, E., Mengistu, A., Takele, T., Oro, A., & Rangaraju, M. (2024). Methylene blue adsorption from aqueous solution using activated carbon of spathodea campanulata. *Results in Engineering*, *21*(February), 101910. https://doi.org/10.1016/j.rineng.2024.101910

Dotto, G. L., Santos, J. M. N., Rodrigues, I. L., Rosa, R., Pavan, F. A., & Lima, E. C. (2015). Adsorption of Methylene Blue by ultrasonic surface modified chitin. *Journal of Colloid and Interface Science*, *446*, 133–140. https://doi.org/10.1016/J.JCIS.2015.01.046

Duan, L., Yun, Q., Jiang, G., Teng, D., Zhou, G., & Cao, Y. (2024). A review of chloride ions removal from high chloride industrial wastewater: Sources, hazards, and mechanisms. *Journal of Environmental Management*, *353*, 120184. https://doi.org/10.1016/J.JENVMAN.2024.120184

Duman, A. K., Özgen, G. Ö., & Üçtuğ, F. G. (2020). Environmental life cycle assessment of olive pomace utilization in Turkey. *Sustainable Production and Consumption*, *22*, 126–137. https://doi.org/10.1016/j.spc.2020.02.008

Duman, G. (2021). Preparation of novel porous carbon from hydrothermal pretreated textile wastes: Effects of textile type and activation agent on structural and adsorptive properties. *Journal of Water Process Engineering*, *43*, 102286. https://doi.org/10.1016/J.JWPE.2021.102286

Dutta, S., Gupta, B., Srivastava, S. K., & Gupta, A. K. (2021). Recent advances on the removal of dyes from wastewater using various adsorbents: a critical review. *Materials Advances*, *2*(14), 4497–4531. https://doi.org/10.1039/D1MA00354B

Feisal, N. A. S., Kamaludin, N. H., Ahmad, M. A., & Tengku Ibrahim, T. N. B. (2024). A comprehensive review of nanomaterials for efficient heavy metal ions removal in water treatment. *Journal of Water Process Engineering*, *64*, 105566. https://doi.org/10.1016/J.JWPE.2024.105566

Fito, J., Abewaa, M., Mengistu, A., Angassa, K., Ambaye, A. D., Moyo, W., & Nkambule, T. (2023). Adsorption of methylene blue from textile industrial wastewater using activated carbon developed from Rumex abyssinicus plant. *Scientific Reports 2023 13:1*, *13*(1), 1–17. https://doi.org/10.1038/s41598-023-32341-w

Fraga, H., Moriondo, M., Leolini, L., & Santos, J. A. (2020). Mediterranean Olive Orchards under Climate Change: A Review of Future Impacts and Adaptation Strategies. *Agronomy 2021, Vol. 11, Page 56*, *11*(1), 56. https://doi.org/10.3390/AGRONOMY11010056

Freha, M., El-Amine Nouairi, M., & Bellil, A. (2024). Method for quantifying catechin in a strawberry extract by measuring optical absorbance, at high sensitivity, under the effect of wavelength and concentration. *Spectrochimica Acta Part A: Molecular and Biomolecular Spectroscopy*, *308*, 123797. https://doi.org/10.1016/J.SAA.2023.123797

Gao, J. J., Qin, Y. B., Zhou, T., Cao, D. D., Xu, P., Hochstetter, D., & Wang, Y. F. (2013). Adsorption of methylene blue onto activated carbon produced from tea (Camellia sinensis L.) seed shells: kinetics, equilibrium, and thermodynamics studies. *Journal of Zhejiang University. Science. B*, *14*(7), 650–658. https://doi.org/10.1631/JZUS.B12A0225

Gayathiri, M., Pulingam, T., Lee, K. T., & Sudesh, K. (2022). Activated carbon from biomass waste precursors: Factors affecting production and adsorption mechanism. *Chemosphere*, *294*(December 2021), 133764. https://doi.org/10.1016/j.chemosphere.2022.133764

GÖK, C. (2017). Equilibrium, Kinetic and Thermodynamic Studies of Europium Adsorption by Biopolymeric Composite. *International Journal of Chemical Engineering and Applications*, *8*(5), 334–339. https://doi.org/10.18178/IJCEA.2017.8.5.679

Hijab, M., Parthasarathy, P., Mackey, H. R., Al-Ansari, T., & McKay, G. (2021). Minimizing adsorbent requirements using multi-stage batch adsorption for malachite green removal using microwave date-stone activated carbons. *Chemical Engineering and Processing - Process Intensification*, *167*, 108318. https://doi.org/10.1016/J.CEP.2021.108318

Ho, Y.-S. (2004). Citation review of Lagergren kinetic rate equation on adsorption reactions. *Budapest Scientometrics*, *59*(1), 171–177.

Inbaraj, B. S., Selvarani, K., & Sulochana, N. (2022). (PDF) Evaluation of a Carbonaceous Sorbent Prepared From Pearl Millet Husk for Its Removal of Basic Dyes. *Journal of Scientific & Industrial Research*, *61*(11), 971–978.

Kavitha, D., & Namasivayam, C. (2007). Experimental and kinetic studies on methylene blue adsorption by coir pith carbon. *Bioresource Technology*, *98*(1), 14–21. https://doi.org/10.1016/J.BIORTECH.2005.12.008

Khan, S., Noor, T., Iqbal, N., & Yaqoob, L. (2024). Photocatalytic Dye Degradation from Textile Wastewater: A Review. *ACS Omega*. https://doi.org/10.1021/ACSOMEGA.4C00887

Kiełbasa, K., Bayar, Ş., Varol, E. A., Sreńscek-Nazzal, J., Bosacka, M., & Michalkiewicz, B. (2022). Thermochemical conversion of lignocellulosic biomass - olive pomace - into activated biocarbon for CO2 adsorption. *Industrial Crops and Products*, *187*. https://doi.org/10.1016/J.INDCROP.2022.115416

Kobya, M., Demirbas, E., Öncel, M. S., & Sencan, S. (2002). Adsorption Kinetic Models Applied to Nickel Ions on Hazelnut Shell Activated Carbons. *Http://Dx.Doi.Org/10.1260/026361702320360595*, *20*(2), 179–188. https://doi.org/10.1260/026361702320360595

Krstić, V., Urošević, T., & Pešovski, B. (2018). A review on adsorbents for treatment of water and wastewaters containing copper ions. *Chemical Engineering Science*, *192*, 273–287. https://doi.org/10.1016/J.CES.2018.07.022

Kumar, N., Pandey, A., Rosy, & Sharma, Y. C. (2023). A review on sustainable mesoporous activated carbon as adsorbent for efficient removal of hazardous dyes from industrial wastewater. *Journal of Water Process Engineering*, *54*, 104054. https://doi.org/10.1016/J.JWPE.2023.104054

Langmuir, I. (1918). The adsorption of gases on plane surfaces of glass, mica and platinum. *Journal of the American Chemical Society*, *40*(9), 1361–1403. https://doi.org/10.1021/JA02242A004/ASSET/JA02242A004.FP.PNG_V03

LibreTexts Chemistry. (n.d.). *Infrared Spectroscopy Absorption Table - Chemistry LibreTexts*. LibreTexts Chemistry. Retrieved May 20, 2024, from https://chem.libretexts.org/Ancillary_Materials/Reference/Reference_Tables/Spectroscopic_Reference_Tables/Infrared_Spectroscopy_Absorption_Table

Liyanaarachchi, H., Thambiliyagodage, C., Lokuge, H., & Vigneswaran, S. (2023). Kinetics and Thermodynamics Study of Methylene Blue Adsorption to Sucrose- and Urea-Derived Nitrogen-Enriched, Hierarchically Porous Carbon Activated by KOH and H3PO4. *ACS Omega*, *8*(18), 16158–16173. https://doi.org/10.1021/ACSOMEGA.3C00339/SUPPL_FILE/AO3C00339_SI_001.PDF

Ma, C., Bai, J., Demir, M., Hu, X., Liu, S., & Wang, L. (2022). Water chestnut shell-derived N/S-doped porous carbons and their applications in CO2 adsorption

and supercapacitor. *Fuel*, *326*, 125119. https://doi.org/10.1016/J.FUEL.2022.125119

Macchi, S., Alsebai, Z., Watanabe, F., Ilyas, A., Atif, S., Viswanathan, T., & Siraj, N. (2021). Influence of phosphorus and nitrogen co-doping of activated carbon from littered cigarette filters for adsorption of methylene blue dye from wastewater. *Sustainable Environment Research*, *31*(1), 1–11. https://doi.org/10.1186/S42834-021-00108-5/FIGURES/10

Macedo, J. de S., da Costa Júnior, N. B., Almeida, L. E., Vieira, E. F. da S., Cestari, A. R., Gimenez, I. de F., Villarreal Carreño, N. L., & Barreto, L. S. (2006). Kinetic and calorimetric study of the adsorption of dyes on mesoporous activated carbon prepared from coconut coir dust. *Journal of Colloid and Interface Science*, *298*(2), 515–522. https://doi.org/10.1016/J.JCIS.2006.01.021

Masudur Rhaman, M., Din Islam, M., Rezaul Karim, M., Ahmed, Y., Mohammad Ziaul Hyder, M. K., & Mohammad Ziaul Hyder, M. (2022). *Fabrication of amine cross-linked magnetic biopolymer adsorbent for the removal of a cationic dye and its isotherm, kinetics and thermodynamic study*. https://doi.org/10.21203/RS.3.RS-1742914/V1

Mohd Faizal, A. N., Meskam, N. N., Putra, N. R., Zaini, A. S., Mohamed Rusli, N., & Ahmad Zaini, M. A. (2023). Preparation of beeswax residue-ZnCl2-activated carbon for adsorption of methylene blue. *Materials Today: Proceedings*. https://doi.org/10.1016/J.MATPR.2023.08.345

Monica, A. V., & Anbalagan, K. (2024). Facile synthesis of activated biomass loaded with ZnCl2 as eco-friendly adsorbent for BPA and BPS removal: Comparative study on Batch, column and breakthrough performance. *Journal of Water Process Engineering*, *64*(February), 105636. https://doi.org/10.1016/j.jwpe.2024.105636

Moreno-Piraján, J. C., & Giraldo, L. (2012). Heavy metal ions adsorption from wastewater using activated carbon from orange peel. *E-Journal of Chemistry*, *9*(2), 926–937. https://doi.org/10.1155/2012/383742

M.R., S., M., H., F., B. A., & S., M. (2009). *Two-parameter isotherms of methyl orange sorption by pinecone derived activated carbon* (vol. 6, issue 4, pp. 285–294). *Iranian Journal Of Environmental Health Science And Engineering* (IJEHSE).

Nampeera, J., Recepoğlu, Y. K., & Yuksel, A. (2024). Valorization of olive tree pruning waste for potential utilization in lithium recovery from aqueous solutions. *Biomass Conversion and Biorefinery*, *14*(4), 4975–4987. https://doi.org/10.1007/S13399-022-02647-2/TABLES/5

Ochando-Pulido, J. M., & Martinez-Ferez, A. (2017). The recovery of added-value compounds from olive mill wastewater. In *Handbook of Olive Oil: Phenolic Compounds, Production and Health Benefits* (pp. 423–438). Nova Science Publishers, Inc.

Ogunmodede, O. T., Ojo, A. A., Adewole, E., & Adebayo, O. L. (2015). Iranica Journal of Energy & Environment Adsorptive removal of anionic dye from aqueous solutions by mixture of Kaolin and Bentonite clay: Characteristics, isotherm, kinetic and thermodynamic studies INTRODUCTION 1. *Iranica Journal of Energy and Environment*, *6*(2), 147–153. https://doi.org/10.5829/idosi.ijee.2015.06.02.11

Onyutha, C., Okello, E., Atukwase, R., Nduhukiire, P., Ecodu, M., & Kwiringira, J. N. (2024). Improving household water treatment: using zeolite to remove lead, fluoride and arsenic following optimized turbidity reduction in slow sand filtration. *Sustainable Environment Research*, *34*(1), 1–15. https://doi.org/10.1186/S42834-024-00209-X/FIGURES/8

Osagie, C., Othmani, A., Ghosh, S., Malloum, A., Kashitarash Esfahani, Z., & Ahmadi, S. (2021). Dyes adsorption from aqueous media through the nanotechnology: A review. *Journal of Materials Research and Technology*, *14*, 2195–2218. https://doi.org/10.1016/J.JMRT.2021.07.085

Ozcan, D. O., Hendekci, M. C., & Ovez, B. (2024). Enhancing the adsorption capacity of organic and inorganic pollutants onto impregnated olive stone derived activated carbon. *Heliyon*, *10*(12), e32792. https://doi.org/10.1016/J.HELIYON.2024.E32792

Pagano, M., Porcino, C., Briglia, M., Fiorino, E., Vazzana, M., Silvestro, S., & Faggio, C. (2017). The Influence of Exposure of Cadmium Chloride and Zinc Chloride on Haemolymph and Digestive Gland Cells from Mytilus galloprovincialis. *International Journal of Environmental Research*, *11*(2), 207–216. https://doi.org/10.1007/s41742-017-0020-8

Pavithra, S., Shyamalagowri, S., Murugesan, S., Akila, N., Raj, S. A., & Dharshini, U. K. D. (2024). Production strategies for carbon composites and carbon-based adsorbents. *Physical Sciences Reviews*. https://doi.org/10.1515/PSR-2023-0040/XML

Piwowarska, D., Kiedrzyńska, E., Jaszczyszyn, K., Álvarez-Ayuso, E., & Bradford, S. (2024). A global perspective on the nature and fate of heavy metals polluting water ecosystems, and their impact and remediation. *Critical Reviews in Environmental Science and Technology*. https://doi.org/10.1080/10643389.2024.2317112

Qalyoubi, L., Al-Othman, A., & Al-Asheh, S. (2021). Recent progress and challenges of adsorptive membranes for the removal of pollutants from wastewater. Part

II: Environmental applications. *Case Studies in Chemical and Environmental Engineering*, *3*, 100102. https://doi.org/10.1016/J.CSCEE.2021.100102

Qasem, N. A. A., Mohammed, R. H., & Lawal, D. U. (2021). Removal of heavy metal ions from wastewater: a comprehensive and critical review. *Npj Clean Water 2021 4:1*, *4*(1), 1–15. https://doi.org/10.1038/s41545-021-00127-0

Qiu, H., Lv, L., Pan, B. C., Zhang, Q. J., Zhang, W. M., & Zhang, Q. X. (2009). Critical review in adsorption kinetic models. *Journal of Zhejiang University: Science A*, *10*(5), 716–724. https://doi.org/10.1631/JZUS.A0820524/METRICS

Rathi, B. S., & Kumar, P. S. (2021). Application of adsorption process for effective removal of emerging contaminants from water and wastewater. *Environmental Pollution*, *280*, 116995. https://doi.org/10.1016/J.ENVPOL.2021.116995

S., L. (1898). *Zur theorie der sogenannten adsorption geloster stoffe* (vol. 24, issue 4, pp. 1–39). Kungliga svenska vetenskapsakademiens handlingar.

Saleh, T. A. (2024). Materials, nanomaterials, nanocomposites, and methods used for the treatment and removal of hazardous pollutants from wastewater: Treatment technologies for water recycling and sustainability. *Nano-Structures & Nano-Objects*, *39*, 101231. https://doi.org/10.1016/J.NANOSO.2024.101231

Satyam, S., & Patra, S. (2024). Innovations and challenges in adsorption-based wastewater remediation: A comprehensive review. *Heliyon*, *10*(9), e29573. https://doi.org/10.1016/J.HELIYON.2024.E29573

Sayed, N. S. M., Ahmed, A. S. A., Abdallah, M. H., & Gouda, G. A. (2024). ZnO@ activated carbon derived from wood sawdust as adsorbent for removal of methyl red and methyl orange from aqueous solutions. *Scientific Reports 2024 14:1*, *14*(1), 1–18. https://doi.org/10.1038/s41598-024-55158-7

Serpil Edebali. (2019). *Advanced Sorption Process Applications*.

Shahrokhi-Shahraki, R., Benally, C., El-Din, M. G., & Park, J. (2021). High efficiency removal of heavy metals using tire-derived activated carbon vs commercial activated carbon: Insights into the adsorption mechanisms. *Chemosphere*, *264*, 128455. https://doi.org/10.1016/J.CHEMOSPHERE.2020.128455

Shahwan, T. (2015). Lagergren equation: Can maximum loading of sorption replace equilibrium loading? *Chemical Engineering Research and Design*, *96*, 172–176. https://doi.org/10.1016/J.CHERD.2015.03.001

Sheraz, N., Shah, A., Haleem, A., & Iftikhar, F. J. (2024). Comprehensive assessment of carbon-, biomaterial- and inorganic-based adsorbents for the removal of

the most hazardous heavy metal ions from wastewater. *RSC Advances*, *14*(16), 11284–11310. https://doi.org/10.1039/D4RA00976B

Siddiqui, S. I., Zohra, F., & Chaudhry, S. A. (2019). Nigella sativa seed based nanohybrid composite-Fe_2O_3-SnO_2/BC: A novel material for enhanced adsorptive removal of methylene blue from water. *Environmental Research*, *178*, 108667–108667. https://doi.org/10.1016/J.ENVRES.2019.108667

Sismanoglu, S., Tayfun, U., Popescu, C. M., & Kanbur, Y. (2023). Effective use of olive pulp as biomass additive for eco-grade TPU-based composites using functional surface modifiers. *Biomass Conversion and Biorefinery*, *13*(13), 12303–12318. https://doi.org/10.1007/S13399-021-01987-9/FIGURES/15

Su, C., Berekute, A. K., & Yu, K. P. (2022). Chitosan@TiO2 composites for the adsorption of copper(II) and antibacterial applications. *Sustainable Environment Research*, *32*(1), 1–15. https://doi.org/10.1186/S42834-022-00138-7/FIGURES/9

Sugumaran, P., Susan, V., Ravichandran, P., & Seshadri, S. (2012). Production and Characterization of Activated Carbon from Banana Empty Fruit Bunch and Delonix regia Fruit Pod. *Journal of Sustainable Energy and Environment*.

Sun, K., Lyu, Q., Zheng, X., Liu, R., Tang, C. Y., Zhao, M., & Dong, Y. (2024). Enhanced water treatment performance of ceramic-based forward osmosis membranes via MOF interlayer. *Water Research*, *254*, 121395. https://doi.org/10.1016/J.WATRES.2024.121395

Sutar, S., & Jadhav, J. (2024). A comparative assessment of the methylene blue dye adsorption capacity of natural biochar versus chemically altered activated carbons. *BiTeR*, *25*, 101726. https://doi.org/10.1016/J.BITEB.2023.101726

Takele, T., Angassa, K., Abewaa, M., Kebede, A. M., & Tessema, I. (2023). Adsorption of methylene blue from textile industrial wastewater using activated carbon developed from H3PO4-activated khat stem waste. *Biomass Conversion and Biorefinery*, *0123456789*. https://doi.org/10.1007/s13399-023-05245-y

Tansel, B., & Nagarajan, P. (2004). SEM study of phenolphthalein adsorption on granular activated carbon. *Advances in Environmental Research*, *8*(3), 411–415. https://doi.org/10.1016/S1093-0191(02)00126-0

Teğin, İ., Demirel, M. F., Alacabey, İ., & Yabalak, E. (2024). Investigation of the effectiveness of waste nut shell–based hydrochars in water treatment: a model study for the adsorption of methylene blue. *Biomass Conversion and Biorefinery*, *14*(9), 10399–10412. https://doi.org/10.1007/S13399-022-02996-Y/TABLES/5

Teweldebrihan, M. D., Gnaro, M. A., & Dinka, M. O. (2024). The application of magnetite biochar composite derived from parthenium hysterophorus for the adsorption of methylene blue from aqueous solution. *Frontiers in Environmental Science*, *12*(April), 1–16. https://doi.org/10.3389/fenvs.2024.1375437

Thommes, M., Kaneko, K., Neimark, A. V, Olivier, J. P., Rodriguez-Reinoso, F., Rouquerol, J., & Sing, K. S. W. (2015). IUPAC Technical Report Physisorption of gases, with special reference to the evaluation of surface area and pore size distribution (IUPAC Technical Report). *Pure Appl. Chem*, aop. https://doi.org/10.1515/pac-2014-1117

Tunalıoglu, R. (2023). Changes in Olive Mill Waste Water Management in Turkey. In *Springer Water* (pp. 213–220). Springer Nature. https://doi.org/10.1007/978-3-031-23449-1_9

Ukanwa, K. S., Patchigolla, K., Sakrabani, R., Anthony, E., & Mandavgane, S. (2019). A review of chemicals to produce activated carbon from agricultural waste biomass. *Sustainability (Switzerland)*, *11*(22), 1–35. https://doi.org/10.3390/su11226204

Valli Nachiyar, C., Rakshi, A. D., Sandhya, S., Britlin Deva Jebasta, N., & Nellore, J. (2023). Developments in treatment technologies of dye-containing effluent: A review. *Case Studies in Chemical and Environmental Engineering*, *7*, 100339. https://doi.org/10.1016/J.CSCEE.2023.100339

Vargas, A. M. M., Cazetta, A. L., Kunita, M. H., Silva, T. L., & Almeida, V. C. (2011). Adsorption of methylene blue on activated carbon produced from flamboyant pods (Delonix regia): Study of adsorption isotherms and kinetic models. *Chemical Engineering Journal*, *168*, 722–730. https://doi.org/10.1016/j.cej.2011.01.067

Wang, H., Li, Z., Yahyaoui, S., Hanafy, H., Seliem, M. K., Bonilla-Petriciolet, A., Luiz Dotto, G., Sellaoui, L., & Li, Q. (2021). Effective adsorption of dyes on an activated carbon prepared from carboxymethyl cellulose: Experiments, characterization and advanced modelling. *Chemical Engineering Journal*, *417*, 128116. https://doi.org/10.1016/J.CEJ.2020.128116

William Kajjumba, G., Emik, S., Öngen, A., Kurtulus Özcan, H., & Aydın, S. (2019). Modelling of Adsorption Kinetic Processes—Errors, Theory and Application. *Advanced Sorption Process Applications*. https://doi.org/10.5772/INTECHOPEN.80495

Yılmaz, O., & Tugrul, N. (2022). Zinc adsorption from aqueous solution using lemon, orange, watermelon, melon, pineapple, and banana rinds. *Water Practice and Technology*, *17*(1), 318–328. https://doi.org/10.2166/wpt.2021.102

Zaidi, Z., Manchanda, A., Sharma, A., Shehnaz, Choudhry, A., Sajid, M., Khan, S. A., Khan, A., & Chaudhry, S. A. (2023). Adsorptive removal of Methylene blue using fruit waste activated carbon and its binary metal oxide nanocomposite. *Chemical Engineering Journal Advances*, *16*, 100571. https://doi.org/10.1016/J.CEJA.2023.100571

Zhang, Y., Lin, X., Hu, C., & Yun, H. (2023). Activated Carbon from Melamine-Impregnated Paper. *BioResources*, *18*(1), 1128–1140. https://doi.org/10.15376/BIORES.18.1.1128-1140

CHAPTER 2

Hydrogeochemical and Isotopic Assessment of the Süleymanli-Ilica Geothermal Waters: Origin, Quality, and Potentıal Uses

Yusuf Uras[1] & Selçuk Yenipınar[2] & Yağmur Uysal[3]

[1] Prof. Dr., Kahramanmaras Sutcu Imam University, Geological Engineering Department, Kahramanmaras, Turkey, ORCID: 0000-0001-5561-3275
[2] MSc., Kahramanmaras Sutcu Imam University, Geological Engineering Department, Kahramanmaras, Turkey
[3] Prof. Dr., Mersin University, Environmental Engineering Department, 33343, Mersin-Turkey. ORCID: 0000-0002-7217-8217,

1. INTRODUCTION

This study aims to investigate the thermal waters of the Süleymanlı-Ilıca region from a hydrogeochemical, isotopic geochemical, and medical geology perspective. The thermal waters in this region are fed by three different springs: Büyükşehir Belediye Hamamı (IJS-1), Özger Hotel (IJS-2), and Vali Saim Çotur Thermal Waters (IJS-3). The lithology of the region is structured in a way that allows for the formation of these water sources (Figure 1). The primary goal of this research is to examine the potential health effects of these thermal waters on local populations from the perspective of medical geology. In this context, the general geology, hydrogeology, isotopic geology, water chemistry, and medical geology of the region were studied. The study area is located approximately 70 km northwest of the city center of Kahramanmaraş, in the northern part of the Onikişubat District. From a medical geology perspective, it was found that the thermal waters in this area are influenced by both natural and anthropogenic sources, particularly in terms of sulfate and sulfur content. These sources have been shaped by contamination from artificial fertilizers and solid waste. The maximum permissible limit for sulfur in thermal waters is 10 mg/L. Previous studies have shown that elevated levels of sulfur and sulfate can lead to kidney diseases and allergic skin conditions. Excessive sulfur content, especially, can negatively affect individuals with asthma.

The study findings suggest that sulfur and sulfate may play a role in the emergence of these diseases. Sulfate enters groundwater primarily through minerals like gypsum and anhydrite. Sulfur compounds can cause significant environmental issues by affecting taste, odor, toxicity, and corrosion through various chemical reactions. Sodium sulfate and magnesium sulfate are particularly limited to a concentration of 250 mg/L due to their laxative effects on humans (Varol et al., 2008).

Hydrogeology is the scientific discipline that studies the formation, distribution, and movement of water beneath the Earth's surface. Subsurface hydrogeology examines the properties of groundwater within the porous features of geological formations. Water is an indispensable resource for all living organisms, and life cannot exist without it. Although approximately one-third of the Earth's surface is covered by water, only about 0.74% of it is drinkable (Akın and Akın, 2007). In the hydrological cycle, groundwater, after moving through various substrates, absorbs surrounding materials. The type and quantity of these materials can change depending on numerous independent factors. Groundwater characteristics are influenced by climate conditions and the water potential of the region. Additionally, isotopic compositions of groundwater provide valuable

information to determine the origin, age, recharge area, and interactions between groundwater and rock formations (Clark and Fritz, 1997).

This study aims to assess the usability of the thermal waters in the Süleymanlı-Ilıca region and examine their potential health effects from a medical geology perspective, with a focus on environmental isotope effects.

Figure 1: General View of the Research Area (Süleymanlı-Ilıca)

1.1. Location and Accessibility

The study area is located approximately 70 km northwest of the city center of Kahramanmaraş, in the northern part of Onikişubat District. A map indicating the location of the study area is presented below (Figure 2). The northern part of the region is surrounded by high mountains, creating a basin-like topography with various elevations. The region experiences a transition between the Mediterranean and continental climates.

The region's morphology is characterized by nearly horizontal plateaus, steep slopes, and shallow valleys. Major mountains in the area include Bezirgan Dağı, Hanın Gediği, Ağa Dağı, Değirmenci Ali Tepesi, Atlık Dağı, and Karagedik Tepeleri. The main rivers in the region are the Ceyhan River and the Zeytin and Ilıca Streams, which flow continuously throughout the year. The region consists of large fertile plains and sparse pine forests. The people living in the mountainous villages primarily engage in forestry, livestock, and agriculture. In the plains and alluvial areas, viticulture, grain farming, and livestock breeding are the main activities. The region is well accessible by paved roads.

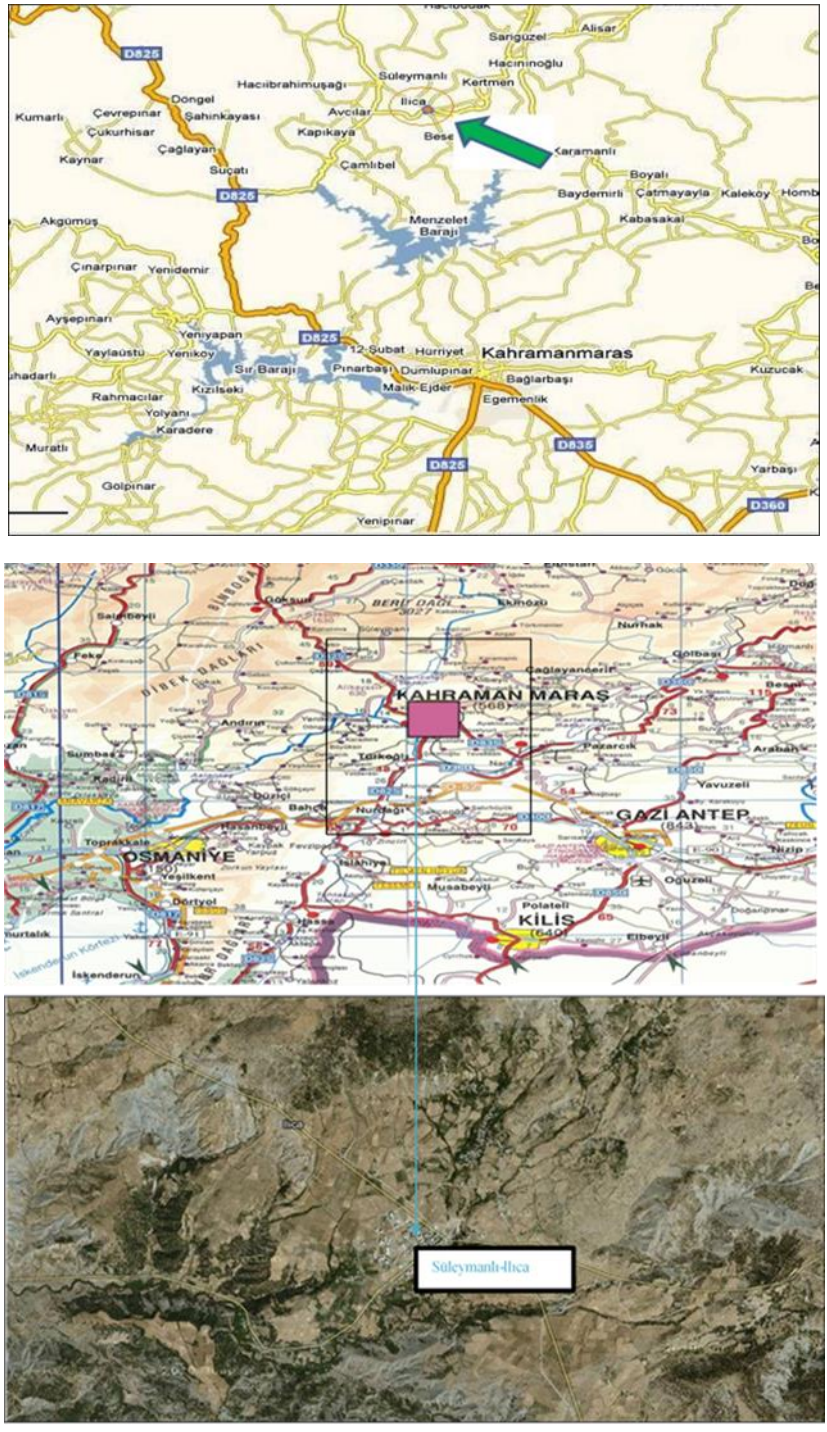

Figure 2: Location Map of the Investigated Area

1.2. Hydrogeochemical Studies Conducted in the Study Area

Hydrogeochemical studies conducted in and around the study area provide a valuable foundation for understanding the chemical properties of water sources and the factors influencing water quality. Hatipoğlu (2004) examined the hydrogeochemistry of the Mersin-Tarsus coastal aquifer, investigating the properties of the alluvial aquifer and the slope aquifer dominated by sedimentary rocks, analyzing the mechanisms shaping groundwater chemistry in the region. Başkan (1970), through research by the MTA Institute, mapped the geological structure and chemical components of the region's water sources, offering fundamental insights into the hydrogeochemical characteristics of the area. Arpacık (2014) focused on the Hopur mineral water source near the Kahramanmaraş Şerefoğlu village, analyzing the chemical composition of the water and providing insight into the region's groundwater properties. Güven (2015) evaluated the physicochemical properties of hot, cold, and mineral springs in the Kahramanmaraş Ilıca region, examining their chemical composition, usage potential, and hydrogeochemical characteristics. Lastly, Dalyan (2017) analyzed the hydrogeology of mineral waters in the Kahramanmaraş Büyükkızılcık region, assessing water quality by examining nitrate, nitrite, and fluoride content. Together, these studies offer a comprehensive understanding of the hydrogeochemical processes in the region and provide valuable context for the current research.

2. MATERIALS AND METHODS

2.1. Materials

Hot water samples were collected from the Suleymanli-Ilica area springs at regular intervals over a one-year period. The samples were initially measured on-site, followed by additional laboratory analyses. Based on these analyses, tables, graphs, and maps were created to represent the data. The geological, geochemical, isotopic geochemistry, and hydrochemical characteristics of the hot springs from the study area were examined to determine the origins and properties of the waters. Detailed analyses were conducted, and all data were evaluated collectively. The chemical analyses also provided insights into the potential usability of the geothermal water sources.

2.2. Methodology

To assess the usability of the hot water springs in the Suleymanli-Ilica area, samples were collected from locations over different months throughout the year. The samples, labeled as IJS-1 (Municipal Bathhouse), IJS-2 (Özger Hotel), and

IJS-3 (Governor Saim Çotur Thermal Baths) were collected using 500 mL and 1000 mL polypropylene containers. These containers were rinsed with natural water at each sampling site to prevent contamination from foreign substances. Heavy metal and anion-cation analyses were conducted using ICP-OES, ICP-MS, and Ion Chromatography (IC) at ACME Analytical Laboratories in Canada. On-site measurements were taken for parameters such as pH, dissolved oxygen (DO), conductivity (EC), and temperature. Additional samples for further analyses were transported to the laboratory and stored at +4°C in a refrigerator. Over the course of one year, a total of 60 water samples were collected from three different sources, with pH measurements taken using a pH meter.

Water samples from the three sources (IJS-1, IJS-2, and IJS-3) were also analyzed at the DSİ TAKK Department Isotope Laboratory using Tritium (^{3}H) and IRMS methods, following IAEA experimental standards. Oxygen-18 (^{18}O) and Deuterium (^{2}H) isotopes were used to determine the origins of the waters, assess rock-fluid interactions, identify boiling-evaporation processes caused by sudden pressure drops underground, investigate the mixing of waters from different aquifers and/or sources, and gather general information about the age of the groundwater.

3. RESULTS and DISCUSSIONS

3.1. Geology of the Study Area

The study area lies within the 1/25,000 scale Kahramanmaraş M37-b4 map sheet. The thermal water sources are found within the Kilisecik Formation, which consists of alternating layers of sandstone and marl intercalated with marly units, dating from the Middle to Upper Miocene. The lithological characteristics of this formation provide the ideal conditions for the development of these water sources. The region features various lithostratigraphic units ranging from Triassic to Quaternary. These units are examined individually, with their chronology arranged from older to younger formations. Figures 3 presents the geological map and cross-section of the study area, highlighting the location of the thermal water sources in Süleymanlı-Ilıca region.

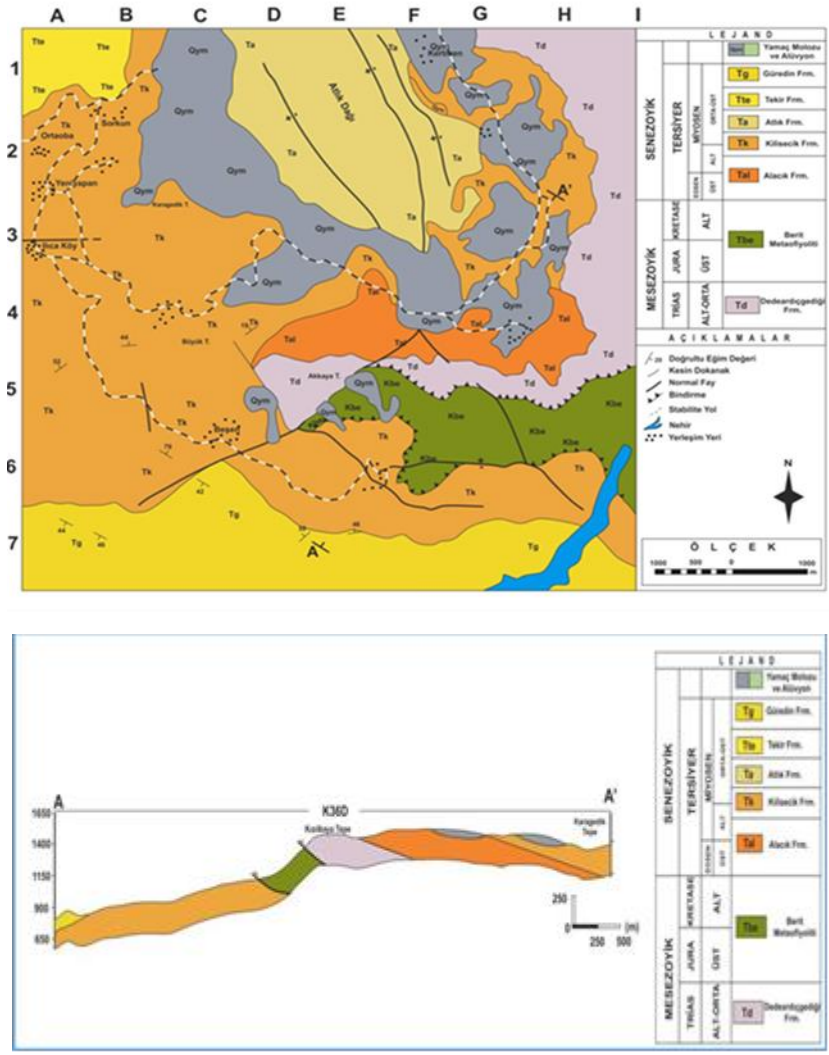

Figure 3: Geological map of the study area (Varol et al. 2012)

3.1.1. Dedeardıçgediği Formation (Td)

This formation, first described by Baydar et al. (1996), is found in the northeastern part of the study area and is predominantly composed of limestone, dolomite, and recrystallized dolomites. The limestones are characterized by beige weathered surfaces, and the dolomites are dark gray when weathered and black when fresh. This unit exhibits a massive, fractured, and durable appearance. Baydar et al. (1996) initially assigned it an age range from Late Permian to Middle Triassic, while Varol et al. (2012) suggested a Triassic age based on regional rock and fossil assemblages. This formation is tectonically overlaid by

the Berit metaophiolite and unconformably overlain by the Kilisecik Formation near Elsen village.

3.1.2. Berit Metaophiolite (Tbe)

The Berit Metaophiolite, first described in Berit Mountain, consists of sedimentary and metamorphic lithologies. It includes peridotites, gabbro, diabase, and schists. Previous studies, including those by Varol et al. (2012), suggested ages of Late Jurassic–Early Cretaceous and Late Cretaceous. The Berit Metaophiolite underlies the Dedeardıçgediği Formation and is itself tectonically overlaid by the Dedeardıçgediği Formation.

3.1.3. Alacık Formation (Tal)

First described by Erdoğan (1975), this Late Eocene formation is characterized by clastic deposits, including fine-to-medium-grained conglomerates and sandstones, along with claystones. The conglomerates are primarily composed of dolomite, radiolarite, and limestone, with angular particles. The sandstones are also angular and coarse-grained, derived mainly from ophiolite and dolomite. The Alacık Formation is unconformably overlain by the Kilisecik Formation.

3.1.4. Kilisecik Formation (Tk)

First described by Gül (2000), this formation consists primarily of alternating layers of shale, marl, and sandstone. The shales are yellowish-green when weathered, while the marls are light to dark green and the sandstones are reddish-yellow with a light green fractured surface. This formation, which forms the aquifer for the thermal springs in the study area, unconformably overlies the Alacık Formation and is conformably overlain by the Tekir Formation in certain regions (Figure 4).

3.1.5. Atlık Formation (Ta)

The Atlık Formation, first named by Varol et al. (2012), consists of limestone with abundant algal and coral fossils, typical of reefal limestone. It overlies the Kilisecik Formation and is conformably overlain by the Tekir Formation. The Atlık Formation is assigned an Early to Middle Miocene age.

3.1.6. Tekir Formation (Tte)

Described by Gül (2000), the Tekir Formation is characterized by well-rounded particles of limestone and dolomite, varying in grain size. It is positioned above the Atlık Limestone and is dated to the Middle to Late Miocene.

Figure 4: Field view of the Kilisecik Formation

3.1.7. Güredin Formation (Tg)

The Güredin Formation, identified by Gül (2000), consists of rubble deposits and sandy conglomerates, with alternating layers of sandstone and claystone. This formation is dated to the Middle to Late Miocene.

3.1.8. Alluvium

The alluvium in the study area consists of unconsolidated gravel, blocks, sand, silt, clay, and marl, typically found in river valleys and floodplains. These layers' exhibit both lateral and vertical transitions.

3.2. Hydrogeological Conditions of the Study Area

The hydrogeological conditions of the study area are influenced by its diverse river systems, geological formations, and the hydrogeological properties of the rocks present. Several rivers, including the Ceyhan River, Zeytindere, and Ilıca Stream, flow continuously through the region, with potential flooding in the winter months. These rivers contribute to the local hydrology and are important in the movement and recharge of groundwater in the area.

The groundwater in the study area is primarily hosted within a combination of Mesozoic limestone and Miocene sediments, with these rock units forming aquifers that are capable of sustaining water flow throughout the year. The Lower and Upper Miocene conglomerates exhibit aquifer properties, particularly where they contact shales, with springs often observed along these contacts, especially in summer. Sandstone layers between shales in the Lower and Upper Miocene also serve as aquifers but typically yield water at lower discharge rates. On the other hand, the Middle Miocene limestones are considered high-quality aquifers, although their discharge volumes are typically higher after significant rainfall due to their elevated locations. Some areas, like the springs beneath Atlık Mountain, discharge water consistently throughout the summer months, a vital water source for the local population. High-volume groundwater discharge is also observed at the contact zones between Middle Miocene limestones and marls, where both normal and karstic springs form. These spring areas are vital to the water supply, as they provide consistent flow even in the hotter months, ensuring a stable water supply for the region.

The geological diversity of Kahramanmaraş province, located at the convergence of the Mediterranean, Eastern Anatolia, and Southeastern Anatolia regions, results in a varied hydrogeological structure. The climate in the region is predominantly Mediterranean, with hot summers and mild winters, although the northern parts experience more continental climate characteristics due to higher elevations. The area's climate and precipitation patterns significantly influence groundwater recharge and the overall water cycle. The average annual precipitation is 717.9 mm, with the temperature averaging 16.5°C between 1929 and 2016, peaking at 28°C during the hottest month (Figure 5).

The lithological characteristics of the Süleymanlı-Ilıca area, with its fractured limestone, sandstone, and shale formations, play a crucial role in the area's permeability. These rocks enable the infiltration and storage of water within aquifers, ensuring groundwater availability. The geothermal sources in the region, including IJS-1 (Municipal Bathhouse), IJS-2 (Özger Hotel), and IJS-3 (Governor Saim Çotur Thermal Baths), are located in areas with high permeability and are important contributors to the local geothermal system, as shown in Figure 6. The high permeability of these formations and their ability to store groundwater contribute to the overall quality of the aquifers in the region, making it a valuable resource for both domestic and industrial use.

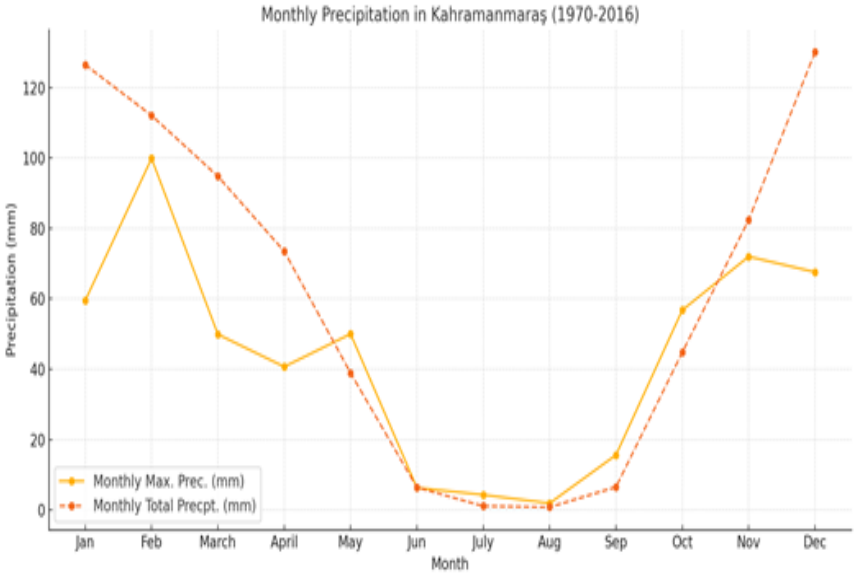

Figure 5: Monthly maximum and total precipitation average change for many years in Kahramanmaraş province and its surroundings, including the region including Süleymanlı location (TSMS, 2017)

IJS-1 (Municipal Bathhouse) Source

IJS-2 (Özger Hotel) Source

IJS-3 (Governor Saim Çotur Thermal Baths) Source

Figure 7: Thermal Soruces of Süleymanlı-Ilıca

3.3. Hydrogeochemistry

The hydrogeochemistry of the hot water sources in the Süleymanlı-Ilıca area was assessed by analyzing several physical and chemical parameters, including temperature, pH, conductivity, alkalinity, trace elements, and ion concentrations over multiple periods (Table 1). The temperature of the hot water sources ranged from 44°C to 47°C at all three sites, categorizing them as "hot water" sources. These temperatures remained consistent across different measurement periods, further confirming the thermal nature of the waters.

The dissolved oxygen (DO) levels in the hot water sources were found to be similar across all three sites, suggesting that the waters have comparable oxygen content, despite being warm. The sodium ion (Na^+) concentrations ranged from 15.49 to 29.12 ppm, which is well below the maximum permissible limit of 200 mg/L for hot waters according to WHO (2017) standards. This indicates that the thermal waters of the region have relatively low salinity. Additionally, the conductivity values, which ranged between 646-679 µS/cm, are also indicative of low ion content and low salinity, further confirming the mild nature of these waters in terms of dissolved salts. The heavy metal content in these hot water sources is also found to be low, suggesting that the thermal waters are relatively free from contamination by potentially harmful metals. This is an important factor in determining the suitability of these waters for therapeutic and recreational purposes.

The U.S. salinity diagram was employed to assess the suitability of these water sources for irrigation. The diagram plots electrical conductivity (EC) on the horizontal axis and the sodium adsorption ratio (SAR) on the vertical axis. These parameters are used to determine the irrigation water class. According to the Wilcox diagram (1955), the hot water sources in the Süleymanlı-Ilıca area are classified as follows (Figure 7):

- IJS-1 falls under the C2-S3 class, indicating it is suitable for irrigation with moderate salinity and sodium content.
- IJS-2 and IJS-3 fall under the C2-S4 class, indicating that they have higher sodium content, but they are still suitable for irrigation in soils that are not highly sensitive to sodium levels.

These classifications indicate that while the waters in the region are generally of good quality, their suitability for irrigation varies, with IJS-1 being more versatile compared to IJS-2 and IJS-3, which may be more suitable for crops that are less sensitive to sodium. The overall chemical quality of the waters suggests their use in both geothermal and agricultural applications, with the added benefit of being low in heavy metals and salinity (Figure 8).

Table 1. Geochemistry of the drinking water sources in the Süleymanlı-Ilıca Region

Geochemical Parameters	IJS-1	IJS-2	IJS-3
Temperature (^{0}C)	44.73±1.24	45.85±1.43	47.49±2.27
pH	8.18±0.06	7.98±0.16	8.41±0.11
EC (µS/cm)	679.8±50.95	650.5±23.78	646.67±21.73
DO (ppm)	6.74±1.03	7.28±0.73	7.24±0.84
Na^+ (ppm)	15.49±5.26	29.12±1.80	26.17±6.38
K^+ (ppm)	1.98±0.50	2.35±0.68	2.41±1.12
Ca^{+2} (ppm)	44.50±8.03	44.85±3.76	39.80±4.18
Mg^{+2} (ppm)	18.84±5.04	21.93±1.92	22.51±1.69
Cl^- (ppm)	10.86±0.48	13.01±1.57	9.80±2.58
HCO_3^- (ppm)	224.71±53.23	258.29±23.03	218.09±67.54
SO_4^{-2} (ppm)	21.46±0.75	15.54±2.06	27.57±7.62
NO_3^- (ppm)	2.79±0.98	2.68±0.67	2.21±0.28
F^{-1} (ppm)	0.56±0.07	0.64±0.15	0.60±0.07
Al (ppb)	1.00±0.09	2.00±0.13	1.00±0.12
Total Cr (ppb)	12.70±1.18	14.70±1.36	1.7±0.93
Cu (ppb)	0.4±0.02	0.3±0.01	0.2±0.05
Mn (ppb)	0.15±0.05	0.14±0.02	0.01±0.00
Ni (ppb)	<0.20	<0.2	<0.2
Si (ppm)	14.29±1.08	2.98±0.32	14.06±0.78
Pb (ppb)	21.9±1.45	11.0±1.40	0.5±0.01
Zn (ppb)	<0.02	<0.02	<0.02

EC: Electrical conductivity, DO: dissolved oxygen

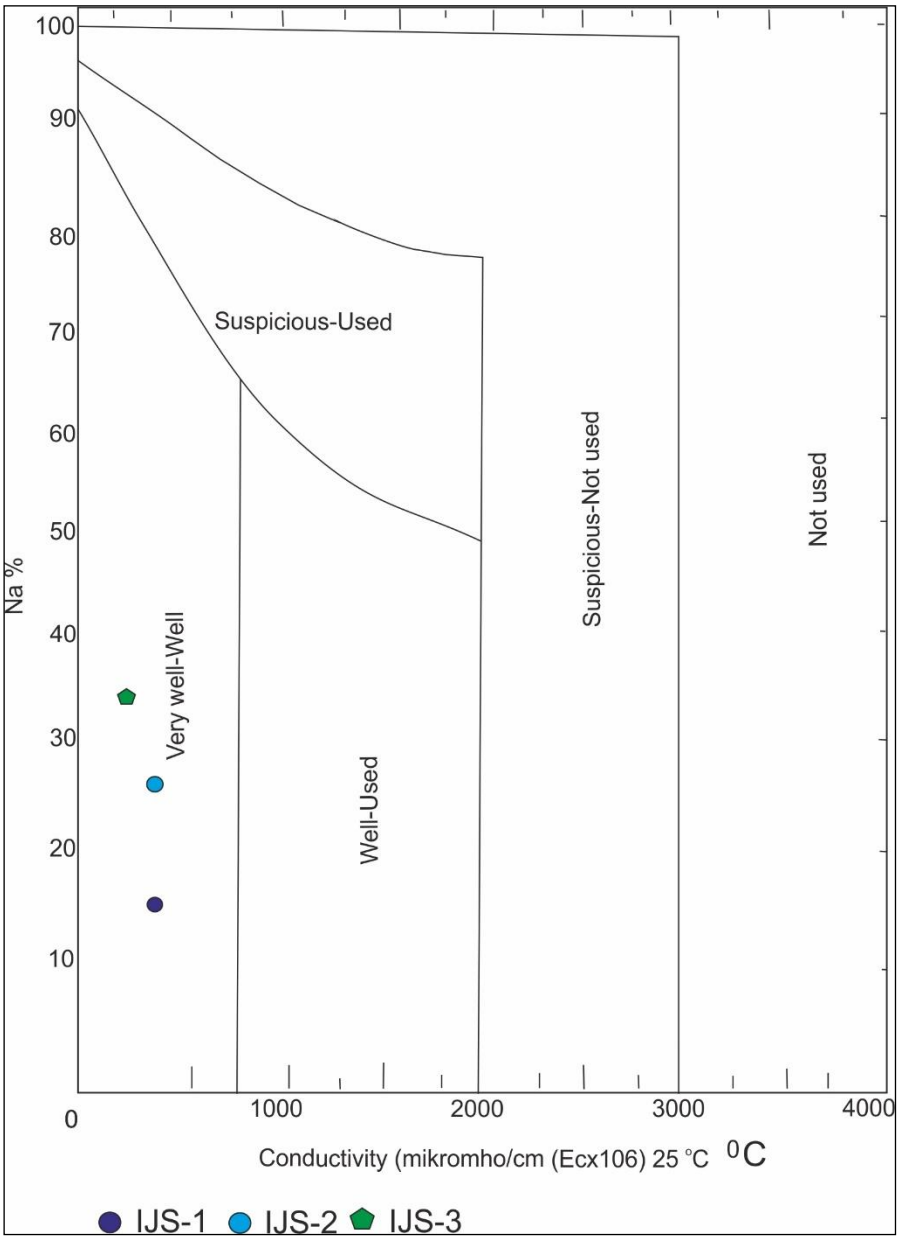

Figure 7: Wilcox Diagram of Hot Water Springs in Suleymanli-Ilıca Area

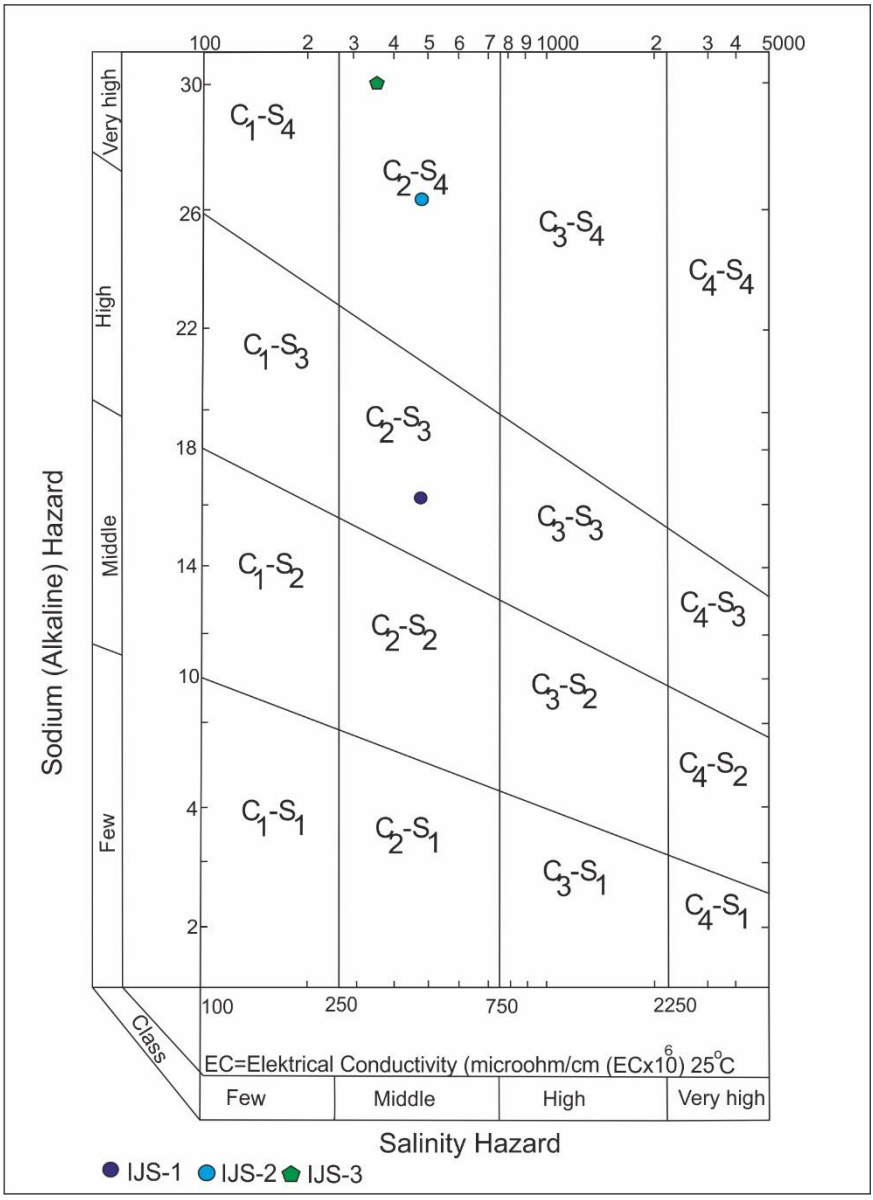

Figure 8: USA Salinity Laboratory Diagram of Hot Water Springs in Süleymanlı-Ilıca Area

The hydrochemical characteristics of the hot springs in the Süleymanlı-Ilıca area were investigated based on anion-cation analysis, with the results presented in Table 2 and illustrated through Piper and Schoeller diagrams. The Piper diagram indicates that the water sources (IJS-1, IJS-2, and IJS-3) contain significant amounts of $CaCO_3$ and $MgCO_3$, suggesting the presence of permanent

hardness components such as $CaSO_4$ and $MgSO_4$, which account for more than 50% of the water hardness. The waters in this region fall into Region 5 of the Piper diagram (Piper, 1944) (Figure 9), representing waters with predominantly calcium and magnesium salts.

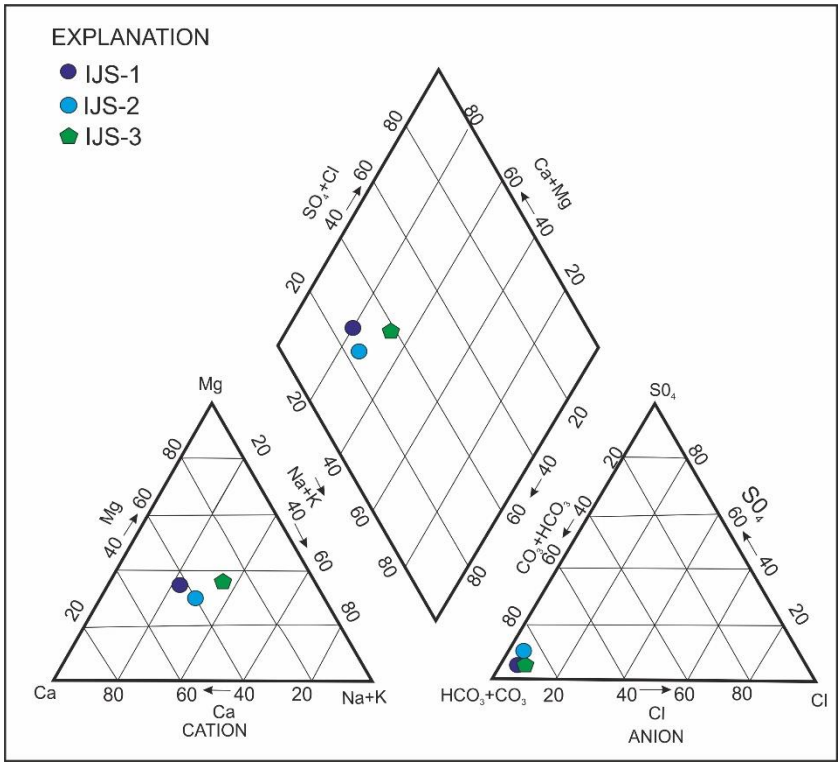

Figure 9. The Piper Diagram Illustrates the Composition of Drinking Water Sources in The Döngele Region

In terms of cation composition, IJS-1 showed the order Ca > Mg > Na+K, IJS-2 as Ca > Na+K > Mg, and IJS-3 as Na+K > Ca > Mg. For anions, all three sources followed a consistent order of HCO_3 > SO_4 > Cl, indicating that bicarbonate ions are the dominant anion in these waters. The Schoeller diagram (Scholler, 1967) reveals that the water sources are categorized as waters with carbonate hardness above 50%, characterized by ions such as $CaSO_4$, $MgSO_4$, $CaCl_2$, and $MgCl_2$ (Figure 10). Based on sulfate concentrations, the waters are classified as Sulfated and Oligosulfated, with sulfate levels ranging from 6-24 mEq/L for the former and 24-58 mEq/L for the latter.

The results from the Schoeller diagram and Piper diagram point to a common aquifer feeding all three hot spring sources. These diagrams,

along with the isotopic analysis, provide insights into the chemical properties and origin of the waters. The isotopes, including tritium (^{3}H), oxygen-18 (^{18}O), and deuterium (^{2}H), were analyzed to explore the interaction between groundwater and the surrounding geology in the region.

Table 2. The anion–cation ranking of drinking water sources of Süleymanlı-Ilıca

Sample	Cation Ranking	Anion Ranking
IJS-1	$Ca^{2+}>Mg^{2+}>Na^{+}+K^{+}$	$HCO_3^{-}> SO_4^{-2}>Cl$
IJS -2	$Ca^{2+}>Na^{+}+K^{+}>Mg^{2+}$	$HCO_3^{-}> SO_4^{-2}>Cl^{-}$
IJS-3	$Na^{+}+K^{+}>Ca^{2+}>Mg^{2+}$	$HCO_3^{-}> SO_4^{-2}>Cl^{-}$

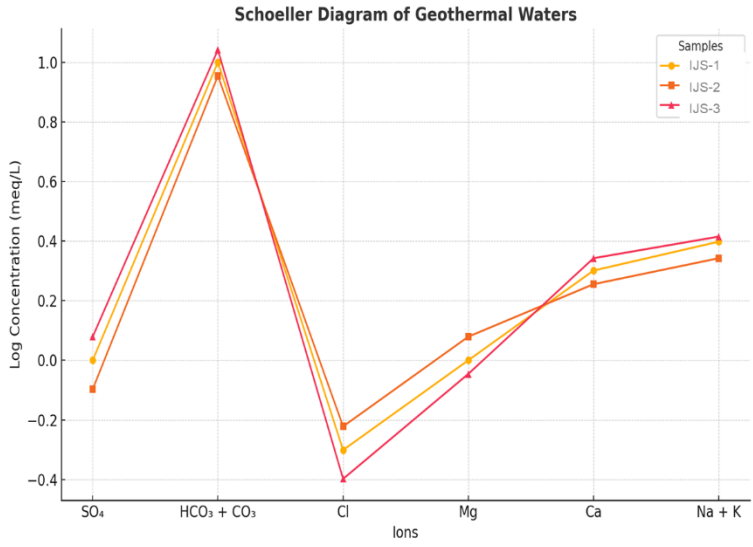

Figure 10: Schoeller diagram of Süleymanlı-Ilıca water sources

Environmental isotopes, including tritium (^{3}H), oxygen-18 (^{18}O), and deuterium (^{2}H), were utilized in this study to gain insights into the aquifer characteristics and the interaction between water and rock in the Süleymanlı-Ilıca groundwater resources. The isotopic analysis conducted on water samples collected seasonally over dry and rainy periods shows the following isotope values:

- For IJS-1 (Büyükşehir Municipality Bathhouse): $\delta^{18}O$ ranged from -9.61 (dry) to -9.58 (rainy), $\delta^{2}H$ ranged from -57.16 (dry) to -56.18 (rainy), and ^{3}H ranged from 0.61 (dry) to 0.93 (rainy).

- For IJS-2 (Özger Hotel): $\delta^{18}O$ values ranged from -9.66 (dry) to -9.73 (rainy), $\delta^{2}H$ from -57.35 (dry) to -56.94 (rainy), and ^{3}H from 0.56 (dry) to 0.59 (rainy).

- For IJS-3 (Vali Saim Çotur Bathhouse): $\delta^{18}O$ values from -9.56 (dry) to -9.57 (rainy), $\delta^{2}H$ from -56.52 (dry) to -56.17 (rainy), and ^{3}H values from 0.79 (dry) to 0.85 (rainy).

These isotopic values indicate that the water sources fall between the Global Meteoric Water Line (GMWL) and the Mediterranean Water Line (MWL) (Figure 11), suggesting that the water is primarily recharged by meteoric precipitation. The comparison of the isotopic data with these lines also shows that the waters have minimal evaporation effects before entering the aquifer.

The presence of deuterium excess (d-excess) values (calculated using the formula: $d = \delta^{2}H - 8*\delta^{18}O$) helps identify regions where continental rather than marine sediments dominate. The d-excess values for the hot water sources in this area range from 19.72 to 20.46, with the lowest recorded at IJS-1. This suggests that the region is influenced by continental-type precipitation, which is typical for the area's geological formation.

The tritium analysis revealed values ranging from 0.56 to 0.93 in the hot springs, with IJS-1 showing the lowest tritium value and thus the shortest water residence time in the aquifer, followed by IJS-2 and IJS-3 with longer residence times. The presence of tritium in these waters points to young groundwater with relatively short transit times, particularly in IJS-1, which has the shortest contact time with the aquifer.

The chloride-tritium diagram further supports the interpretation of young groundwater with short transit times, as evidenced by high tritium and low chloride concentrations in the waters. However, the Deuterium-Tritium relationship suggests that IJS-3 has slightly deeper circulation compared to the other two sources (Figure 11).

The lithological conditions of the region, including the presence of shale, marl, sandstone, and limestone layers, support the groundwater's deep circulation and its relatively young age, as suggested by the isotopic data. These findings indicate

that the chemical composition of the waters and their origin are closely linked to the geological features of the Süleymanlı-Ilıca area.

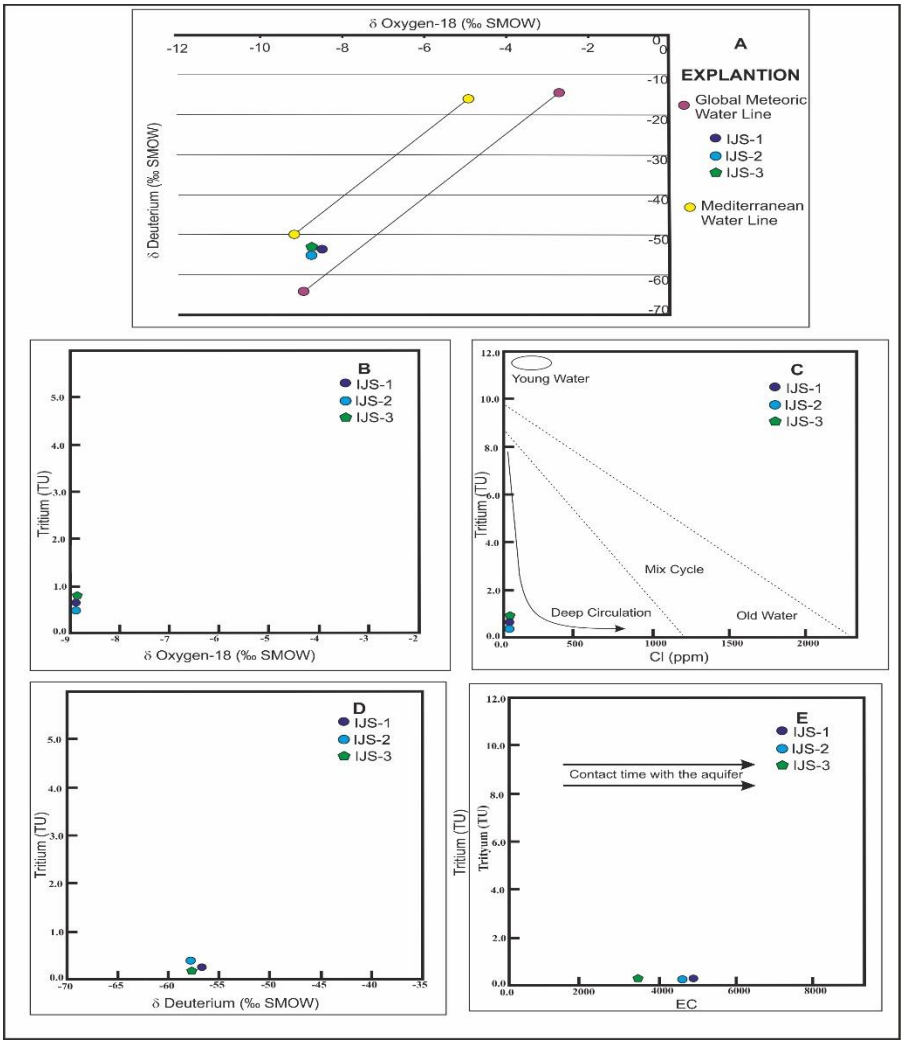

Figure 11: The Relationship Between Isotopes of Drinking Water Sources of Süleymanlı-Ilıca (a) $\delta^{18}O$-^{3}H; TU relationship, b) Cl-TU relationship, c) (δ2H)–TU relationship, d) (EC; µS/cm)–TU) relationship

CONCLUSION

The geothermal waters of Süleymanlı-Ilıca, sourced from the Kilisecik Formation, exhibit distinct geochemical and isotopic signatures that indicate their meteoric origin and young groundwater age. The Schoeller and Piper diagrams confirm their classification as sulfate and hyper-carbonated waters, with significant non-carbonate hardness. The presence of calcium, sulfate, and chloride in high concentrations aligns with $CaSO_4$, $MgSO_4$, and $CaCl_2$ water types, contributing to their unique hydrochemical profile.

The Wilcox and US Salinity Laboratory diagrams categorize IJS-1 as "C2-S3" (moderate salinity, high sodium) and IJS-2 and IJS-3 as "C2-S4" (moderate salinity, very high sodium), indicating variations in their suitability for agricultural use. Additionally, the isotopic analysis (^3H, $\delta^{18}O$, and δ^2H) confirms that these waters have undergone minimal evaporation before entering the aquifer, further supporting their meteoric recharge classification.

Medical geology evaluations suggest that the waters' mineral content has potential therapeutic applications, particularly in dermatology and musculoskeletal treatments. However, the elevated sulfate levels warrant caution for individuals with asthma and kidney-related conditions. While the waters comply with nitrate and sulfate safety standards, continuous monitoring is recommended to ensure their long-term usability for human consumption and balneotherapy.

Overall, this study provides a comprehensive hydrogeochemical and isotopic assessment of the Süleymanlı-Ilıca geothermal waters, offering valuable insights for their sustainable management and potential health benefits.

REFERENCES

Akın, M., and Akın, G. (2007). Suyun Önemi, Türkiye'de Su Potansiyeli, Su Havzaları ve Su Kirliliği. Ankara Üniversitesi Dil ve Tarih-Coğrafya Fakültesi Dergisi, 47(2), 105- 118.

Arpacık, F. (2014). Hopur içmesi (Kahramanmaraş) mineralli su kaynağının hidrojeokimyasal özellikleri. Yüksek Lisans Tezi, Kahramanmaraş Sütçü İmam Üniversitesi, Fen Bilimleri Enstitüsü, Kahramanmaraş. 83s.

Başkan, E. (1970). Mersin Güney yolu Kaplıca ve İçmesi Hidrojeoloji Etüdü, Ankara, MTA Rapor No: 4370.

Baydar, O., and Yergök A.F. (1996). Güneydogu Anadolu-Kenar Kıvrım Kuşağı-Amanos Dağları Kuzeyi ve Dogu Torosların Jeolojisi. Jeoloji Etütleri Dairesi, 90 pp, Ankara.

Clark, I., and Fritz, P. (1997). Environmental Isotopes in Hydrogeology. CRC Press, New York, 328 p.

Dalyan, V. (2017). Büyükkızılcık (Göksun-K.Maraş)ve Çevresindeki Mineralli Su Kaynaklarının Çevresel İzotop Özellikleri. Yüksek Lisans Tezi, Kahramanmaraş Sütçü İmam Üniversitesi, Fen Bilimleri Enstitüsü, Kahramanmaraş, 71s.

Erdoğan, T. (1975). VI. Bölge Gölbaşı Dolayının Jeolojisi, TPAO, Ankara, Rapor No: 929.

Gleıck, P.H. (1996). Water resources. In Encyclopedia of Climate and Weather, ed. By S.H. Schneider, Oxford University Pres, New York, 2:.817-823

Gül, M.A. (2000). Kahramanmaraş Yöresinin Jeolojisi. Doktora tezi, Hacettepe Üniversitesi, Fen Bilimleri Enstitüsü, Ankara, 304s,

Güven, H. (2015). Ilıca Kaplıcası (Kahramanmaraş) sıcak ve mineralli sularının hidrokimyasal özellikleri. Selçuk Üniversitesi, Yüksek Lisans Tezi, Fen Bilimleri Enstitüsü, Konya, 114s.

Hatipoğlu, Z. (2004). Mersin–Tarsus kıyı akiferinin hidrojeokimyası, Doktora Tezi, Hacettepe Üniversitesi Fen Bilimleri Enstitüsü, Ankara, 142s.

Piper A.M. (1944). A graphic procedure in geochemical interpretation of water analyses. Transactions. American Geophysical Union, 25:914–923. https://doi.org/10.1029/TR025i006p00914

Schoeller, H. (1967). Geochemistry of groundwater. An international guide for research and practice. UNESCO, 1967, chap 15, pp 1-18.

TSMS, Turkish State Meteorological Service, (2017). Available at: www.dmi. gov.tr

Varol, L., Kop, A., Darbaş, G. (2012). Koçlar-Sarıgüzel (Kahramanmaraş Kuzeyi) Arasında Kalan Bölgenin Jeolojik Özellikleri, Doğu Toroslar. Kahramanmaraş Sütçü İmam Üniversitesi Mühendislik Bilimleri Dergisi, 15(1):43-56.

Varol, S., Davraz, A., Varol, E. (2008). Yeraltı suyu Kimyası ve Sağlığa Etkisinin Tıbbi Jeoloji Açısından Değerlendirilmesi. TAF Prev Med Bull, 7(4):351-356

Wilcox, L.V. (1955). Classification and use of irrigation water. US Department of Agriculture, Circular 969, Washington DC.

World Health Organization (2017). Guidelines for Drinking-Water Quality: Fourth Edition Incorporating the First Addendum, Geneva. https://www.ncbi.nlm.nih.gov/books/NBK442373

CHAPTER 3

Supplier Selection in an Electric Distribution Company Using the Analytic Hierarchy Process

Nimet Karabacak[1] & Yunus Emre Demir[2] & Doğukan Abeş[3] & Yıldıray Saklıca[4] & Dilara Sönmez[5]

[1] Asst. Prof. Department of Industrial Engineering, Faculty of Engineering and Architecture, Istanbul Nişantaşı University, ORCID: 0000-0003-3361-1265
[2] B.Eng.Std., Department of Industrial Engineering, Faculty of Engineering and Architecture, Istanbul Nişantaşı University
[3] B.Eng.Std. Department of Industrial Engineering, Faculty of Engineering and Architecture, Istanbul Nişantaşı University
[4] B.Eng.Std. Department of Industrial Engineering, Faculty of Engineering and Architecture, Istanbul Nişantaşı University
[5] B.Eng.Std. Department of Industrial Engineering, Faculty of Engineering and Architecture, Istanbul Nişantaşı University

1. Introduction

In the dynamic and competitive landscape of the electricity distribution industry, selecting the right suppliers is crucial for ensuring operational efficiency, cost-effectiveness, and high service quality. Supplier selection, however, is a complex and multifaceted decision-making process that requires careful consideration of various criteria such as cost, reliability, technical capabilities, and sustainability. Traditional methods of supplier selection often fail to capture the full range of these interrelated factors. This is where the Analytic Hierarchy Process (AHP) is used a powerful decision-making tool that simplifies complex problems by structuring them into a multi-level framework, allowing decision-makers to evaluate and compare alternatives based on a set of well-defined criteria. This research explores the application of the AHP method to supplier selection in an electricity distribution company. By using AHP, companies can systematically prioritize criteria, assess multiple suppliers, and make more informed, transparent, and objective decisions.

The aim of this study is to demonstrate how AHP can enhance the supplier selection process by offering a structured approach to managing the inherent complexities of this decision. Through this exploration, the research will provide insights into the potential benefits of AHP in improving supplier selection outcomes in the energy sector. The electricity distribution sector plays a pivotal role in ensuring the continuous and efficient delivery of power to consumers. One of the key challenges faced by companies in this sector is the selection of reliable suppliers that can meet both operational and strategic needs, all while optimizing costs and ensuring service quality. Given the increasing complexity of supply chains, influenced by factors such as technological advancements, regulatory changes, and the need for sustainability, traditional supplier selection methods often fall short in addressing the multi-dimensional nature of the decision-making process. In response to these challenges, AHP has emerged as a valuable tool for making informed, objective, and systematic supplier selection decisions.

AHP is a structured decision-making methodology that decomposes complex problems into smaller, manageable components, allowing decision-makers to evaluate multiple alternatives across various criteria in a hierarchical manner. This approach enables companies to weigh both quantitative and qualitative factors, ensuring a balanced assessment of suppliers. This article aims to explore the application of AHP in the context of supplier selection within an electricity distribution company, providing both theoretical insights and practical implications for industry practitioners. The rationale behind this research stems from the need for a more rigorous, transparent, and scientifically grounded

approach to supplier selection in a rapidly evolving industry. By incorporating AHP into the decision-making process, electricity distribution companies can improve the accuracy and reliability of their supplier choices, ultimately contributing to enhanced operational performance. This article concludes by offering recommendations for future research and practical strategies for implementing AHP in supplier selection processes within the energy sector. Through this research, the article aims to highlight the effectiveness of AHP as a decision-making tool in improving supplier selection outcomes, while also contributing to the broader discourse on best practices within the electricity distribution industry.

2. Background

Supplier selection is a critical determinant of operational efficiency and long-term sustainability in electricity distribution companies. The procurement of high-quality materials and services such as transformers, cables, and maintenance equipment directly influences the reliability, safety, and overall quality of electrical distribution networks. In this context, suppliers are not only tasked with delivering essential components but are also responsible for maintaining the consistency and reliability of the supply chain. Supplier reliability and service quality are, therefore, of paramount importance; any disruptions or inefficiencies in the supply chain can result in severe operational challenges, increased costs, and diminished customer satisfaction.

The highly regulated and competitive nature of the electricity distribution industry further complicates the supplier selection process, necessitating the consideration of a wide array of factors, including cost, quality, delivery timelines, adherence to safety standards, and environmental considerations. Inadequate supplier selection can expose companies to significant risks, such as operational delays, equipment failures, and potential legal liabilities. Thus, it is imperative for electricity distribution companies to adopt a structured and systematic approach to supplier selection. Such an approach not only enhances decision-making but also helps minimize risks, ultimately contributing to the improved performance and resilience of the electrical distribution network. In electricity distribution companies, supplier selection is a strategic and pivotal decision-making process that directly influences the company's operational performance. The key criteria to be considered in supplier selection encompass several dimensions, including cost analysis, reliability and performance, technical competence, legal and regulatory compliance, and financial evaluation. Cost analysis involves the assessment of unit electricity prices offered by the supplier, the long-term stability of these prices, and the total cost of procurement.

Reliability and performance criteria focus on the supplier's capacity to ensure uninterrupted power supply, the speed of fault repair, and the robustness of their technical infrastructure. Technical competence pertains to the supplier's ability to modernize the grid, implement advanced technological infrastructure, and integrate renewable energy sources into the distribution network. Legal and regulatory compliance involves evaluating the supplier's adherence to relevant regulations, possession of necessary licenses and permits, and conformity with environmental standards. Finally, financial evaluation encompasses an analysis of the supplier's financial performance, credit rating, and investment capacity, which are crucial indicators of long-term viability and stability. To ensure optimal decision-making, the supplier selection process should be conducted objectively, incorporating a comprehensive and systematic evaluation of these factors. This structured approach helps mitigate risks and enhances the overall performance and sustainability of the electricity distribution network. Over the years, several studies have explored the methodology and importance of supplier selection in the electricity distribution sector, highlighting various decision-making tools and criteria for evaluating suppliers. Saaty (1980) introduced AHP, a widely adopted decision-making method used to address complex supplier selection problems. AHP facilitates the prioritization of multiple criteria and alternatives by transforming subjective assessments into quantitative measures. Ho, Xu, and Dey (2010) explored various multi-criteria decision-making (MCDM) methods, including AHP, in supplier selection across different industries, including electricity distribution, emphasizing the significance of cost, quality, and delivery performance. Gencer and Gürpinar (2007) examined a hybrid decision-making model combining AHP with linear programming to assess suppliers in an electricity distribution company, focusing on criteria such as price, quality, and delivery reliability. Sahu and Das (2011) demonstrated the application of AHP in selecting suppliers for critical components in the electricity distribution sector, with a particular emphasis on cost, quality, and environmental impact. Chan and Kumar (2007) proposed a decision model for global supply chain supplier selection, highlighting the importance of quality, cost, and delivery time, factors which are equally critical in the electricity distribution industry. Pereira and Tavares (2009) suggested the application of fuzzy logic to manage uncertainty and subjectivity in evaluating supplier performance, especially in high-risk sectors such as electricity distribution. Kannan and Barani (2015) integrated AHP with the Technique for Order Preference by Similarity to Ideal Solution (TOPSIS) to evaluate multiple supplier selection criteria in a case study within the electricity distribution industry. Rao and Kumanan (2014) employed a hybrid model combining AHP and the Analytic Network Process (ANP) for supplier

selection in the electricity distribution sector, accounting for interdependencies between criteria and the capabilities of suppliers. Vaidya and Kumar (2006) reviewed the wide-ranging applications of AHP, specifically in supply chain management and supplier selection, particularly within the electricity sector.

Kukiełka and Czichowsky (2014) demonstrated the application of multi-criteria decision analysis (MCDA) techniques to evaluate supplier performance in power distribution companies, focusing on energy efficiency, compliance, and cost-effectiveness. Zhang and Sun (2012) integrated AHP with decision tree analysis to identify the most suitable suppliers for an electricity distribution company, taking reliability and risk factors into consideration. Güngör and Aydın (2007) discussed how electricity utility companies can enhance their supplier selection processes, particularly for infrastructure components such as cables and transformers. Hsu and Chiu (2010) examined how AHP can be utilized to evaluate and select suppliers in the power distribution sector, emphasizing product quality, pricing strategies, and vendor reliability. Tzeng and Huang (2011) provided a comprehensive review of AHP applications, particularly in industries such as electricity distribution, for supplier evaluation. Chien and Lin (2011) demonstrated the application of AHP for supplier evaluation in the electric utility industry, focusing on technical expertise, delivery performance, and financial stability. Kannan and Dev (2012) investigated how fuzzy AHP can incorporate environmental and sustainability considerations into supplier selection, which is particularly relevant for electricity distribution companies facing stringent environmental regulations. Ming and Hsieh (2010) highlighted the importance of selecting suppliers that adhere to regulatory standards and safety protocols, using AHP to quantify supplier performance. Koca and Topal (2013) presented a hybrid decision-making model integrating AHP with other techniques, such as cost-benefit analysis and risk assessment, for supplier selection in electric distribution companies. Wang and Yang (2013) combined AHP with a genetic algorithm to optimize supplier selection, considering the dynamic and complex nature of electricity distribution networks. Liu and Zhang (2012) evaluated the integration of sustainability criteria, such as environmental impact and carbon footprint, into supplier selection decisions using a multi-criteria decision-making approach in the electricity distribution sector. These studies illustrate the continued development and application of decision-making models, particularly AHP, to address the complexities of supplier selection in the electricity distribution sector, incorporating various criteria such as cost, quality, delivery performance, and sustainability.

3. Material and Method

The selection of suppliers is a complex and critical decision for electricity distribution companies, as it directly influences cost, quality, and operational efficiency. Traditional supplier selection methods often fail to adequately account for multiple, conflicting criteria. This research investigates the application of the AHP as a decision-making tool to systematically evaluate and rank potential suppliers, aiming to improve the supplier selection process in electricity distribution companies by incorporating a structured, multi-criteria approach that aligns with organizational goals. The application of the AHP to the supplier selection process in electricity distribution companies is significant for several reasons:

Complex Decision-Making: Supplier selection involves evaluating multiple factors, including cost, reliability, quality, and service. Traditional decision-making methods often struggle to handle the complexity and interdependencies of these criteria. AHP offers a structured, multi-criteria decision-making framework that enables decision-makers to systematically evaluate and rank suppliers based on both quantitative and qualitative factors.

Optimization of Supply Chain Operations: By utilizing AHP, electricity distribution companies can make more informed and rational supplier selection decisions. This can lead to cost savings, better quality of service, improved efficiency, and reduced operational risks, all of which are critical in maintaining reliable electricity distribution and minimizing service disruptions.

Strategic Alignment: Supplier selection is not only a tactical decision but also a strategic one that impacts long-term relationships with suppliers, compliance with regulatory standards, and sustainability goals. AHP's ability to incorporate diverse strategic and operational objectives makes it a valuable tool for aligning supplier selection with the company's broader goals.

Enhanced Transparency and Consistency: AHP helps ensure that the decision-making process is transparent and consistent. The model's hierarchical structure facilitates clear communication and documentation of the decision rationale, which can be valuable for accountability, audits, and justifying decisions to stakeholders.

The rapid transformations occurring in the modern business landscape have heightened the uncertainties faced by organizations, thereby complicating business management. Coupled with the increasing number of alternatives available for selection, decision-making processes have become increasingly

complex. In organizations with extensive decision-making processes, decision-making is not merely about gathering information but involves making informed choices using advanced decision-making techniques. These methods are inherently multi-purpose and operate in uncertain environments.

3.1. Multi-Criteria Decision Model

Many mathematical programming models rely on combining objective functions within the constraints set by the decision-maker. In numerous decision-making scenarios, multiple quantitative and qualitative criteria and objectives must be considered. When these criteria interact or conflict with one another, the situation is classified as a multi-criteria decision-making (MCDM) problem. The challenge lies in selecting the optimal alternative due to the inherent conflicts between the criteria that need to be optimized simultaneously. To address this issue, various methods have been developed to facilitate a compromise between the criteria and identify the most suitable alternative. The supplier selection problem, by its very nature, constitutes a multi-criteria decision-making problem because it requires decision-makers to evaluate suppliers based on multiple criteria. Linear weighting methods, in particular, are used to solve the supplier selection problem by assigning importance weights to the various criteria involved.

3.2. Analytical Hierarchy Process (AHP) in Supplier Selection

The Analytical Hierarchy Process (AHP) is a widely recognized multi-criteria decision-making method employed in the evaluation and selection of suppliers. One of the key distinguishing features of AHP is its ability to incorporate both qualitative and quantitative criteria into the decision-making process. In complex decision-making scenarios, AHP facilitates managerial decision-making by assigning relative importance values to both decision alternatives and criteria, thereby providing a structured approach to evaluating multiple factors (Timor, 2011). The application of AHP in supplier selection can be described in eight stages, as outlined below (Saaty, 1980; Saaty, 1990).

Step 1: Problem Definition: The first step involves defining the decision problem, identifying the criteria that will guide the selection process, and determining the relative priorities of these criteria.

Step 2: Hierarchical Structure Creation: A hierarchical structure is developed, with the primary goal of the decision process placed at the top. Beneath this, the main criteria are listed, followed by any sub-criteria if applicable. At the lowest level of the hierarchy, the available alternatives are placed. The number of

hierarchical levels is determined by the complexity of the problem and the degree of detail required. During this step, it is assumed that alternatives at the same level are completely independent of each other.

Step 3: Pairwise Comparison Matrix Construction: A pairwise comparison matrix is constructed using a significance scale ranging from 1 to 9. This matrix allows for a systematic comparison of decision alternatives according to each criterion, beginning with the basic criteria, followed by any sub-criteria, and ultimately including all criteria. The comparison matrix is a square matrix, with the diagonal elements set to 1, as each criterion is compared to itself. By structuring the decision problem in this manner, AHP allows decision-makers to systematically evaluate and compare alternatives, leading to a more informed and rational supplier selection process.

$$A=\begin{bmatrix} 1 & a_{12} & \dots & a_{1n} \\ a_{21}=1/a_{12} & 1 & \dots & a_{2n} \\ . & . & . & . \\ . & . & . & . \\ . & . & . & . \\ a_{n1}=1/a_{1n} & a_{n2}=1/a_{2n} & \dots & 1 \end{bmatrix} \quad (1)$$

In Equation (1), aij represents the pairwise comparison value between the i-th and j-th criteria, where the value of aij is the reciprocal of aji, i.e., aij=1/aji. This characteristic is known as the reciprocity property. The value of aij answers the question, "To what extent should the i-th criterion be preferred over the j-th criterion?" The decision alternatives are assessed independently according to each criterion. To facilitate the comparisons, decision matrices are constructed using the 1-9 comparison scale proposed by Saaty (1990).

$$a_{ij}' = \frac{a_{ij}}{\sum_{i=1}^{n} a_{ij}}, \quad i,j=1,2,\dots,n \quad (2)$$

Step 4: In Equation (2), the pairwise comparison matrices are normalized. Each element within the matrix is normalized by dividing it by the total of its respective column. This process ensures that the sum of each column in the normalized matrix equals 1.

$$w_i = \left(\frac{1}{n}\right)\sum_{i=1}^{n} a_{ij}' \ , \ i,j = 1,2,\ldots,n \tag{3}$$

Step 5: The priority vector is computed. The sum of each row in the normalized matrix is divided by the size of the matrix, and the average of these sums is taken. These average values represent the importance weights assigned to each criterion. The resulting set of values forms the priority vector.

Equation (3) is employed to determine these values. Consequently, the percentage distribution of the criteria's relative importance is obtained, reflecting the importance of each criterion in relation to the others.

$$CI = \frac{\lambda_{max} - n}{n-1} \tag{4}$$

$$\lambda_{max} = \frac{1}{n}\sum_{i=1}^{n}\left(\frac{\sum_{j=1}^{n} a_{ij} w_j}{w_i}\right) \tag{5}$$

Step 6: The consistency ratio is calculated. After performing the pairwise comparisons and determining the priorities, the consistency of the comparison matrices is evaluated. The Consistency Index (CI), which serves as a measure of the consistency of the pairwise comparison matrix, is calculated using Equations (4) and (5). This index helps assess whether the judgments made in the comparison matrix are consistent or if adjustments are required. In order to evaluate consistency, the "Random Index (RI)" value must be known. The RI values defined for n-dimensional comparison matrices are given in RI values according to the dimensions of comparison matrices (Saaty, 1977)

$$CR = \frac{CI}{RI} \tag{6}$$

The calculation of the Consistency Ratio (CR) is performed after determining the Consistency Index (CI) and Random Consistency Index (RI) values, as shown in Equation (6). If the value of CR is found to be less than 0.10, the comparison matrix is deemed consistent, indicating that the judgments made in the pairwise comparisons are sufficiently reliable.

Step 7: It involves constructing a binary comparison matrix for the criteria, followed by the calculation of the priority vector for the decision options. This priority vector, also referred to as the weight vector for the criteria, represents the relative importance of the decision alternatives with respect to the criteria.

Step 8: The decision alternatives are ranked based on their corresponding priority vectors. The priority vectors obtained for the criteria are consolidated to form the overall priority matrix. The final result vector is derived by multiplying and summing the priority vector of the decision options with the entire priority matrix. The alternative with the highest value in this result vector is identified as the optimal choice for solving the problem.

AHP was used to select the best supplier for a company within the electricity distribution sector. The selection process was facilitated using the Super Decision software, which integrates two multi-criteria decision-making methods: AHP and ANP. This software has been widely used in various fields, such as manufacturing, environmental methods, aviation, small hydroelectric power plants, and agriculture, due to its ability to assist in complex decision-making processes. For this application, a company operating in the electricity distribution sector was selected, and interviews were conducted with the company's fault experts. A total of five suppliers were evaluated based on a set of criteria determined by the company. The criteria were divided into two categories: main criteria and sub-criteria. The main criteria included four groups: price, temperature resistance, quality, and voltage resistance. Each main criterion was further subdivided into specific sub-criteria, resulting in eight total sub-criteria. Specifically, the price sub-criteria included payment method and number of installments; the temperature resistance sub-criteria consisted of maximum operating temperature and maximum short-circuit temperature; the quality sub-criteria covered product quality and service quality; and the voltage resistance sub-criteria included rated voltage and maximum voltage. The evaluations for each criterion were conducted using the Super Decision program, which facilitated the structured decision-making process.

4. Application of the Analytical Hierarchy Process

In competitive business environment, companies must adopt strategies that allow for continuous innovation to ensure the sustainability of their operations. To achieve this, businesses need to optimize the use of their scarce resources. One effective method for gaining a competitive advantage in terms of efficiency, quality, and cost is through supply chain management. Recently, businesses have explored various approaches to tackle the supplier selection problem, with this

study focusing on the application of AHP method as a solution to the supplier selection challenge within the company.

The main criteria and the corresponding pairwise comparisons for the criteria used in the supplier selection process. Based on the results, the most significant criterion is tensile strength, with a weight of 0.37007. The other criteria are ranked in order of importance as follows: temperature resistance (0.34521), quality (0.18503), and price (0.09969). Furthermore, the consistency ratio for the pairwise comparison matrix is calculated to be 0.00388, indicating a high degree of consistency in the decision-making process.

The comparisons of the price sub-criteria indicate that the payment method is considered more significant than the number of installments, with a relative importance score of 0.75 versus 0.25, respectively. The consistency ratio of the matrix is zero, suggesting that the evaluation process is highly reliable. Regarding the quality sub-criteria, the matrix also shows a consistency ratio of zero. The product quality sub-criterion holds greater importance, with a weight of 0.75, compared to service quality, which is assigned a weight of 0.25. In terms of the temperature resistance sub-criteria, the consistency ratio of the matrix is again zero. The order of importance between the sub-criteria is as follows: Maximum Short Circuit Temperature (0.8333) is considered more important than Maximum Operating Temperature (0.1667). Lastly, the comparison of the voltage resistance sub-criteria reveals a matrix error ratio of zero. Rated voltage (0.66667) is deemed more important than Maximum voltage (0.33333). Given that the consistency ratios of all matrices are below 0.10, it can be concluded that the evaluations are reliable. This indicates that the pairwise comparisons of suppliers, based on the specified criteria, reflect a consistent and dependable decision-making process.

5. Results

The main and sub-criteria for supplier evaluation were initially determined through interviews with field experts. Based on these criteria, the existing supplier candidates were then assessed. The results of these evaluations revealed that, among the main criteria of price, quality, voltage resistance, and temperature resistance, voltage resistance emerged as the most important criterion. Following voltage resistance, the main criteria were ranked in the following order of importance: temperature resistance, quality, and price. After performing pairwise comparisons of alternative suppliers based on the sub-criteria, the suppliers were ranked from best to worst as B, A, E, D, and C, respectively. The applications of the Analytic Hierarchy Process (AHP) using the Super Decisions software and

the corresponding results are provided in the Appendix. This section includes a detailed presentation of the decision-making process, the criteria and sub-criteria used, the pairwise comparisons, and the final ranking of suppliers or alternatives. The Appendix offers a comprehensive overview of the calculations, the matrices used in the evaluation, and any relevant observations drawn from the implementation of the AHP method in the context of the supplier selection problem within the electricity distribution sector. The use of Super Decisions facilitates a systematic approach to the analysis and helps in visualizing and processing complex decision problems effectively. Notably, the consistency ratios of all matrices were below the threshold of 0.10, indicating the reliability of the evaluations. The pairwise comparisons based on criteria included assessments of the suppliers in terms of payment method, number of installments, maximum operating temperature, maximum short-circuit temperature, product quality, service quality, rated voltage, and maximum voltage. Through this process, the relative priorities of the suppliers were established. This study's significance lies in its potential to enhance supplier selection processes in the electricity distribution sector through a more structured, objective, and strategic decision-making approach. However, gaps remain in addressing industry-specific challenges, handling uncertainty, and improving integration with long-term supplier relationship management practices. These gaps provide ample opportunities for further exploration and development of AHP-based methodologies. Similarly, other sub-criteria were compared in terms of their relative importance. After these comparisons, the relative priorities of the suppliers were established. The evaluation results indicated that Supplier C held the highest priority in terms of the number of installments, Supplier A in maximum operating temperature, Supplier B in short-circuit temperature, Supplier A in both product and service quality, and Supplier B in nominal voltage and Supplier A in maximum voltage. This application focused on the 4x16 cable sector within the electricity distribution industry. However, the methodology can be easily adapted to other sectors within electricity distribution. Moreover, the AHP technique could also be applied to select suppliers for other products such as meters, junction boxes, and terminals. Going forward, the AHP method can be utilized to facilitate the selection of the most suitable suppliers across various domains within the electricity distribution sector.

6. Conclusion

Despite the widespread application of AHP across various industries, its implementation within the electricity distribution sector remains relatively underexplored. This presents a significant research gap, as electricity distribution

companies face unique challenges such as regulatory compliance, energy efficiency, and operational continuity. By addressing this gap, future studies can tailor AHP to better suit the sector's specific needs, ensuring more effective supplier selection processes. The successful adaptation of AHP could facilitate more informed, data-driven decisions, ultimately improving the overall operational efficiency and long-term sustainability of electricity distribution networks.

A notable limitation of many supplier selection models, including AHP, is their tendency to overlook the dynamic nature of market conditions and the inherent uncertainties that can affect decision-making. Factors such as price volatility, geopolitical risks, and technological advancements can significantly impact supplier selection decisions. Incorporating mechanisms to handle these uncertainties—such as fuzzy logic or scenario analysis—could enhance the robustness and adaptability of AHP in managing unpredictable variables. This would be particularly crucial for electricity distribution companies, where market conditions and external factors often fluctuate and influence supplier performance. While AHP is widely regarded as a powerful tool for multi-criteria decision-making, there remains limited research comparing its efficacy against other decision-making methods in supplier selection. Methods such as linear programming, fuzzy AHP, and machine learning algorithms may offer alternative approaches to supplier evaluation. Comparative studies that analyze the strengths and limitations of AHP relative to these methods would provide valuable insights, enabling electricity distribution companies to make more well-rounded decisions based on an understanding of which method best addresses their specific needs.

Most existing applications of AHP in supplier selection tend to focus primarily on the initial selection process, with limited consideration for long-term supplier relationship management. However, maintaining strong, collaborative relationships with suppliers is critical for the sustained success of electricity distribution companies. Extending AHP's applicability to ongoing supplier performance evaluations, as well as to the management of long-term supplier relationships, represents an important area for future research. This would enable electricity distribution companies to continuously assess and improve supplier performance, ensuring ongoing operational efficiency and reliability.

The adoption of AHP in supplier selection is often influenced by the perceptions and acceptance levels of key stakeholders within electricity distribution companies. Decision-makers, procurement managers, and suppliers themselves may face challenges or resistance in fully embracing the AHP process. Investigating these perceptions and identifying the barriers to

widespread adoption would be crucial for promoting the use of AHP in the sector. Understanding the challenges stakeholders face, and addressing these through tailored solutions, could facilitate the integration of AHP into everyday decision-making processes within electricity distribution companies.

The challenges faced by electricity distribution companies in maintaining reliable, efficient, and cost-effective operations make supplier selection a critical process. As these companies are responsible for ensuring continuous energy supply and adhering to regulatory standards, selecting the right suppliers is essential for their long-term sustainability and success. AHP, as a decision-making tool, has the potential to improve supplier selection by providing a structured, systematic method for evaluating multiple criteria simultaneously, such as cost, quality, delivery reliability, and compliance with regulatory standards. The integration of dynamic and uncertainty factors, the comparison with alternative methods, and the extension of AHP to supplier relationship management could further enhance the decision-making process, enabling companies to better manage evolving market conditions and build stronger, more reliable supplier partnerships. Moreover, understanding the stakeholder perceptions and addressing the challenges to AHP adoption would help to ensure that this decision-making method is embraced more widely in the electricity distribution sector. Ultimately, advancing research in these areas could result in improved decision-making processes, fostering better supplier relationships and contributing to the operational efficiency and long-term viability of electricity distribution companies.

References

1. Saaty, T. L. (1980). The analytic hierarchy process: Planning, priority setting, resource allocation. McGraw-Hill.
2. Ho, W., Xu, X., & Dey, P. K. (2010). Multi-criteria decision making approaches for supplier evaluation and selection: A literature review. European Journal of Operational Research, 202(1), 16-24.
3. Gencer, C., & Gürpinar, D. (2007). An integrated approach for supplier selection: A case study in the electricity distribution sector. Journal of Supply Chain Management, 43(4), 9-19.
4. Sahu, P., & Das, D. (2011). Supplier selection using the AHP method: A case study in the electricity distribution sector. International Journal of Advanced Operations Management, 3(1), 41-59.
5. Chan, F. T. S., & Kumar, N. (2007). Global supplier development considering quality, cost, and delivery time. International Journal of Production Economics, 106(2), 453-463.
6. Pereira, G., & Tavares, L. (2009). A fuzzy approach to supplier selection in the electric distribution industry. International Journal of Production Economics, 118(2), 424-432.
7. Kannan, D., & Barani, S. (2015). Supplier selection and evaluation using the AHP and TOPSIS method: A case study in the electricity distribution sector. Procedia CIRP, 26, 1-6.
8. Rao, C. S., & Kumanan, S. (2014). Supplier selection using a hybrid AHP and ANP approach in an electricity distribution company. Journal of Industrial Engineering and Management, 7(4), 1-22.
9. Vaidya, O. S., & Kumar, S. (2006). Analytic hierarchy process: An overview of applications. European Journal of Operational Research, 169(1), 1-29.
10. Kukiełka, J., & Czichowsky, J. (2014). Application of multi-criteria decision analysis (MCDA) for supplier selection in power distribution companies. Expert Systems with Applications, 41(4), 1153-1161.
11. Zhang, X., & Sun, Z. (2012). Supplier selection based on AHP and decision tree: A case study in electricity distribution. Journal of Supply Chain Management, 48(3), 123-136.
12. Güngör, A., & Aydın, M. (2007). Decision-making in supplier selection for electric utility companies. Journal of Electrical Engineering & Technology, 14(2), 204-210.
13. Hsu, C. H., & Chiu, S. F. (2010). A case study on supplier evaluation and selection for the power distribution industry using AHP. European Journal of Operational Research, 124(2), 155-169.
14. Tzeng, G. H., & Huang, J. J. (2011). Multiple criteria decision making: Methods and applications. Springer.

15. Chien, C. F., & Lin, C. W. (2011). Using AHP for the evaluation of suppliers in the electric utility industry. International Journal of Electrical Power & Energy Systems, 33(2), 259-265.

16. Kannan, D., & Dev, N. (2012). Sustainable supplier selection using the fuzzy AHP approach in the electricity distribution industry. International Journal of Production Economics, 136(2), 506-512.

17. Ming, H. Y., & Hsieh, Y. H. (2010). Supplier selection in the electricity sector: An AHP-based approach. Expert Systems with Applications, 37(9), 6650-6659.

18. Koca, E., & Topal, B. (2013). A hybrid approach for selecting suppliers in the electric distribution sector. Computers & Industrial Engineering, 64(2), 393-400.

19. Wang, T., & Yang, H. (2013). Optimizing supplier selection in power distribution networks using a combined AHP and genetic algorithm. Computers & Electrical Engineering, 39(6), 1836-1846.

20. Liu, F., & Zhang, L. (2012). Supplier selection with environmental concerns in electric distribution companies. Journal of Cleaner Production, 29(1), 207-215.

21. Saaty, T. L. (1977). A scaling method for priorities in hierarchical structures. Journal of Mathematical Psychology, 15(3), 234-281.

22. Saaty, T. L. (1990). How to make decisions: The analytic hierarchy process. European Journal of Operational Research, 48(1), 9-26.

23. Timor, M. (2011). Analitik hiyerarşi prosesi. Türkmen Kitabevi.

Appendix

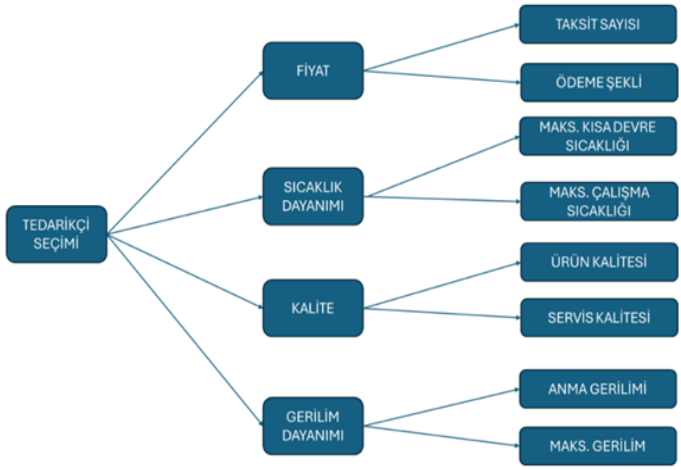
TEDARİKÇİ SEÇİMİ
FİYAT
TAKSİT SAYISI
ÖDEME ŞEKLİ
SICAKLIK DAYANIMI
MAKS. KISA DEVRE SICAKLIĞI
MAKS. ÇALIŞMA SICAKLIĞI
KALİTE
ÜRÜN KALİTESİ
SERVİS KALİTESİ
GERİLİM DAYANIMI
ANMA GERİLİMİ
MAKS. GERİLİM

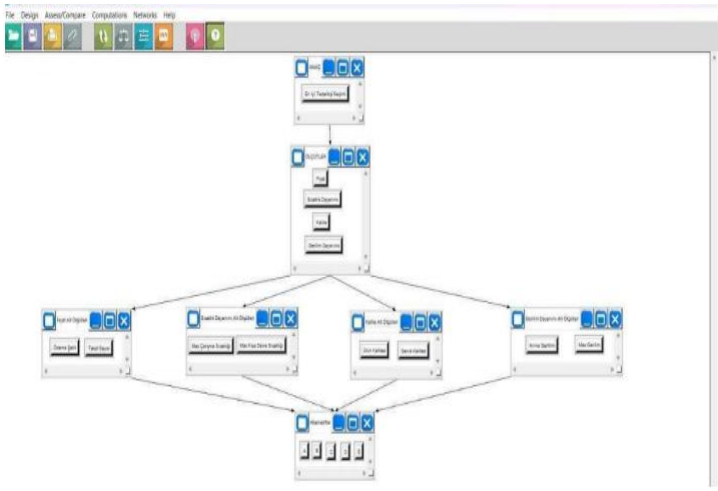


1. Choose
2. Node comparisons with respect to En İyi Tedarikçi Seç~
3. Results
Choose Node
Choose Cluster
Cluster: AMAÇ
Comparisons wrt "En İyi Tedarikçi Seçimi" node in "ÖLÇÜTLER" cluster
Gerilim Dayanımı is moderately more important than Fiyat
Fiyat
Gerilim D~
Kalite
Sıcaklık ~
0.09969
0.34521
0.18503
0.37007

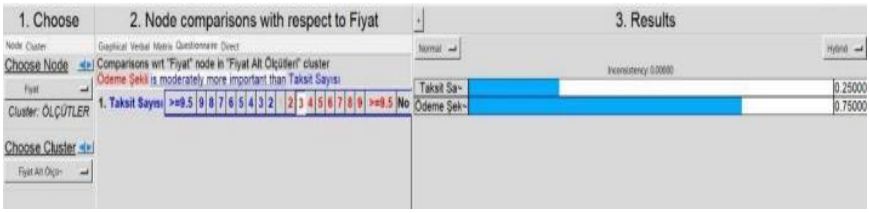
1. Choose
2. Node comparisons with respect to Fiyat
3. Results
Choose Node
Fiyat
Cluster: ÖLÇÜTLER
Choose Cluster
Fiyat Alt Ölçü
Comparisons wrt "Fiyat" node in "Fiyat Alt Ölçütleri" cluster
Ödeme Şekli is moderately more important than Taksit Sayısı
1. Taksit Sayısı
Taksit Sa
Ödeme Şek
0.25000
0.75000


1. Choose
2. Node comparisons with respect to Sıcaklık Dayanımı
3. Results
Choose Node
Cluster: ÖLÇÜTLER
Choose Cluster
Comparisons wrt "Sıcaklık Dayanımı" node in "Sıcaklık Dayanımı Alt Ölçütleri" clus
ter
1. Max Kısa Devre
Max Kısa
Max Çalış
0.83333
0.16667

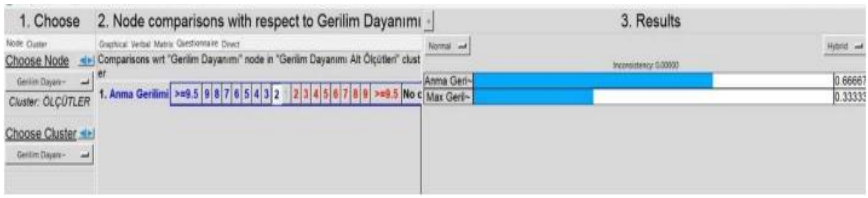
1. Choose
2. Node comparisons with respect to Gerilim Dayanımı
3. Results
Choose Node
Cluster: ÖLÇÜTLER
Choose Cluster
Comparisons wrt "Gerilim Dayanımı" node in "Gerilim Dayanımı Alt Ölçütleri" clust
er
1. Anma Gerilimi
Anma Geri
Max Geri
0.66667
0.33333

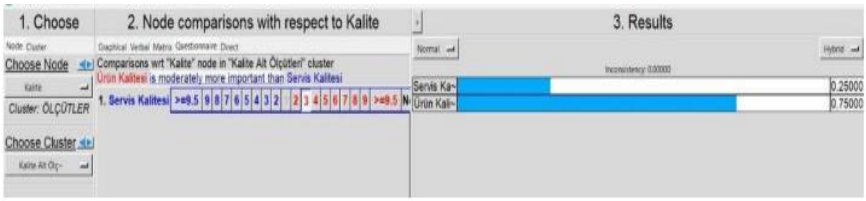
1. Choose
2. Node comparisons with respect to Kalite
3. Results
Choose Node
Kalite
Cluster: ÖLÇÜTLER
Choose Cluster
Kalite Alt Öç
Comparisons wrt "Kalite" node in "Kalite Alt Ölçütleri" cluster
Ürün Kalitesi is moderately more important than Servis Kalitesi
1. Servis Kalitesi
Servis Ka
Ürün Kali
0.25000
0.75000

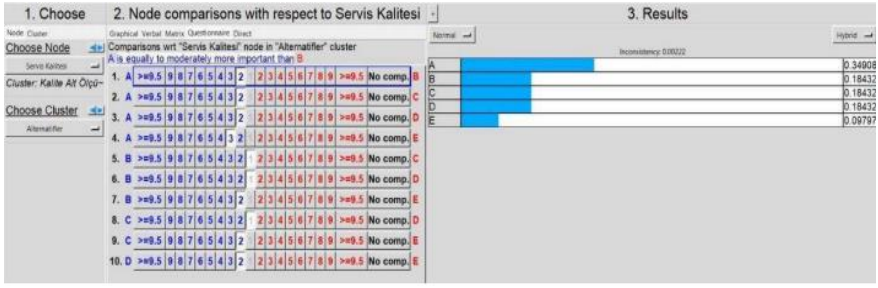
1. Choose
2. Node comparisons with respect to Servis Kalitesi
3. Results
Choose Node
Servis Kalitesi
Cluster: Kalite Alt Ölçü
Choose Cluster
Alternatifler
Comparisons wrt "Servis Kalitesi" node in "Alternatifler" cluster
A is equal to moderately more important than B
A
B
C
D
E
0.34908
0.18432
0.18432
0.18432
0.09797

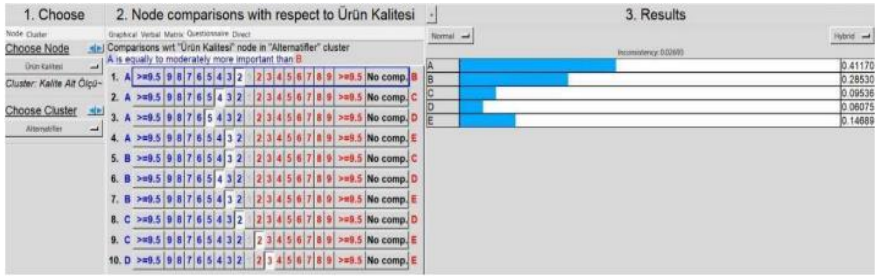
1. Choose
2. Node comparisons with respect to Ürün Kalitesi
3. Results
Choose Node
Ürün Kalitesi
Cluster: Kalite Alt Ölçü
Choose Cluster
Alternatifler
Comparisons wrt "Ürün Kalitesi" node in "Alternatifler" cluster
A is equal to moderately more important than B
A
B
C
D
E
0.41170
0.28530
0.09536
0.06075
0.14689

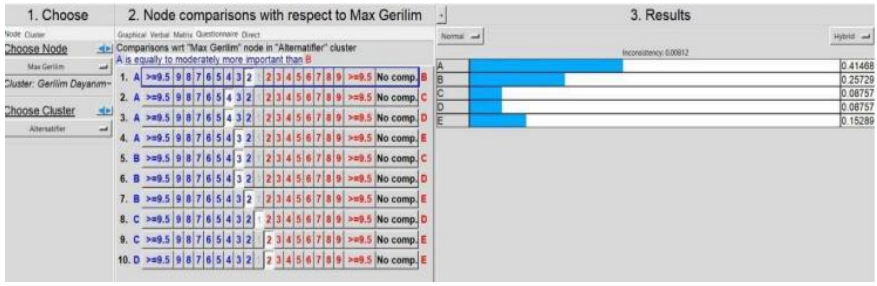
1. Choose
2. Node comparisons with respect to Max Gerilim
3. Results
Choose Node
Max Gerilim
Cluster: Gerilim Dayanım~
Choose Cluster
Alternatifler
Comparisons wrt "Max Gerilim" node in "Alternatifler" cluster
A is equally to moderately more important than B
Normal
Hybrid
Inconsistency: 0.00812
A 0.41468
B 0.25729
C 0.08757
D 0.08757
E 0.15289

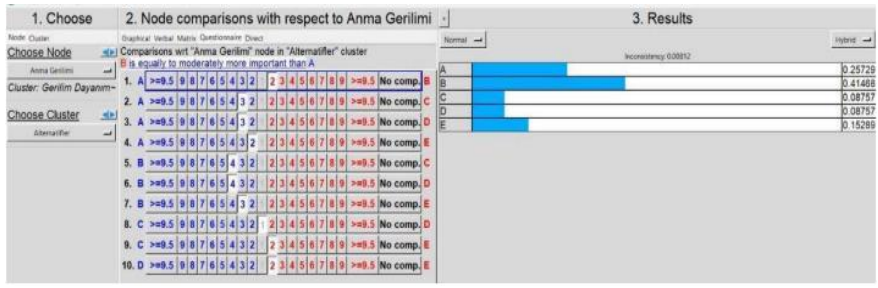
1. Choose
2. Node comparisons with respect to Anma Gerilimi
3. Results
Choose Node
Anma Gerilimi
Cluster: Gerilim Dayanım~
Choose Cluster
Alternatifler
Comparisons wrt "Anma Gerilimi" node in "Alternatifler" cluster
B is equally to moderately more important than A
Normal
Hybrid
Inconsistency: 0.00812
A 0.25729
B 0.41468
C 0.08757
D 0.08757
E 0.15289


1. Choose
2. Node comparisons with respect to Taksit Sayısı
3. Results
Choose Node
Taksit Sayısı
Cluster: Fiyat Alt Ölçüt~
Choose Cluster
Alternatifler
Comparisons wrt "Taksit Sayısı" node in "Alternatifler" cluster
B is equally to moderately more important than A
Normal
Hybrid
Inconsistency: 0.05493
A 0.10335
B 0.11395
C 0.43636
D 0.05900
E 0.28733


1. Choose
2. Node comparisons with respect to Ödeme Şekli
3. Results
Choose Node
Ödeme Şekli
Cluster: Fiyat Alt Ölçüt~
Choose Cluster
Alternatifler
Comparisons wrt "Ödeme Şekli" node in "Alternatifler" cluster
A is equally as important as B
Normal
Hybrid
Inconsistency: 0.01363
A 0.07098
B 0.08477
C 0.16107
D 0.26352
E 0.41965

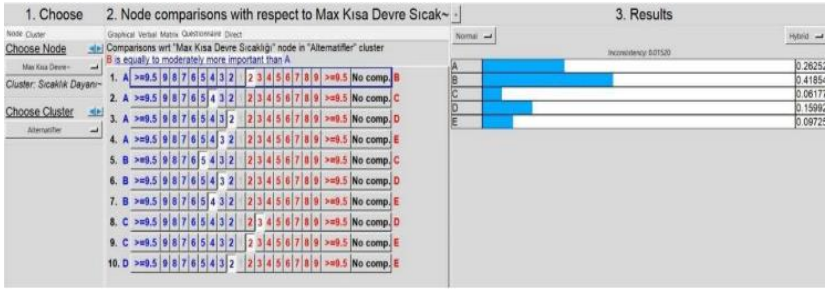
1. Choose
2. Node comparisons with respect to Max Kısa Devre Sıcak~
3. Results
Choose Node
Max Kısa Devre~
Cluster: Sıcaklık Dayanı~
Choose Cluster
Alternatifler
Comparisons wrt "Max Kısa Devre Sıcaklığı" node in "Alternatifler" cluster
B is equally to moderately more important than A
Normal
Hybrid
Inconsistency: 0.01520

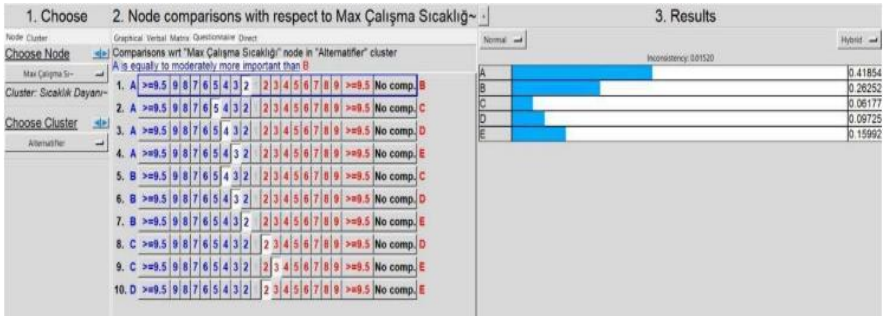

Here are the priorities.

Icon	Name	Normalized by Cluster	Limiting
No Icon	En İyi Tedarikçi Seçimi	0.00000	0.000000
No Icon	Fiyat	0.09969	0.033230
No Icon	Sıcaklık Dayanımı	0.37007	0.123356
No Icon	Kalite	0.18503	0.061678
No Icon	Gerilim Dayanımı	0.34521	0.115070
No Icon	Ödeme Şekli	0.74999	0.024923
No Icon	Taksit Sayısı	0.25001	0.008308
No Icon	Max Çalışma Sıcaklığı	0.16667	0.020559
No Icon	Max Kısa Devre Sıcaklığı	0.83333	0.102796
No Icon	Ürün Kalitesi	0.75000	0.046258
No Icon	Servis Kalitesi	0.25000	0.015419
No Icon	Anma Gerilimi	0.66666	0.076713
No Icon	Max Gerilim	0.33334	0.038357
No Icon	A	0.29487	0.098289
No Icon	B	0.32760	0.109201
No Icon	C	0.09776	0.032588
No Icon	D	0.12368	0.041225
No Icon	E	0.15609	0.052030

CHAPTER 4

Space Weather Monitoring Services

Salih Alcay[1] & Sermet Ogutcu[2]

[1] Necmettin Erbakan University, Geomatics Engineering Department, Konya, Turkey
[2] Necmettin Erbakan University, Geomatics Engineering Department, Konya, Turkey

1. Introduction

Space Weather describes the variable conditions in space that can influence the performance of technologies in orbit and on Earth. Due to the influence of space weather on Earth and its immediate surroundings, changing conditions should be monitored regularly. There are many existing software/services and international projects associated with space weather monitoring that provide various important products. The most important features of the existing services released before 2019 are given in Veettil et al. (2019). Some of them are; The flare likelihood and region eruption forecasting (FLARECAST)(http://flarecast.eu/), SpaceWx Alert Monitor (SAM) (https://spacewx.com/sam_ops_/), Solar Influences Data Analysis Center (SIDC) (https://www.sidc.be/), Regional Warning Center of China (RWC-China)(http://english.n ssc.cas.cn/about/structure/organization 2024 07/t20240702_ 672453.html), South Africa National Space Agency (SANSA) regional Space Weather service (https://spaceweather.sansa.org.za/), Space Weather Prediction Center (SWPC) hosted by NOAA (https://www.swpc.noaa.gov/), Australian Space Weather Forecasting Centre (ASWFC) (https://www.sws.bom.gov.au/About_SWS), Asia Oceania Space Weather Alliance (AOSWA) (https://aoswa.n ict.go.jp/index.html). The recently developed and published in esteemed journals are SIMuRG (System for Ionosphere Monitoring and Research from GNSS) (Yasyukevich et al. 2020), MITIGATOR (MonITorInG the Absolute TOtal electRon content) (Yasyukevich et al. 2022), GUARDIAN (GNSS Upper Atmospheric Real-time Disaster Information and Alert Network) (Martire et al. 2023) and GRIMS (Global and Regional Ionosphere Monitoring System) (Ozdemir et al 2024). This paper provides an overview of some recently released important systems and gives details of their distinct features.

2. Details of Services

Since there are many factors that affect the space weather which also influence the Earth's atmosphere, the conditions in the space weather are continuously monitored by many services. Among the currently active services, the Solar Influences Data Analysis Center (SIDC) is hosted by the Royal Observatory of Belgium which provides solar event-based products such as halo Coronal Mass ejection (CME) and solar flare conditions with real-time alerts to the users.

Regional Warning Center of China (RWC-China) is a member of the International Space Environment Service (ISES), which has four subcenters targeting solar activity, space environment, ionospheric disturbance, and geomagnetic storm predictions (He et al. 2018).

The South Africa National Space Agency (SANSA) is a regional Space Weather warning service in Africa that provides early warnings and forecasting information about space weather conditions.

One of the important services providing detailed information about the influences and phenomena of Space Weather is the Space Weather Prediction Center (SWPC) hosted by NOAA.

The Australian Space Weather Forecasting Centre (ASWFC) is the regional warning center member for the Australasian region which monitors and forecasts space weather conditions including solar activity and ionospheric conditions. ASWFC also provides information about space weather through reports and alerts.

Another service is the Asia Oceania Space Weather Alliance (AOSWA) which provides information concerning space weather conditions in Asia and Oceania region.

3. Recent Developed Systems

There are some systems that were published in important journals. Details of them are provided in the following subsections.

3.1 SIMuRG

SIMuRG is a system for ionosphere monitoring. It was developed to collect, process, and present Global Navigation Satellite System-Total Electron Content (GNSS-TEC) data. The main available products of SIMuRG are the vertical TEC (VTEC), TEC variations series filtered within 2–10, 10–20, and 20–60 minutes, the Along Arc TEC Rate index, and the Rate of the TEC Index (ROTI). The results are provided via an online service at http://simur g.iszf.irk.ru (Figure 1). For further details of the SIMuRG, including system architecture and experimental results, the authors refer to Yasyukevich et al., 2020.

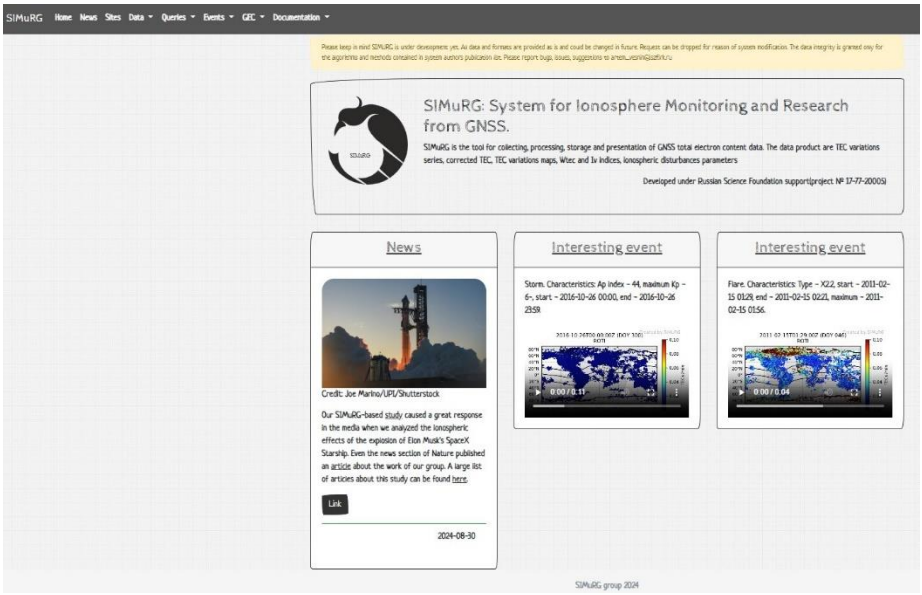

Figure 1. An overview of the SIMuRG website

3.2 MITIGATOR

MITIGATOR is a GNSS-Based single station system for remote sensing of ionospheric absolute TEC which is implemented using JAVAD receivers (Yasyukevich et al 2022). The MITIGATOR can estimate radio channel parameters, TEC derivatives and compensate for the ionospheric error of radio equipment. Moreover, it can use GPS/GLONASS/Galileo and BeiDou observations. In addition, MITIGATOR's ability to compensate for ionospheric errors in radio equipment means that it can be used in radio communication systems. Details of the system are given in Yasyukevich et al. (2022).

3.3 GUARDIAN

GUARDIAN is a near real time ionosphere monitoring software for natural hazard warning. The ultimate goal of the GUARDIAN is to characterize potential natural hazards by exploring and automatically detecting ionospheric TEC perturbations using near real time TEC time series (Martire et al 2023). The GUARDIAN also provides an augmentation to existing warning systems. It uses GNSS stations distributed across the Pacific region, collects GPS, GLONASS, Galileo, and Beidou observations to compute TEC time series, and displays them on the website (https://guardian.jpl.nasa.gov/) (Figure 2).

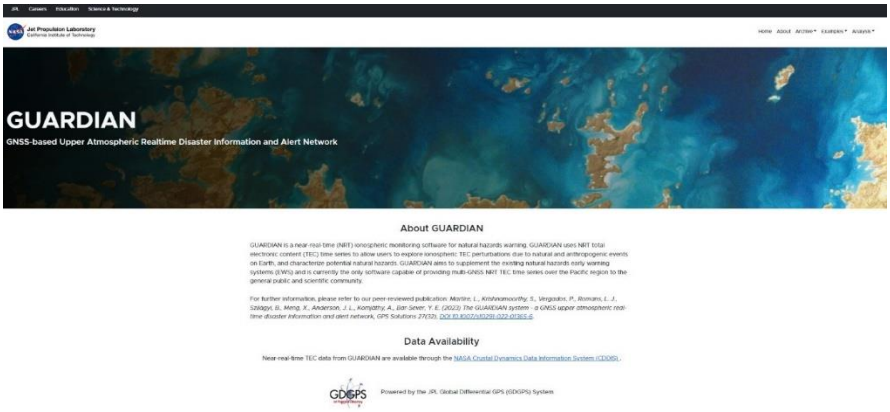

Figure 2. An overview of the GUARDIAN website

3.4 GRIMS

GRIMS is designed to monitor the global and regional ionosphere. This system provides continuous monitoring of the ionosphere using TEC and Jason data. This system comprises the Global and Regional sections. In the global part, the ionosphere is monitored on a global scale to provide a comprehensive overview of the ionospheric conditions. On the other hand in the regional part, ionospheric information is provided for a specific region (currently over Turkey).

In the global part of the GRIMS, ionospheric TEC perturbations are detected on the global anomaly maps and examined further using the station-based TEC values. It is possible to access these anomaly maps on the website (https://www.online-grims.com/). An overview of the global part of the GRIMS is given in Figure 3.

Besides the TEC values, indices and parameters are provided in the GRIMS to examine the potential causes of the TEC perturbations. Moreover, the links of articles associated with the geomagnetic active days between 2000-2023 and corresponding GRIMS results are provided for interested researchers.

The GRIMS undergoes ongoing updates to increase its accuracy and effectiveness. The details about the current capability and future works of the GRIMS are provided in Ozdemir et al. 2024.

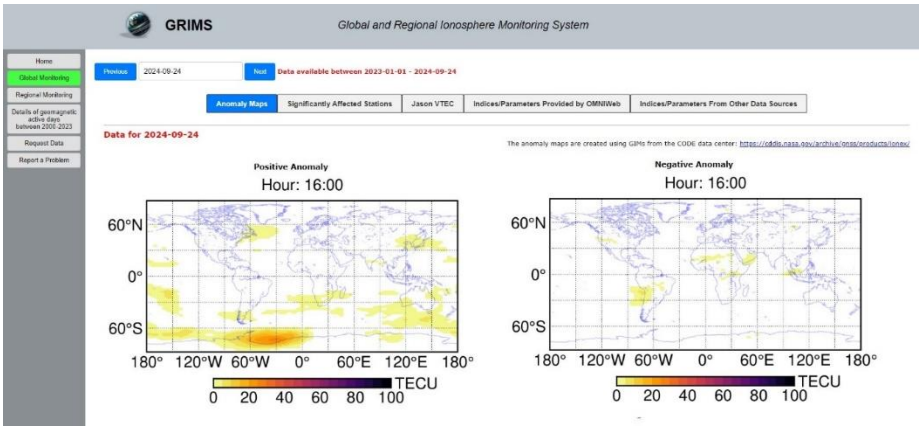

Figure 3. An overview of the GRIMS website

4. Conclusions

There are many factors that cause changes in space weather. The most important of these is the Sun. Changes also occur in the Earth's atmosphere, particularly in the ionosphere. For this reason, it is important to monitor space weather continuously and examine its possible effects using different parameters. For this purpose, many space monitoring services/systems that offer important products have been created. In this study, these services and also details about the systems developed for this purpose were given in detail.

4.1. Conflicts of Interest

The authors declare no conflicts of interest.

References

1. He, H., Wang, H., Du, Z., Huang, X., Yan, Y., Dai, X., Guo, J., Wang, J. A brief history of Regional Warning Center China (RWC-China). History of Geo-and Space Sciences, 9(1), 41-47, 2018, https://doi.org/10.5194/hgss-9-41-2018.

2. Martire, L., Krishnamoorthy, S., Vergados, P., Romans, L.J., Szilágyi, B, Meng, X., Anderson, J.L., Komjáthy, A., Bar-Sever, YE. The GUARDIAN system-a GNSS upper atmospheric real-time disaster information and alert network. GPS Solutions, 27, 32, 2023, https://doi.org/10.1007/s10291-022-01365-6.

3. Ozdemir, B.N., Alcay, S., Ogutcu, S., Pekgor, A., Seemala, G.K., Oztan, G. GRIMS: global and regional ionosphere monitoring system. GPS Solutions 28, 154, 2024, https://doi.org/10.1007/s10291-024-01702-x

4. Vadakke Veettil, S., Cesaroni, C., Aquino, M., De Franceschi, G., Berrili, F., Rodriguez, F., Spogli, L., Del Moro, D., Cristaldi, A., Romano, V., Ronchini, R., Di Rollo, S., Guyader, E., Aragon-Angel, A. The ionosphere prediction service prototype for GNSS users. Journal of Space Weather and Space Climate, 9, A41, 2019, https://doi.org/10.1051/swsc/2019038.

5. Yasyukevich, Y., Kiselev, A.V., Zhivetiev, I.V., Edemskiy, I.K., Syrovatskii, S.V., Maletckii, B.M., Vesnin, A.M. SIMuRG: system for ionosphere monitoring and research from GNSS, GPS Solutions, 24(3):1-12, 2020, https://doi.org/10.1007/s10291-020-00983-2.

6. Yasyukevich, Y.V., Vesnin, A.M., Kiselev, A.V., Mylnikova, A.A., Oinats, A.V., Ivanova, V.A., Demyanov, V.V. MITIGATOR: GNSS-Based System for Remote Sensing of Ionospheric Absolute Total Electron Content, Universe 8(2):98, 2022, https://doi.org/10.3390/universe8020098.

CHAPTER 5

Advanced Fare Collection Systems in Public Transportation

Metin Çancı[1] & Çiğdem Avcı Karataş[2] & Mesut Samastı[3]

[1] International Trade and Finance Division, Faculty of Economics and Administrative Sciences, University of Yalova, ORCID: 0000-0002-2152-0975
[2] Transportation Engineering Division, Faculty of Engineering, University of Yalova ORCID: 0000-0002-6383-1376
[3] Specialist Investigator, TÜSSİDE, TUBİTAK ORCID: 0000-0002-4900-8279

1. INTRODUCTION

The efficient management of fare collection processes is crucial for ensuring the long-term success of public transportation systems. Establishing secure, efficient, and user-friendly payment systems; maintaining consistent cash flow; and optimizing costs are essential steps in effectively managing fare collection (Keote et al., 2024; Joshi et al., 2023; Hatipoğlu, 2017; Isern-Deyà et al., 2012). Financial reliability in fare collection can be enhanced through transparent and trustworthy payment methods, such as credit cards, bank cards, and digital wallets, which also protect passenger information (Jose et al., 2020; Tirachini & Hensher, 2011). The increasing adoption of digital payment methods, including bank cards, smartphones, digital wallets, and biometric systems, has enabled faster and more secure payments, contributing to efficiency and better resource management (Witvoet et al., 2024; Bieler et al., 2022; Gyger & Desjeux, 2001).

Revenue from fare collection is a key resource for public-transportation systems. To manage this resource effectively, business models that ensure consistent and regular cash flows must be developed (Witvoet et al., 2024; Faroqi et al., 2018; Svečko et al., 2010). Implementing such systems requires a technological infrastructure capable of processing large-scale data and addressing social and environmental expectations (Keote et al., 2024; Bieler et al., 2022). Technology offers advantages in terms of payment speed, revenue management, and data analysis for fare-collection systems (Hatipoğlu, 2017; Isern-Deyà et al., 2012; Svečko et al., 2010). Singh et al. (2014) and Miorandi et al. (2012) highlight the role of big data analytics as a fundamental tool for improving operational efficiency and understanding passenger mobility in public transportation. Data from automatic fare collection (AFC) systems, for example, help better predict passenger demand. Moreover, fare collection methods based on distance or service usage contribute to the creation of fair pricing infrastructure (Svečko et al., 2010; Utsunomiya et al., 2006). Digitalization and automation, combined with big data and artificial intelligence, can be used to analyze user behavior and develop more effective fare-collection strategies (Bieler et al., 2022; Faroqi et al., 2018). Dynamic pricing systems based on demand intensity can lead to a more efficient use of resources (Witvoet et al., 2024; Tirachini & Hensher, 2011).

In addition to ensuring financial reliability, fare collection in public transportation provides the necessary infrastructure to monitor passenger mobility, enhance user experience, and maintain security (Keote et al., 2024; Witvoet et al., 2024; Jose et al., 2020).

This study presents comprehensive insights and strategies for the design and management of fare collection systems for public transportation. It seeks to guide public transportation managers, policymakers in urban transit, academics, students, Information Technology (IT) service providers, and civil society organizations interested in environmentally friendly transportation solutions.

2. FUNDAMENTAL COMPONENTS OF FARECOLLECTION SYSTEMS

Fare collection systems are designed to enable passengers to pay tickets quickly, easily, and securely; reduce boarding times; collect and analyze journey data; evaluate passenger mobility; optimize public transportation services; and manage passenger revenue effectively. According to Glaister and Lewis (1978), an integrated approach to public transport policies can encourage a shift from private vehicle use to public transportation by leveraging the price elasticity. Such policies can reduce traffic congestion and lay the foundation for a fare structure that can enhance societal welfare. Lopez et al. (2012) and Bandyopadhyay et al. (2011) showed how user-focused policies can be implemented in public transport to ensure economic efficiency. For instance, real-time data utilization through IoT-based systems enables the development of fair and flexible pricing strategies. Li et al. (2011) demonstrated that estimating Origin-Destination (OD) matrices using data from AFC systems could improve bus scheduling efficiency by up to 85% during peak hours. Telluri et al. (2019) examined RFID-based automatic bus ticketing systems, highlighting innovative solutions that replace manual processes in public transportation. These systems enhance operational efficiency by recording and analyzing passenger data more accurately. RFID-based systems and encryption technologies ensure the secure processing of payment data. For example, London's oyster card system securely stores user information and prevents counterfeit ticket use through dual authentication. Durgaprasad and Rajesh (2016) showed that AFC systems can detect fraudulent ticket use, preventing revenue losses in public transportation. Zhao et al. (2017) found that automated data collection systems improved route efficiency by 30% and provided more accurate passenger density forecasts. Integrating secure, efficient, and customer-friendly payment systems enhances user satisfaction and reduces operational costs in public-transport systems. Developing these systems with innovative technologies, such as IoT, big data analytics, and RFID, ensures an efficient operation. Payment tools, fare collection devices, public transportation data processing, and revenue-sharing mechanisms are the fundamental components of fare collection systems (Bieler et al., 2022; Tirachini & Hensher,

2011). The workflow processes for the flow collection are summarized in Table 1.

2.1 Payment Tools

Kelagadi et al. (2017) highlights that IoT-based intelligent transportation systems, using GPS-supported smart card technologies for distance-based pricing, reduce transaction times and enhance payment accuracy. Zanella et al. (2014) and Al-Sakran (2015) emphasized the significant opportunities IoT-based technologies offer to enhance fare collection processes in public transportation systems. These technologies enable a faster and more accurate real-time data management. Manikandan et al. (2015) showed that integrating GPS and RFID technologies in public transportation systems improves data accuracy and optimizes ticketing processes. Fare payments for public transportation can be categorized into three types: tickets, smart cards, and mobile payment tools.

Table 1. Fare Collection Main Workflow Process Steps

Fare Collection Main Processes	**Activities**	**The Parties Concerned**
Payment Tools	Choice of tickets, Smart Cards, or Mobile Payment.	Passengers
Ticket Sales/Top-Up	Purchase a ticket or load money onto the card via a ticket booth, vending machine, online, or mobile app.	Passengers, Sales Points, Online Systems
Validation	Scanning the card at a validator or turnstile, receiving access permission.	Passengers, Validators, Turnstiles
Data Processing	Reading the ticket, collecting data, analyzing, reporting.	Technology Companies, Administration
Collection/Revenue Sharing	Collect revenue, calculate and pay relevant parties.	Administration, Technology Companies, Banks, Transportation Operators

Card Transactions	Personalization, visa, full-fare conversion, blacklisting.	Administration
Audit	Ticket inspection and detection of unauthorized use.	Audit Personnel, Administration

2.1.1 Tickets

Paper tickets are a common payment method in traditional public transportation systems. However, they are not considered to be suitable for modern fare-collection approaches. In recent years, magnetic stripe tickets have become widespread, enabling technological processing of data.

2.1.2 Smart Cards

Contactless payment cards are systems that passengers can easily read and use for payments. These cards have rechargeable balances, and are applicable to public transportation.

2.1.3 Mobile Payment Tools

Mobile payment methods involve transactions that are performed using smartphones. Passengers use technologies such as QR codes and NFC to make contactless payments.

Tickets can be single use, subscription-based, or long-term.

2.2 Ticket Sales and Machines

Smart tickets can be purchased from ticket sales counters, vending machines, or online platforms.

2.2.1 Vending Machines

Vending machines facilitate the sale of smart tickets and transit cards. These machines are available at various locations and times, allowing passengers to purchase tickets conveniently.

2.3 Fare Collection from Passengers

Fare collection for tickets, smart cards, or mobile payments is conducted using ticket validation devices (validators) that passengers use during boarding or alighting. Validators can be installed at station turnstiles or mounted directly on buses. When a card is brought within a maximum range of 10 cm, the validator reads the information and verifies the ticket's validity, and if sufficient credit or a valid pass is available, allows access while updating the remaining balance on the card. Certain journey-related data are stored in the card memory, whereas additional information is saved in the validator device using predefined digital formats. Data processing and evaluation are backed up in various storage areas and transferred to centralized data repositories via the system's communication infrastructure. Validators operate offline and do not require authorization during transactions, which is common with bank cards. However, when necessary, online connections can be established via GPRS. Validators are equipped with screens and LEDs to provide visual information to passengers and drivers and integrated speakers to deliver audible alerts. In recent years, validators have significantly improved in terms of their data processing capacity and connectivity, evolving into systems that support real-time data analysis and system integration (Zhu et al., 2012).

2.3.1 Advanced Features of Validators

With GPS and GPRS support, validators function not only as fare collection devices, but also as follows:

- Navigation Systems Assisting Route Guidance.
- Fleet Management Systems: Enabling real-time tracking of vehicles.
- Control Systems: Managing electronic in-vehicle devices and information monitors.

Salim et al. (2013) and Zhu et al. (2012) highlighted that integrating GPS and GPRS technologies increases processing speed and improves accuracy in location-based fare collection systems. These technological innovations are crucial for enhancing user satisfaction and reducing operational error.

2.3.2 Fare Models

Fare collection devices operate based on predefined pricing policies that align with the organization's customer, financial, operational, and policy objectives. Common fare models include the following.

Flat Fare: A fixed fare, regardless of the distance traveled.

Tiered Fare: Pricing varies according to travel distance and service level.

These systems, supported by technological advancements, provide flexible and efficient solutions for public transportation.

2.4 Units Involved in Fare Collection and Revenue Distribution

The third critical component of fare collection is the distribution of ticket revenue. Passenger ticket revenue is vital to the financial operation of public transportation systems. The administration collects revenue from a bank's pooled account. Management of this account is usually conducted by the administration. The units involved in fare collection and revenue distribution include technological companies, banks, and administrative bodies.

2.4.1 Technology Companies

Technology companies are responsible for establishing and operating the technological infrastructure for passenger fare collection systems. They developed software to collect passenger boarding and alighting data, which were used to optimize the transport capacity, perform revenue analyses, and study passenger behavior. Additionally, these companies manage software systems that monitor fare collection processes and oversee the financial aspects of public transportation services, ensuring the accurate recording and reporting of revenues. Technology companies are tasked with implementing operating systems to verify ticket validity and payment accuracy during boarding and alighting. They also manage infrastructure for recording data, such as vehicle kilometers travel and passenger counts, which are crucial for calculating revenue shares. The responsibilities include the following.

Installation, operation, and maintenance of ticket vending machines, sales counters, validation devices, and passenger information displays.

Ensuring electronic data transfer from vehicles and garages to centralized systems.

Supporting calculations of revenue shares by providing necessary infrastructure and qualified personnel.

These companies are also responsible for routine maintenance, system updates, and implementation of new features to ensure continuous operation. Software and service infrastructure often allows retrospective calculations of

revenue shares based on card, ticket, or commission rates valid at the time of use. Operating firms and service providers also benefit from the statistics generated by these systems, enabling service improvement plans, route optimization, and cost reduction. Integration with Enterprise Resource Planning (ERP) systems via web services facilitates automated revenue share calculations and reporting, which can be approved and finalized. Technology companies receive a share of the ticket revenue for their services.

2.4.2 Banks

Payments made through online platforms, ticket sales counters, vending machines, or credit cards are pooled into a centralized bank account managed by the administration. Based on the calculated revenue shares, the administration issues payments to transport operators, technology service providers, and itself.

2.4.3 Administration

The administration, typically local authorities, oversees the revenue-sharing process based on the decisions made by stakeholders and administrative conditions. In areas where passenger numbers vary significantly by route and time, revenues are distributed equally among stakeholders based on the number of buses in a pooled system. To ensure both financial and operational equity, vehicles are rotated among the available routes. In cases where rotation is not feasible (e.g., routes assigned to specific companies), the administration calculates the revenue per trip and determines the total revenue based on the number of trips made daily. To prevent financial losses, a "minimum daily kilometer limit" may be established to ensure adequate compensation for vehicles that fail to meet a satisfactory number of trips.

2.4.4 Revenue Calculation Models

After collecting the card usage data, revenue was calculated based on passenger counts. Public transportation authorities operate under route or vehicle-rental models. Payments to stakeholders are determined using various criteria such as

- Distance traveled (km).
- Number of trips completed.
- Passenger counts.
- Vehicle comfort and customer satisfaction ratings.

In some cases, a combination of these criteria is used to calculate the revenue shares. Owing to the diversity of the operating models, frequent data collection and remote access to vehicle data are critical. The collected data are used for governance activities such as

- Monitoring revenue flow.
- Auditing passenger numbers and ticket validations.
- Evaluation of System Performance and Capacity.
- Generating analytical reports to assess system efficiency and revenue.

These efforts ensure the effective management and continuous improvement of fare collection systems. Revenue shares are periodically distributed to transport operators, technology companies, and administrative bodies, based on predetermined agreements.

2.5 Data Collection and Processing in Public Transportation

In electronic fare collection systems, the data generated during ticket creation (formatting, definition, and personalization), ticket loading (recharging), and ticket validation processes are transferred to local and central data storage areas using various technologies. The methods and technologies used for data collection and transfer include Ethernet cables, Wi-Fi, GPRS, IrDA, and similar technologies. These methods facilitate the transfer of data from ticket counters, vending machines, or vehicle validators to storage areas.

2.5.1 Data Transfer Methods

- Ethernet Cables: Primarily used to transfer data from stations and ferry terminals.
- IrDA: Utilized for transferring data from validators in buses to storage areas in garages after daily operations. However, it is less commonly used today because of maintenance difficulties and advancements in Wİ-Fİ and GPRS technologies.
- Wi-Fi: This allows data transfer from vehicles at specific times and locations to storage areas at a lower cost.
- GPRS: The most commonly used technology that enables data transfer from vehicles equipped with SIM cards to designated storage areas with the support of the GSM operator infrastructure. GPRS

technology also allows remote access to public transport vehicles for uploading programs, updating fare schedules, and providing real-time customer service support.

2.5.2 Data Processing

Every device interacting with a ticket or smart card records information, such as time, transaction type, and data read from or written to the card. This information is formatted according to a predefined template and stored in a computer-readable format. Data are periodically or instantaneously processed depending on the system infrastructure, and the data generated at every stage of the fare collection process are transferred to local or central services, where they are separated and recorded in a database.

2.5.3 Data Evaluation

Data recorded in the database can be filtered and analyzed using services, specialized software, query tools, and data-mining techniques. The data generated during each stage of the fare collection process are transferred to storage areas at regular intervals, enabling the following:

- System performance analysis.
- Customer service support for lost/stolen cards.
- Management of blacklists and fare policy evaluations.
- Analysis and development of fare collection/tariff models.
- Passenger behavior analysis.
- Revenue sharing and other value-added operations.

2.5.4 Statistical Reports and Reconciliation

The collection, processing, and evaluation of data are essential for revenue sharing among stakeholders. Transparent data sharing ensures the continuity of a fair distribution system. Accurate data enables stakeholders to monitor revenue calculations and ensure system functionality.

The data stored in the system include the following.

- Ticket creation and usage times (dates and times).
- Ticket type and validity period.

- Recharged amounts (currency or usage rights).
- Device information for the last transaction.
- Fare deductions and remaining balance.
- Vehicle and route details for each transaction.

2.5.5 Applications for Data Insights

The statistical reports generated from the data can be used as follows:

- Improving passenger satisfaction through targeted actions.
- Optimization of routes and schedules.
- Adjust fares and transfer policies.
- Plan additional services during peak demand.
- Reduce the number of vehicles on underutilized routes.
- Analysis of passenger profiles and ticket usage patterns.
- Passenger distribution maps were generated across the network.

Additionally, data are critical for calculating financial revenue shares, enabling effective governance and operational decision making.

2.6 Calculation of Revenue Shares

The revenue shares among public transportation operators, administrative bodies, infrastructure providers, and technology companies are periodically distributed based on predefined regulations. The calculations rely on data such as passenger boarding counts and vehicle kilometers traveled. The revenue distribution was designed to be standardized, secure, and conducted in real-time.

2.6.1 Criteria for Revenue Allocation

The key performance criteria for revenue allocation include the following.

- Compliance with traffic and system rules.
- Adherence to operational schedules.
- Technical adequacy of vehicles and services.

- Cleanliness and passenger satisfaction.
- Avoidance of bus stop violations.

Inspections were conducted to ensure compliance, and penalties were applied for any deficiencies or errors according to performance standards. Payments to transportation operators are determined based on kilometers traveled or passenger counts, depending on the agreed-upon model.

2.6.2 Revenue Distribution Models

Revenue-sharing ratios vary according to city and stakeholder agreements. Common models include:

- Kilometer-Based Payments: Operators are compensated based on the distance traveled by their vehicles.
- Passenger-based Payments: Payments are determined by the number of passengers transported.
- Combined Models: A combination of kilometers traveled and passenger counts was used to calculate payments.

Specialized software and services facilitate the implementation of varying revenue-sharing ratios for different cities or stakeholders within the same city. This allows each bus to be evaluated as an independent entity with separate revenue-share calculations.

2.6.3 Payment Schedules

Payments to operators are typically weekly or monthly. Additionally, revenues from advertisements displayed on metros, trams, ferries, and buses were partially or fully allocated to local authorities under the agreement.

2.6.4 Customization and Flexibility

Revenue distribution systems incorporate software tools that enable flexible adjustments to satisfy the unique needs of various regions and stakeholders. This ensures equitable and transparent revenue sharing, and enhances the financial efficiency of public transportation systems.

3. PASSENGER TICKET TYPES

Passenger tickets can vary from paper tickets to different versions of electronic tickets. While small- and medium-sized settlements may not require complex technologies and infrastructure, relying instead on cash, tokens, or paper ticket applications, larger cities with high passenger volumes and tiered fare systems necessitate more advanced technologies such as magnetic or smart cards.

3.1 Magnetic Stripe Tickets

Magnetic stripe tickets are made from paper or plastic materials, and store information about the ticket's value and usage on the back. This fare payment method involves electronic readers who check the ticket's validity for a boarded vehicle or deduct the appropriate fare amount from the ticket balance. Magnetic technology can be either read-only (e.g., for daily use) or read-written (e.g., when balance decreases with each use). Magnetic stripe tickets, which address many of the disadvantages of paper tickets, are still used in some cities, particularly single-use tickets. The use of magnetic stripe tickets in fare collection systems dates to the 1960s, when they were first implemented in rail systems. These tickets can be made from paper or plastic, and depending on the context, they may feature printed information such as the remaining balance. Magnetic stripe tickets made of paper contained printed data.

3.1.1 Advantages of Magnetic Stripe Tickets

- Cost Efficiency: Compared to other electronic systems, magnetic strip tickets are more affordable.
- Adaptability: These can easily be integrated into various payment systems in different regions.

3.1.2 Disadvantages of Magnetic Stripe Tickets

- Longer Validation Times: Magnetic stripe tickets require longer processing times than smart cards do.
- Duplication Risks: Magnetic stripes are more susceptible to copying.
- Higher Maintenance Costs: Equipment maintenance for magnetic stripe ticket systems is costlier than for smart card systems.
- Infrastructure Dependency: A support system involving a sales network and an electronic fare collection infrastructure is necessary.

- Reader Costs: Magnetic stripe ticket readers are more expensive than contactless smart-card readers (Manikandan et al., 2015).

Despite their limitations, magnetic stripe tickets remain an essential element in the evolution of fare-collection systems, particularly in specific urban contexts or single-use applications.

3.2 Smart Cards

Smart cards such as magnetic stripe cards contain computer chips. Contactless smart cards communicate with a terminal (reader) via radio waves to read, evaluate, and store the data. They are designed to fit into a wallet or pocket and operate through integrated circuits. The card itself is passive, and the reader accesses the card to perform the read/write operations. Contactless smart cards adhere to ISO/IEC 14443 standards, which are of two types: A and B. An alternative standard, ISO/IEC 15693, supports reading distances up to 50 mm but is more commonly used for highway tolls and parking fees than public transportation ticketing.

3.2.1 Components of Smart Card Systems

Smart card systems may include the following.

- Fareboxes with smart-card readers.
- Smart Cards (Paper or Plastic).
- Station Software/Hardware.
- Garage Software/Hardware.
- Central Unit Software/Hardware.
- Contactless smart cards are categorized as follows.
- Memory Cards: Store basic data.
- Chip Cards: Incorporate microprocessors for advanced functionality.

These cards can be used by tapping them on a reader or bringing them within a certain proximity. They are versatile and are applicable to public transportation, parking payments, shopping, and university systems. Additionally, smart cards facilitate fare integration across different transportation modes.

3.2.2 Applications for Smart Cards

Smart-friendly cards have gained worldwide popularity and are the most widely used fare-collection tools in public transport systems. Prominent examples include the following.

- Easycard (Taiwan).
- Octopus Card (Hong Kong).
- T-Money (South Korea).
- Pasmo Card (Tokyo).
- Oyster Card (London).
- Istanbulkart (Istanbul).

3.2.3 Historical Development

The first smart cards were contact-based and were introduced in Europe in 1980 as prepaid phone cards. Microprocessor-enabled chip cards appeared later, allowing encrypted data storage on both the card and the reader. This innovation expanded its usage to include commerce, banking, and so on. The data processing time for these cards was approximately one-fifth of a second. Early smart cards required longer processing times for added security; however, advancements in microprocessors significantly reduced these delays.

3.2.4 Dual-Interface Cards

The demand for multifunctionality has led to the development of dual-interface cards that combine contactless and contactless capabilities. These cards allow a seamless transition between retail transactions (using POS devices) and public transportation (via contactless readers).

3.2.5 Advantages of Smart Cards

- Faster Processing: Reduces boarding time in driver-controlled systems.
- Convenience: Allows usage without removing the card from wallets or bags.
- Durability: Less prone to damage from foreign objects and requires less maintenance.
- Security: Offers enhanced protection against fraud and duplication.

- Flexible Installation: Compact devices provide installation versatility.
- Versatile Applications: Usable beyond public transport in areas such as banking, shopping, and university campuses.
- 3.2.6 Disadvantages of Smart Cards
- Infrastructure Requirements: Requires an electronic fare collection system with a sales network.
- Higher Production Costs: More expensive than magnetic stripe cards.

Smart cards represent a significant technological advancement in fare collection systems, balancing speed, security, and adaptability for a wide range of applications.

3.3 Mobile Payments

In many cities, along with systems ranging from paper tickets to smart cards, payment options are available through bank cards issued by financial institutions and smartphones. However, payments made using bank cards are often not appealing because of their limited flexibility for single use and lack of integration with ticketing systems. Mobile payments are particularly advantageous for occasional users such as those visiting from outside the city.

3.3.1 Challenges of Mobile Payments

- Coordination Issues: Coordination difficulties between private institutions and public transport operators.
- Lack Of Integration: Incomplete integration with ticketing systems.
- Limited Transfers: Lack of options for multiple transfers.
- Higher Costs: Unit fare charges are typically higher than those of the other payment methods.

3.3.2 Mobile Ticketing Applications

In addition to bank cards, mobile ticketing applications installed on smartphones allow phones to function as smart cards. These applications enable users to use

- They use their phones as tickets for compatible recharging and spending devices.

- Recharge smart cards are defined on smartphones that use mobile credit card applications.
- Automate the top-ups when the balance falls below a preset threshold, as observed in highway and bridge toll systems.

Mobile payment systems offer flexibility and convenience but require better integration with public transportation networks to become more widely adopted.

3.4 Passenger Tickets by Usage Type

Passenger tickets can be categorized into two main types based on their usage: disposable and reloadable tickets**.**

3.4.1 Disposable Tickets

Disposable tickets are primarily designed for individuals who do not live in the city or use public transportation infrequently, typically for single-entry trips. Depending on the size of the city and its transportation system, these tickets are available as one-, three-, five, or 10-ride options and are still in active use. Although disposable tickets are made from paper, they can also be produced using thin PVC or PET materials. These tickets can be defined as transfer or non-transfer tickets, with limited usage rights.

3.4.2 Reloadable Tickets

Reloadable tickets are tailored to regular public transport users, who can add credit as needed. These tickets can be used until the end of their physical lifespan and may vary based on passenger and travel profiles. Types of reloadable tickets

Credit-Based Tickets: Deduct fares according to the specific fare rates of the boarded vehicle.

Subscription Tickets: Provides access based on travel rights. Examples include:

- 7-Day, 15-Day, Or 30-Day Tickets: Valid for the specified duration from the purchase date or first use.
- Seasonal Tickets (3-Month Validity): This includes options such as tourist cards with limited duration and usage rights.
- Single-tickets: Allow one journey or multiple trips within a set time (e.g., 1–1.5 h).

- Round-trip tickets: Provides a journey to and from a destination.
- Multi-Ride Tickets: Offered in 5-, 10-, or 20-ride bundles.
- Seasonal asses: Available daily, weekly, monthly, or yearly.
- Combined Tickets: Enable parking and continuation of public transit.
- Group or Family Tickets: Designed for multiple users.

3.4.3 Special Fare Categories

The system also supports free, discounted, or restricted access tickets based on decisions made by public transport authorities and central administration.

- Senior Citizens (60+, 65+ years).
- Persons With Disabilities and Their Caregivers.
- Military Personnel and Police.
- Public Sector Employees (e.g., PTT Workers, Municipal Staff).
- Professionals (Judges, Prosecutors, Teachers, Journalists).
- Students.
- National Athletes (Annual Ride Limits).
- Martyrs' families, war veterans, and relatives.
- Public Transportation Inspectors.

These tickets provide equitable access to public transportation services and cater to diverse passenger demographics.

4. PASSENGER TICKET PRICING IN PUBLIC TRANSPORTATION

Passenger ticket pricing plays a crucial role in public transportation policy. Decisions regarding pricing should be made during the initial stages of transportation planning because they directly affect the operational processes and design of the system.

4.1 Passenger Ticket Pricing

There are two primary types of passenger ticket pricing policies for public transportation: flat fare and tiered fare policies.

4.1.1 Flat Fare Policies

Flat fare systems charge the same price, regardless of the passenger, distance traveled, travel day, or service quality. This system simplifies fare payments and prevents potential confusion and disputes among the operators. This is straightforward to implement. However, applying the same fare to long-distance trips or special service routes with higher operational costs may be unfair. Additionally, flat fare systems have lower revenue potential than tiered fare policies.

4.1.2 Tiered Fare Policies

Tiered fare systems enhance revenue potential and increase the system complexity. For example, London's zonal fare system has successfully distributed passenger densities more evenly (Glaister and Lewis, 1978). The tiered fare policies were implemented in four ways.

- Distance-Based or Zonal Pricing: Fares are determined based on the distance traveled.
- Time-Based Pricing: Fares vary depending on the day of the week or the time of travel (e.g., lower fares during weekends or off-peak hours).
- Service-Based Pricing: Fares differ based on the type and quality of service provided (e.g., higher fares for express routes or tourist-oriented city tours).
- Free or Discounted Pricing Based on Service or Region: In specific areas (e.g., parts of city centers) or special-purpose routes (e.g., those integrated with other transportation modes), fares may be waived or offered at a discounted rate.

4.2. Comparison of Flat and Tiered Fare Policies

- Flat Fare Policies are simpler and easier to understand but may be perceived as less fair and generate lower revenue.
- Tiered Fare Policies are considered fairer and have a higher revenue potential but may be harder for passengers to comprehend owing to the variety of fare structures.

Tiered fare systems balance equity and financial efficiency but require careful communication and design to ensure passenger understanding and satisfaction.

4.3. Passenger Ticket Fare Collection Methods

Modern electronic ticketing systems enable fare collection through validators in vehicles, stops, stations, and piers, similar to paper tickets. Validators for rubber-tired systems are usually located inside vehicles, whereas metro, tram, and ferry systems often feature turnstile-based validators at stations or piers. Another widely implemented approach in countries with developed public transportation cultures is the open-access system, where ticket validation is not required at entry. Periodic in-vehicle inspections impose heavy fines on fare evaders to ensure compliance.

4.3.1 Driver-Controlled Onboard Validator Fare Collection Systems

In these systems, the driver directly monitors payment immediately after boarding. Typically, a fare collection box and/or a separate device for magnetic or smart-card transactions is positioned next to the driver. The subsystems for this method include the following.

- Smart Card Readers with Electronic Fare Boxes
- Validators For Magnetic and Contactless Cards
- Vehicle-Based Validator Counter Readers
- Validator Counter Readers at Stations, Garages, And Terminals

These systems are cost-effective because they do not require an external infrastructure. They also effectively prevent fare evasion. However, requiring passengers to board through a single door and pay upon entry significantly increases waiting times at stops, particularly on busy routes. In addition, the processing and consolidation of data from individual validators as well as maintenance and revenue calculations require additional manpower.

4.3.2 Conductor-Controlled Onboard Validator Fare Collection Systems

In these systems, conductors onboard check tickets or sell them to the passengers. All passengers were verified. The required subsystems include the following.

- Station Software/Hardware
- Garage Software/Hardware
- Central Unit Software/Hardware

Unlike driver-controlled systems, passenger boarding times are shorter as payments are processed onboard, thereby reducing waiting times at stops. However, these systems require a higher workforce than alternatives.

- Supervisors (1 per 350-400 passengers)
- Maintenance Personnel (1 per 25 validators)
- Revenue Calculation Officers (1 per 25 validators)
- Data Processing/Recording Officers (1 per 15,000 boardings)
- Security Personnel (1 per 15 stops)
- Ticket Sales Personnel (1 per 3,000 passengers)

Conductor-controlled systems are more suitable for long-distance routes in less urbanized areas but are less efficient for high-traffic or short-distance routes.

4.3.3 Turnstile-Based Offboard Fare Collection Systems

In metro, tram, and ferry systems, passengers validate tickets using turnstiles, either by inserting tickets or by tapping smart cards. Turnstile systems are also used in rubber-tired systems such as Bus Rapid Transit (BRT). Because fare collection occurs offboard, delays caused by payments during boarding are minimized. Turnstiles reduce fare evasion compared with open-access systems. However, turnstiles require additional physical space at stops, which makes their implementation in confined areas challenging. They also need separate accessible passageways for the disadvantaged groups. Turnstile-based systems are the most expensive to implement, owing to the additional cost of turnstiles. The workforce requirements include the following.

- Maintenance Personnel (1 per 25 validators)
- Revenue Calculation Officers (1 per 25 validators)
- Security Personnel (1 per stop)
- Data Processing/Recording Officers (1 per 15,000 boardings)
- Ticket Sales Personnel (1 per 3,000 passengers)

4.3.4 Open-Access Fare Collection Systems Without Turnstiles

In open-access systems without turnstiles, passengers validate their tickets randomly during onboard inspections conducted by the roving personnel. The required subsystems include the following.

- Validators
- Smart Card Processors for Validators
- Wall-Mounted Validators at Stops And Stations
- Handheld Validators
- Station Software/Hardware
- Garage Software/Hardware
- Central Unit Software/Hardware

Passenger boards through multiple doors, thereby reducing the stop waiting times. Onboard inspections focus on ticket validation rather than fare collection, which requires less supervision than conductor-controlled systems do. However, these systems carry a high risk of evading fares. Inspection strategies should be planned to mitigate this risk effectively. The workforce requirements include the following:

- Roving Inspection Officers (1 per 3,000 passengers)
- Maintenance Personnel (1 per 25 validators)
- Revenue Calculation Officers (1 per 25 validators)
- Data Processing/Recording Officers (1 per 15,000 boardings)
- Security Personnel (1 per 15 stops)
- Ticket Sales Personnel (1 per 3,000 passengers)

These methods provide flexibility in various public transportation contexts by balancing costs, efficiency, and passenger convenience. The structure of passenger fare collection systems varies depending on the city, operator, fleet size, and the technology employed. The cost of fare collection for operators ranges from approximately 1% to 3% of the total revenue collected. A significant portion of this expense is attributed to payments made to technology companies. Other costs include commissions paid to ticket sellers as a percentage of each

ticket's price; labor, energy, and maintenance required for ticket and token machines; and salaries for personnel involved in the overall development and management of the system. Another aspect of passenger fare collection systems is their ability to provide datasets related to trips, including information on the time, region, and passenger profiles. These data are crucial for urban public transportation planning, enabling route and network optimization, and the creation of new lines and routes. Such insights contribute significantly to the enhancement of urban mobility and transportation system efficiency. A comparison of the fare collection systems is presented in Table 2.

Table 2. Comparison of Passenger Fare Collection Methods

Factor	**Offboard Fare Collection without Turnstiles**	**Offboard Fare Collection with Turnstiles**	**Onboard Conductor-Controlled Validator**	**Onboard Driver-Controlled Validator**
Equipment Required	Ticket vending machines, validators, retail sales equipment, manual inspection devices	Turnstiles, ticket vending machines	Ticket vending machines, validators, retail sales equipment, manual inspection devices	Validators, ticket processing units
Stop Characteristics	Open or platform stops	Additional physical space for turnstiles and vending machines, planned entry and exits	Open platforms	-
Passenger Density	May cause challenges with inspections in crowded vehicles; require numerous validators	Fare collection is unaffected by density	Inspections may be challenging in crowded vehicles	Slow boarding
Fare Evasion	Depends on inspection frequency, deterrent penalties, and passenger density	Passengers may jump over turnstiles	Minimal as all fares are collected by the conductor; issues may arise during peak times	It depends on fraudulent cards and extreme passenger density
Transfers Between Modes	Possible	Requires shared equipment between systems	Managed by conductors	Requires special arrangements
Regional Pricing	Difficult to implement; requires origin-based validation	Requires turnstiles at exits and refund machines	-	Passengers must inform drivers of destination for payment
Automatic Fare Collection (AFC)	Electronic tickets and cards; inspectors require handheld readers	Cards are tapped at turnstiles; errors are immediately detected, and access is denied	Conductors require handheld readers and	Processing units and card readers required; fare changes may cause issues

			processing units	
Security and Customer Services	Inspectors are present at stops and on vehicles; additional security may be needed	Security may be required at stops and on vehicles if no staff are present	Conductors are present on all vehicles	Driver is responsible for security and customer services
Ease of Payment	Queues may form for top-ups on multi-use or stored-value cards, but boarding is smooth	Depending on accepted payment types at turnstiles; cash payments may cause queues	No preloading required; no queues during payments or boarding	Requires pre-payment or instant payment; queues may form

5. CONCLUSION AND EVALUATION

The study of Fare Collection Systems emphasizes the importance of public transportation, highlighting its role not only in generating revenue, efficiently utilizing resources, and ensuring financial viability but also in improving passenger satisfaction, accessibility, and operational efficiency. Fare collection in public transportation refers to the process of collecting fees from passengers to access and use the transportation. This process typically involves tickets, cards, and mobile applications (apps). Effective functioning of these systems is critical for the efficiency and operational success of public transportation services. Achieving efficiency in fare collection systems is essential for improving the service quality and addressing passenger needs. An accessible and easy-to-understand fare-collection system is necessary for all passengers. Ticketing operations should be simple, fast, and practical, enabling seamless payments through integrated systems across various transportation modes (e.g., buses, subways, trams, and ferries). Such integration is crucial for achieving system-wide optimization and user convenience. Another important aspect is the management of revenue distribution and operational oversight by public-transport authorities. This includes fee collection from passengers, revenue allocation to operators, monitoring payment processes, tracking passenger counts, and ensuring the system performance. Fare policies should be fair to all passengers and include supportive tariffs for special groups, such as students, elderly individuals, and people with disabilities. Additionally, fare structures should encourage the widespread usage of the public transport network, ensuring its long-term viability.

Accurate fare collection and effective management of this process are critical for covering the operational costs of public-transport systems and making them

accessible to everyone. Historically, fare collection has relied on low-cost, straightforward methods such as paper tickets, cash payments, and manual processes requiring minimal technological input. However, advancements have shifted the focus to technology-driven applications that offer faster payment options, revenue management, and data-analysis capabilities. Modern fare collection systems contribute not only to financial efficiency but also to improving accessibility, service quality, and digital transformation. These systems facilitate seamless ticketing across transportation modes, thereby allowing passengers to use the same cards across buses, metros, and trams. They also supported the data collection and analysis for better urban mobility planning. Adopting fair pricing policies and offering concessions to specific groups, such as students, elderly individuals, and people with disabilities, exemplify inclusive transportation systems. Additionally, innovations such as electronic tickets, smart cards, and mobile payment methods reduce reliance on paper tickets and minimize environmental impact. The digitization of fare collection enhances data management and analysis, improves efficiency, and enables more effective transportation planning. In conclusion, sustainable fare collection systems in public transportation serve as critical tools not only to ensure financial viability but also to enhance user satisfaction and reduce environmental impacts. Technological advancements such as digitization, automation, and data analytics will further enhance the success and effectiveness of these systems in the future.

Acknowledgment

The authors declare no conflicts of interest. This research was conducted independently and adhered to scientific ethics and academic standards. This book chapter, based on the chapter titled 'Sustainable Fare Collection Systems in Public Transportation' in Turkish, from the book Advancements in Engineering (Platanus Publishing, December 2024, ISBN: 978-625-6634-59-6, DOI: 10.5281/zenodo.14576846), has been prepared to meet the needs of institutions and organizations providing English-language education on this topic in academic settings.

REFERENCES

Al-Sakran, H. O. (2015). Intelligent traffic information system based on integration of IoT and agent technology. *International Journal of Advanced Computer Science and Applications (IJACSA), 6*(2), 23–29. http://dx.doi.org/10.14569/IJACSA.2015.060206.

Bandyopadhyay, D., Sen, J. (2011). The Internet of Things - Applications and challenges in technology and standardization. *Wireless Personal Communications, 58*(1), 49–69. http://dx.doi.org/10.1007/s11277-011-0288-5.

Bieler, M., Skretting, A., Büdinger, P., Grønli, T. M. (2022). Survey of automated fare collection solutions in public transportation. *IEEE Transactions on Intelligent Transportation Systems, 23*(9), 14248–14252. https://doi.org/10.1109/TITS.2022.3161606.

Durgaprasad, C., & Rajesh, G. (2016). Automatic fare collection system in public transportation. *International Journal of Scientific Engineering and Technology Research, 5*(47), 9631–9633.

Faroqi, H., Mesbah, M., Kim, J. (2018). Applications of transit smart cards beyond a fare collection tool: A literature review. *Advances in Transportation Studies: An International Journal, Section B, 45*, 107–110. https://doi.org/10.4399/978255166098.

Glaister, S. and Lewis, D. (1978). An integrated fares policy for transport in London. *Journal of Public Economics 9*(3): 341–355. https://doi.org/10.1016/0047-2727(78)90015-4.

Gyger, T., and Desjeux, O. (2001). EasyRide: Active transponders for a fare collection system. *IEEE Micro, 21*(6), 36–42. https://doi.org/10.1109/40.977756.

Hatipoğlu, S. (2017). Otobüs sistemi ücret ödeme şekli ve çeşitliliğinin dünya örnekleri incelenerek Ankara için modellenmesi. *Ankara Araştırmaları Dergisi, 5*(2), 273–282. (in Turkish). https://doi.org/10.5505/jas.2017.30932.

Isern-Deyà, A. P., Vives-Guasch, A., Mut-Puigserver, M., Payeras-Capellà, M., & Castellà-Roca, J. (2012). A secure automatic fare collection system for time-based or distance-based services with revocable anonymity for users. *The Computer Journal, 56*(10), 1198–1215. https://doi.org/10. 1093/comjnl/bxs033.

Jose, S., Anto, D., Robin, K. M., & Kumar, S. (2020). Literature Survey on Current Public Bus Transportation. *International Journal of Scientific Research & Engineering Trends, 6*(1), ISSN (Online): 2395-566X.

Joshi, A., Chavan, Y., Kale, A., Patkar, P., & Tawde, G. (2023). Automated public transport fare collection system using RFID. *International Journal of Engineering Research & Technology (IJERT) 12*(8): 1–8. https://doi.org/10.17577/IJERTV12IS080104.

Keote, M., Gaykwad, U., Sontakkey, S., Deshmukh, S., & Bansod, K. (2024). Design and development of automatic bus fare collection system using RFID technology. *Proceedings of the 5th International Conference for Emerging Technology (INCET)*, Karnataka, India. 1–5. https://doi.org/10.1109/INCET61516.2024.10592980.

Kelagadi, H. M., Kumar, N., Laxmikant, S. A., & Mrityunjaya, D. H. (2017). Smart transportation using IoT technologies. *International Conference on IoT in Social, Mobile, Analytics, and Cloud (I-SMAC)*, 1–5, IEEE Catalog Number: CFP17OSV-POD, ISBN: 978-1-5090-3244-0, Palladam, Tamil Nadu, India 10-11 February.

Li, D., Lin, Y., Zhao, X., Song, H., & Zou, N. (2011). Estimating a transit passenger trip origin-destination matrix using automatic fare collection systems. *Lecture Notes in Computer Science, 6637*, 502–513. https://doi.org/10.1007/978-3-642-20244-5_48.

Lopez, T. S., Ranasinghe, D. C., & McFarlane, D. (2012). Adding sense to the Internet of Things: An architecture framework for smart object systems. *Personal and Ubiquitous Computing, 16*(3), 291–308. https://doi.org/10.1007/s00779-011-0399-8.

Manikandan, T., Kalaiyarasi, G., & Priyadarshini, P. K., & Priyaranga, P. R. (2015). Conductorless bus ticketing system using RFID and information through GPS and GSM. *International Journal of Innovative Science, Engineering & Technology, 2*(9), 884–893.

Miorandi, D., Sicari, S., Pellegrini, F. D., Chlamtac, I. (2012). Internet of Things: Vision, applications and research challenges. *Ad Hoc Networks, 10*(2012), 1497–1516. http://dx.doi.org/10.1016/j.adhoc.2012.02.016.

Salim, K. A., & Idrees, I. M. (2013). Design and implementation of web-based GPS-GPRS vehicle tracking system. *International Journal of Computer Science and Engineering Technology, 3*(12), 443–448.

Singh, D., Tripathi, G., Jara, A.J. (2014). A survey of Internet-of-Things: Future vision, architecture, challenges and services. *IEEE World Forum on Internet of Things, 1*, 287–292.

Svečko, J., Kotnik, B., Mezgec, Z., & Chowdhury, A. (2010). The Margento automated fare collection system solution for public transport. *Proceedings of the 7th International Conference on Logistics & Sustainable Transport, Maribor*, June 24–26, 2010, Slovenia.

Tellluri, P., Manam, S., Oli, J. (2019). Automated bus ticketing system using RFID. *IEEE 2nd International Conference on Intelligent Computing, Instrumentation, and Control Technology*, https://doi.org/10.1109/ICICICT46008.2019.8993159.

Tirachini, A., & Hensher, D. A. (2011). Bus congestion, optimal infrastructure investment, and the choice of a fare collection system in dedicated bus corridors. *Transportation Research Part B: Methodological, Elsevier*, *45*(5), 828–844. https://doi.org/10.1016/j.trb.2011.02.006.

Utsunomiya, M., Attanucci, J., and Wilson, N. (2006). Potential uses of transit smart card registration and transaction data to improve transit planning. *Transportation Research Record: Journal of the Transportation Research Board, 1971(1)*: 119–126. https://doi.org/10.1177/0361198106197100114.

Witvoet, K., Vidal, C., Stiene, T., & Emadi, A. (2024). Towards frictionless public transit: A brief review of automatic fare collection. *IEEE International Conference on Smart Mobility 87–92, Niagara Falls, ON, Canada*. https://doi.org/10.1109/SM63044.2024.10733519.

Zanella, A., Bui, N., Castellani, A., Vangelista, L., Zorzi, M. (2014). Internet of Things for smart cities. *IEEE Internet of Things Journal, 1*(1), 22–32. https://doi.org/10.1109/JIOT.2014.2306328.

Zhao, J., Rahbee, A., & Wilson, N. H. M. (2007). Estimating a rail passenger trip origin-destination matrix using automatic data collection systems. *Computer-Aided Civil and Infrastructure Engineering*, *22*(5), 376–387. https://doi.org/10.1111/j.1467-8667.2007.00494.x.

Zhu, Y., Zhu, X., Zhu, S., & Guo, S. (2012). Intelligent transportation system based on Internet of Things. *Proceedings of WAC*, 1–3, Puerto Vallarta, Mexico.

CHAPTER 6

Non-Invasive Blood Glucose Level Monitoring

Muhammed Selman Erel[1] & İlyas Çankaya[2]

[1] Arş. Gör., Ankara Yıldırım Beyazıt Üniversitesi Elektrik-Elektronik Mühendisliği Bölümü
Orcid: 0000-0001-6719-0433
[2] Prof. Dr., Ankara Yıldırım Beyazıt Üniversitesi Elektrik-Elektronik Mühendisliği Bölümü
Orcid: 0000-0002-6072-3097

Technological developments, globalization and lifestyle-changing bring drawbacks in addition to benefits. Diabetes mellitus is one of such drawbacks brought by modernization. Diabetes mellitus is a disease in which physiological dysfunctions characterized by hyperglycemia due to insulin resistance, inadequate insulin secretion, or excessive glucagon secretion (Ignatavicius & Workman, 2016; Lewis, Dirksen, Heitkemper, & Bucher, 2014). There are many people suffering from diabetes in both developing and developed countries. In 2021, globally, 537 million people is diagnosed as diabetes mellitus and this is expected to rise to 783 million adults with diabetes by 2045 Forouhi & Wareham (2022). It remarkable changes not only societies, political systems and environment, but also economical systems. Economic burden of diabetes is 1.32 trillion $ in 2015, which is 1.8% of global GDP, and it is projected that baseline scenario, past trends scenario and target scenario are 2.25, 2.48 and 2.12 trillion $ for economic burden of diabetes mellitus for 2030, respectively (Bommer et al., 2018). Although researchers have not identified a definitive reason through academic inquiry for diabetes mellitus, there are several factors contribute to development of diabetes: Genetics, obesity, insulin resistance, autoimmune factors, age, physical inactivity, ethnicity, hormonal changes (see figure 1). There are mainly two types of diabetes mellitus: type-1 diabetes and type-2 diabetes. Type-1 diabetes (T1D) is an autoimmune disorder in which pancreatic insulin-producing beta cells are destructed by immune system. Without insulin, human body cannot consume blood glucose properly and blood sugar level is increased. Type-2 diabetes (T2D) is chronic metabolic disorder, which is more common than T1D, in which body's cells cannot respond properly to insulin due to insulin resistance. Therefore, pancreas loses it's ability to produce enough insulin. As the concentration of insulin diminishes, a concomitant reduction in blood glucose levels is observed.

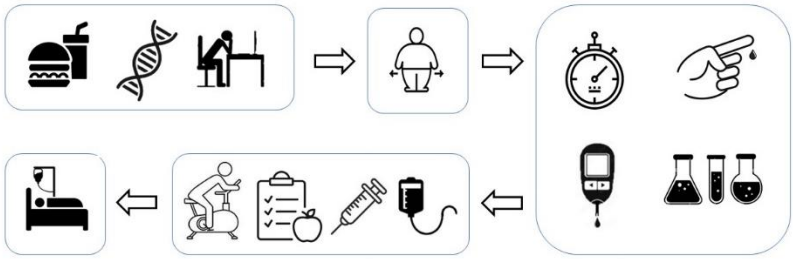

Figure 1. Progression-flow of Diabetes Mellitus

Self-monitoring of Blood Glucose Monitoring

Self-monitoring of blood glucose (SMBG) is one of the important methods for continuous glucose monitoring (CGM). It is important because it provides short-term and long-term glycemic control, immediate feedback for nutritional intakes, physical exercises and drugs. It can benefit to prognose diabetes by developing an individualized blood glucose profile, providing people with diabetes day-by-day blood glucose monitoring, improving personal consciousness for the people with diabetes and their relatives to hyperglycemia and hypoglycemia, intervening during severe illnesses and mild stress periods, improving quality of life by reducing risk of acute and chronic complications, providing long-term monitoring trend for blood glucose during illnesses, endocrinal or psychological problems, motivating to fight diabetes. SMBG is recommended for T1D patients, T2D patients, individuals receiving insulin support, pregnant, athletes, people with the risk of hyperglycemia and hypoglycemia. Frequency of SMBG varies from person to person. SMBG is done during fasting, before meals, before sleeping, before and after insulin treatment. Most experts recommend that patients with insulin treatment should monitor their blood glucose level four times a day(Benjamin, 2002). Blood glucose test results can be recorded in logbook. Modern SMBG devices have electronic memory. It is possible to recall previous test results. SMBG is performed by "point-of-care" (POC) devices called portable glucose meter.

Figure 2. Needle Anxiety developed in children

Portable Glucose Meter

Portable glucose meter (PGM) as a “point-of-care” (POC) device is used to measure glucose level in blood. It is a compact but powerful gadget democratizing diabetes management with its portability and immediate monitoring capabilities. By taking minimum amount of blood, which is done by pricking the finger with a specialized tool named lancet, blood is analyzed. Lancet is a tool having sharp but sterile needle to prick the finger for blood sampling easily. Sanitation should be concerned while using it. After pricking the finger, blood is placed on a test strip thanks to capillary effect. These test strips having several layers of materials include specialized enzymes. Reaction between blood sample and the test strip enzyme creates an electron flow. This electrical current is sensed by the device and conditioned to monitor glucose level in blood. The amperometry utilized in glucometer is favored in many devices because of instant but reliable test results (Jaffari & Turner, 1995). The portable glucose meter device is recommended for individuals having diabetes managements who need frequent glucose monitoring, individuals at the risk of diabetes, people with concern of self-healthcare to regulate dietary, medication, exercise, illness, stress and dehydration. Thanks to giving instant test results on the go and at home, this point-of-care device can be utilized by diabetic patients, obese people, caregivers of patients, athletes, security officers and astronauts. Advantages of PGMs are portability, immediate test results and improved management. Without hospitalization, It can give immediate test results in almost anywhere at anytime. Thanks to it’s digital storage features, it is possible to monitor the trend of blood glucose level for a desired interval. Contrary to advantages, PGMs have drawbacks, too. Accuracy concern is the first drawback for PGMs. Although PGMs have same working principal, accuracy can differ from device to device. Also, test strip quality, calibration issue and user error are other sources for accuracy problem. Second drawback is limitation in monitoring. PGMs determine a single blood glucose level at a specific time. To obtain more results, pricking the fingers more is needed and it hurts patient. The last and the major drawback is discomfort. To obtain a test result, sampling is based on an invasive principle and pricking is essential. It is uncomfortable and painful for especially frequent monitoring. Also, needle phobia builds anxiety to PGMs.

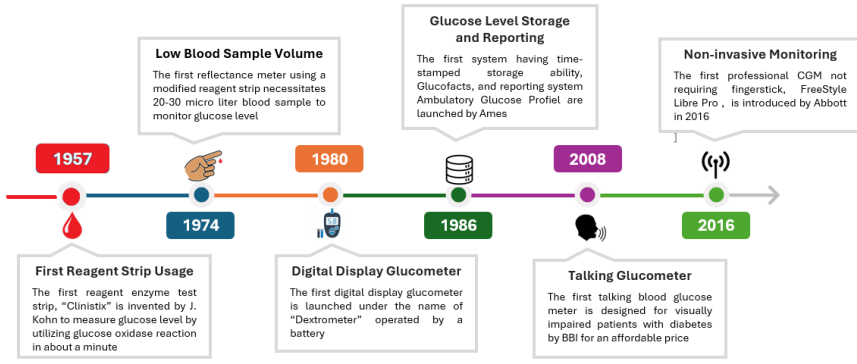

Figure 3. Timeline of Blood Glucose Meter

Non-invasive Glucose Monitoring

Traditional blood glucose monitoring methods have many drawbacks like finger-pricking, risk of infection and limited data. Addressing all disadvantages related to invasive blood glucose monitoring, non-invasive glucose monitoring (NIGM) presents a potential alternative to PGMs. Non-invasive glucose monitoring (NIGM) method is a technique for measuring glucose levels of diabetic patients non-invasively from body fluids. It does not require pricking the fingers or drawing blood. This technique eliminates all inconveniences and pains related to in-vivo monitoring. In NIGM, glucose level is monitored in multiple ways: electrical, optical and ultrasound. There are numerous benefits of non-invasive glucose monitoring (NIGM) over traditional glucose monitoring. NIGM is painless compared to traditional monitoring. It eliminates pricking needless and it is less invasive for diabetic people. NIGM is more convenient to use than conventional methods. It often includes wearable devices or sensors as a point of care devices to measure blood level continuously in the natural course of life. Unlike the old-fashioned methods, which provides single-shot measurement, NIGM presents real-time monitoring to regulate diet, physical activities and therapy to obtain ideal glucose level. By eliminating painful in-vivo measurement, it reduces the risk of infection and skin irritation related to pricking. It enhances quality of life for people with diabetes and with the risk of diabetes. It can be utilized by diabetic people, athletes, bedridden patients and health-conscious individuals with peace of mind.

1.1. Human Blood Composition and Glucose

Human Blood Components (HBC) are vital for maintaining overall health, homeostasis and body functions. Blood is made up of four components: Plasma, red blood cells, white blood cells and platelets. Red blood cells responsible for transmitting oxygen in body, white blood cells are responsible for defending the body against infections and foreign invaders and platelets are responsible for wound healing. Plasma is the majority of blood, making up about %55 of whole volume, including proteins, hormones, waste products and nutrients. Glucose is one of the most important component providing energy for body's cells. It should be regulated without fluctuations, ups or downs, to provide homeostasis. Components of human blood plasma and their concentrations and weights in the whole are given in the table 1.

Table 1. Human Blood Composition

Component	**Concentration (mg/dL)**	**mg/100g (Range)**	**mg/100g (Average)**	**% weight for mg/100g**
Total Proteins	6000-8000	5714.29-7619.05	6666.67	6.66667
Albumin	3500-5000	3333.33-4761.90	4047.62	4.04762
Globulins	2000-3500	1904.76-3333.33	2619.05	2.61905
Fibrinogen	200-450	190.48-428.57	309.53	0.30953
Sodium (Na^+)	3100-3300	2952.38-3142.86	3047.62	3.04762
Potassium (K^+)	140-200	133.33-190.48	161.91	0.16191
Calcium (Ca^{2+})	8.5-10.5	8.10-10.00	9.05	0.00905
Chloride (Cl^-)	3500-3800	3333.33-3619.05	3476.19	3.47619
Bicarbonate (HCO_3^-)	1300-1700	1238.10-1619.05	1428.58	1.42858
Glucose	**70-100**	**66.67-95.24**	**80.96**	**0.08096**
Cholesterol (Total)	140-200	133.33-190.48	161.91	0.16191
Triglycerides	50-150	47.62-142.86	95.24	0.09524
Urea (BUN)	7-20	6.67-19.05	12.86	0.01286
Creatinine	0.6-1.2	0.57-1.14	0.86	0.00086
Vitamin A	0.02-0.06	0.02-0.06	0.04	0.00004
Vitamin D	0.03-0.1	0.03-0.10	0.07	0.00007
Vitamin E	0.5-1.5	0.48-1.43	0.96	0.00096

Vitamin K	0.00002-0.00032	0.00-0.00	1.14	0.00114
Vitamin C	0.4-2.0	0.38-1.90	0.01	0.00001
Vitamin B1 (Thiamine)	0.0025-0.0075	0.00-0.01	0.01	0.00001
Vitamin B2 (Riboflavin)	0.001-0.02	0.00-0.02	0.01	0.00001
Vitamin B3 (Niacin)	0.0005-0.008	0.00-0.01	0.02	0.00002
Vitamin B6 (Pyridoxine)	0.005-0.03	0.00-0.03	0	0

2. Non-INVASIVE GLUCOSE MONITORING METHODS

NIGM methods are basically under three modalities: Electrical methods, optical methods and physiological methods. They are given in the block-representation graph below.

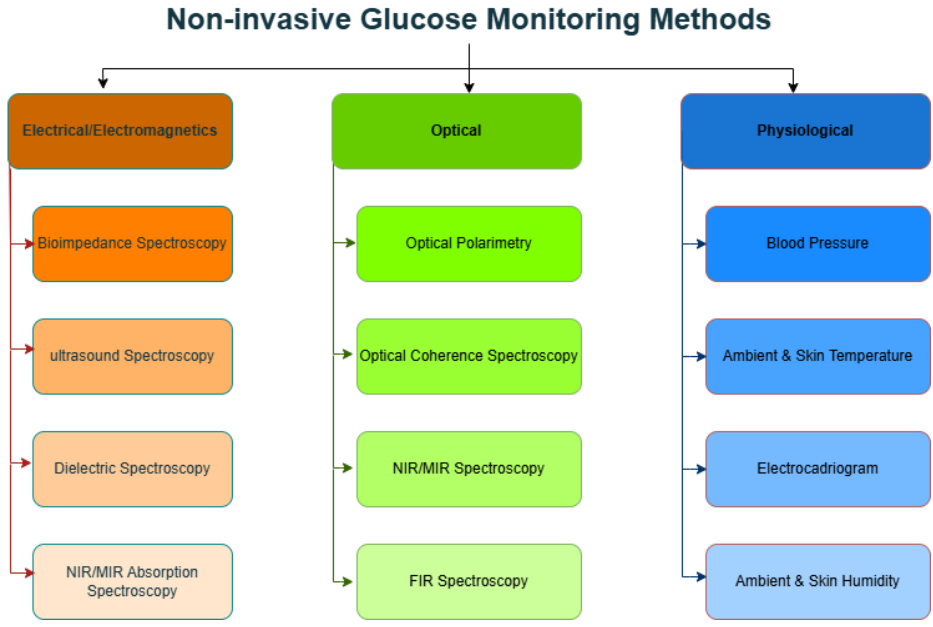

Figure 4. NIGM Methods under Electrical, Optical and Physiological

2.1. Electrical and Electromagnetics Methods

Electrical measurement technique holds a key position in non-invasive glucose monitoring by providing bright results for precise and convenient glucose level measurement as an alternative for traditional blood glucose monitoring

techniques. Dielectric spectroscopy, bioimpedance spectroscopy, RF/Microwave spectroscopy and ultrasound spectroscopy are electrical methods to measure blood glucose level in a non-invasive manner. By using electrical signals and processing responses from the target tissue or body fluids, such methods provide useful results without pricking. Although some methods appear as an end-user-friendly, some of them are still under development to boost portability, accuracy, precision and reliability while being a glimmer of hope for diabetes.

2.1.1. Dielectric Spectroscopy

Dielectric Spectroscopy is one of the painless solution that researchers studying dielectric properties of tissues or targets affected by glucose concentration variations. Dielectric is a material which is polarized under electric field. Due to being a polar molecule of glucose, dielectric property changes with the concentration of it, which provides indirect prediction of blood glucose level. Interaction of electric field with biological tissue includes relative permittivity and electrical conductivity. Conductivity is the ability to conduct electrical current. Relative permittivity is the ability to store electrical energy in electric field. Such figure of merits affected by concentration of glucose, hydration level and tissue composition. By considering both of these parameters, dielectric methods can provide an idea about glucose concentrations in tissues. Relative complex permittivity and underlying mathematical relations between glucose concentrations and dielectric properties are given below, derived from Debye's relaxation theory.

$$\varepsilon_r(\omega) = \varepsilon_r'(\omega) - j\varepsilon_r''(\omega) \quad (1)$$

$$\varepsilon_r = \varepsilon_\infty + \frac{\varepsilon_s - \varepsilon_\infty}{1 + j\omega\tau(\chi)} \quad (2)$$

$$\varepsilon_r = \varepsilon_\infty + \frac{\varepsilon_s - \varepsilon_\infty}{1 + j\omega\tau} + \frac{\sigma}{j\omega\varepsilon_\infty} \quad (3)$$

$$\varepsilon_r = \varepsilon_\infty + \frac{\varepsilon_s - \varepsilon_\infty}{1 + j\omega\tau^{1-\alpha}} \quad (4)$$

$$\varepsilon_r = \varepsilon_\infty + \frac{\varepsilon_s - \varepsilon_\infty}{1 + j\omega\tau^{1-\alpha}} + \frac{\sigma}{j\omega\varepsilon_\infty} \quad (5)$$

$\varepsilon_r'(\omega)$ is real part of the relative complex permittivity representing amount of stored energy inside the material whereas $\varepsilon_r''(\omega)$ is imaginary part of the relative complex permittivity representing amount of energy stored inside the material

(Farrugia et al., 2024)ε_s is static permittivity at lower frequencies, ε_∞ is permittivity at high frequencies, τ is characteristic relaxation time of the medium and χ is glucose concentration (Laha, Rajput, Laha, & Jadhav, 2022).

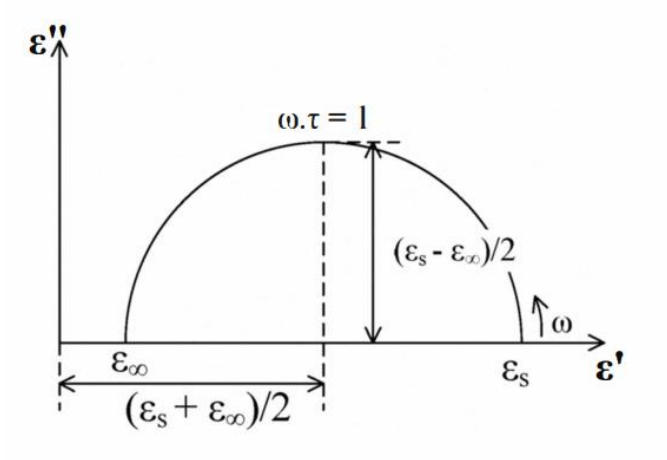

Figure 5. Complex Cole-cole Plane

Dextrose, known for its ability to mimic blood, stands as a pivotal component in non-invasive glucose monitoring (NIGM) research, offering a straightforward starting point for advancing studies in this field. ("EUCAP," n.d.) (Smulders, Buysse, & Huang, 2013) are some examples for dextrose studies in NIGM. In ("EUCAP," n.d.), they simulated blood with solutions by adding from %10 to %50 with steps of %10 weight into de-ionized water. They measured dielectric properties of solutions for the frequencies ranging from 200 MHz to 5 GHz. They observed that permittivity of solutions decreased as sugar concentration is increased whereas electrical conductivity increased. Although this study shows dielectric properties of dextrose in broad terms, results are still relatively far to represent realistic blood glucose levels. Nevertheless, this study serves as a valuable initial step towards illuminating blood glucose level monitoring despite the current limitations in accurately representing realistic blood glucose levels. In (Smulders et al., 2013), they measured dielectric properties of dextrose solutions with seven different glucose levels ranging from 0 mg/dl to 108,000mg/dl with the steps of 18,000 mg/dl. Although this study showed that increase in glucose level reduces permittivity of the dextrose solution in lower frequencies and vice versa for higher frequencies and increase in glucose level has effect on conductivity, which is smaller compared to effect on permittivity, dextrose glucose levels in this study is relatively far from human blood glucose

ranges,72 mg/dl – 216 mg/ dl for a healthy person (Yilmaz, Foster, & Hao, 2019) and ambulatory device's measurement range, up to 600 mg/dl (Philis-Tsimikas, Chang, & Miller, 2011). This study cannot be used to model blood glucose level. Nevertheless, studies having the wide glucose range are used to model glucose-dependent dielectric property change at room temperature (Turgul & Kale, 2015, 2016, 2018).

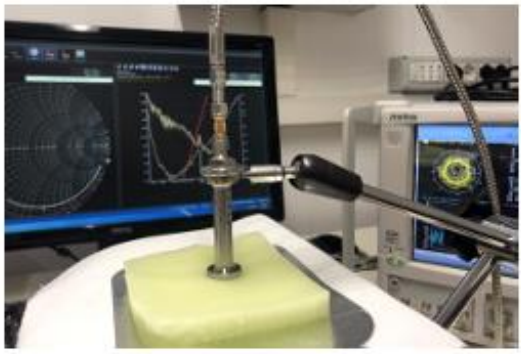

Figure 6. Test Setup in MW Lab at University of Calabria (Costanzo, Cioffi, Qureshi, & Borgia, 2021)

In the realm of non-invasive glucose monitoring, where complexity of real tissues introduce significant challenges, phantom studies emerge as pivotal studies emerge as pivotal research tools in early stages by providing invaluable insights and validations.(Yilmaz, Foster, & Hao, 2014) (Beam & Venkataraman, 2011) are key studies in phantom studies in NIGM. In (Yilmaz et al., 2014), they mimicked the dielectric properties of blood and other biological tissues they modeled wet skin, fat, blood and muscle by using deionized water, gelatine, NaCl, oil, detergent and food coloring in different concentrations. They fabricated each layer of phantom by stirring, heating and leaving overnight to solidify one by one. They utilized a food coloring to distinguish each layer of the phantom. In (Beam & Venkataraman, 2011), they mixed components of water, sugar, salt and flour for blood mimicking phantom. Their recipe includes certain weight of components stated in (Karacolak, Moreland, & Topsakal, 2013a). They utilize sugar to imitate glucose in blood. They built a consensus on results between blood measurements and phantom measurements at higher frequencies, not for lower frequencies.

Exploring the biological tissue studies in non-invasive glucose measurement opens a gateway to dielectric property changes with higher precision and non-invasive manner. (Topsakal, Karacolak, & Moreland, 2011a) (Karacolak,

Moreland, & Topsakal, 2013b) are such of them. They studied blood plasma taken from 10 adults with the ages of 18 to 40 years by tuning blood glucose concentration from 0 mg/dl to 16000 mg/dl. They measured dielectric properties of blood plasma with a commercial coaxial dielectric probe for the frequency of between 0.5 GHz to 20 GHz. They fitted results to quadratic coefficients to obtain Cole-Cole parameters and they derived polynomials for model parameters. They concluded that as the glucose concentration increases relative permittivity and conductivity decreases gradually. (Venkataraman & Freer, 2011) is another work studied dielectric permittivity for non-invasive blood glucose monitoring. They studied 40 blood samples from 8 diabetic and 12 non-diabetic patients. Blood glucose concentrations of samples range from 79mg/dl to 330mg/dl. Just like previous work, they utilized dielectric probe kit to measure dielectric permittivity of blood samples. They fitted their results to two-pole Cole-Cole model and they concluded that for five blood samples between 80 mg/dl to 140 mg/dl, relative permittivity decreases. For other concentrations, results are not meaningful. It is due to noisy results due to low volume sample.

Antenna and resonator play a key role in advancing NIGM research, serving crucial components for transmission and reception of signals by enabling accurate and reliable monitoring advantage for diabetes mellitus. Various studies have proposed significant designs to measure glucose levels. (Megdad, Aldhaheri, & Sobahi, 2023a) (Mahnashi, Qureshi, Al-Shehri, & Attia, 2023a) can be considered among such studies. In study (Megdad et al., 2023a)they designed a narrowband and compact antenna resonating at 6.1 GHz with a gain of 3.3 dBi to measure blood glucose level without pricking. Their design is based on low-cost FR-4 substrate. They utilized finger phantom model constructed on electromagnetic simulation environment. Their phantom model has multiple layers including skin, fat, muscle, blood and bone. They conducted parametric analysis to determine best dimension values. They found different dielectric constants and resonant frequencies for different glucose concentrations. Another study having antenna design based on low-cost FR-4 materials is (Mahnashi et al., 2023a). In this study, they designed RF microstrip patch antennas working at 5.7 GHz. They not only designed antenna part but also whole RF-chain involving low-noise amplifier, bandpass filter and RF detector. This system differs from other studies having two individual antennas for transmission and reception. It ranges a very wide range of glucose concentration like(Topsakal, Karacolak, & Moreland, 2011b). Operating frequency of(Megdad, Aldhaheri, & Sobahi, 2023b) and (Mahnashi, Qureshi, Al-Shehri, & Attia, 2023b)resides in U-NII bands. They design their antenna for dual-band five rectangular slots. They not

only measured scattering parameters experimentally but also simulated glucose in water model empirically in simulation environment.

Operating frequency embodies a cornerstone of NIGM due to it's impact on penetration depth, signal strength and interaction with biological tissues. In spectroscopy of NIGM, electromagnetic (EM) waves interact with biological tissues to determine glucose level without blood sample. Frequency selection decide the depth at which EM waves can penetrate into the skin affecting accuracy and reliability seriously. While higher frequencies can penetrate shallow depths, convenient for surface-level measurements, lower frequencies can penetrate deeper depths by encountering higher signal attenuation and more interference affecting measurement accuracy and reliability. Numerous studies have utilized different frequency bands. Some of them are suitable for unlicensed usage, some of them are not.(Xiao, Yu, Li, Song, & Kikkawa, 2021) (Mohammadi, Mohammadi, Demir, & Kara, 2021) utilized microwave frequencies 0.4-2GHz, 2-3.5 GHz, 1.8-1.9 GHz, and 2-3 GHz bands, respectively. Although study used whole 2-3 GHz band and showed best S_{21} Magnitude performance for 2-2.5 GHz, it is possible to being prototyped and work on 2.4 GHz ISM band independently. Contrary to other studies,(Mohammadi et al., 2021) used 4-port antenna circuit. They used S_{31} in their study to measure glucose concentration and it showed best performance at different frequencies at different glucose levels. However, it is also possible to being prototyped and work on 2.4 GHz ISM band independently though some optimizations should be performed for out-of-band frequencies. (Jang, Park, Lee, Yun, & Yook, 2020) is another study to work on 2.4 GHz ISM band. Transmission and resonance frequencies of the system are 2.45 and 2.42 GHz residing in ISM band.

2.1.2. Bioimpedance Spectroscopy

Bioimpedance spectroscopy is one of the recently emerged crucial method to measure blood glucose levels (BGL) without pricking in a non-invasive manner. By cultivating tissue's electrical properties, it provides a reliable, trustworthy approach to accurately and comfortably measure BGL. It has mainly four monitoring parts: tiny electrical stimulation, electrical impedance as tissue response, impedance change as blood sugar impact and signal conditioning.

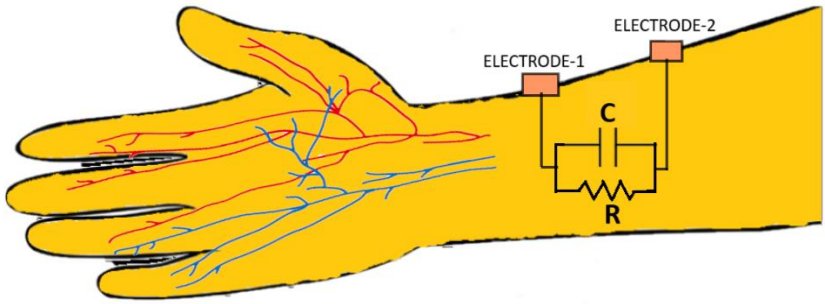

Figure 7. Bioimpedance Glucose Level Measurements

Tiny electrical stimulation plays a key role in bioimpedance spectroscopy as an alternative method for non-invasive glucose monitoring by measuring impedance response under low-level electrical current. Level of stimuli is important and should be in a cooperation between sensitivity and resolution of impedance measurement and safety limit. Contrary to other devices-under-test (DUTs), bioimpedance spectroscopy is applied to human tissues. Safety should be concerned for level of electrical input level because tissue damage, discomfort, and patient safety. High level of stimuli may present a hazard of tissue damages, like nerve stimulation, thermal injury, and electrolytic effects. Applied person may be discomforted or feel pain due to not only stimuli level but also duration of it. Therefore, it is minimized the stimuli level and duration for a proper working. Patient safety is another concern for stimuli level. Magnitude of electrical input should be so adjusted that the risk of unfavorable events and complications are prevented.

Electrical impedance is obtained as a measure of tissue response characterizing the tissue's reaction to electrical current providing meaningful information about tissue composition and physiological properties. When an electric field is applied to a tissue, which is a dielectric material, polarization occurs. Polarization is a response of a dielectric material's permittivity, which is the ability to store energy. Impedance of a dielectric material is given below (Popov, Ishai, Khamzin, & Feldman, 2016).

$$Z = \frac{\sigma - j\omega\varepsilon_0\varepsilon}{\sigma^2 + (\omega\varepsilon_0\varepsilon)^2} \qquad (6)$$

Relative permittivity of a material decreases as the frequency increases. Relative permittivity, also impedance, varies over four principle dispersion regions: alpha

dispersion, 100Hz-10kHz where ion diffusion is dominant; beta dispersion, sub MHz - 10 MHz where charge accumulation at cellular membrane is dominant, delta dispersion, sub-GHz where rotation of macromolecular side chains is dominant, gama dispersion about 10 GHz where dipolar rotation of water molecules is dominant.

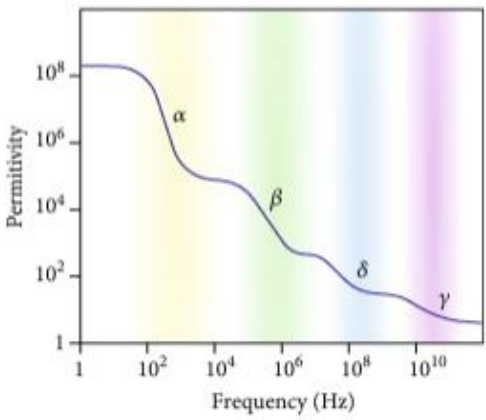

Figure 8. Different Dispersion Regions (Bounik, Cardes, Ulusan, Modena, & Hierlemann, 2022)

Change in BGL can induce important shifts in impedance, representing changes in body's electrical conductivity, which severely influence the effect of electrical polarization of cell membranes, bheta dispersion. Therefore, it is important that applying frequency of impedance analysis should be within ionic conductivity and bheta dispersion intervals. Not too high to dominate bheta dispersion, <200 MHz, not too low to have problem in electrode polarization and to suppress signals of alpha dispersion over bheta dispersion, >100 kHz. Study by Caduff et. al. (Tura, Sbrignadello, Barison, Conti, & Pacini, 2007a), also verifies this frequency range. In their study, they have meaningful results for impedance modulus and impedance phase up to 1 MHz for various glucose concentrations. They claimed that although they studied a wider spectrum, up to 10 MHz, glucose variations severely affect the dielectric properties of solution, especially physiological solutions, certainly evident at low frequencies, on the order of 100 kHz.

In BIS, both current and voltage electrodes are applied to DUT. In current electrode, a proper tiny current is applied. In voltage electrodes, voltage through the tissue is observed. Ratio between them is explained as impedance. Magnitude

and phase of impedance are introduced due to tissue properties and glucose concentrations. Due to the fact that tiny current is applied, tiny voltage signal is sensed by the voltage electrodes. Therefore, signal amplification is required to process the signal. Then, sophisticated noise reduction and interference elimination algorithms are applied. Later on, calibration procedures are carried out to establish a strong correlation between impedance measurement and glucose concentration. Signal conditioning is essential for researchers, engineers and scientists to improve the quality of signal, to eliminate the undesired effects and to solidify a robust association between sugar concentration and impedance.

Skin impedance plays a critical role in NIGM where impedance is measured over the skin. Impedance can be affected by skin hydration, thickness of stratum corneum (SC), which is the most significant layer for transdermal transport (BLAIR, 1968). There are many sophisticated skin impedance models to develop reliable and realistic measurement results. By adding dermis, hypodermis, vessels and hair follicles to SC, Montague Model, Tregear Model and Lykken model are the most-well known and best-representing models to understand skin behaviour. Montague Model is famous it's simplistic and accurate model with three components, two resistors and one capacitor. Although Montague model performs better with shallow layers from surface, it fails to model deeper layers from surface. For deeper layers modeling, Tregear model is introduced to increase inaccuracies and inadequacies. One layer of the model is a series connection of three parallel connected resistor capacitor pairs. The more layers considered, the higher the level of the model. By considering major contributions of layers, maximum of level 3 can be considered for Tregear model. As an alternative to Tregear model to improve the accuracy of Montague model, Lykken model is another model. Just like Tregear model, it includes 3-elements except capacitor is replaced with impedance.

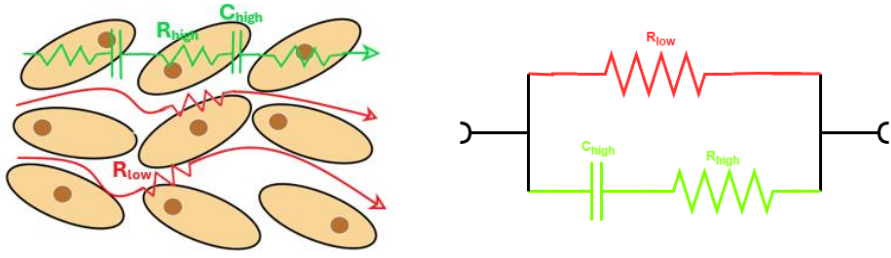

Figure 9. Bioimpedance Signal Pathway and Equivalent Circuit

In Bioimpedance NIGM, basically, capacitive sensors are utilized to measure BGL. Capacitive coupling between sensor and skin is a method of AC conduction

mechanism, capacitive sensing is performed on the lowest impedance, bypassing the high impedance introduced by stratum corneum. Changes in dielectric properties lead to impedimetric changes. Glucose level in blood affects dielectric properties of the tissue. By measuring impedance affected by dielectric changes, it is possible to measure BGL. Capacitive reading can be affected by some factors. Skin roughness can lead to reading error due to contact area issue. When skin area is not uniform, there may be a bad attachment between the sensor and skin surface. This mismatch can cause air between sensor and skin, introducing inconsistency in electrical contact. When capacitive sensors are designed larger sensor area is considered for reliable bioimpedance measurement. Sweating and state of hydration are other factors for sensor reading. Sweating decreases internal body water including intracellular and extracellular water. Water as a primary conductor in the body decreases impedance reading in bioimpedance analysis. Electrolyte imbalance is other result of sweating. In sweating process not only water but also some electrolytes like sodium, potassium and chloride are expelled from the body. Electrolytes as charge carrying ions decrease impedance reading in bioimpedance analysis. Ejection of them from body cells and tissues increases the actual impedance value in bioimpedance analysis. Moisture on the skin surface is another result of sweating. Moisture including electrolytes creates an alternative electrical path from the outside of body, those are conductive substances and decrease reliability of bioimpedance analysis. Pressure on the sensor is another factor for sensor reading. Interface issue is one of the results of pressure on the sensor. When excessive pressure is applied, interface properties between the sensor and the tissue are changed. Extracellular fluid movement is another result of pressure on the sensor. High pressure on the sensor can cause the movement of fluids between cells, those are major contributor of bioimpedance. Shift in fluid distribution changes normal bioimpedance properties of tissues. Change in tissue thickness is another result of pressure on the sensor.

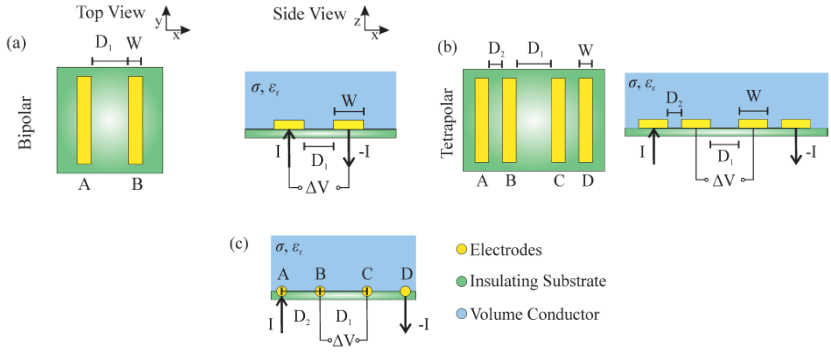

Figure 10. Bipolar and Tetrapolar Capacitive Sensors (Kassanos, 2021)

There are three types of capacitive sensors in NIGM: Bipolar, tetrapolar, and interdigitated sensors. The most straightforward method for assessing electrical impedance involves employing a pair of electrodes. One of these electrodes may serve as a grounding point, or alternatively, it's recommended that the alternating current signal administered to the second electrode be precisely out of phase by 180 degrees from the signal applied to the other electrode. This configuration entails a differential excitation. Ensuring that the direct current voltage remains identical on each electrode is essential for imparting a net zero direct current signal onto the biomaterial under examination (BUS). The layout and configuration of the electrodes determine how the electric field is distributed, thereby determining which regions of the biomaterial under study (BUS) are influencing the recorded impedance. The situation involving two electrodes positioned opposite each other with the biomaterial under study (BUS) sandwiched between them is widely recognized, resembling a parallel plate capacitor with a mostly uniform electric field in the central region of the electrodes and a fringing field at the edges. This setup is particularly relevant, for instance, when employing large electrodes to assess bulk tissue characteristics and has found application in impedance cell cytometry. Tissue impedance is lowered when low frequency signals are applied. By considering the sensor interface impedance, which is on the order of Mega ohm, configuration of electrodes should be revised to improve the monitoring performance of the low impedance of bulk tissue compared to higher impedance of electrode contact impedance. Tetrapolar sensor system is one of the alternative solution for the problem. In tetrapolar sensor system there are four electrodes and two of them are used for current injection and two of them are used for voltage measurement. For voltage measurement electrodes, a high input impedance amplifier is utilized

and no current passes through the electrodes, consequently no voltage drop occurs across the electrode interface impedance.

2.1.3. Ultrasound

Ultrasound (US) technology is a hopeful for NIGM and offering a strong alternative to traditional ways like finger-pricking or CGM devices. Working philosophy of US is to emit high-frequency sound waves interacting with skin and underlying deeper materials allowing monitoring the glucose levels via tissue properties changes like elasticity, viscosity, density, acoustic impedance and thickness. Although many research activities are carried out in this field, US technology is still painless, invasive and a strong potential method for real-time monitoring.US technology for NIGM purposes are based on hybrid sensor technology. Generally, optical and ultrasound or biosensor and ultrasound technologies are combined. One of such technology is a combination of US sensors and electrochemical bio sensors by S. Lee et al. (Lee, Nayak, Dodds, Pishko, & Smith, 2005). They studied to monitor blood glucose levels of rats by applying insulin to hyperglycemic rats. They observed the BGL decrease by 233.3 mg/dl within 5 min. They utilized a impedance matching solution between US sensor and rat body. Ultrasound and biosensor application are compared with commercial glucose meter results. It showed that no statistically significant difference is seen between two groups, $p>0.05$.

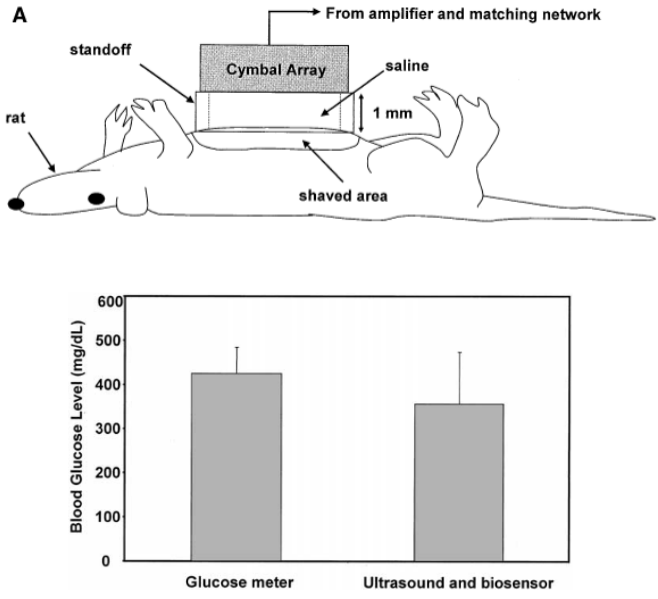

Figure 11. Ultrasound Glucose Monitoring Experiment and Results (Lee et al., 2005)

Table 2. Literature Review Table for Electrical Methods for NIGM

Study Reference	**Technology**	**Biophysiological factor**	**Statistical Outcome**	**Machine Learning Utilization**	**Advantage**	**Disadvantage**
(Sanai et al., 2023) Sanai et. Al., 2023	Bioelectrical Impedance Analysis	Bioimpedance of skin tissue	%17.9 MARD	Gradient boosted model is developed	• Portable • As accurate as SMBG meter • Real-time Monitoring	• Lower noise immunity • Personal Calibration Necessity
(Tura, Sbrignadello, Barison, Conti, & Pacini, 2007b)Tura et. Al., 2007	Bioelectrical Impedance Analysis	Electrical Impedance Difference of different liquids	125% for Mean Standard deviation for Modulus Signal	Not utilized	• Different liquid samples have different impedance • Applicable to different stimulus frequencies	• Dependency of Hydration level • Long Response Time after food intake
(Klyve et al., 2024)Klyve et. Al., 2024	Broadrange RF Spectroscopy	Dielectric Property of tissues	%12.9 MARD	LightGBM model is developed	• Deep Tissue Penetration • No need for consumables	• Limited biological population • No person with diabetes in participants
(Woo, Lee, & Yook, 2024) Woo et. Al., 2024	Dielectric Spectroscopy	Different dielectric characteristics of liquid solutions	0.5 mdB per $mgdL^{-1}\mu L$ Sensitivity	Not utilized	• No ionizing Radiation • potential for multi-analyte detection	• Limited spatial resolution • Tissue heterogeneity
(Farhoudi, Laurentius, Magda, Reiche, & Solzbacher, 2021) Farhoudi et. Al., 2021	Ultrasound Spectroscopy	Ultrasound-induced Resonance	65.6 MARD Value	Not utilized	• Compatibility with Wearable Devices • Reduced risk of infection	• Dependence of blood flow • Limited sensitivity to glucose

Literature review of electrical methods for NIGM is given in table 2. Sanai et al. (2023) explored bioelectrical impedance analysis (BIA) to measure skin tissue bioimpedance, achieving a 17.9% MARD with a gradient-boosted model, making it a portable and accurate alternative to standard glucose meters. However, its effectiveness is limited by personal calibration requirements and lower noise immunity. Similarly, Tura et al. (2007) examined BIA in liquid impedance differentiation, though hydration dependency and slow response times hinder real-time applications. Klyve et al. (2024) advanced glucose sensing using broad-range RF spectroscopy, utilizing a LightGBM model and achieving 12.9% MARD, offering deep tissue penetration without consumables, but lacking biological validation in diabetic populations. Woo et al. (2024) investigated dielectric spectroscopy, which enables multi-analyte detection without ionizing radiation, yet struggles with spatial resolution and tissue heterogeneity. Finally,

Farhoudi et al. (2021) demonstrated ultrasound spectroscopy as a wearable-compatible method with a lower risk of infection, though it remains dependent on blood flow and has limited glucose sensitivity. Collectively, these studies underscore the growing need for precise, non-invasive glucose monitoring, highlighting technological advancements and existing challenges that must be addressed for clinical adoption and widespread accessibility.

2.1.4. Pros/Cons Analysis

Electrical / Electromagnetic Methods

Advantages

1. High penetration depth at low frequencies for electromagnetic method
2. For mmW and MW, they are highly sensitive with a fast response in real-time, flexible, low power, robust, small in size
3. For BIS, it is inexpensive, safe, small in size, reliable, fast acting.
4. For ultrasound, penetrate long distances into tissue, high sensitivity, indifference to skin color variations unlike optical sensing.
5. For ultrasound, it is easier to differentiate glucose from other blood compounds.

Disadvantages

1. Low penetration depth at high frequencies especially for fat and skin
2. Dielectric spectroscopy affected by environment and physiological parameters like movement, sweat, ambient, temperature, humidity, water content, electrolyte concentration,
3. Dangerous for continuous monitoring, as repetitive exposure could cause damage to tissue due to penetration depth.
4. For bio impedance spectroscopy, it does not predict the electrical impedance due to cell-membrane capacitance.
5. For BIS, main disadvantages, sensor's complexity, instability with sweat or movement.
6. For ultrasound, high cost, sensitivity to temperature and pressure.

2.2. Optical

Optical methods in NIGM provides a strong key position to diabetes management by measuring glucose levels without pricking. These methods are based on the light-based technologies interacting with glucose molecules in tissues with the natural properties of optics like absorption, scattering, reflection to predict glucose concentrations. NIR spectroscopy, Raman Spectroscopy, optical coherence tomography are frequently studied techniques due to their reliable, robust, sensitive and versatile nature. These technologies can offer more accurate, efficient and innovative solutions by transforming our understanding of non-invasive glucose monitoring in human blood. Although some methods appear as an end-user-friendly, some of them are still under development to boost portability, accuracy, precision and reliability while being a glimmer of hope for diabetes.

2.2.1. Near Infrared Spectroscopy

Near-Infrared spectroscopy utilizes the light in the 750-2500 nm band of the spectrum, while Middle-Infrared Spectroscopy utilizes 2500-25000 nm of the spectrum and visible light utilizes 400-700 nm, covering from violet, around 400 nm to red, around 700 nm of the spectrum. Although NIR band is located neither on the left nor on the right of the spectrum, i.e. intermediate of the spectrum, radiation of it can penetrate the skin much deeper than visible or MIR light. NIR has many appropriate frequency bands where hemoglobin, lipid and water absorption intensities are low enough to allow light to diffuse in to the tissue making near-infrared spectral measurements possible. NIR spectral measurement is a more effective tool for clinical and scientific applications. Thanks to the developments of semiconductor and microelectronics area, it has gained popularity for monitoring many biological indicators due to its straightforward, cost-effective, safe and convenient real-time monitoring. It is possible to monitor in a real-time manner due to it's non-destructive, fast, no-reagent usage working principle.

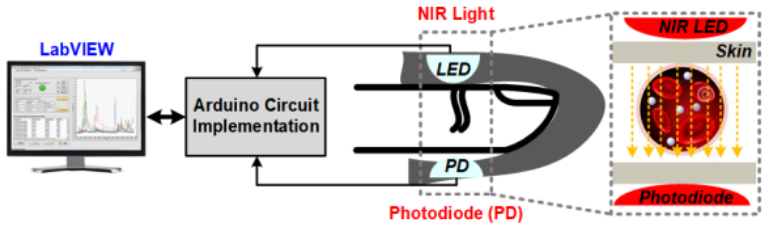

Figure 12. NIR-based NIGM System Prototype (Haxha & Jhoja, 2016)

Although many prototypes are reported in the literature, one of the most applicable and cost-effective study is by Shyqyri H. and Jaspreet J . In their study, they designed a optical based NIGM prototype involving Arduino, NIR LED and a photodetector. Post-processing of the sensor data is performed in LabView. They designed the system so that it operates at 940nm wavelength. Working principle of the system is based on Beer-Lambert Law. Attenuation is calculated by considering both transmitted and received signal. Output voltage is correlated with invasive BGL results and a model is proposed on LabView. Schematic representation of the system is given in figure 13.

2.2.2. Optical Polarimetry

Optical Polarimetry is a prominent technique for NIGM offering a good alternative for conventional blood glucose monitoring techniques. Interaction of light with biological tissues, in which glucose can affect optical properties of tissue, can change the polarity of light. This technique works by taking advantage of the fact that glucose affects the rotation of polarized light, named optical rotation. This method is a good hope for continuous monitoring in diabetic patients without issues related to conventional methods, like finger-pricking. On the other hand, technical challenges are still remained related to sensitivity, accuracy and signal conditioning algorithm efficiency.

$$\theta = \alpha l c \qquad (7)$$

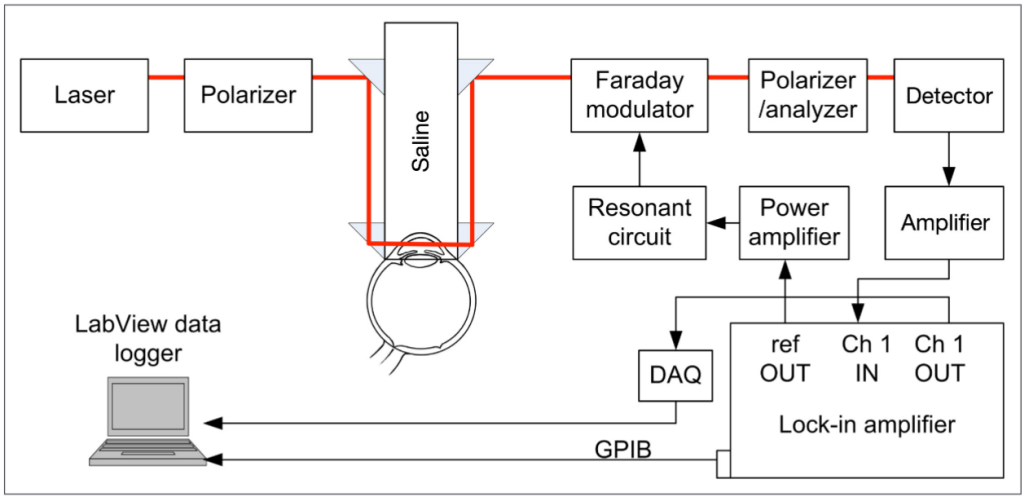

Figure 13. Optical Polarimetry Setup [57]

Although few studies conducted in literature about polarimetric-based NIGM, the study by Georgeanne P. et al. (Purvinis, Cameron, & Altrogge, 2011) is a strong study for this topic. In this study, they experimented in a total of seven New Zealand white (NZW) rabbits and they are anesthetized properly to experiment with anterior chamber of the eyes. They set up the system involving of 632.8 nm laser, polarizer, modulator and amplifiers. The system is depicted as below. They derived a optical signal intensity model based on modulation frequency, modulation depth, rotation angle due to glucose.

2.2.3. Pros/Cons Analysis of Optical Methods

Advantages

1. For OCT, good SNR independent of heartrate, blood pressure, osmolytes, red blood cell ratio
2. For OP, it is accurate, it has high resolution, and compact in size.
3. For Raman Spectrometry, it is less affected by water. It is robust against scattering lights due to filtering
4. For NIR, high sensitivity of photoconductive detectors.
5. For NIR, measuring signal has higher energy than MIR Spectroscopy.
6. For NIR, water is in transparent band in NIR device.
7. For MIR, glucose is detected at specific MIR wavelengths.
8. For MIR, peak responses are higher compared to NIR.

Disadvantages

1. For OCT, low sensitivity, high sensitivity to movement, limited skin temperature to continuous monitoring
2. For OP, it can be hard to obtain good optical rotation signals in case of low blood glucose levels. High lag times and high sensitivity to motion, temperature and other compounds.
3. For NIR Spectroscopy, it is rather sensitive to physiological parameters, environment factors like tissue thickness, temperature, skin tone, composition in tissue and ambient light.
4. For MIR, penetration depth is shorter than NIR.

5. For Raman Spectrometry, Raman signal is weak due to its low-occurrence nature.
6. For NIR, it is difficult to differentiate blood glucose from other blood compounds.
7. For MIR, water is one of the primary interference for glucose measurement.

For MIR, poor penetration.

Table 3. Literature Review for Optical Methods in NIGM

(Shokrekhodaei, Cistola, Roberts, & Quinones, 2021)SHOKREKHODAEI et. Al., 2021	Infrared Spectropscopy	Skin Tissue – Light İnteractio n	99.75% Clarke Error Grid	KNN, DT, SVM for classificatio n, MLR, ANN for regression models	• High Sensitivity • High Specificity	• Sensitivity to skin color • Motion Artifacts
(Hina & Saadeh, 2020) Hina et. Al., 2020	Infrared Spectroscop y	Skin Tissue – Light İnteractio n	7.62% mARD	Support Vector Regression for BGL prediction	• Reduced risk of infection • Pain-free	• Lower SNR • Sensitivity to motion artifacts
(Rachim & Chung, 2019) Rachim et. Al., 2019	Infrared Spectroscop y	Skin Tissue – Light İnteractio n	6.16 mg/dl standard predictio n error	Not utilized	• Integration with wearable devices • Improved Quality of life	• Aging effect • Signal Processing Challenges
(Pors et al., 2023) Pors et. Al., 2023	Raman Spectroscop y	Molecula r Vibration and Raman Scatterin g	14.3% mARD	Partial Least Square Regression	• Continuous monitoring potential • High Specificity	• Weak Signal level • Skin Variability
(Song, Ha, Park, Bae, & Yoo, 2015) Song et. Al., 2015	Infrared Spectroscop y	Molecula r Vibration and Raman Scatterin g	RMSEP of 0.27 mmol/L and R^2 of 0.98	Principle Component Analysis + Back Propagation Artificial Neural Network	• Miniaturizati on • Portability	• Ambient Light Interferenc e • Temperatu re sensitiivty

In table.3, literature review for optical methods of NIGM is given. SHOKREKHODAEI et al. (2021) investigated infrared spectroscopy, demonstrating 99.75% accuracy on the Clarke Error Grid while employing KNN, DT, SVM, MLR, and ANN models for classification and regression. Despite its high sensitivity and specificity, challenges such as skin color variations and motion artifacts limit its widespread application. Similarly, Hina et al. (2020) utilized infrared spectroscopy with support vector regression (SVR) for blood

glucose level (BGL) prediction, achieving a 7.62% mARD while ensuring a pain-free and infection-free experience, though lower signal-to-noise ratio (SNR) and motion sensitivity remain concerns. Rachim et al. (2019) explored infrared spectroscopy integration with wearable devices, reporting a standard prediction error of 6.16 mg/dL, significantly enhancing quality of life but facing aging-related signal degradation and processing challenges. Meanwhile, Pors et al. (2023) examined Raman spectroscopy, leveraging molecular vibration and Raman scattering to achieve a 14.3% mARD using Partial Least Squares Regression, though weak signal levels and skin variability impact accuracy. Lastly, Song et al. (2015) explored infrared spectroscopy with PCA and Back Propagation ANN, achieving RMSEP of 0.27 mmol/L and R^2 of 0.98, emphasizing miniaturization and portability but suffering from ambient light interference and temperature sensitivity. These studies underscore the growing potential of infrared and Raman spectroscopy in non-invasive glucose monitoring, while also highlighting the technological and physiological challenges that must be addressed for clinical viability.

2.3. Physiological Methods

Physiological methods in non-invasive glucose monitoring are studied to measure BGL without need for conventional requirements. Key features in the body are utilized to monitor BGL. The methods utilizing such features rely on the detection of physiological signals such as light absorption, skin temperature or blood pressure. Tear, sweat are other biological fluids to study BGL.

2.3.1. Blood Pressure

Blood pressure plays a crucial role in the development of certain non-invasive glucose monitoring techniques, as it can influence the distribution and flow of blood in the body, potentially affecting glucose concentrations in tissues. Photoplethysmography (PPG) is one of the technique to monitor blood pressure and BGL. One of study utilizing the method is by Enric Monte-Moreno. He collected PPG signals via finger pulse oximeter and related BGL, systolic (SBP) and diastolic (DBP) blood pressures. They obtained satisfactory results for BGL estimation. System designed is given as below.

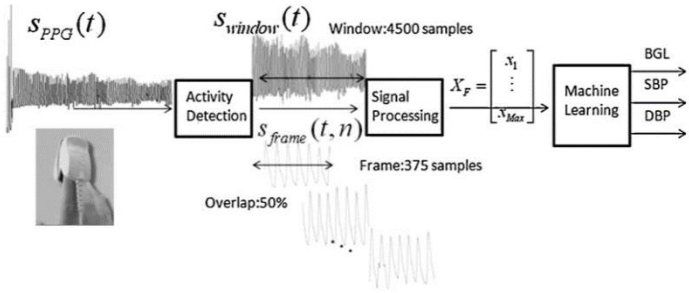

Figure 14. Blood Pressure Setup [80]

2.3.2. Tear

Tear became a promising biofluid for NIGM because of the glucose involvement. Glucose concentration in tears correlates with glucose level in blood. Optical sensors, biosensors are devices to monitor glucose level continuously. One of the study utilized tear to monitor glucose level is by Justin T. B. et al.(Baca, Finegold, & Asher, 2007). They studied tear biofluid to estimate blood glucose level by collecting samples from diabetic and nondiabetic subjects. Subjects are given oral glucose load and glucose level in tears and time lag after glucose intake are monitored.

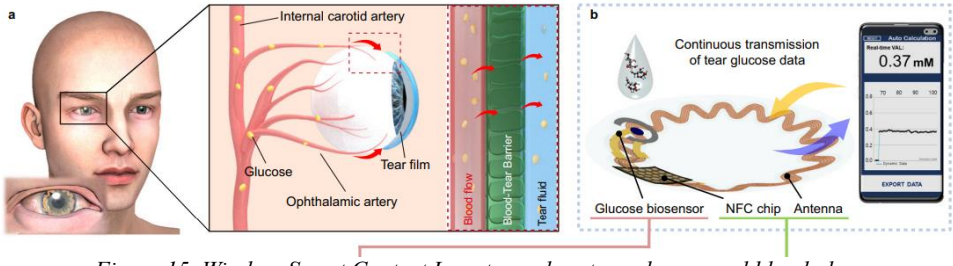

Figure 15. Wireless Smart Contact Lens to analyse tear glucose and blood glucose (Park et al., 2024)

2.3.2. Pros/Cons Analysis of Physiological Methods

Advantages

1. Various body fluids, urine, sweat, saliva can hold various information about glucose levels.
2. Risk of infection is eliminated.

3. Glycemic Control is improved based on insulin dosage, exercise etc.
4. Multimeter parameter monitoring can be performed with a single device.
5. It has potential for integration with wearable smart devices.

Disadvantages

1. It has low correlation for glucose levels in physiological fluids. Accuracy and precision are low.
2. High response time compared to blood in the event of real-time changes of glucose levels.
3. High risk of interferences of external factors. Hydration level, temperature, humidity can affect glucose level in body fluids.
4. Sensor design and calibration are difficult for body fluids.

Comparison of Non-invasive Realtime Methods

The trade-off analysis compares optical and RF/microwave technologies for non-invasive sensing. Optical methods (e.g., infrared, Raman spectroscopy) face challenges like component limitations, design complexity, and shallow depth penetration, making them costly and harder to implement. In contrast, RF/microwave methods (e.g., bioimpedance, RF spectroscopy) offer greater flexibility, easier integration, lower costs, and better depth penetration. They benefit from well-defined safety regulations and existing infrastructure, making them more suitable for wearable applications. However, RF/microwave methods may still face interference and calibration challenges. The choice between these technologies depends on balancing precision, cost, and feasibility, with RF-based methods emerging as a strong contender for future non-invasive glucose monitoring.

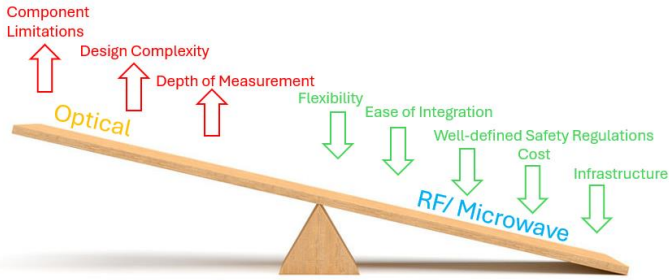

Figure 16. Trade-off Analysis for NIGM Methods

RF/Microwave (RF/MW) methods for non-invasive glucose monitoring (NIGM) offer several strong advantages, making them promising for future applications, given in Figure 17. They provide high spectrum coverage, allowing for precise glucose detection across different frequencies. Their penetration depth enables deeper tissue analysis, improving accuracy compared to surface-limited optical methods. RF/MW also exhibits high sensitivity, enhancing glucose measurement reliability. Additionally, these methods have the flexibility to integrate with other sensing technologies, increasing adaptability. Most importantly, RF/MW techniques hold great potential for continuous glucose monitoring (CGM), paving the way for wearable, real-time diabetes management solutions.

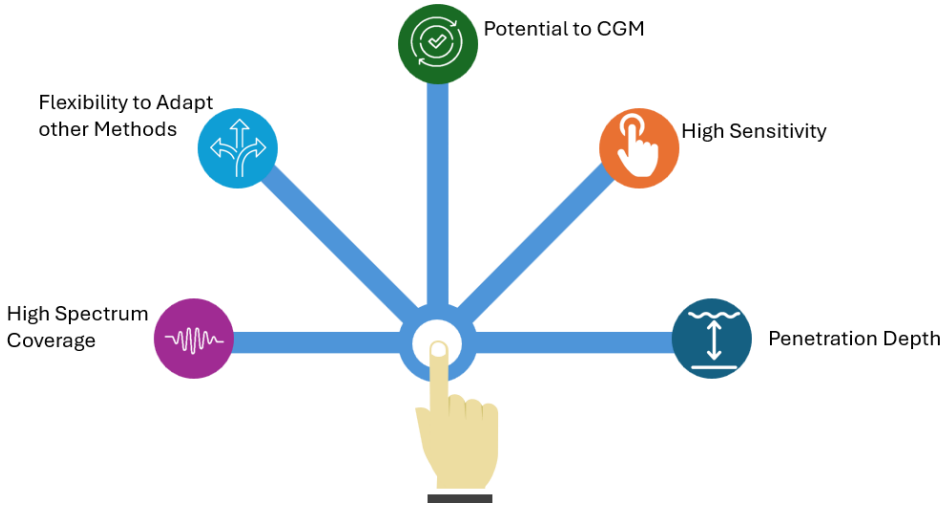

Figure 17. Strong Ways of RF/Microwave Methods

Tablo 4. Literature Review for Physiological Methods in NIGM

(Soni & Jha, 2015) Soni and Jha, 2014	Glucoseoxydase (GOD) activity	Reaction of Glucose in saliva with GOD enzyme	0.95 correlation coefficient	Not utilized	• Ease of collection • Dynamic Relationship	• Late response time • Calibration Challenge
[(Chopra, Rao, Kamath, Akhila Arun, & Shettigar, 2024)Chopra et. Al., 2024	Glucoseoxydase (GOD) activity	Reaction of Glucose in saliva with GOD enzyme	23.821 MAE	Feature selection and ML models Development	• Child-friendly • Safer-for Long-term Usage	• Contaminants • Individual difference
[(Monte-Moreno, 2011) Monte-Moreno, 2011	photoplethysmograph	Absorption and scattering of light with skin tissue	87.7% Clarke Error grid in zone A	Linear Regression, Neural Network, Support Vector Machine	• Lower Cost • Suitability of all ages	• Skin Variability • Ambient Light Interference
(Geelhoed-Duijvestijn et al., 2021)Geelhoed-Duijvestijn et. Al., 2020	Glucoseoxydase (GOD) activity	Reaction of Glucose in tear with GOD enzyme	16.7% MARD	Neural Network	• Minimal sample necessity • Smart contact lens compatibility	• Delay in response time • Risk of infection
[(Greyling, Madhurantakam, Lin, Muthukumar, & Prasad, 2023) Greyling et. Al., 2023	Glucoseoxydase (GOD) activity	Reaction of Glucose in sweat with GOD enzyme	0.9864 correlation coefficient	One-way ANOVA Analysis	• Minimal sample necessity • Wearable Device compatibility	• Influence of skin contamination • Delay in response time

Soni and Jha (2014) investigated glucose oxidase (GOD) activity in saliva, achieving a 0.95 correlation coefficient with blood glucose levels, emphasizing the ease of collection and the dynamic relationship of glucose in saliva. However, the method faces challenges such as delayed response time and calibration difficulties, which can limit real-time applicability. Chopra et al. (2024) investigated glucose oxidase (GOD) activity in saliva, utilizing machine learning-based feature selection models and reporting a mean absolute error (MAE) of 23.821, making it a child-friendly and safer long-term option, though challenges such as contaminants and individual differences persist. Similarly, Monte-Moreno (2011) explored photoplethysmography, which leverages light absorption and scattering in skin tissue, achieving 87.7% Clarke Error Grid accuracy (Zone A). While this method is low-cost and suitable for all ages, issues such as skin variability and ambient light interference remain significant obstacles. Geelhoed-Duijvestijn et al. (2020) studied tear-based glucose monitoring using glucose oxidase activity, obtaining a mean absolute relative difference (MARD) of 16.7% and highlighting the minimal sample requirement and compatibility with smart contact lenses, though delayed response times and infection risks pose challenges. Lastly, Greyling et al. (2023) focused on sweat-

based glucose detection, reporting a strong correlation coefficient of 0.9864 and demonstrating wearable device compatibility, though it is still affected by skin contamination and slow response times. These studies illustrate the growing feasibility of non-invasive glucose monitoring, while also emphasizing the need for enhanced sensitivity, faster response times, and robust calibration techniques to make these methods clinically viable.

3. Conclusion

Diabetes is a chronic condition requiring continuous glucose monitoring to prevent complications. Blood glucose is essential for metabolic stability, but traditional monitoring methods are often invasive and inconvenient. Non-invasive glucose monitoring (NIGM) offers alternatives using electrical, optical, and physiological methods. Electrical techniques (e.g., bioimpedance, RF spectroscopy) provide real-time tracking but require calibration. Optical methods (e.g., infrared, Raman spectroscopy) offer high specificity but face skin variability issues. Physiological approaches (e.g., saliva, tear, sweat glucose sensing) are minimally invasive but suffer from delayed response times. While NIGM holds great promise, further advancements in sensor accuracy and real-world validation are essential for clinical adoption and improved diabetes management.

4. References

Baca, J. T., Finegold, D. N., & Asher, S. A. (2007). Tear Glucose Analysis for the Noninvasive Detection and Monitoring of Diabetes Mellitus. *The Ocular Surface*, *5*(4), 280–293. https://doi.org/10.1016/S1542-0124(12)70094-0

Beam, K., & Venkataraman, J. (2011). Phantom models for in-vitro measurements of blood glucose. *2011 IEEE International Symposium on Antennas and Propagation (APSURSI)*, 1860–1862. IEEE. https://doi.org/10.1109/APS.2011.5996860

Benjamin, E. M. (2002). Self-Monitoring of Blood Glucose: The Basics. *Clinical Diabetes*, *20*(1), 45–47. https://doi.org/10.2337/diaclin.20.1.45

BLAIR, C. (1968). MORPHOLOGY AND THICKNESS OF THE HUMAN STRATUM CORNEUM. *British Journal of Dermatology*, *80*(7), 430–436. https://doi.org/10.1111/j.1365-2133.1968.tb11978.x

Bommer, C., Sagalova, V., Heesemann, E., Manne-Goehler, J., Atun, R., Bärnighausen, T., … Vollmer, S. (2018). Global Economic Burden of Diabetes in Adults: Projections From 2015 to 2030. *Diabetes Care*, *41*(5), 963–970. https://doi.org/10.2337/dc17-1962

Bounik, R., Cardes, F., Ulusan, H., Modena, M. M., & Hierlemann, A. (2022). Impedance Imaging of Cells and Tissues: Design and Applications. *BME Frontiers*, *2022*. https://doi.org/10.34133/2022/9857485

Chopra, A., Rao, R. R., Kamath, S. U., Akhila Arun, S., & Shettigar, L. (2024). Predicting blood glucose level using salivary glucose and other associated factors: A machine learning model selection and evaluation study. *Informatics in Medicine Unlocked*, *48*, 101523. https://doi.org/10.1016/j.imu.2024.101523

Costanzo, S., Cioffi, V., Qureshi, A. M., & Borgia, A. (2021). Gel-Like Human Mimicking Phantoms: Realization Procedure, Dielectric Characterization and Experimental Validations on Microwave Wearable Body Sensors. *Biosensors*, *11*(4), 111. https://doi.org/10.3390/bios11040111

EUCAP. (n.d.). *2024 18th European Conference on Antennas and Propagation (EuCAP)*. IEEE.

Farhoudi, N., Laurentius, L. B., Magda, J. J., Reiche, C. F., & Solzbacher, F. (2021). *In Vivo* Monitoring of Glucose Using Ultrasound-Induced Resonance in Implantable Smart Hydrogel Microstructures. *ACS Sensors*, *6*(10), 3587–3595. https://doi.org/10.1021/acssensors.1c00844

Farrugia, L., Porter, E., Conceição, R. C., Meo, S. Di, Godinho, D. M., Bonello, J., … Peyman, A. (2024). The Complex Permittivity of Biological Tissues: A

Practical Measurement Guideline. *IEEE Access*, *12*, 10296–10314. https://doi.org/10.1109/ACCESS.2024.3352728

Forouhi, N. G., & Wareham, N. J. (2022). Epidemiology of diabetes. *Medicine*, *50*(10), 638–643. https://doi.org/10.1016/j.mpmed.2022.07.005

Geelhoed-Duijvestijn, P., Vegelyte, D., Kownacka, A., Anton, N., Joosse, M., & Wilson, C. (2021). Performance of the Prototype NovioSense Noninvasive Biosensor for Tear Glucose in Type 1 Diabetes. *Journal of Diabetes Science and Technology*, *15*(6), 1320–1325. https://doi.org/10.1177/1932296820964844

Greyling, C. F., Madhurantakam, S., Lin, K.-C., Muthukumar, S., & Prasad, S. (2023). Tracking Active Glucose-Galactose [TAGG] dynamics in human sweat. *Biosensors and Bioelectronics: X*, *14*, 100357. https://doi.org/10.1016/j.biosx.2023.100357

Haxha, S., & Jhoja, J. (2016). Optical Based Noninvasive Glucose Monitoring Sensor Prototype. *IEEE Photonics Journal*, *8*(6), 1–11. https://doi.org/10.1109/JPHOT.2016.2616491

Hina, A., & Saadeh, W. (2020). A Noninvasive Glucose Monitoring SoC Based on Single Wavelength Photoplethysmography. *IEEE Transactions on Biomedical Circuits and Systems*, *14*(3), 504–515. https://doi.org/10.1109/TBCAS.2020.2979514

Ignatavicius, D., & Workman, M. L. (2016). Medical-Surgical Nursing Patients-Centered Collaborative Care. In *Elsevier* (Vol. 53).

Jaffari, S. A., & Turner, A. P. F. (1995). Recent advances in amperometric glucose biosensors for in vivo monitoring. *Physiological Measurement*, *16*(1), 1–15. https://doi.org/10.1088/0967-3334/16/1/001

Jang, C., Park, J.-K., Lee, H.-J., Yun, G.-H., & Yook, J.-G. (2020). Non-Invasive Fluidic Glucose Detection Based on Dual Microwave Complementary Split Ring Resonators With a Switching Circuit for Environmental Effect Elimination. *IEEE Sensors Journal*, *20*(15), 8520–8527. https://doi.org/10.1109/JSEN.2020.2984779

Karacolak, T., Moreland, E. C., & Topsakal, E. (2013a). Cole–cole model for glucose-dependent dielectric properties of blood plasma for continuous glucose monitoring. *Microwave and Optical Technology Letters*, *55*(5), 1160–1164. https://doi.org/10.1002/mop.27515

Karacolak, T., Moreland, E. C., & Topsakal, E. (2013b). Cole–cole model for glucose-dependent dielectric properties of blood plasma for continuous glucose monitoring. *Microwave and Optical Technology Letters*, *55*(5), 1160–1164. https://doi.org/10.1002/mop.27515

Kassanos, P. (2021). Bioimpedance Sensors: A Tutorial. *IEEE Sensors Journal*, *21*(20), 22190–22219. https://doi.org/10.1109/JSEN.2021.3110283

Klyve, D., Lowe, S., Currie, K., Anderson, J. H., Ward, C., & Shelton, B. (2024). Noninvasive Blood Glucose Measurement Using RF Spectroscopy and a LightGBM AI Model. *IEEE Sensors Journal*, *24*(17), 28049–28055. https://doi.org/10.1109/JSEN.2024.3405800

Laha, S., Rajput, A., Laha, S. S., & Jadhav, R. (2022). A Concise and Systematic Review on Non-Invasive Glucose Monitoring for Potential Diabetes Management. *Biosensors*, *12*(11), 965. https://doi.org/10.3390/bios12110965

Lee, S., Nayak, V., Dodds, J., Pishko, M., & Smith, N. B. (2005). Glucose measurements with sensors and ultrasound. *Ultrasound in Medicine and Biology*, *31*(7), 971–977. https://doi.org/10.1016/j.ultrasmedbio.2005.04.004

Lewis, S. L., Dirksen, S. R., Heitkemper, M. M., & Bucher, L. (2014). Medical-Surgical Nursing: Assessment and Management of Clinical Problems, 9th Edition. In *Elsevier*.

Mahnashi, Y., Qureshi, K. K., Al-Shehri, A. A., & Attia, H. (2023a). Design and Experimental Validation of a Noninvasive Glucose Monitoring System Using RF Antenna-Based Biosensor. *IEEE Sensors Journal*, *23*(3), 2856–2864. https://doi.org/10.1109/JSEN.2022.3227382

Mahnashi, Y., Qureshi, K. K., Al-Shehri, A. A., & Attia, H. (2023b). Design and Experimental Validation of a Noninvasive Glucose Monitoring System Using RF Antenna-Based Biosensor. *IEEE Sensors Journal*, *23*(3), 2856–2864. https://doi.org/10.1109/JSEN.2022.3227382

Megdad, A. R., Aldhaheri, R. W., & Sobahi, N. M. (2023a). Noninvasive Method for Measuring the Blood Glucose Level Using a Narrow Band Microstrip Antenna. *The Applied Computational Electromagnetics Society Journal (ACES)*. https://doi.org/10.13052/2022.ACES.J.371102

Megdad, A. R., Aldhaheri, R. W., & Sobahi, N. M. (2023b). Noninvasive Method for Measuring the Blood Glucose Level Using a Narrow Band Microstrip Antenna. *The Applied Computational Electromagnetics Society Journal (ACES)*. https://doi.org/10.13052/2022.ACES.J.371102

Mohammadi, P., Mohammadi, A., Demir, S., & Kara, A. (2021). Compact Size, and Highly Sensitive, Microwave Sensor for Non-Invasive Measurement of Blood Glucose Level. *IEEE Sensors Journal*, *21*(14), 16033–16042. https://doi.org/10.1109/JSEN.2021.3075576

Monte-Moreno, E. (2011). Non-invasive estimate of blood glucose and blood pressure from a photoplethysmograph by means of machine learning techniques. *Artificial Intelligence in Medicine*, *53*(2), 127–138. https://doi.org/10.1016/j.artmed.2011.05.001

Park, W., Seo, H., Kim, J., Hong, Y.-M., Song, H., Joo, B. J., … Park, J.-U. (2024). In-depth correlation analysis between tear glucose and blood glucose using a wireless smart contact lens. *Nature Communications*, *15*(1), 2828. https://doi.org/10.1038/s41467-024-47123-9

Philis-Tsimikas, A., Chang, A., & Miller, L. (2011). Precision, Accuracy, and User Acceptance of the OneTouch SelectSimple Blood Glucose Monitoring System. *Journal of Diabetes Science and Technology*, *5*(6), 1602–1609. https://doi.org/10.1177/193229681100500638

Popov, I., Ishai, P. Ben, Khamzin, A., & Feldman, Y. (2016). The mechanism of the dielectric relaxation in water. *Physical Chemistry Chemical Physics*, *18*(20), 13941–13953. https://doi.org/10.1039/C6CP02195F

Pors, A., Rasmussen, K. G., Inglev, R., Jendrike, N., Philipps, A., Ranjan, A. G., … Weber, A. (2023). Accurate Post-Calibration Predictions for Noninvasive Glucose Measurements in People Using Confocal Raman Spectroscopy. *ACS Sensors*, *8*(3), 1272–1279. https://doi.org/10.1021/acssensors.2c02756

Purvinis, G., Cameron, B. D., & Altrogge, D. M. (2011). Noninvasive Polarimetric-Based Glucose Monitoring: An *in Vivo* Study. *Journal of Diabetes Science and Technology*, *5*(2), 380–387. https://doi.org/10.1177/193229681100500227

Rachim, V. P., & Chung, W.-Y. (2019). Wearable-band type visible-near infrared optical biosensor for non-invasive blood glucose monitoring. *Sensors and Actuators B: Chemical*, *286*, 173–180. https://doi.org/10.1016/j.snb.2019.01.121

Sanai, F., Sahid, A. S., Huvanandana, J., Spoa, S., Boyle, L. H., Hribar, J., … Telfer, T. J. (2023). Evaluation of a Continuous Blood Glucose Monitor: A Novel and Non-Invasive Wearable Using Bioimpedance Technology. *Journal of Diabetes Science and Technology*, *17*(2), 336–344. https://doi.org/10.1177/19322968211054110

Shokrekhodaei, M., Cistola, D. P., Roberts, R. C., & Quinones, S. (2021). Non-Invasive Glucose Monitoring Using Optical Sensor and Machine Learning Techniques for Diabetes Applications. *IEEE Access*, *9*, 73029–73045. https://doi.org/10.1109/ACCESS.2021.3079182

Smulders, P. F. M., Buysse, M. G., & Huang, M. D. (2013). Dielectric Properties of Glucose Solutions in the 0.5–67 GHz Range. *Microwave and Optical Technology Letters*, *55*(8), 1916–1917. https://doi.org/10.1002/mop.27672

Song, K., Ha, U., Park, S., Bae, J., & Yoo, H.-J. (2015). An Impedance and Multi-Wavelength Near-Infrared Spectroscopy IC for Non-Invasive Blood Glucose Estimation. *IEEE Journal of Solid-State Circuits*, *50*(4), 1025–1037. https://doi.org/10.1109/JSSC.2014.2384037

Soni, A., & Jha, S. K. (2015). A paper strip based non-invasive glucose biosensor for salivary analysis. *Biosensors and Bioelectronics*, *67*, 763–768. https://doi.org/10.1016/j.bios.2014.09.042

Topsakal, E., Karacolak, T., & Moreland, E. C. (2011a). Glucose-dependent dielectric properties of blood plasma. *2011 XXXth URSI General Assembly and Scientific Symposium*, 1–4. IEEE. https://doi.org/10.1109/URSIGASS.2011.6051324

Topsakal, E., Karacolak, T., & Moreland, E. C. (2011b). Glucose-dependent dielectric properties of blood plasma. *2011 XXXth URSI General Assembly and Scientific Symposium*, 1–4. IEEE. https://doi.org/10.1109/URSIGASS.2011.6051324

Tura, A., Sbrignadello, S., Barison, S., Conti, S., & Pacini, G. (2007a). Impedance spectroscopy of solutions at physiological glucose concentrations. *Biophysical Chemistry*, *129*(2–3), 235–241. https://doi.org/10.1016/j.bpc.2007.06.001

Tura, A., Sbrignadello, S., Barison, S., Conti, S., & Pacini, G. (2007b). Impedance spectroscopy of solutions at physiological glucose concentrations. *Biophysical Chemistry*, *129*(2–3), 235–241. https://doi.org/10.1016/j.bpc.2007.06.001

Turgul, V., & Kale, I. (2015). On the accuracy of complex permittivity model of glucose/water solutions for non-invasive microwave blood glucose sensing. *2015 E-Health and Bioengineering Conference (EHB)*, 1–4. IEEE. https://doi.org/10.1109/EHB.2015.7391450

Turgul, V., & Kale, I. (2016). Characterization of the complex permittivity of glucose/water solutions for noninvasive RF/Microwave blood glucose sensing. *2016 IEEE International Instrumentation and Measurement Technology Conference Proceedings*, 1–5. IEEE. https://doi.org/10.1109/I2MTC.2016.7520546

Turgul, V., & Kale, I. (2018). Permittivity extraction of glucose solutions through artificial neural networks and non-invasive microwave glucose sensing. *Sensors and Actuators A: Physical*, *277*, 65–72. https://doi.org/10.1016/j.sna.2018.03.041

Venkataraman, J., & Freer, B. (2011). Feasibility of non-invasive blood glucose monitoring: In-vitro measurements and phantom models. *2011 IEEE*

International Symposium on Antennas and Propagation (APSURSI), 603–606. IEEE. https://doi.org/10.1109/APS.2011.5996782

Woo, H., Lee, H.-J., & Yook, J.-G. (2024). Noninvasive Detection of Glucose and NaCl Solutions With Environment Correction Using a Dual IDC-Based Microwave Sensor. *IEEE Sensors Journal*, *24*(12), 19039–19049. https://doi.org/10.1109/JSEN.2024.3390544

Xiao, X., Yu, Q., Li, Q., Song, H., & Kikkawa, T. (2021). Precise Noninvasive Estimation of Glucose Using UWB Microwave With Improved Neural Networks and Hybrid Optimization. *IEEE Transactions on Instrumentation and Measurement*, *70*, 1–10. https://doi.org/10.1109/TIM.2020.3010680

Yilmaz, T., Foster, R., & Hao, Y. (2014). Broadband Tissue Mimicking Phantoms and a Patch Resonator for Evaluating Noninvasive Monitoring of Blood Glucose Levels. *IEEE Transactions on Antennas and Propagation*, *62*(6), 3064–3075. https://doi.org/10.1109/TAP.2014.2313139

Yilmaz, T., Foster, R., & Hao, Y. (2019). Radio-Frequency and Microwave Techniques for Non-Invasive Measurement of Blood Glucose Levels. *Diagnostics*, *9*(1), 6. https://doi.org/10.3390/diagnostics9010006

CHAPTER 7

Current Developments in Waste Valorization in Turkey and Worldwide

Zehra Gülten Yalçın[1] & Mustafa Dağ[2] & Muhammed Bora Akın[3]

[1] Asst. Prof. Dr. Çankırı Karatekin University, Faculty of Engineering, Department of Chemical Engineering, Uluyazı Campus, 18100, Çankırı, Turkey, ORCID: 0000-0001-5460-289X
[2] Res. Asst. Dr. Çankırı Karatekin University, Faculty of Engineering, Department of Chemical Engineering, Uluyazı Campus, 18100, Çankırı, Turkey, ORCID: 0000-0001-9540-3475
[3] Asst. Prof. Dr. Çankırı Karatekin University, Faculty of Engineering, Department of Chemical Engineering, Uluyazı Campus, 18100, Çankırı, Turkey, ORCID: 0000-0003-3841-1633

Introduction

A study conducted by Washington Carver emphasized that there is no true waste in nature, as discarded products can serve as raw materials for new production. Various studies have also highlighted that waste, including tree leaves and farm manure, can be utilized as raw materials for other production processes. In the 1930s, Henry Ford developed a method to extract soybean meal from certain automobile parts and successfully implemented the reuse of waste bottles and other discarded materials, achieving significant cost savings. As pioneers in waste valorization and zero waste principles, Carver and Ford laid the foundation for modern waste management strategies (Gül & Yaman, 2021).

Numerous studies have explored waste valorization methods, waste minimization, recycling, and eco-friendly technologies. Given the economic, social, and environmental costs, reducing household solid waste has attracted significant attention. The disposal of solid waste in landfills imposes financial burdens, and waste reduction strategies can mitigate economic losses while minimizing social and environmental impacts (Cheah et al., 2022). Solid waste management remains a central research topic (Khan et al., 2022). Studies indicate that household solid waste recycling rates (67%) are notably higher than those observed in workplaces (39%) and holiday resorts (38%) (Liu et al., 2023). Additionally, Lee et al. (2024) investigated waste management and recycling behaviors in South Korea, identifying that environmental awareness significantly influences recycling and waste disposal behaviors.

In Malaysia, the rapid urbanization process has led to an increase in waste generation, particularly food waste, posing a critical challenge for sustainable waste management. Studies have focused on improving contemporary waste management efforts by utilizing anaerobic digestion and Hydrothermal Carbonization (HTC) technologies to manage the increasing volume of food waste (Shukla et al., 2024).

Developing countries face significant challenges in municipal solid waste separation and processing due to high population densities and economic constraints. Ineffective waste management can exacerbate environmental and socioeconomic concerns. Therefore, municipal solid waste management and energy recovery are essential for sustainable development. Studies emphasize the advancement of energy recovery technologies, particularly in thermochemical and biochemical waste conversion, as an economic and sustainable approach (Khan et al., 2022).

The historical development of zero waste initiatives can be traced back to 1973 when Dr. Paul Palmer first introduced the term while founding Zero Waste Systems Inc. (ZWI) in the United States. The company focused on reusing chemicals from electronic applications. Zero waste efforts gained prominence in the 1980s, driven by global environmental developments. In 1986, the National Coalition Against Mass Burn Incineration was established in the U.S., followed by the introduction of the Pay-As-You-Throw (PAYT) system in Seattle in 1988. In 1989, California implemented waste management regulations aimed at diverting 25% of existing waste from landfills by 1995 and 50% by 2000, culminating in the Integrated Waste Management Act (Gül & Yaman, 2021).

In 1990, Thomas Lindqvist introduced the Extended Producer Responsibility (EPR) concept in Sweden, advocating for the use of recyclable raw materials during production. In 1995, Canberra became the first city to officially adopt a zero waste target, with a municipal commitment to achieving a waste-free city by 2010 (Black & Nakanishi, 2024). The term "zero waste" was formally defined in a 2009 peer-reviewed panel as an ethical, economic, efficient, and visionary goal that guides individuals in adopting sustainable lifestyles and practices that mimic natural cycles. It was further emphasized that all discarded materials should be designed as resources for future use (Zhang et al., 2021).

The Zero Waste (ZW) process requires systematically preventing and eliminating waste materials by reducing their volume and toxicity while preserving all resources. This involves designing and managing products and processes in a way that prevents waste generation, maximizes recovery, and avoids incineration or landfill disposal (Saira & Shanthakumar, 2023). Implementing the Zero Waste system helps mitigate pollution factors in soil, water, and air, thereby reducing threats to human, animal, and plant health (Khalid et al., 2023).

Zero Waste represents an ethical approach and practice that aims to close resource loops and eliminate single-use habits. It is defined as a natural, sustainable cycle in which materials discarded by one entity become resources for another. The Zero Waste concept focuses on minimizing waste volume and its harmful effects while optimizing resource use, enhancing recovery, and eliminating incineration and landfilling. Achieving Zero Waste requires a strong foundation in environmental awareness and advanced research on waste management.

Zero Waste initiatives are typically structured into four key stages:

- Design Phase: Developing innovative designs before production begins to enhance efficiency and prevent waste.
- Sustainable Consumption and Responsible Purchasing: Reducing waste through informed consumption choices and responsible procurement behaviors.
- Waste Minimization: Diverting and reducing waste through efficient waste management practices.
- Policy and Regulatory Evaluation: Assessing waste processes and implementing regulations and policies accordingly (Conlon, 2023).

At an urban level, Zero Waste encompasses awareness of material, food, water, and energy flows. In 2012, the Zero Waste Business Council (ZWBC) was established in the United States, aiming to promote Zero Waste practices globally. Many cities worldwide have adopted Zero Waste strategies and set ambitious targets, including Vancouver (Canada), San Francisco (USA), Adelaide (Australia), Flanders (Belgium), Dubai (UAE), and Buenos Aires (Argentina) (Conlon, 2023).

In today's world, industrialization and globalization have further emphasized the importance of sustainable development. Recognizing this urgency, world leaders adopted the United Nations (UN) 2030 Agenda for Sustainable Development in 2015, establishing a comprehensive global framework for sustainable development. This agenda includes 17 Sustainable Development Goals (SDGs), designed to eradicate poverty and promote sustainability worldwide by 2030. Among these goals, Goal 12 focuses on ensuring responsible production and consumption, reinforcing the principles of sustainable waste management and resource efficiency.

Waste Recycling in Turkey and Worldwide

Waste recycling plays a crucial role in environmental sustainability and the conservation of natural resources. In both Turkey and the global landscape, research and initiatives in this field have increased significantly. However, implementation and success rates vary across countries (Koçak & İkizoğlu, 2020). In Turkey, substantial progress has been made in the Zero Waste initiative, particularly through national projects such as the Zero Waste Project. Despite these efforts, the country's recycling rates remain lower than those observed in European Union (EU) member states. Municipal waste management data indicate

that approximately 32 million tons of household waste are generated annually, yet only a small fraction of this waste is successfully recycled (Genç et al., 2019).

Zero Waste Project in Turkey: Launched in 2017, this initiative aims to develop recycling infrastructure for public institutions, municipalities, and private sector enterprises (Erdur, 2019).

Industrial Waste Management: The recycling of plastic, glass, and metal industrial waste is primarily handled by private companies in Turkey (Salihoğlu et al., 2021).

Recycling Facilities in Turkey: According to 2018 data from the Turkish Statistical Institute (TÜİK), there were 2,223 registered recycling facilities across the country. However, several key challenges hinder recycling efforts, including inadequate recycling infrastructure, low public awareness, lack of standardized waste separation systems among municipalities, and deficiencies in hazardous waste management (Freitas & Michelangelo, 2025).

Global Waste Recycling: Recycling rates vary significantly across countries, with developed nations exhibiting higher success rates, while developing countries struggle with inadequate waste management systems (Liu et al., 2023).

In 2020, the EU generated 2.154 billion metric tons of waste across all economic sectors and households, equivalent to 4,815 kg per capita. Household waste accounted for 9.4% of this total, while the construction (37.5%) and mining & quarrying (23.4%) industries were responsible for more than 60% of total EU waste. Waste and water services contributed 10.8%, and manufacturing accounted for 10.6% of total waste production. Notably, Germany and France collectively generated one-third of all EU waste (Chioatto & Sospiro, 2023).

Among EU nations, Germany (401 million tons) and France (310 million tons) were the largest waste producers in 2020, together accounting for 33% of total EU waste, contributing 19% and 14%, respectively (Weghmann, 2023). The United Kingdom (282 million tons) ranked third, followed by Italy (175 million tons) and Poland (170 million tons) (Di & Beccarello, 2022).

Since mining waste represents the largest waste stream in the EU, excluding it from statistics facilitates cross-country comparisons. According to Eurostat, in 2020, the EU generated 4.8 tons of waste per capita, with 3.08 tons originating from mining waste and 1.735 tons from other sources. In other words, 64% of total EU waste was attributed to the mining sector, including waste rock and tailings from ore processing (Pyrgaki et al., 2021).

Unlike traditional household waste, electronic waste (e-waste) contains hazardous components (Abalansa et al., 2021). However, e-waste materials, particularly their metal and non-metal compositions, exhibit high recycling potential (Dutta et al., 2023). The concentration of valuable metals in e-waste is often dozens or even hundreds of times higher than that found in raw ore (Thakur & Kumar, 2022). E-waste contains up to 60 different metals, including copper, gold, silver, palladium, aluminum, and iron (Gamage et al., 2023).

As of 2017, the estimated value and reserves of recyclable materials within e-waste were as follows:

- Iron/steel: 16,500 kt (€9 billion)
- Copper: 1,900 kt (€10.6 billion)
- Aluminum: 220 kt (€3.2 billion)
- Gold: 0.3 kt (€10.4 billion)
- Silver: 1.0 kt (€0.58 billion)
- Plastic: 8,600 kt (€12.3 billion) (Nithya & Thirunavukkarasu, 2021).

The cost of recycling metals from e-waste is significantly lower than the cost of extracting virgin raw materials, making e-waste recycling an energy-efficient and environmentally friendly solution (Tabelin et al., 2021). Furthermore, the total economic value of recoverable materials in e-waste is estimated to be around $57 billion, surpassing the GDP of many nations (Vishwakarma & Hait, 2024).

In Turkey, managing e-waste issues in the long term requires regulatory adjustments based on an understanding of its potential impacts within the framework of sustainability and digitalization. With the increasing adoption of digital technologies, e-waste volumes are expected to rise significantly. However, current collection and classification systems remain inadequate, necessitating the development of new, technology-driven sustainable collection and sorting models for effective e-waste management. Currently, Turkey's existing e-waste management strategies rely primarily on recycling rather than digitalization-based solutions (Kazancıoğlu et al., 2021). Figure 1 presents the estimated annual e-waste generation in Turkey over the years.

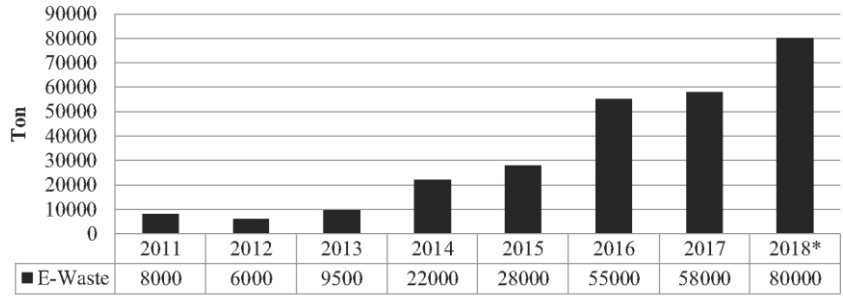

Note(s): 2018* approximate data of the amount of collected e-waste in Turkey (Ministry of Environment and Urbanization, 2017)

Figure 1. Estimated Annual E-Waste Generation in Turkey (Ministry of Environment and Urbanization, 2017; National Waste Management and Action Plan, 2016–2023).

In line with the Waste Electrical and Electronic Equipment (WEEE) Directive of the European Parliament, Turkey has developed a national WEEE regulation to manage electronic waste. The annual e-waste collection targets for the coming years have been published on the official website of the Ministry of Environment, Urbanization, and Climate Change.

According to the 2017 E-Waste Monitor Report, Turkey generated approximately 623,000 tons of electronic waste in that year. Statistics indicate that in 2016, per capita e-waste generation ranged between 6.8 and 7.8 kg. Additionally, Vodafone, a major telecommunications company, reported the amount of e-waste generated in each city in Turkey in 2016. However, beyond these reports, no new comprehensive data on Turkey's e-waste have been made publicly available (Simşek & Satoglu, 2022).

The latest figures show that per capita waste generation among EU member states varies significantly, ranging from 1.5 tons in Croatia to 21 tons in Finland. Finland is followed by Bulgaria (16.8 tons) and Sweden (14.7 tons). Germany and France report figures close to the EU average of 4.8 tons per capita (Tsimnadis & Kyriakopous, 2024).

Conclusion

Global environmental challenges, such as plastic pollution and electronic waste accumulation, require effective and sustainable solutions. A significant portion of plastic waste remains unrecycled and continues to contaminate marine ecosystems, posing severe environmental risks. Additionally, the rapid increase in electronic waste necessitates the implementation of sustainable recycling strategies to mitigate its environmental impact.

Raising public awareness and encouraging participation in recycling initiatives through education and incentive programs is essential for improving waste management systems. While Turkey has made notable progress in recycling and waste management, it still lags behind global leaders in this field. To further enhance recycling efforts, improving waste separation systems, increasing public awareness, and investing in industrial waste management infrastructure are crucial.

On a global scale, countries such as Germany, South Korea, and Sweden serve as leading examples of successful recycling policies. With technological advancements and sustainable waste management policies, it is evident that global recycling rates will continue to improve in the future.

References

Abalansa, S., El Mahrad, B., Icely, J., & Newton, A. (2021). Electronic waste, an environmental problem exported to developing countries: The GOOD, the BAD and the UGLY. Sustainability, 13(9), 5302.

Apollon, W., Rusyn, I., González-Gamboa, N., Kuleshova, T., Luna-Maldonado, A. I., Vidales-Contreras, J. A., & Kamaraj, S. K. (2022). Improvement of zero waste sustainable recovery using microbial energy generation systems: A comprehensive review. Science of The Total Environment, 817, 153055.

Black, J., & Nakanishi, H. (2024). Towards Net-Zero Emissions from Urban Transport: Ex Post Policy Evaluation in Canberra, the Australian Capital Territory. Sustainability, 16(19), 8656.

Cheah, C. G., Chia, W. Y., Lai, S. F., Chew, K. W., Chia, S. R., & Show, P. L. (2022). Innovation designs of industry 4.0 based solid waste management: Machinery and digital circular economy. Environmental Research, 213, 113619.

Chioatto, E., Khan, M. A., & Sospiro, P. (2023). Sustainable solid waste management in the European Union: Four countri regional analysis. Sustainable Chemistry and Pharmacy, 33, 101037.

Conlon, K. (2023). Emerging transformations in material use and waste practices in the Global South: Plastic-Free and Zero Waste in India. Urban Science, 7(2), 47.

Dutta, D., Rautela, R., Gujjala, L. K. S., Kundu, D., Sharma, P., Tembhare, M., & Kumar, S. (2023). A review on recovery processes of metals from E-waste: A green perspective. Science of the Total Environment, 859, 160391.

Erdur, E. (2019). Türkiye'de sıfır atık projesi ve projenin kamu kurumlarında uygulanması; süleymanpaşa belediyesi örneği. Yayımlanmamış yüksek lisans tezi, Ankara Gazi Üniversitesi Fen Bilimleri Enstitüsü Çevre Bilimleri Ana Bilim Dalı, Ankara.

Freitas De Lima, A. P., & Michelangelo Giglio, E. (2025). The Human Factor in The Problems, Challenges And Solutions of Implementing Technologies In Recycling Networks. Environmental & Social Management Journal/Revista de Gestão Social e Ambiental, 19(1).

Gamage, L. E., Basak, A. K., Pramanik, A., Prakash, C., Shankar, S., Debnath, S., ... & Ramakrishana, S. (2023). Recycling of Gold and Silver from Electronic Waste—A Review. Materials Circular Economy, 5(1), 8.

Genç, A., Zeydan, O., & Saraç, S. (2019). Cost analysis of plastic solid waste recycling in an urban district in Turkey. Waste Management & Research, 37(9), 906-913.

Gül, M., & Yaman, K. (2021). Türkiye'de atık yönetimi ve sıfır atık projesinin değerlendirilmesi: Ankara örneği. Atatürk Üniversitesi İktisadi ve İdari Bilimler Dergisi, 35(4), 1267-1296.

Khan, A. H., López-Maldonado, E. A., Khan, N. A., Villarreal-Gómez, L. J., Munshi, F. M., Alsabhan, A. H., & Perveen, K. (2022). Current solid waste management strategies and energy recovery in developing countries-State of art review. Chemosphere, 291, 133088.

Khan, A. H., López-Maldonado, E. A., Alam, S. S., Khan, N. A., López, J. R. L., Herrera, P. F. M., ... & Singh, L. (2022). Municipal solid waste generation and the current state of waste-to-energy potential: State of art review. Energy Conversion and Management, 267, 115905.

Kazancoglu, Y., Ozbiltekin, M., Ozkan Ozen, Y. D., & Sagnak, M. (2021). A proposed sustainable and digital collection and classification center model to manage e-waste in emerging economies. Journal of Enterprise Information Management, 34(1), 267-291.

Koçak, E., & İkizoğlu, B. (2020). Types of waste in the context of waste management and general overview of waste disposal in Turkey. International Journal of Agriculture Environment and Food Sciences, 4(4), 520-527.

Kurniawan, T. A., Maiurova, A., Kustikova, M., Bykovskaia, E., Othman, M. H. D., & Goh, H. H. (2022). Accelerating sustainability transition in St. Petersburg (Russia) through digitalization-based circular economy in waste recycling industry: A strategy to promote carbon neutrality in era of Industry 4.0. Journal of cleaner production, 363, 132452.

Lee, E., Shurson, G., Oh, S. H., & Jang, J. C. (2024). The mana-gement of food waste recycling for a sustainable future: A case study on South Korea. Sustainability, 16(2), 854.

Liu, K., Tan, Q., Yu, J., & Wang, M. (2023). A global perspec-tive on e-waste recycling. Circular Economy, 2(1), 100028.

Lee, E., Shurson, G., Oh, S. H., & Jang, J. C. (2024). The mana-gement of food waste recycling for a sustainable future: A case study on South Korea. Sustainability, 16(2), 854.

Liu, K., Tan, Q., Yu, J., & Wang, M. (2023). A global perspective on e-waste recycling. Circular Economy, 2(1), 100028.

Nguyen, T. T. T., Malek, L., Umberger, W. J., & O'Connor, P. J. (2022). Household food waste disposal behaviour is driven by perceived personal benefits,

recycling habits and ability to compost. Journal of Cleaner Production, 379, 134636.

Nithya, R., Sivasankari, C., & Thirunavukkarasu, A. (2021). Electronic waste generation, regulation and metal recovery: a review. Environmental Chemistry Letters, 19, 1347-1368.

Shittu, O. S., Williams, I. D., & Shaw, P. J. (2021). Global E-waste management: Can WEEE make a difference? A review of e-waste trends, legislation, contemporary issues and future challenges. Waste Management, 120, 549-563.

Shukla, K. A., Sofian, A. D. A. B. A., Singh, A., Chen, W. H., Show, P. L., & Chan, Y. J. (2024). Food waste management and sustainable waste to energy: Current efforts, anaerobic digestion, incinerator and hydrothermal carbonization with a focus in Ma-laysia. Journal of Cleaner Production, 448, 141457.

Simsek, E., Ozdemir, Z., & Satoglu, S. I. (2022). Sustainable planning of precious and rare elements' recycling from waste electronic products: a multi-objective model and application. Process Integration and Optimization for Sustainability, 6(3), 7

Tabelin, C. B., Park, I., Phengsaart, T., Jeon, S., Villacorte-Tabelin, M., Alonzo, D., ... & Hiroyoshi, N. (2021). Copper and critical metals production from porphyry ores and E-wastes: A review of resource availability, processing/recycling challenges, socio-environmental aspects, and sustainability issues. Resources, Conservation and Recycling, 170, 105610.23-735.

Tsimnadis, K., & Kyriakopoulos, G. L. (2024). Investigating the Role of Municipal Waste Treatment within the European Union through a Novel Created Common Sustainability Point System. Recycling, 9(3), 42.

Thakur, P., & Kumar, S. (2022). Evaluation of e-waste status, management strategies, and legislations. International Journal of Environmental Science and Technology, 19(7), 6957-6966.

TÜİK waste disposal and recovery facilities statistics, 2018. Access date 25.02.2025.

Van Yken, J., Boxall, N. J., Cheng, K. Y., Nikoloski, A. N., Moheimani, N. R., & Kaksonen, A. H. (2021). E-waste recycling and resource recovery: A review on technologies, barriers and enablers with a focus on oceania. Metals, 11(8), 1313.

Vishwakarma, A., & Hait, S. (2024). E-Waste Valorization and Resource Recovery. Management of Electronic Waste: Resource Recovery, Technology and Regulation, 202-233.

Zhang, P., Xie, Y., Wang, Y., Li, B., Li, B., Jia, Q., ... & Cai, Y. (2021). Water-Energy-Food system in typical cities of the world and China under zero-waste: Commonalities and asynchronous experiences support sustainable development. Ecological Indicators, 132, 108221.

CHAPTER 8

Synthesis of Lithium Titanium Oxide From Boron Ore Wastes

Ayşegül Yücel[1] & Musa Sarıkaya[2] & Tolga Depci[3]

[1] Asst. Prof. İskenderun Technical University, İskenderun Vocational School, Department of Envıronmental Protectıon Technologies, Hatay, Türkiye, ORCID: 0000-0001-7069-7518
[2] Prof. Dr. Inönü University, Department of Mining Engineering, Malatya, Türkiye, ORCID: 0000-0003-4942-4472
[3] Prof. Dr., Iskenderun Technical University, Faculty of Engineering and Natural Science, Department of Petroleum and Natural Gas Engineering, Iskenderun, Hatay, Türkiye, ORCID: 0000-0001-9562-8068

1. Introduction

Lithium titanium oxide (LTO) compounds are being investigated to improve lithium-ion batteries' energy storage capacities (Liu et al., 2017 a, b; Meng et al., 2014). LTOs are produced by sol-gel (Zhang et al., 2013) or combustion methods (Wang et al., 2013). However, solid-state reactions are preferred because these methods are complex and expensive procedures (Ribeiro et al., 2019; Michalska et al., 2014). The solid-state method is one of the simplest synthesis methods (Smida et al., 2020). This method widely produces complex oxides from simple oxides, carbonates, nitrates, hydroxides, oxalates, alkoxides, and other metal salts. In the solid-state method, the primary purpose is to mix the powder mixture very homogeneously and reduce the powder's particle size. Then the second step is the heat treatment application (Buekenhoudt et al., 2010).

The solid-state chemical reaction process occurs in four steps: diffusion (i), reaction (ii), nucleation (iii), and growth (iv). In the mechanical process, described as the conventional method and using a mortar, the force required to break up the particles cannot be accurately controlled. For this reason, planetary ball mills, where the grinding speed and time can be controlled, are used today (Cova & Luque, 2019). The process in the grinder can be described in three steps (Figure 1. a). The first step is, to begin with, the rearrangement and re-stacking of particles. At this stage, the particles pass each other with minimal deformation and breakage, producing fine, irregularly shaped particles. The second step involves the elastic and plastic deformation of the particles. At this stage, welding may occur between metallic particles. The third step involves particle fracture, which results in further deformation and/or fragmentation of the particles. As the size of the particles decreases, the tendency to form aggregates and the fracture resistance increase. As the grinding continues and maximum energy is consumed, the particle fineness approaches a limit (Kopp et al., 2013; Arzt et al., 2001; Do et al., 2000).

The next stage of the solid-state synthesis method is the sintering roasting method. Many different mechanisms can occur, such as sintering events in polycrystalline materials, the presence of grain boundaries, and diffusion at grain boundaries. In practice, more than one mechanism may operate during any sintering method. The emergence of multiple mechanisms complicates the analysis of sintering rates and the determination of sintering mechanisms. The most critical consequence of grain boundaries can occur as grain growth and pore growth during sintering.

Figure 1. b examines the sintering mechanism of a structure consisting of three particles. At least six different sintering mechanisms can be counted in this polycrystalline material. Surface diffusion, lattice diffusion, and vapor transport from particle surfaces (mechanisms 1, 2, and 3) lead to neck growth without condensation and are non-descriptive mechanisms. Grain boundary diffusion and lattice diffusion from grain boundary to pores (4 and 5) are polycrystalline ceramics' most important densification mechanisms. Diffusion from the grain boundary to the pores allows neck growth and condensation. Plastic flow by dislocation (linear) action (mechanism 6) also leads to neck growth and densification but is more common in the sintering of metal powders (Rahaman, 2017).

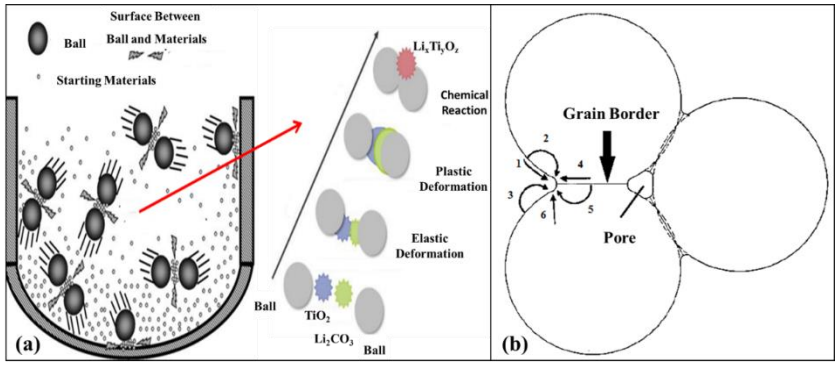

Figure 1. Schematic representation of the events that may occur in (a) the ball mill and (b) sintering theory (Rahaman, 2017). (b: 1: Surface diffusion; 2: Lattice diffusion (from the surface); 3: Vapor transport; 4: Grain boundary diffusion; 5: Lattice diffusion (from grain boundary); 6: Plastic flow)

Raj et al. (2019) synthesized a solid state using mechanical activation with $Li_4Ti_5O_{12}$, Li_2CO_3, and anatase starting reagents to examine supercapacitor properties. The ball mill was operated at a rotational speed of 900 rpm for 12 hours, and ethanol was added to the mill chamber as a solvent. After mechanical activation, the material was calcined at 800°C for 10 hours. During the heat treatment, Li^+ ion diffused into TiO_2, and $Li_4Ti_5O_{12}$ formation started from the outer surface. For this reason, they stated that mixing the raw materials homogeneously and finely is essential for a complete reaction.

Researchers examined the photocatalytic application to examine the effect of ethanol added to the medium during mechanical activation. Walenta et al. (2015) stated that ethanol is adsorbed on rutile as dissolution in an oxygen space. They also mentioned water as a by-product since this can be defined as a surface defect.

Lithium titanium oxides have two important uses. One is its use as an anode electrode material due to the rapid progress in lithium-ion batteries (Liu et al., 2017). For example, the $LiTi_2O_4$ compound is a superconducting oxide system as a thin film (Maruyama et al., 2015; Jin et al., 2015) and the other as bulk material (Johnston et al., 1973). In addition, many researchers have turned to research lithium titanium oxide systems to increase lithium-ion batteries' energy storage capacity (Liu et al., 2017).

Lithium titanates ($Li_4Ti_5O_{12}$, $Li_2Ti_2O_4$, and $Li_7Ti_5O_{12}$) have lithium intercalation and de-intercalation reversibility, superior capacity retention, and long cycle lives unless there is significant structural change (Ziebarth et al., 2014; Ra et al., 2005; Guerfi et al., 2003; Ohzuku et al., 1995).

However, these electrochemical insertion processes create volume changes in the electrodes, leading to the formation of cracks that damage cells. Therefore, $Li_{1+y}Ti_{2-y}O_4$ ($x = 1$, $0 \leqslant y \leqslant 1/3$) has become a potential electrode material as it is a zero voltage insertion material (Scharner et al., 1999; Cava et al., 1984).

It has been reported that nanometer-sized $LiTi_2O_4$ can be synthesized by the hydrothermal method, but this may result in an incomplete reaction and side reaction product (Fattakhova et al., 2005).

A small crystal size can be preferred in lithium titanium oxides to be used as the electrode material to increase the active surface area and accelerate the electrochemical reaction (Kashkooli et al., 2016; Pohjalainen et al., 2015; Wang et al., 2014).

Yue et al. (2018) reported that as a result of various electrochemical analyses such as charge/discharge profiles and cyclic voltmeter with synthesized $Li_4Ti_5O_{12}$, 7 nm nanoparticles exhibited as good reversible capacity as those with larger crystal sizes.

In using lithium titanium oxides as lithium-ion sieves, their different specific morphologies may affect various properties such as lithium uptake capacity, Li^+ adsorption equilibrium time, selective lithium performance, and reproducibility. In general, it is stated that the smaller the adsorbent crystal size, the greater the lithium uptake capacity can be and the shorter the Li^+ adsorption equilibrium time will be, and this is because smaller particles usually produce larger specific areas (Xu et al., 2016).

$Li_2Ti_2O_4$ ceramic is tough to synthesize. The reason for this is the evaporation of lithium ions and oxidation of titanium ions at high reaction temperatures (Yang

et al., 2010). In addition, various defects that may occur during synthesis play an essential role in determining the material's thermodynamic, electrical, and optical properties (Liu et al., 2017 – b; Deiss et al., 1997).

Despite their high performance, they are expensive systems (Wegmann et al., 2018). In the literature reviews, lithium titanium oxide batteries offer a potential use in the battery industry due to their higher C rate (C, a current value used to estimate and/or indicate the expected adequate time of the battery under variable charge/discharge conditions) charge/discharge feature (Zaghib et al., 2011), longer life, power density (Giuliano et al., 2018) and safety performances (Cicconi et al., 2019).

As a result of technological developments in electronic devices that require high-performance batteries, the demand for lithium has increased at the same rate. Since lithium sources could not meet this increasing demand (Paranthaman et al., 2017; Swain, 2017; Hanisch et al., 2015; Grosjean et al., 2012), lithium was tried to be obtained from different sources. Many different processes (adsorption, solvent extraction, membrane, electrodialysis, etc.) are applied to take lithium into solution from lithium sources (minerals, brines, geothermal waters, clays, etc.) (Xu et al., 2021; Liu et al., 2019; Xu et al., 2016). To remove lithium ions in the solution medium, lithium-ion sieves with effective adsorbent properties have been synthesized, and many researchers continue to work. (Chitrakar et al., 2014; Yu et al., 2014). There are two types of lithium-ion sieves used in lithium adsorption. One is LiMnO (LMO), and the other is $LiTi_2O_4$ (LTO). Compared with manganese-type lithium-ion sieves, titanium-type lithium-ion sieves with stronger Ti-O bonds have a stable structure, good acid resistance, lower dissolution loss of Ti, relatively stable adsorption performance, and multiple recycling (Zhang et al. et al., 2021).

Yücel (2022) in her doctoral thesis conducted a comprehensive characterization of boron ore waste. Through X-ray Fluorescence (XRF) analysis, it was determined that the loss on ignition was 35.06%. Elemental analysis revealed predominant oxidized compounds including CaO (24.16%), MgO (16.13%), and SiO_2 (15.50%). Further analysis using Inductively Coupled Plasma Mass Spectrometry (ICP-MS) indicated the presence of lithium at 1131,9 ppm. X-ray Diffraction (XRD) analysis, employing the Reference Intensity Ratio (RIR) method, identified the composition as 11,8% $CaMg(CO_3)_2$, 81% $Ca_7Mg_{7.25}Si_{14}$, and 7,2% $LiAlSiO_4$. To recover lithium from the boron ore waste, a series of sequential processes including calcination and water leaching were conducted. Auxiliary agents such as $CaSO_4.2H_2O$ and $CaCO_3$ were incorporated

during calcination to facilitate the extraction process, resulting in lithium dissolution. The highest lithium concentration (1099,76 ppm) was achieved through water leaching. Subsequently, a 1000 ppm Na solution was introduced to the solution containing the highest lithium concentration, precipitating lithium carbonate. This study aims to synthesize $Li_xTi_yO_z$ using Li_2CO_3 obtained from boron wastes. For this purpose, two different pretreatments were used, one conventional and the other mechanochemical. Obtained Li_2CO_3 was subjected to a calcination process at 850°C. The effect of different parameters used in pretreatments on $Li_xTi_yO_z$ synthesis was investigated in the study.

2. Materials and Methods

In the analysis of boron ore waste obtained from Eti Maden İşletmeleri Eskişehir Kırka Boron Operations Directorate, a lithium content of 1131,9 ppm was detected using ICP-MS analysis. To recover the lithium, a mixture of calcium sulfate ($CaSO_4.2H_2O$) and calcium carbonate ($CaCO_3$) reagents was added to the waste in specific mass proportions. The resulting mixture was subjected to roasting at 900°C for 120 minutes. Subsequently, water leaching was performed on the cooled material using a solid/liquid ratio of 5%. The leaching process involved stirring the mixture at 400 rpm under ambient conditions for a contact time of 120 minutes, resulting in a lithium recovery yield of 97.16% (Yücel, 2022).

Next, to obtain Li_2CO_3, Na_2CO_3 dissolved in water (1000 ppm Na solution) was added dropwise to the previously obtained solution, and the reaction temperature was maintained at 80°C. Following a 72-hour reaction period, the solid product was separated by centrifugation and subsequently dried at 105°C overnight (Yücel, 2022). The obtained material was then subjected to structural analysis using XRD (Fig.2.a) and SEM (Fig.2.b) analysis.

The subsequent objective was to synthesize $Li_xTi_yO_z$ (LTO) by combining the obtained Li_2CO_3 with specific amounts of commercial TiO_2 (CAS number: 13463-67-7, Sigma-Aldrich). Two different methods, conventional and mechanochemical, were investigated for their potential to produce LTO.

In the experimental studies, 10 mg Li_2CO_3 and 10 mg TiO_2 were mixed in a 1:1 ratio, and 10 mg Li_2CO_3 and 20 mg TiO_2 were mixed in a 1:2 ratio. The chemical reaction that can occur in both methods is given below.

$$Li_2CO_3 + TiO_2 \rightarrow Li_xTi_yO_z + CO_2 \qquad (2.1)$$

Retsch brand PM100 model ball mill was used to synthesize $Li_xTi_yO_4$ ceramic material, and Protherm brand PLF120 model chamber furnace was used for the sintering process. First, Li_2CO_3 and TiO_2 obtained from the waste were mixed in a 1:1 and 1:2 ratio in 5 mL ethanol (the same amount in all studies) in a ball mill at 200 and 400 rpm rotational speed for 15, 30, 45, 60, and 90 minutes. Next, each sample was dried in an oven at 80°C for 60 minutes to remove ethanol and then was heat treated in an oven at 850°C for 30, 60, 90, and 120 minutes for calcination (Yücel, 2022).

3. Results and Discussion

3.1. Characterization of Lithium Carbonate

The characterization of Li_2CO_3, derived from boron ore tailings, was conducted using X-ray diffraction (XRD) and scanning electron microscopy (SEM) analyses. XRD analysis was performed using the Rigaku Brand Miniflex 600 Model, employing X-rays at 40 kV and 15 mA. The range of 2θ (Theta) values investigated spanned from 10 to 80 degrees. The obtained XRD pattern was compared with the monoclinic crystal structure of Li_2CO_3 available in the ICDD (International Centre for Diffraction Data) library of the device. The comparison confirmed the presence of Li_2CO_3 in the sample, as indicated by the match with the corresponding PDF Card No: 01-083-1454.

In their study, Wang et al. (2019) aimed to produce Li_2CO_3 through a solution containing LiCl and Na_2CO_3 at various temperatures ranging from 5 to 80 °C. During the X-ray diffraction (XRD) analysis conducted in their research, they observed that the peaks between 20 and 40 ° (2θ values) closely resembled the XRD peaks of Li_2CO_3 obtained in this current study. This similarity in the XRD patterns suggests that the Li_2CO_3 produced in both studies exhibited comparable crystal structures. Furthermore, Wang et al. (2019) performed thermal analysis on the obtained Li_2CO_3 samples, spanning a temperature range of 5 to 80 °C. It was observed that the Li_2CO_3 sample synthesized at 80 °C showed a relatively smaller mass loss, and this mass loss occurred at approximately 700 °C. This finding indicates that Li_2CO_3 synthesized at 80 °C in their study exhibited higher thermal stability, as it required a higher temperature (around 700 °C) for significant mass loss to occur.

Aguilar and Graber (2018) focused on examining the reaction kinetics between lithium sulfate and sodium carbonate solutions in their study. They employed the calorimetric method to investigate the relationship of the reaction rate with both temperature (at 60, 70, and 80°C) and concentration of the

solutions. Through their experimentation, Aguilar and Graber (2018) determined that the reaction between these two solutions is characterized as an endothermic reaction. An endothermic reaction absorbs heat from the surroundings, resulting in a decrease in the temperature of the reaction mixture. Interestingly, the study revealed that increasing the temperature had a positive effect on the reaction time. In an endothermic reaction, the reaction time decreases as the temperature rises. This finding implies that the rate of reaction between lithium sulfate and sodium carbonate solutions is enhanced with higher temperatures, allowing for faster reaction kinetics. Overall, the investigation conducted by Aguilar and Graber provided valuable insights into the temperature-dependent reaction kinetics of lithium sulfate and sodium carbonate, highlighting the endothermic nature of the reaction and its positive correlation with reaction time at elevated temperatures. The similarities and differences observed between the XRD patterns and thermal analysis results of both studies provide valuable insights into the structural and thermal properties of the Li_2CO_3 synthesized under different conditions.

Additionally, SEM analysis was conducted to visualize and characterize the morphology and microstructure of the Li_2CO_3 sample (Fig.2.b). As evident from the figure, the material exhibits a relatively uniform and foliated appearance, although there is variation in crystal size. Applying the Scherrer equation, the crystal size was determined to be approximately 24.92 nm. In the microstructure, rounded structures were observed on the leafy-looking formations. These rounded structures were believed to be unreacted Na_2CO_3 residues. These residues may have resulted from incomplete reaction processes during the synthesis of the material.

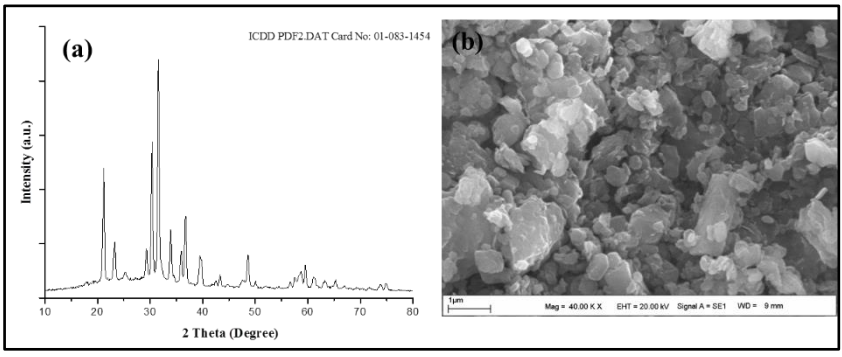

Figure 2. XRD (a) and SEM (b) images of the obtained Li_2CO_3

3.2. Synthesis with the Conventional Method

In the conventional method of synthesizing LTO, agate mortar was utilized to mix the materials for 15 minutes before calcination at 850°C. The study investigated the influence of TiO_2 amount and calcination time on the resulting product. When Li_2CO_3 and TiO_2 were mixed in a 1:1 ratio by mass, it was observed that two phases were formed in the structure regardless of the calcination time. These phases were identified as dilithium titanate (D-LTO) and TiO_2 (Figure 3. a). The content of the D-LTO phase within the structure was found to be 79.4% (30 minutes), 86.7% (60 minutes), 91% (90 minutes), and 91.7% (120 minutes), respectively. The remaining amounts represented the TiO_2 phase. The chemical formula of these D-LTO phases was determined to be $(Li_2TiO_3)_{10.667}$, and they corresponded to card number 01-075-1602 in the ICDD PDF2.DAT library. In the calculations using the Scherrer equation, it was noted that the calcination time did not significantly affect the crystal size. The crystal size was measured to be 7.37 nm (30 minutes), 25.30 nm (60 minutes), 27.33 nm (90 minutes), and 25.1 nm (120 minutes), respectively. Analyzing the structures of TiO_2 involved in the reaction, it was found that TiO_2 existing at 30 minutes and 60 minutes corresponded to card number 00-021-1276 in the ICDD PDF2.DAT library, and TiO_2 formed at 90 minutes and 120 minutes matched card number 01-078-1510 in the same library. Despite the difference in their unit cell dimensions, it was observed that both TiO_2 structures shared the same crystal structure.

Tangkas et al. (2021) used XRD to define the structure and compound of lithium titanium oxide (LTO) in their study with Li_2TiO_3, which they synthesized by the solid-state method. In their analysis, they stated that the LTO product has a significant monoclinic structure at 2θ (theta) 18° and 43°, and the size of the formed crystals is affected by temperature and solid Li/Ti ratio. They found that the maximum dimension at 600°C and 750°C was 512 nm and 50 nm, respectively. Furthermore, they reported that the higher the temperature, the smaller the crystal size formed, and the higher the Li/Ti solid ratio, the larger the crystal size formed. In our study, it was observed that the crystal sizes found in the experiments performed at the 1:2 ratio (Li_2CO_3:TiO_2) increased compared to the crystal sizes in the experiments at 1:1 ratio (Li_2CO_3:TiO_2). The crystalline dimensions were below 50 nm at 850°C supporting the study of Tangkas et al. (2021).

Obtaining lithium titanate by doubling the amount of TiO_2 used with the same method was also studied. XRD analyses of the obtained products are given in

Figure 2. b. In addition to the dilithium titanate phase with ICDD PDF2.DAT Card number 01 – 075 – 1602 and chemical formula $(Li_2TiO_3)_{10.667}$, the unreacted TiO_2 (ICDD PDF2.DAT Card no: 00 – 021 – 1276) phase was also detected. As the calcination time increases, the percentage of dilithium titanate formed in the structure also increases. 62% of D-LTO was formed in 30 minutes, 81.6% in 60 minutes, 77% in 90 minutes, and 93% in 120 minutes of calcination time. By using the Scherrer equation the crystal size of D – LTOs was calculated as 24.77, 28.46, 23.13, and 27.74 nm, respectively.

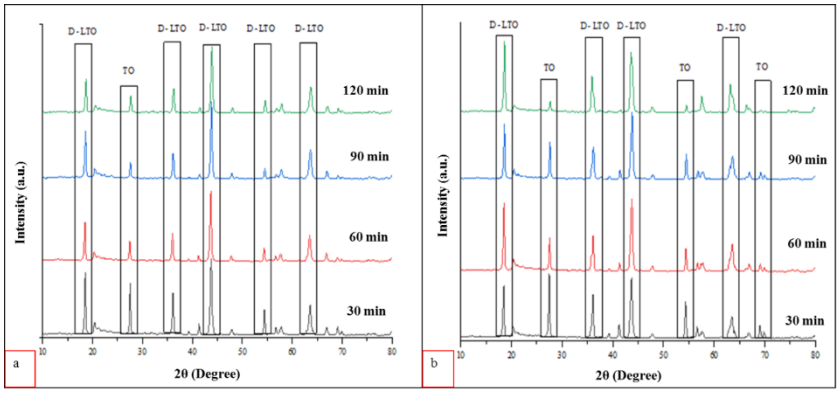

Figure 3. XRD analysis of lithium titanates obtained using the conventional method (a: Mixing ratio 1:1 (Li_2CO_3:TiO_2), b: Mixing ratio 1:2 (Li_2CO_3:TiO_2))

3.2. Synthesis with The Mechanochemical Pretreatment

It was observed that the lithium titanate oxide structure formed in the synthesis process with the conventional method did not change depending on calcination time and remained the same. For this reason, different structured lithium titanate oxide production was investigated with the help of a ball mill using Li_2CO_3 precipitated from waste. For this purpose, in addition to 5 different grinding times and four different calcination time parameters, the 1:1 and 1:2 (Li_2CO_3:TiO_2)ratios, whose chemical reactions are given below, were also studied.

$$Li_2CO_3 + TiO_2 \rightarrow Li_xTi_yO_z + mCO_2 \quad (3.1)$$

$$Li_2CO_3 + 2TiO_2 \rightarrow Li_aTi_bO_c + nCO_2 \quad (3.2)$$

Studies were carried out at 200 and 400 rpm rotation speeds to examine the effect of the rotational speed of the ball mill. The number of balls (agate) and the amount of ethanol placed in the chamber (agate) were kept constant in the mill. Working conditions are presented in Table 1, and XRD analyses of the obtained lithium titanates are presented in Figure 3. In these operating conditions, only

dilithium titanium oxide with the chemical formula of $(Li_2TiO_3)_{10.667}$ is formed, and its ICDD PDF2.DAT Card number is 01 – 075 – 1602. When compared with the conventional method, it was observed that dilithium titanium oxides with the same structure were formed. However, TiO_2 peaks, which did not react in the conventional method, were also found.

The smallest crystalline size was found to be 17.06, 19.51, 20.73, and 18.72 nm, respectively, in the study in which the calcination time was kept as 30, 60, 90, and 120 minutes at 850°C at a mixing ratio of 1:1 for 60 minutes grinding time. On the other hand, the largest crystal size was obtained as 31.29 nm at 15 minutes of grinding and 90 minutes of calcination time. The highest crystalline size was reached at a mixing ratio of 1:2 (Li_2CO_3:TiO_2) and calcination times of 60, 90, and 120 minutes at 90 minutes of grinding time. These values were 44.90, 44.60, and 46.41 nm, respectively, depending on the calcination time.

Table 1. Operating conditions and obtained results at 200 rpm.

Working conditions			Results	
Mixing ratio	Grinding time (min)	Oven Time (min)	Obtained Products	Size of the Crystal (nm)
1:1	15	30	$(Li_2TiO_3)_{10,667}$ 01 – 075 – 1602*	22,78
	30			20,82
	45			21,22
	60			17,06
	90			17,46
1:1	15	60		28,63
	30			23,27
	45			22,49
	60			19,51
	90			24,14
1:1	15	90		31,29
	30			24,68
	45			24,54
	60			20,73
	90			22,40
1:1	15	120		28,14
	30			26,21
	45			20,49
	60			18,72
	90			24,79
1:2	15	30	$(Li_2TiO_3)_{10,667}$ 01 – 075 – 1602*	29,35
	30			19,61
	45			36,76

	60		$Li_4Ti_5O_{12}$	41,90
	90		00 – 049 – 0207*	37,86
1:2	15	60	$(Li_2TiO_3)_{10,667}$ 01 – 075 – 1602*	21,69
	30		$Li_4Ti_5O_{12}$ 00 – 049 – 0207	28,04
	45			39,18
	60			39,25
	90			44,90
1:2	15	90	$Li_4Ti_5O_{12}$ 00 – 049 – 0207*	25,86
	30			33,93
	45		$Li_2Ti_2O_4$ 00 – 038 – 0270*	34,91
	60		$Li_4Ti_5O_{12}$ 00 – 049 – 0207*	36,79
	90			44,60
1:2	15	120	$Li_2Ti_2O_4$ 00 – 038 – 0270*	31,66
	30			31,37
	45		$Li_4Ti_5O_{12}$ 00 – 049 – 0207*	37,21
	60		$Li_2Ti_2O_4$ 00 – 038 – 0270*	40,20
	90		$Li_4Ti_5O_{12}$ 00 – 049 – 0207*	31,66

* ICDD PDF2.DAT Card number

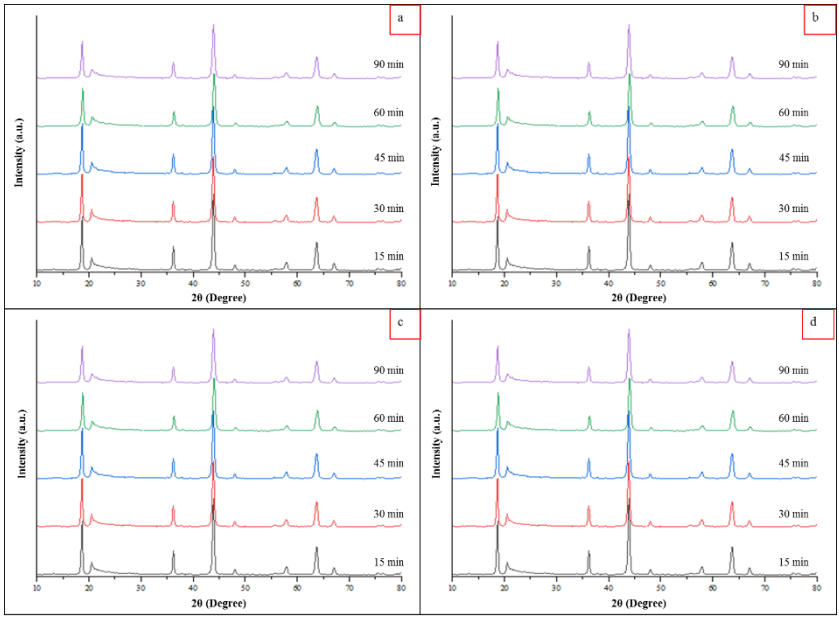

Mixing Ratio 1:1

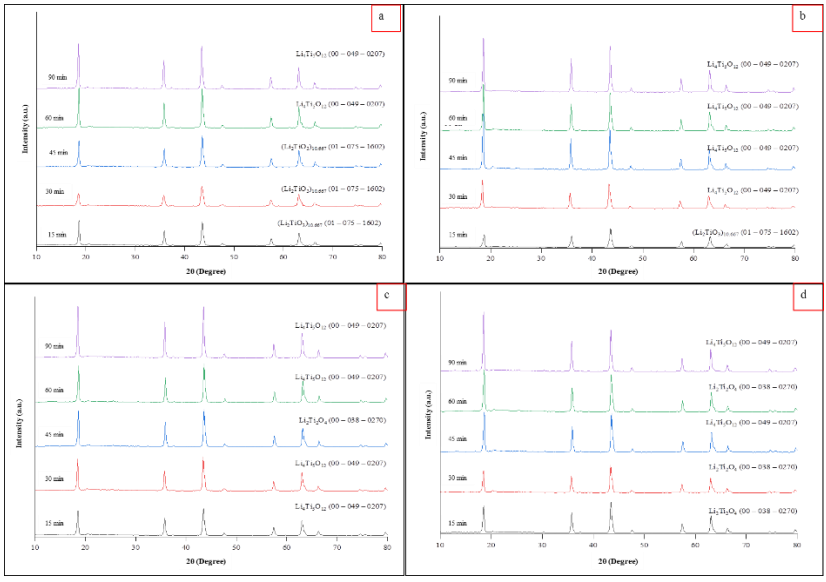

Mixing Ratio 1:2

Figure 4. XRD analysis of lithium titanate oxides synthesized at 200 rpm grinding speed (Oven time a: 30 min, b: 60 min, c: 90 min, and d: 120 min)

During the study, it was tried to synthesize lithium titanate oxides by changing the mill rotation speed to 400 rpm in the mechanochemical pretreatment stage.

The experimental conditions, obtained products, chemical formulas, PDF2.DAT card numbers, and crystalline dimensions are given in Table 2. At the same grinding and calcination times, it was observed that dilithium oxide (Figure 4), which has a similar structure to the studies carried out at 200 rpm grinding speed, was observed in the studies performed at a Li_2CO_3: TiO_2 (1:1) ratio at 400 rpm. Its ICDD PDF2.DAT Card number is 01 – 075 – 1602, and its chemical formula is $(Li_2TiO_3)_{10.667}$. The average crystal size was calculated as 22.19 nm.

In the study performed at the ratio of Li_2CO_3:TiO_2 (1:2) $(Li_2TiO_3)_{10,667}$ (ICDD PDF2.DAT Card number 01 – 075 – 1602) is formed in 30 minutes calcination and 60 minutes grinding time, while $Li_4Ti_5O_{12}$ (ICDD PDF2.DAT Card number 00 – 049 – 0207) is formed in other operating conditions. In 60 minutes of calcination time and 15 and 60 minutes of grinding times $(Li_2TiO_3)_{10,667}$ (ICDD PDF2.DAT Card number 01 – 075 – 1602) was formed The material with the chemical formula $Li_2Ti_2O_4$ (ICDD PDF2.DAT card number) was formed both in 60 minutes of grinding and 90 minutes of calcination and 120 minutes calcination, 30 and 90 minutes of grinding time. At the end of the studies, three different lithium titanium oxides were obtained. When the average of the crystalline sizes of these species among themselves (Table 2) is calculated, the values of 31.20 nm for the material with the chemical formula $(Li_2TiO_3)_{10,667}$, 38.40 nm for the material with the chemical formula $Li_4Ti_5O_{12}$ and 37.35 nm for the material with the chemical formula $Li_2Ti_2O_4$ has been obtained. In the grinding and calcination study performed at the ratio (1:2), the highest crystal size was obtained with 46.47 nm in 90 minutes of calcination and 45 minutes of grinding time. The smallest crystal size was obtained at 28.50 nm in 60 minutes of grinding and calcination time (Table 2).

Table 2. Operating conditions and obtained results at 400 rpm.

Operating Conditions			Results	
Mixing Ratio	Grinding time (min)	Oven Time (min)	Obtained Products	Crystal Size (nm)
1:1	15	30	$(Li_2TiO_3)_{10,667}$ 01 – 075 – 1602*	19,22
	30			23,65
	45			17,21
	60			20,71
	90			22,40
1:1	15	60		21,18
	30			28,90
	45			21,58
	60			21,40
	90			24,19
1:1	15	90		20,35
	30			25,02
	45			21,02
	60			23,43
	90			21,54
1:1	15	120		21,17
	30			19,33
	45			21,85
	60			25,14
	90			24,49
1:2	15	30	$Li_4Ti_5O_{12}$ 00 – 049 – 0207*	34,91
	30			30,12
	45			38,38
	60		$(Li_2TiO_3)_{10,667}$ 01 – 075 – 1602*	30,32
	90		$Li_4Ti_5O_{12}$ 00 – 049 – 0207*	34,07
1:2	15	60	$(Li_2TiO_3)_{10,667}$ 01 – 075 – 1602*	30,75
	30		$Li_4Ti_5O_{12}$	40,58

	45		00 – 049 – 0207*	41,89
	60		$(Li_2TiO_3)_{10,667}$ 01 – 075 – 1602*	28,50
	90		$Li_4Ti_5O_{12}$ 00 – 049 – 0207*	35,44
1:2	15	90	$Li_4Ti_5O_{12}$ 00 – 049 – 0207*	39,27
	30			38,02
	45			46,47
	60		$Li_2Ti_2O_4$ 00 – 038 – 0270*	41,60
	90		$Li_4Ti_5O_{12}$ 00 – 049 – 0207*	40,05
1:2	15	120	$Li_4Ti_5O_{12}$ 00 – 049 – 0207*	38,86
	30		$Li_2Ti_2O_4$ 00 – 038 – 0270*	38,69
	45		$Li_4Ti_5O_{12}$ 00 – 049 – 0207*	41,18
	60		$(Li_2TiO_3)_{10,667}$ 01 – 075 – 1602*	35,23
	90		$Li_2Ti_2O_4$ 00 – 038 – 0270*	31,76

* ICDD PDF2.DAT Card number

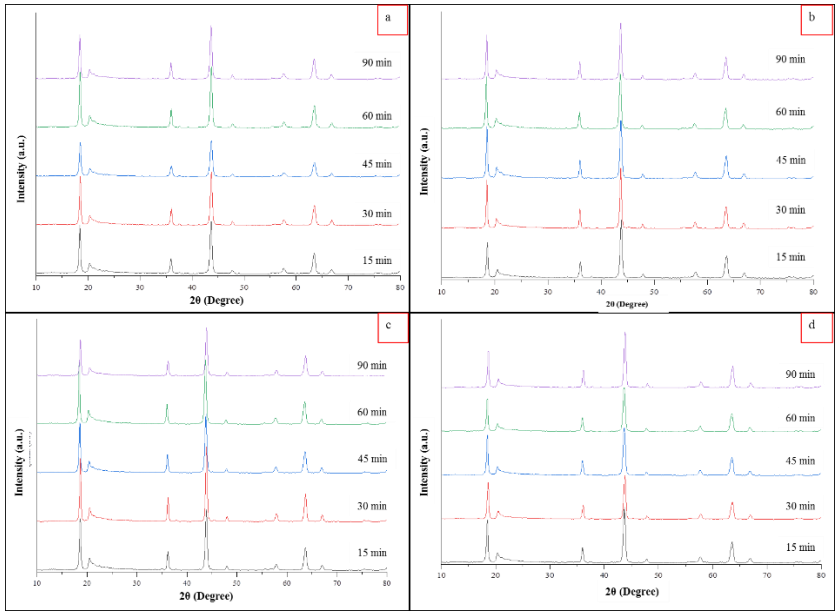

Mixing Ratio 1:1

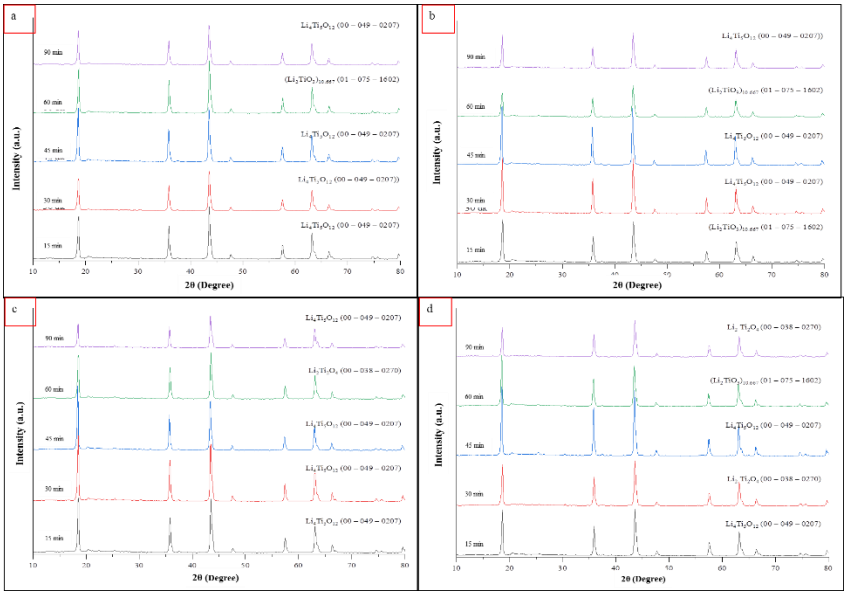

Mixing Ratio 1:2

Figure 5. XRD analysis of lithium titanate oxides synthesized at 400 rpm grinding speed (Oven time a: 30 min, b: 60 min, c: 90 min, and d: 120 min)

Synthesis by the conventional method initially occurs at the reagents' interface. Therefore, non-homogeneous phases may occur. The disadvantages of solid-state synthesis, without distinguishing the intended use of lithium titanium oxides, are that the required particle size cannot be obtained and does not provide the desired morphology and homogeneity (Yi et al., 2010). In addition, high calcination is needed to sustain the reaction. For example, in solid-state reactions of Li_2CO_3 and TiO_2, a calcination temperature of at least 850°C is generally needed (Yuan et al., 2011; Yuan et al., 2009).

In this study, Li_2CO_3 obtained from boron wastes and TiO_2 starting reagents were used and studied with the conventional solid-state method. However, the products obtained were in two phases. In the study performed at the ratio of Li_2CO_3:TiO_2 (1:1), as the calcination time increased, TiO_2 decreased by 12.3%. This showed that the formation reaction of lithium titanium oxide continued with increasing calcination time. On the other hand, at the ratio of Li_2CO_3:TiO_2 (1:2), it was observed that the calcination time did not affect the formation of lithium titanium oxide so much, and the TiO_2 phase remained at an average of 26.03%.

Babu et al. (2018) synthesized solid-state using Li_2CO_3 and TiO_2 starting reagents. After calcining for 16 hours in air at 850°C, they were pelleted and sintered for another 16 hours at 900°C. They stated that the mass loss up to 500°C is due to the water and crystal water in the structure, and the mass loss between 500-700°C is due to the conversion of the carbonate compound. The development of the reactions between Li_2O and TiO_2 and the stabilization of the mass loss after 700°C were also considered as the formation of lithium titanium oxide. The crystal size calculated using the XRD peaks and the Scherrer equation was 46.02 nm. It was determined that the average value of the crystalline dimensions obtained from our study was close to this result.

In their study, Yuan et al. (2011) used stoichiometric TiO_2 (anatase) and Li_2CO_3 to produce $Li_4Ti_5O_{12}$. The mixtures were calcined for 300 minutes (5 hours) at 700, 750, and 800°C and in different atmospheres (air, nitrogen, and argon) after 60 minutes of grinding at 400 rpm rotation speed. When XRD analyses were examined, impurities (unreacted) with another definition of rutile phase were observed at 700°C. Therefore, their study suggested that the reagents for forming $Li_4Ti_5O_{12}$ should be at 800°C in an air atmosphere.

When the XRD analyses of the $Li_4Ti_5O_{12}$ structure formed at different temperatures were examined, it was determined that it showed similar peaks with the same structures obtained in our study.

The rutile phase was used as the starting reagent due to the conversion of the anatase phase to the rutile phase in high-temperature operation. Byrne et al. (2016) stated that 600 - 700°C is sufficient in their study on converting anatase to the rutile phase, but this temperature can be increased with additives added at the initial stage.

Zhukov et al. (2020) calcined at 650-850°C for 2 hours after mechanical activation using a ball mill (400 rpm) for 1-120 minutes with Li_2CO_3 and rutile starting reagents to synthesize $Li_4Ti_5O_{12}$. They investigated the activation between lithium carbonate and rutile with their thermogravimetric analysis. CO_2 decomposition from the carbonate structure was observed at approximately 745°C, and the weight loss was determined to be approximately 15.9%. The absence of a change in mass loss when the temperature reached 866°C was associated with the formation of $Li_4Ti_5O_{12}$. In addition, the synthesis of Li_2TiO_3 was also carried out in the same study. It has been reported that increasing the mechanical activation time for both materials significantly decreases temperature. Li_2TiO_3 formation temperature decreased from 743°C to 490°C, $Li_4Ti_5O_{12}$ formation temperature decreased from 866°C to 814°C and this result was obtained in 60 minutes of mechanical activation.

In this study, $Li_4Ti_5O_{12}$ was obtained at Li_2CO_3:TiO_2 (1:1) mixing ratio, 200 rpm grinder rotation speed, 60 minutes grinding time, 850°C oven operating temperature, and 60 minutes calcination time. The fact that the rotation speed of the mill and the calcination time are lower in the process of obtaining $Li_4Ti_5O_{12}$ provides an advantage to this study.

When the XRD analyses of the product obtained at the end of the mechanical activation performed in the study are examined, the presence of Li_2CO_3 and TiO_2 phases can be seen. Considering that ethanol added to the medium for synthesizing lithium titanate oxides may cause defects on the TiO_2 surface (oxygen vacancies), Li^+ ion likely settles in these defects at high temperatures. At the same time, it is thought that by-product water, which may be formed by adding ethanol, is removed by drying the material in the oven after mechanical activation.

4. Conclusions

Lithium titanium oxide synthesis was made by mixing Li_2CO_3 obtained from boron ore wastes and TiO_2 in certain proportions. Conventional solid-state and mechanochemical pretreatment methods were used for this purpose. In both

methods, the oven temperature was kept constant at 850°C, and its time-dependent (30, 60, 90, and 120 minutes) variation was investigated.

In the conventional method, $(Li_2TiO_3)_{10,667}$ was formed at the end of all the above-mentioned calcination times. However, it was observed that TiO_2 was also present as a second phase (Figure 3). In the study where the mixing ratios were 1:1 the percentage of lithium titanium oxides formed at the end of 30, 60, 90, and 120 minutes were 79.4%, 86.7%, 91%, and 91.7%, respectively; on the other hand in the study where mixing ratios were 1:2, 62%, 81.6%, 77%, and 93% lithium titanium oxides were obtained. By using the Scherrer equation, the crystal size of D – LTOs was calculated as 27,37, 25,30, 27,33 ve 25,1 nm for (1:1) ratio and 24.77, 28.46, 23.13, and 27.74 nm for (1:2) ratio, respectively.

In the synthesis with the mechanochemical pretreatment method, the same mixing ratios (1:1 and 1:2), the same temperature (850°C), and calcination times (30, 60, 90, and 120 minutes) were used as in the conventional method. In addition, two different rotation speeds of the ball mill used were chosen as 200 and 400 rpm. The chemical formulas of lithium titanium oxides obtained under different conditions were $(Li_2TiO_3)_{10,667}$, $Li_4Ti_5O_{12}$, and $Li_2Ti_2O_4$ (Table 1, Figure 4, Table 2, and Figure 5).

At 200 and 400 rpm a mixing ratio of (1:1) $(Li_2TiO_3)_{10,667}$ was formed with the average crystal dimensions of 22.96 nm at 200 rpm and 22.18 nm at 400 rpm.

In the synthesis process, the $Li_4Ti_5O_{12}$ phase was obtained at a 1:2 ratio of Li_2CO_3 to TiO_2, and this occurred under both grinding speeds (200 rpm and 400 rpm). The grinding and calcination times did not show a significant effect on the formation of this phase or the resulting particle size. Another important compound, the $Li_2Ti_2O_4$ phase, also occurred at a 1:2 ratio of Li_2CO_3 to TiO_2, and this happened under both grinding speeds (200 rpm and 400 rpm). In this case, the grinding time did not seem to have a substantial impact on the formation of the phase. However, the calcination time played a crucial role, at 90 minutes and especially at 120 minutes. Notably, the operating conditions, including grinding and calcination, did not significantly influence the particle size in this phase. Overall, these findings suggest that the formation of the $Li_4Ti_5O_{12}$ and $Li_2Ti_2O_4$ phases is primarily dependent on the ratio of Li_2CO_3 to TiO_2, and the calcination time appears to be a more critical factor in controlling the formation of the $Li_2Ti_2O_4$ phase.

The average crystalline size of the products obtained in the studies with a mixing ratio of 1:2 and ball mill rotation speed of 200 rpm was 34.34 nm (Table

1). The average crystal size of the products obtained in the studies with the mixing ratio of 1:2 and ball mill rotation speed of 400 rpm was calculated as 36.80 nm (Table 2).

Credit authorship contribution statement

Ayşegül Yücel: Conceptualization, Methodology, Formal analysis, Investigation, Resources, Writing – original draft, Writing – review & editing.

Musa Sarıkaya: Project administration, Writing – review & editing, Visualization, Supervision

Tolga Depci: Investigation, writing — review, and editing.

Declaration of Competing Interest

The authors declare that this work has yet to be previously published or evaluated for publication elsewhere. At the same time, the authors declare that there is no conflict of interest regarding the publication of this study.

Data availability

No data was used for the research described in the article.

Acknowledgments

The authors wish to frankly thank the management and employees of İnönü University Scientific and Technological Research Center (İBTAM), the management and employees of İskenderun Technical University Science and Technology Application and Research Center (İSTE-BTM), the Eti Maden Enterprises General Directorate Technology, and the Development Department and the İnönü University Scientific Research Projects (BAP) Coordination Unit, which provided financial support to my doctoral thesis with the project number **FDK-2020-2114** (Doctoral Thesis Project).

References

Aguilar, P. G., and Graber, T. A. (2018). Determination of the reaction kinetic parameters for Li_2CO_3 crystallization from Li_2SO_4 and Na_2CO_3 solutions using calorimetric measurements. Industrial and Engineering Chemistry Research, 57(14), 4815-4823.

Arzt, E., Dehm, G., Gumbsch, P., Kraft, O., and Weiss, D. (2001). Interface controlled plasticity in metals: dispersion hardening and thin film deformation. Progress in Materials Science, 46(3-4), 283-307.

Babu, B. V., Babu, K. V., Aregai, G. T., Devi, L. S., Latha, B. M., Reddi, M. S., & Veeraiah, V. (2018). Structural and electrical properties of $Li_4Ti_5O_{12}$ anode material for lithium-ion batteries. Results in Physics, pp. 9, 284–289.

Buekenhoudt, A., Kovalevsky, A., Luyten, J., Snijkers, F., and Giorno, L. B. T. C. M. S. (2010). 1.11 Basic Aspects in Inorganic Membrane Preparation. in-Chief: Enrico, G. Lidietta (Eds.), Comprehensive Membrane Science and Engineering, Elsevier, Oxford, 217-252.

Byrne, C., Fagan, R., Hinder, S., McCormack, D. E., & Pillai, S. C. (2016). New approach of modifying the anatase to rutile transition temperature in TiO_2 photocatalysts. RSC advances, 6(97), 95232-95238.

Cava, R. J., Murphy, D. W., Zahurak, S., Santoro, A., & Roth, R. S. (1984). The crystal structures of the lithium-inserted metal oxides $Li_{0.5}TiO_2$ anatase, $LiTi_2O_4$ spinel, and $Li_2Ti_2O_4$. Journal of Solid State Chemistry, 53(1), 64–75.

Chitrakar, R., Makita, Y., Ooi, K., and Sonoda, A. (2014). Lithium recovery from salt lake brine by H_2TiO_3. Dalton transactions, 43(23), 8933-8939.

Cicconi, P., Postacchini, L., Pallotta, E., Monteriù, A., Prist, M., Bevilacqua, M., and Germani, M. (2019). A life cycle costing of compacted lithium titanium oxide batteries for industrial applications. Journal of Power Sources, 436, 226837.

Cova, C. M., and Luque, R. (2019). Advances in mechanochemical processes for biomass valorization. BMC Chemical Engineering, 1(1), 1-12.

Deiss, E., Wokaun, A., Barras, J. L., Daul, C., and Dufek, P. (1997). Average Voltage, Energy Density, and Specific Energy of Lithium-Ion Batteries: Calculation Based on First Principles. Journal of the Electrochemical Society, 144(11), 3877.

Do Kim, Y., Chung, J. Y., Kim, J., and Jeon, H. (2000). Formation of nanocrystalline Fe–Co powders produced by mechanical alloying. Materials Science and Engineering: A, 291(1-2), 17–21.

Fattakhova, D., Petrykin, V., Brus, J., Kostlánová, T., Dědeček, J., and Krtil, P. (2005). Solvothermal synthesis and electrochemical behavior of nanocrystalline cubic Li–Ti–O oxides with the cationic disorder. Solid State Ionics, 176(23-24), 1877-1885.

Giuliano, M. R., Prasad, A. K., and Advani, S. G. (2012). Experimental study of an air-cooled thermal management system for high-capacity lithium–titanate batteries. Journal of power sources, 216, 345-352.

Grosjean, C., Miranda, P. H., Perrin, M., and Poggi, P. (2012). Assessment of world lithium resources and consequences of their geographic distribution on the expected development of the electric vehicle industry. Renewable and Sustainable Energy Reviews, 16(3), 1735-1744.

Guerfi, A., Sevigny, S., Lagacé, M., Hovington, P., Kinoshita, K., and Zaghib, K. (2003). Nanoparticle $Li_4Ti_5O_{12}$ spinel as electrode for electrochemical generators. Journal of Power Sources, 119, 88-94.

Hanisch, C., Loellhoeffel, T., Diekmann, J., Markley, K. J., Haselrieder, W., and Kwade, A. (2015). Recycling of lithium-ion batteries: a novel method to separate coating and foil of electrodes. Journal of cleaner production, 108, 301-311.

Jin, K., He, G., Zhang, X., Maruyama, S., Yasui, S., Suchoski, R., & Takeuchi, I. (2015). Anomalous magnetoresistance in the spinel superconductor LiTi2O4. Nature communications, 6(1), 1–8.

Johnston, D. C., Prakash, H., Zachariasen, W. H., & Viswanathan, R. (1973). High-temperature superconductivity in the Li- Ti-O ternary system. Materials Research Bulletin, 8(7), 777–784.

Kashkooli AG, Lui G, Farhad S, Lee DU, Feng K, Yu AP, Chen ZW (2016). Nanoparticle size effect on the performance of $Li_4Ti_5O_{12}$ spinel. Electrochim Acta 196:33–40

Kopp Alves, A., Bergmann, C. P., and Berutti, F. A. (2013). High-energy milling. In Novel synthesis and characterization of nanostructured materials (pp. 77-85). Springer, Berlin, Heidelberg.

Liu, G., Zhao, Z., & Ghahreman, A. (2019). Novel approaches for lithium extraction from salt-lake brines a review. Hydrometallurgy, pp. 187, 81–100.

Liu, Y., Lian, J., Sun, Z., Zhao, M., Shi, Y., and Song, H. (2017-a). The first-principles study for the novel optical properties of $LiTi_2O_4$, $Li_4Ti_5O_{12}$, $Li_2Ti_2O_4$, and $Li_7Ti_5O_{12}$. Chemical Physics Letters, 677, 114–119,

Liu, Y., Lian, J., Yang, X., Zhao, M., Shi, Y., Song, H., and Dai, K. (2017-b). First-principles calculation for point defects in $Li_2Ti_2O_4$. Materials Research Express, 4(10), 106502.

Maruyama, S., Shin, J., Zhang, X., Suchoski, R., Yasui, S., Jin, K., & Takeuchi, I. (2015). Reversible electrochemical modulation of the superconducting transition temperature of $LiTi_2O_4$ ultrathin films by ionic liquid gating. Applied Physics Letters, 107(14), 142602.

Meng, X., Wang, X., Zhou, Y., Tong, L., Zeng, X., and Chen, X. (2014). Spinel lithium titanate from brookite nanocrystallites. Ceramics International, 40(3), 4989-4993.

Michalska, M., Krajewski, M., Ziolkowska, D., Hamankiewicz, B., Andrzejczuk, M., Lipinska, L., and Czerwinski, A. (2014). Influence of milling time in solid-state synthesis on structure, morphology, and electrochemical properties of $Li_4Ti_5O_{12}$ of spinel structure. Powder Technology, 266, 372-377.

Ohzuku, T., Ueda, A., and Yamamoto, N. (1995). Zero-strain insertion material of Li $[Li_{1/3}Ti_{5/3}]O_4$ for rechargeable lithium cells. Journal of the Electrochemical Society, 142(5), 1431.

Paranthaman, M. P., Li, L., Luo, J., Hoke, T., Ucar, H., Moyer, B. A., & Harrison, S. (2017). Recovery of lithium from geothermal brine with lithium–aluminum layered double hydroxide chloride sorbents. Environmental science & technology, 51(22), 13481–13486.

Pohjalainen E, Rauhala T, Valkeapää M, Kallioinen J, Kallio T (2015). Effect of $Li_4Ti_5O_{12}$ particle size on the performance of lithium ion battery electrodes at high C rates and low temperatures. J Phys Chem C 119(5):2277–2283

Ra, W., Nakayama, M., Uchimoto, Y., and Wakihara, M. (2005). Experimental and computational study of the electronic structural changes in $LiTi_2O_4$ spinel compounds upon electrochemical Li insertion reactions. The Journal of Physical Chemistry B, 109(3), 1130-1134.

Rahaman, M. N. (2017). Ceramic processing and sintering. CRC press.

Raj, H., Saxena, S., and Sil, A. (2019). $Li_4Ti_5O_{12}$/AC Hybrid Supercapacitor combining High Power of Supercapacitor and High Energy of Li-ion battery. Materials Today: Proceedings, 18, 2625-2631.

Ribeiro, L. S., Nogueira, A. E., Aquino, J. M., and Camargo, E. R. (2019). A new strategy to obtain nano-scale particles of lithium titanate ($Li_4Ti_5O_{12}$) by the oxidant peroxo method (OPM). Ceramics International, 45(18), 23917-23923.

Scharner, S., Weppner, W., and Schmid-Beurmann, P. (1999). Evidence of Two-Phase Formation upon Lithium Insertion into the $Li_{1.33}Ti_{1.67}O_4$ Spinel. Journal of the Electrochemical Society, 146(3), 857.

Smida, Y. B. , Marzouki, R., Kaya, S., Erkan, S., Zid, M. F. , and Hamzaoui, A. H. (2020). Synthesis Methods in Solid-State Chemistry. In (Ed.), Synthesis Methods and Crystallization. IntechOpen.

Swain, B. (2017). Recovery and recycling of lithium: A review. Separation and Purification Technology, pp. 172, 388–403.

Tangkas, I. W. C. W. H., Astuti, W., Sumardi, S., and Petrus, H. T. B. M. (2021). Lithium titanium oxide synthesis by solid-state reaction for lithium adsorption from artificial brine source. In IOP Conference Series: Earth and Environmental Science Vol. 882, No. 1, p. 012005

Walenta, C. A., Kollmannsberger, S. L., Kiermaier, J., Winbauer, A., Tschurl, M., and Heiz, U. (2015). Ethanol photocatalysis on rutile TiO_2 (110): the role of defects and water. Physical Chemistry Chemical Physics, 17(35), 22809-22814.

Wang, Y., Du, S., Wang, X., Sun, M., Yang, Y., and Gong, J. (2019). Spherulitic growth and morphology control of lithium carbonate: the stepwise evolution of core-shell structures. Powder Technology, 355, 617-628.

Wang D, Wu XY, Zhang YY, Wang J, Yan P, Zhang CM, He D N (2014) The influence of the TiO_2 particle size on the properties of $Li_4Ti_5O_{12}$ anode material for lithium-ion battery. Ceram Int 40:3799–3804

Wang, J., Zhao, H., Wen, Y., Xie, J., Xia, Q., Zhang, T., & Du, X. (2013). High-performance $Li_4Ti_5O_{12}$ material as anode for lithium-ion batteries. Electrochimica Acta, 113, 679-685.

Wegmann, R., Döge, V., and Sauer, D. U. (2018). Assessing the potential of a hybrid battery system to reduce battery aging in an electric vehicle by studying the cycle life of a graphite NCA high energy and a LTO metal oxide high power battery cell considering realistic test profiles. Applied Energy, 226, 197-212.

Xu, P., Hong, J., Qian, X., Xu, Z., Xia, H., Tao, & Ni, Q. Q. (2021). Materials for lithium recovery from salt lake brine. Journal of Materials Science, 56(1), 16–63.

Xu, X., Chen, Y., Wan, P., Gasem, K., Wang, K., He, T., Adidharma, H. and Fan, M. (2016). Extraction of lithium with functionalized lithium ion sieves. Progress in Materials Science, 84, 276-313

Yang, J., Zhao, J., Chen, Y., & Li, Y. (2010). Preparation and characterization of $LiTi_2O_4$ anode material synthesized by one-step solid-state reaction. Ionics, 16(5), 425–429.

Yi, T. F., Jiang, L. J., Shu, J., Yue, C. B., Zhu, R. S., & Qiao, H. B. (2010). Recent development and application of $Li_4Ti_5O_{12}$ as anode material of lithium ion battery. Journal of Physics and Chemistry of Solids, 71(9), 1236–1242.

Yu, C. L., Yanagisawa, K., Kamiya, S., Kozawa, T., and Ueda, T. (2014). Monoclinic Li_2TiO_3 nano-particles via hydrothermal reaction: Processing and structure. Ceramics International, 40(1), 1901-1908.

Yuan, T., Cai, R., and Shao, Z. (2011). Different effect of the atmospheres on the phase formation and performance of $Li_4Ti_5O_{12}$ prepared from ball-milling-assisted solid-phase reaction with pristine and carbon-precoated TiO_2 as starting materials. The Journal of Physical Chemistry C, 115(11), 4943-4952.

Yuan, T., Wang, K., Cai, R., Ran, R., and Shao, Z. (2009). Cellulose-assisted combustion synthesis of $Li_4Ti_5O_{12}$ adopting anatase TiO_2 solid as raw material with high electrochemical performance. Journal of alloys and compounds, 477(1-2), 665-672.

Yue, J., Badaczewski, F. M., Voepel, P., Leichtweiß, T., Mollenhauer, D., Zeier, W. G., and Smarsly, B. M. (2018). Critical role of the crystallite size in nanostructured $Li_4Ti_5O_{12}$ anodes for lithium-ion batteries. ACS applied materials & interfaces, 10(26), 22580-22590

Yücel, A. (2022). Investıgatıon Of The Productıon Of Lıthıum Tıtan Oxıde From Boron Ore Wastes, (PhD Thesis), İnönü University Institute of Natural and Applied Sciences, Türkiye

Zaghib, K., Dontigny, M., Guerfi, A., Charest, P., Rodrigues, I., Mauger, A., and Julien, C. M. (2011). Safe and fast-charging Li-ion battery with long shelf life for power applications. Journal of power sources, 196(8), 3949-3954.

Zhang, C., Zhang, Y., Wang, J., Wang, D., He, D., & Xia, Y. (2013). $Li_4Ti_5O_{12}$ prepared by a modified citric acid sol–gel method for lithium-ion battery. Journal of power sources, pp. 236, 118–125.

Zhang, Y., Liu, J., Yang, Y., Lin, S., & Li, P. (2021). Preparation of granular titanium-type lithium-ion sieves and recyclability assessment for lithium recovery from brines with different pH value. Separation and Purification Technology, 267, 118613.

Zhukov, A. V., Chizhevskaya, S. V., Merkushkin, A. O., and Htun, Y. K. K. (2020). Kinetic analysis of the second stage of the solid-phase synthesis of $Li_4Ti_5O_{12}$ from a mechanically activated mixture of rutile and lithium carbonate. Solid State Ionics, 357, 115440.

Ziebarth, B., Klinsmann, M., Eckl, T., and Elsässer, C. (2014). Lithium diffusion in the spinel phase $Li_4Ti_5O_{12}$ and in the rocksalt phase $Li_7Ti_5O_{12}$ of lithium titanate from first principles. Physical Review B, 89(17), 174301.

CHAPTER 9

Soft Robotics: Advances, Challenges, and Future Perspectives

Merdan Özkahraman[1]

*

[1] Asst. Prof., Faculty of Technology, Department of Mechatronic Engineering, Isparta Applied Sciences University West Campus, Merkez 32260 Isparta/Turkey, Orcid: 0000-0002-3501-6497

INTRODUCTION

Soft robotics is an interdisciplinary field that combines materials science, mechanical engineering, and bio-inspired design to develop robotic systems with enhanced flexibility, adaptability, and safety. Unlike conventional rigid robots, which rely on hard materials such as metal and plastic to create structured mechanical systems, soft robots are primarily composed of highly deformable and compliant materials, including elastomers, hydrogels, liquid crystal polymers, and shape-memory alloys (Albu-Schaffer et al., 2008; Cianchetti, Laschi, Menciassi, & Dario, 2018; Whitesides, 2018). These materials allow soft robots to achieve smooth, continuous, and biomimetic movements, enabling them to interact more safely with humans and fragile objects while adapting to unstructured or dynamic environments. As a result, soft robotics represents a significant paradigm shift in the field of robotics, moving away from traditional kinematic structures toward more versatile, lifelike systems.

One of the fundamental distinctions between soft robots and their rigid counterparts lies in their mode of operation and motion generation. Traditional rigid robots are typically designed with well-defined joints, linkages, and actuators, which provide precise, repeatable movements but limit their ability to interact safely with complex and uncertain environments. These robots are often optimized for industrial settings, where speed, accuracy, and efficiency are prioritized over adaptability and compliance. However, such rigid structures pose challenges when robots need to navigate unpredictable terrains, handle delicate materials, or collaborate closely with humans (Iida & Laschi, 2011; S. Kim, Laschi, & Trimmer, 2013; Yasa et al., 2023). In contrast, soft robots exploit deformable structures and unconventional actuation mechanisms, such as pneumatic, hydraulic, dielectric elastomer, and magnetically responsive actuators, to achieve highly adaptive and reconfigurable behaviors. These capabilities enable soft robots to squeeze through confined spaces, conform to irregular surfaces, and demonstrate enhanced resilience against mechanical impact and external perturbations.

Due to these distinctive characteristics, soft robotics has rapidly expanded into a wide range of applications across multiple disciplines. In biomedical engineering, soft robotic systems are revolutionizing minimally invasive surgery, prosthetics, and rehabilitation devices, offering improved dexterity and patient comfort (Lee et al., 2017; Trivedi, Rahn, Kier, & Walker, 2008). Unlike traditional robotic surgical instruments, which are constrained by rigid components, soft robotic manipulators can navigate delicate anatomical

structures with greater precision, reducing the risk of tissue damage. Similarly, in the field of assistive technologies, soft robotic exosuits and prosthetic devices are being designed to provide more natural and intuitive movements for individuals with mobility impairments.

In industrial and manufacturing settings, soft robotic grippers and manipulators are addressing long-standing challenges in automation by enabling the handling of objects with varying shapes, sizes, and fragilities (Kumar, 2018; Schmitt, Piccin, Barbé, & Bayle, 2018). Traditional rigid robotic arms require precise pre-programming and structured environments to operate efficiently, whereas soft robotic grippers can passively conform to objects, reducing the need for complex sensing and control algorithms (Shintake, Cacucciolo, Floreano, & Shea, 2018; Terrile, Argüelles, & Barrientos, 2021). This capability is particularly valuable in logistics, food processing, and electronic assembly, where delicate and irregularly shaped items must be manipulated safely and efficiently.

Beyond industrial and biomedical applications, soft robotics is also playing a crucial role in exploration and search-and-rescue missions. Traditional robotic systems often struggle to operate in hazardous environments, such as collapsed buildings, underwater terrains, or extraterrestrial surfaces, due to their rigid structures and limited adaptability. Soft robots, with their ability to deform and maneuver through constrained spaces, offer a promising alternative for disaster response teams and autonomous exploration systems (Sebastian, 2025; Wen, Hu, Zhang, Li, Kang, & Zhang, 2024). Additionally, the development of bio-inspired soft robots, such as robotic octopuses, caterpillars, and worms, is opening new possibilities for locomotion strategies that are not feasible with conventional rigid robots.

As research in soft robotics continues to advance, new challenges and opportunities are emerging. The field is currently grappling with critical issues such as improving the durability and longevity of soft materials, enhancing control precision, and developing energy-efficient actuation mechanisms. Despite these challenges, the potential of soft robotics to redefine robotic applications across multiple domains is undeniable. This review aims to provide a comprehensive overview of the fundamental principles, design methodologies, fabrication techniques, control strategies, and real-world applications of soft robotics. Furthermore, key challenges and future research directions will be discussed to highlight the next steps required to fully unlock the capabilities of soft robotic systems. Through this discussion, we seek to offer insights into how

soft robotics can continue to revolutionize automation, healthcare, and human-robot interaction in the coming years.

1. FUNDAMENTAL PRINCIPLES AND DESIGN APPROACHES IN SOFT ROBOTICS

Soft robotics is founded on principles that prioritize compliance, adaptability, and biomimicry. Unlike traditional rigid robots that rely on precise jointed mechanisms, soft robots utilize deformable materials and unconventional actuation methods to achieve flexible movement and environmental interaction. The design approaches in soft robotics integrate insights from materials science, mechanical engineering, and control theory to develop systems that can morph, stretch, and navigate complex terrains. This section explores the core components of soft robotic systems, including compliant materials, actuation mechanisms, and modeling techniques.

1.1. Material Science And Compliant Materials

Material selection plays a crucial role in the development of soft robotic systems, as it directly influences their mechanical properties, adaptability, and durability. Soft robots primarily utilize elastomers, hydrogels, shape-memory alloys, and liquid crystal polymers due to their high deformability and resilience (Coyle, Majidi, LeDuc, & Hsia, 2018; Yap, Sing, & Yeong, 2020).

Elastomers, such as silicone rubbers and polyurethane, are widely used in soft robotics due to their high elasticity and durability. Their ability to undergo large deformations without permanent damage makes them suitable for actuators and artificial muscles (Bira, Dhagat, & Davidson, 2020; Gupta, Qin, Wang, Godaba, & Zhu, 2019). Hydrogels, composed of hydrophilic polymer networks, exhibit unique properties such as swelling, biocompatibility, and shape transformation in response to stimuli like temperature or pH changes, making them ideal for biomedical applications.

Shape-memory alloys (SMAs) and liquid crystal elastomers (LCEs) are another class of materials that enable programmable shape transformations. SMAs, such as nickel-titanium (NiTi), exhibit phase-transition behavior, allowing them to return to a pre-defined shape when heated. This property is utilized in soft robotic actuators that require controlled deformations. LCEs, on the other hand, undergo macroscopic deformations when exposed to light, heat, or electric fields, offering an alternative approach to achieving movement in soft robots (Huang et al., 2019; Jin, Dong, Xu, Liu, Alici, & Jie, 2016; Yubai Zhang et al., 2020).

The selection of compliant materials must balance flexibility with mechanical robustness. One of the critical challenges in soft robotics is maintaining durability while ensuring sufficient compliance for functional movements. Future advancements in materials science, such as self-healing polymers and programmable metamaterials, are expected to further enhance the capabilities of soft robots.

1.2. Actuation Mechanisms in Soft Robotics

Soft robots utilize a variety of actuation mechanisms that differ significantly from conventional electric motors and servos. The most commonly used actuation strategies in soft robotics include pneumatic, hydraulic, dielectric elastomer, shape-memory, and magnetic actuation.

Pneumatic and hydraulic actuators generate movement through pressurized air or liquid, respectively. Soft pneumatic actuators (SPAs) are among the most widely used due to their simplicity, rapid response, and high compliance (Moseley, Florez, Sonar, Agarwal, Curtin, & Paik, 2016; Walker et al., 2020; Xavier et al., 2022). The governing equation for a pneumatic actuator's expansion can be approximated by:

$$V = \frac{nRT}{P} \tag{1}$$

where V is the volume expansion, n is the number of moles of gas, R is the universal gas constant, T is the absolute temperature, and P is the applied pressure. By carefully controlling the pressure levels, soft robots can achieve a wide range of deformations and locomotion patterns.

Dielectric elastomer actuators (DEAs) function by applying an electric field across a soft elastomer membrane sandwiched between compliant electrodes. This causes electrostatic forces that lead to membrane compression and expansion in the perpendicular direction (Gu, Zhu, Zhu, & Zhu, 2017; Youn et al., 2020). The mechanical deformation of a DEA is governed by the Maxwell stress equation:

$$\sigma = \frac{\varepsilon_0 \varepsilon_r E^2}{2} \tag{2}$$

where σ is the induced stress, ε_0 is the permittivity of free space, ε_r is the relative permittivity of the elastomer, and E is the applied electric field. DEAs are lightweight, energy-efficient, and capable of high-speed actuation, making them ideal for bio-inspired robotic systems.

Shape-memory materials, including shape-memory alloys (SMAs) and shape-memory polymers (SMPs), undergo phase transitions in response to external stimuli such as temperature or stress (M. S. Kim et al., 2023; Naresh, Bose, & Rao, 2016). The deformation and recovery of SMAs follow the constitutive equation:

$$\epsilon = \frac{\sigma}{E} + \sigma \Delta T \tag{3}$$

where ϵ is the strain, σ is the applied stress, E is the elastic modulus, α is the thermal expansion coefficient, and ΔT is the temperature change. These actuators are particularly useful for applications requiring slow but powerful movements, such as robotic grippers and surgical tools.

Magnetically responsive soft robots use embedded magnetic particles or layers to generate motion under an external magnetic field (Ebrahimi et al., 2021; Y. Kim & Zhao, 2022). The torque and force generated by a magnetic actuator depend on the field strength and material properties and can be described as:

$$F = \nabla (M \cdot B) \tag{4}$$

where F is the force, M is the magnetization of the material, and B is the applied magnetic field. Magnetic soft robots have demonstrated remarkable capabilities for remote actuation, enabling applications such as minimally invasive medical robots and untethered locomotion in constrained environments. Each actuation method has distinct advantages and limitations, and hybrid actuation strategies are being explored to optimize performance for specific applications.

1.3. Modeling and Simulation Techniques for Soft Robots

The highly deformable nature of soft robots poses challenges for traditional robotic modeling approaches, which typically rely on rigid-body kinematics and dynamics. Instead, soft robots are often modeled using continuum mechanics and finite element analysis (FEA) to predict their deformations and interactions with the environment.

Continuum Mechanics Modeling: Soft robots are commonly described using beam and plate theories or hyperelastic material models, such as the Mooney-Rivlin and Ogden models (Ding et al., 2022; Natarajan, Hassan, Kit, Santhosh, Ramesh, & Sasikumar, 2021). The strain energy function W for a hyperelastic material is often represented as:

$$W = C_1(I_1 - 3) + C_2(I_2 - 3) \quad (5)$$

where C_1 and C_2 are material parameters, and I_1 and I_2 are the first and second invariants of the Cauchy-Green deformation tensor. These models help predict the large deformations characteristic of soft robotic structures.

Finite Element Analysis (FEA) is a numerical approach widely used to simulate the mechanical behavior of soft robots. By discretizing the robot's structure into finite elements and solving for stress and strain distributions under different loading conditions, FEA provides insights into the robot's performance and failure points. Advanced FEA techniques also incorporate multiphysics simulations, including fluid-structure interaction and electromechanical coupling, to optimize soft robotic designs (Duriez, 2013).

Machine Learning-Based Modeling: Given the high complexity of soft robot behavior, machine learning approaches, particularly deep learning and reinforcement learning, are increasingly being used for control and modeling. Neural networks can approximate nonlinear dynamics and predict soft robot deformations under various conditions, offering an alternative to traditional physics-based simulations (Chin, Hellebrekers, & Majidi, 2020; Daekyum Kim et al., 2021).

Modeling and simulation remain essential for optimizing soft robotic performance, reducing development time, and ensuring reliable operation. As computational power and data-driven techniques advance, hybrid approaches combining physics-based models with machine learning algorithms are expected to further improve soft robot design and control. Soft robotics continues to evolve through innovations in materials, actuation mechanisms, and computational modeling. The next sections will explore fabrication methods and control strategies, which are essential for translating these principles into functional robotic systems.

2. FABRICATION METHODS

The fabrication of soft robots requires advanced manufacturing techniques that can accommodate the complexity of compliant materials, intricate geometries, and multifunctional components. Unlike traditional rigid robots, which rely on machining, casting, and assembly of metal and plastic components, soft robots necessitate fabrication strategies that ensure seamless integration of soft actuators, flexible electronics, and deformable structures. The development of scalable and efficient fabrication methods is critical for enhancing the functionality, durability, and reproducibility of soft robotic systems. This section

explores key fabrication techniques, including 3D printing, material processing, and sensor-actuator integration.

Additive manufacturing, particularly 3D printing, has become one of the most promising techniques for soft robot fabrication due to its ability to create complex, multi-material, and highly customizable structures (Stano & Percoco, 2021). Unlike traditional subtractive or molding-based approaches, 3D printing enables layer-by-layer deposition of soft materials, allowing for the direct fabrication of compliant robotic systems with embedded functionalities.

Among the most commonly used 3D printing technologies in soft robotics are stereolithography (SLA), fused deposition modeling (FDM), and direct ink writing (DIW). SLA-based 3D printing utilizes photopolymerization to solidify liquid resins into highly detailed and complex geometries, making it suitable for fabricating intricate soft robotic components. FDM, on the other hand, relies on the extrusion of thermoplastic filaments and elastomeric materials to create compliant structures. DIW techniques enable the printing of viscoelastic and functional inks, including conductive and responsive materials, which are essential for integrating actuation and sensing capabilities (Gul et al., 2018; Wallin, Pikul, & Shepherd, 2018).

Multi-material 3D printing has further revolutionized the fabrication of soft robots by allowing different material properties to be combined within a single printed structure (Fang, Matte, Kwok, & Wang, 2018; Joyee & Pan, 2019). By integrating stiff and soft materials, researchers can engineer gradient mechanical properties that enhance robotic performance. The mechanical behavior of 3D-printed soft structures can often be described using continuum mechanics models, such as the nonlinear strain-stress relationship:

$$\sigma = E\epsilon + D\epsilon^2 \tag{6}$$

where σ is the stress, E is the linear elastic modulus, D is a nonlinear deformation coefficient, and ϵ is the applied strain. These models help predict the deformation behavior of 3D-printed soft actuators under external loads.

Despite its advantages, 3D printing still faces challenges in scalability, print resolution, and the limited availability of functional soft materials. Future advancements in high-resolution, multi-material, and bio-compatible 3D printing techniques will further expand the possibilities of soft robotic fabrication.

The fabrication of soft robots also involves specialized processes to prepare and mold soft materials into functional robotic components. These processes

include casting, molding, and laser cutting, each of which is tailored to different material properties and design requirements (Bell, Becker, & Wood, 2022; Silva, Fonseca, Neto, Babcinschi, & Neto, 2024). Casting and molding techniques are widely used for fabricating soft robotic actuators, particularly those based on silicone elastomers, hydrogels, and shape-memory materials. In these methods, liquid polymers are poured into custom molds and cured to form flexible structures. The curing process can be modeled using reaction kinetics equations, where the degree of polymerization P(t) follows an exponential growth model:

$$P(t) = 1 - e^{-kt} \tag{7}$$

where k is the polymerization rate constant, and t is the curing time. By optimizing curing conditions, researchers can fine-tune the mechanical properties of soft robotic components.

Laser cutting and heat-sealing techniques are commonly employed in the production of soft pneumatic actuators and origami-inspired robots (Jia et al., 2024; Yang & Asbeck, 2018). By precisely cutting thin layers of elastomers and thermoplastic films, engineers can create lightweight, foldable, and air-tight robotic structures. These techniques are particularly useful for fabricating soft grippers, wearable robotic devices, and inflatable actuators. Microfabrication and self-assembly methods are also gaining attention in soft robotics, particularly for miniaturized and bio-integrated robotic systems. Techniques such as photolithography and soft lithography allow for the precise patterning of microscale soft materials, enabling the development of highly sensitive artificial skins, stretchable circuits, and bio-hybrid robots. As material science advances, new self-healing and stimuli-responsive materials are being developed to enhance the durability and adaptability of soft robots.

The seamless integration of sensors and actuators is essential for enabling autonomous and adaptive behavior in soft robotic systems. Unlike rigid robots, where electronic sensors and actuators can be easily attached to hard surfaces, soft robots require flexible, stretchable, and deformable components that can conform to dynamic shapes and movements.

Soft sensors are designed to detect mechanical deformations, temperature changes, and environmental stimuli while maintaining compliance with the robot's structure. Some of the most commonly used soft sensors include resistive, capacitive, and optical-based strain sensors (Hegde, Su, Tan, He, Chen, & Magdassi, 2023; Polygerinos et al., 2017). The resistance of a stretchable sensor, for example, follows the equation:

$$R = R_0(1 + k\epsilon) \quad (8)$$

where R_0 is the initial resistance, k is the gauge factor, and ϵ is the strain. By embedding such sensors into soft robotic skins, researchers can achieve real-time proprioception and environmental feedback.

Similarly, the integration of soft actuators with embedded control circuits allows for the development of untethered and autonomous soft robots. Emerging techniques such as liquid-metal-based stretchable electronics and conductive polymer composites enable the creation of deformable circuits that maintain electrical functionality even under extreme deformations. Flexible power sources, including stretchable batteries and energy-harvesting systems, further enhance the autonomy of soft robotic platforms.

One of the major challenges in sensor-actuator integration is ensuring the durability and reliability of flexible electronics under repeated mechanical loading. Current research is focused on developing self-healing conductors and bio-inspired neural networks that can adapt to material fatigue and environmental changes. Future advancements in printed electronics, artificial synapses, and neuromorphic computing will further expand the possibilities for intelligent soft robotic systems.

In summary, fabrication methods in soft robotics continue to evolve, incorporating cutting-edge manufacturing technologies, novel material processing techniques, and seamless integration of sensors and actuators. These advancements pave the way for more sophisticated, autonomous, and multifunctional soft robotic platforms capable of addressing real-world challenges. The next section will explore control strategies that enable precise movement and adaptive behavior in soft robots.

3. CONTROL STRATEGIES

Soft robots present unique control challenges due to their highly deformable and continuum structures (J. Wang & Chortos, 2022). Unlike rigid robots, which can be controlled using well-established kinematic and dynamic models, soft robots exhibit complex, nonlinear, and often unpredictable behavior. Traditional robotic control methods based on rigid-body dynamics and classical control theory are not directly applicable to soft robotic systems. Instead, novel control strategies inspired by biological organisms, artificial intelligence (AI), and sensory feedback mechanisms have been developed to achieve precise and adaptive motion control. This section explores bio-inspired motion control, AI-

driven learning-based approaches, and feedback integration strategies in soft robotics.

Soft robots are often designed to replicate the movement strategies found in biological systems, such as the locomotion of cephalopods, worms, and muscle-like actuations in vertebrates. These bio-inspired control strategies leverage distributed actuation, compliance, and decentralized coordination to achieve adaptive movement (Ahmed et al., 2022; Coyle et al., 2018).

One of the fundamental bio-inspired approaches is central pattern generator (CPG)-based control, which mimics the rhythmic motor patterns observed in biological nervous systems. CPGs are neural circuits that generate periodic signals for rhythmic motions, such as walking or swimming, without requiring continuous sensory input (Ishige, Umedachi, Taniguchi, & Kawahara, 2019; X. Liu, Onal, & Fu, 2023). Mathematically, CPGs are often modeled using coupled nonlinear oscillators:

$$\dot{x_i} = f(x_i) + \sum_j w_{ij} g(x_j) \tag{9}$$

where x_i represents the state of the i-th oscillator, $f(x_i)$ defines the intrinsic dynamics of the oscillator, w_{ij} is the coupling weight between oscillators, and $g(x_j)$ represents the interaction function. These coupled oscillators enable soft robots to generate smooth and adaptive locomotion patterns. Another widely used bio-inspired control strategy is tendon-driven and muscle-like actuation, which relies on variable stiffness and compliance to mimic biological muscle functions. In these systems, forces are controlled using Hill-type muscle models:

$$F = F_{max} \cdot \left(\frac{l}{l_0}\right) \cdot (1 - v/v_{max}) \tag{10}$$

where F_{max} is the maximum force, l is the muscle length, l_0 is the optimal length, v is the contraction velocity, and v_{max} is the maximum contraction velocity. By tuning these parameters, soft robotic actuators can replicate biological muscle behaviors, leading to more natural and adaptive movement. Bio-inspired controllers also incorporate morphological computation, where the robot's body structure itself contributes to motion efficiency. For example, octopus-inspired soft robots utilize their compliant limbs to generate propulsion without requiring precise trajectory planning. This form of passive compliance reduces the need for complex control algorithms and enhances energy efficiency.

Given the highly nonlinear and dynamic nature of soft robots, traditional model-based control approaches often struggle to predict and regulate their

movements accurately. To address this challenge, AI-driven and machine learning-based control strategies have emerged as powerful alternatives. These techniques allow soft robots to learn from experience, adapt to unknown environments, and optimize their control policies over time.

Reinforcement learning (RL) is one of the most effective machine learning techniques used in soft robotics. RL enables robots to autonomously discover optimal control policies by interacting with their environment and maximizing a reward function (Bhagat, Banerjee, Ho Tse, & Ren, 2019; X. Liu, Onal, & Fu, 2023). The learning process follows the Bellman equation:

$$Q(s,a) = r + \gamma max_{a'} Q(s',a') \tag{11}$$

where $Q(s,a)$ represents the expected cumulative reward for taking action a in state s, r is the immediate reward, γ is the discount factor, and $max_{a'}, Q(s',a')$ is the maximum expected reward in the next state. By iteratively updating $Q(s,a)$ through trial-and-error interactions, soft robots can learn optimal motion strategies without requiring explicit dynamic models.

Another AI-driven approach is deep learning-based predictive control, where deep neural networks (DNNs) are trained to approximate the robot's dynamic behavior. A neural network controller can be represented as:

$$y = f(W \cdot X + b) \tag{12}$$

where y is the predicted output, W is the weight matrix, X is the input feature vector (e.g., sensor readings and actuator states), and b is the bias term. By training the network with large datasets of robot motion, deep learning models can generalize complex deformation patterns and generate real-time control commands.

Hybrid approaches combining model-based control with machine learning are also being explored. For example, model predictive control (MPC) combined with neural networks can improve real-time motion planning by leveraging both physical models and data-driven corrections (Best, Gillespie, Hyatt, Rupert, Sherrod, & Killpack, 2016; Bruder, Gillespie, Remy, & Vasudevan, 2019). This synergy enhances control robustness and enables adaptive behavior in soft robotic systems. To achieve autonomous and precise movement, soft robots rely on real-time feedback from embedded sensors. Unlike rigid robots, where encoders and gyroscopes provide well-defined state estimates, soft robots require flexible and stretchable sensors that can conform to their deformable structures. Strain and pressure sensors play a crucial role in proprioception by measuring deformations

in soft robotic actuators. These sensors often use resistive, capacitive, or optical sensing principles (Shih et al., 2019; Thuruthel, Shih, Laschi, & Tolley, 2019). For instance, the resistance R of a stretchable strain sensor changes according to Equation 8. Tactile sensing is also essential for enabling soft robots to interact safely with objects and humans. Flexible capacitive sensors detect contact forces using the relationship:

$$C = \frac{\varepsilon A}{d} \tag{13}$$

where C is the capacitance, ε is the permittivity of the dielectric material, A is the electrode area, and d is the separation distance. By continuously monitoring capacitance changes, soft robots can perceive and respond to external forces, improving grasping and manipulation capabilities.

Closed-loop feedback control is commonly used to regulate soft robot behavior based on sensory data. The most widely used approach is proportional-integral-derivative (PID) control, described by:

$$u(t) = K_p e(t) + K_i \int e(t)dt + K_d \frac{de(t)}{dt} \tag{14}$$

where $e(t)$ is the error signal, K_p is the proportional gain, K_i is the integral gain, and K_d is the derivative gain. PID controllers enable real-time error correction and stabilization in soft robotic systems.

In advanced sensory integration strategies, sensor fusion techniques combine multiple data sources, such as strain, pressure, and vision sensors, to create a comprehensive understanding of the robot's state. Kalman filters and Bayesian estimation methods are often employed to refine sensor readings and improve control accuracy (DongWook Kim, Park, & Park, 2021). As sensor technology continues to advance, the integration of neuromorphic computing and artificial sensory networks is expected to further enhance the intelligence and autonomy of soft robots. Future research will focus on developing bio-inspired reflexive control systems that mimic human sensory-motor loops, enabling soft robots to exhibit lifelike movement and adaptability.

Soft robotics control strategies are evolving rapidly, incorporating bio-inspired methods, AI-driven learning, and real-time feedback mechanisms to achieve adaptive and intelligent behavior. By combining flexible actuation with advanced computational approaches, researchers are paving the way for next-generation soft robots capable of dynamic interaction with their environment. Continued progress in these areas will enable soft robotic systems to be deployed

in increasingly complex real-world applications, from healthcare and industrial automation to search-and-rescue and human-assistive technologies.

4. APPLICATIONS OF SOFT ROBOTICS

Soft robotics has gained significant attention across various fields due to its ability to provide adaptable, safe, and biomimetic solutions that rigid robots cannot achieve. The intrinsic compliance and flexibility of soft robotic systems make them highly suitable for applications that involve interaction with delicate environments, human contact, and unstructured terrains. This section explores four key domains where soft robotics has made a substantial impact: biomedical applications, industrial and manufacturing processes, exploration and search-and-rescue missions, and wearable robotics.

4.1. Biomedical Applications (Surgical Robots, Rehabilitation Devices)

One of the most promising areas of soft robotics is biomedical engineering, where soft robots are being developed to enhance surgical precision, rehabilitation therapies, and patient assistance. Traditional surgical robots, such as the da Vinci system, rely on rigid-link mechanisms that offer high precision but limited compliance. In contrast, soft surgical robots use deformable actuators and flexible end-effectors to perform minimally invasive procedures with greater adaptability (Ashuri, Armani, Jalilzadeh Hamidi, Reasnor, Ahmadi, & Iqbal, 2020; Cianchetti et al., 2018). For example, soft continuum robots inspired by octopus tentacles and snake-like structures can navigate inside the human body with minimal tissue damage (Olson, Hatton, Adams, & Mengüç, 2020). Their deformation can be modeled using continuum mechanics, where the bending of a soft robotic arm can be approximated using an Euler-Bernoulli beam equation for flexible structures:

$$M = EI\frac{d^2\theta}{ds^2} \tag{15}$$

where: M is the bending moment, E is the Young's modulus of the soft material, I is the moment of inertia, θ is the bending angle, and s is the arc length along the robot's body.

In rehabilitation, soft exoskeletons and assistive robotic devices are being developed to support patients with mobility impairments. Unlike traditional exoskeletons, which use rigid frames and motors, soft robotic exosuits employ textile-based actuators and pneumatic artificial muscles to provide lightweight, unobtrusive support. These systems integrate adaptive control algorithms to

adjust the assistance level based on real-time feedback from embedded sensors, allowing for personalized rehabilitation therapy. Soft robots are also being integrated into prosthetics, where they offer greater dexterity and lifelike motion. Soft robotic hands with embedded tactile sensors can provide intuitive and natural movement control by responding to electromyographic (EMG) signals from the user's muscles. These advancements are paving the way for the next generation of medical robots that seamlessly interact with biological systems.

4.2. Industrial And Manufacturing Processes

Soft robotics is transforming industrial automation by providing safe and flexible robotic manipulators capable of handling delicate objects. Traditional industrial robots are highly efficient but often lack adaptability, requiring precise pre-programming and structured environments. Soft robotic grippers, on the other hand, leverage compliant materials and deformable structures to passively adapt to various objects without complex sensing and control (G. Zhang, Li, Wu, & Zhu, 2021). A widely studied model for soft robotic gripping is the Fin Ray Effect, where a flexible fin deforms around an object upon contact (Crooks, Vukasin, O'Sullivan, Messner, & Rogers, 2016). The gripping force F of a soft robotic gripper can be approximated as:

$$F = k \cdot d \tag{16}$$

where: k is the stiffness coefficient of the soft material, d is the displacement caused by object contact. Soft grippers are increasingly used in food processing, pharmaceuticals, and electronics manufacturing, where objects of varying shapes and fragilities must be handled without causing damage. For example, vacuum-powered soft grippers and pneumatically actuated fingers enable efficient packaging of irregularly shaped produce, while dielectric elastomer actuators (DEAs) provide high-speed object manipulation in assembly lines.

Additionally, soft robots are playing a critical role in human-robot collaboration (HRC) by offering intrinsically safe interactions. Unlike rigid robotic arms that require strict safety barriers, soft robotic arms are designed to absorb impacts and work alongside human operators in shared workspaces. AI-driven adaptive control strategies further enhance their ability to respond to unpredictable industrial environments.

4.3. Exploration And Search-And-Rescue Robots

Soft robotics is also revolutionizing exploration and disaster response, where robots must navigate complex and hazardous environments. Traditional wheeled

and legged robots often struggle in rubble-filled, underwater, or extraterrestrial terrains, whereas soft robots can deform, squeeze through confined spaces, and survive mechanical shocks (Sebastian, 2025; Wen et al., 2024). Soft crawling robots inspired by earthworms and caterpillars use peristaltic motion to traverse through narrow gaps (Seok, Onal, Wood, Rus, & Kim, 2010). Their movement can be mathematically described using a wave propagation model:

$$x(t) = Asin(2\pi ft + \phi) \tag{17}$$

where: $x(t)$ is the displacement at time t, A is the amplitude of contraction, f is the frequency of undulation, ϕ is the phase shift. These robots are particularly useful in search-and-rescue operations, where they can enter collapsed buildings to locate survivors without risking further structural collapse.

Another critical area of soft robotics is underwater exploration, where bio-inspired robots, such as robotic fish and octopuses, mimic aquatic locomotion using fluidic actuators. Unlike propeller-driven underwater vehicles, soft robotic swimmers exhibit low energy consumption and silent propulsion, making them ideal for environmental monitoring and marine research. In space exploration, NASA and other research institutions are exploring inflatable soft robots that can deploy on extraterrestrial surfaces (Ng & Lum, 2023; Spenko, 2023). These robots offer a lightweight and compact alternative to rigid planetary rovers, enhancing adaptability to uneven terrains.

4.4. Wearable Robotics

Wearable robotics is another area where soft robotic technology is making a profound impact, particularly in human augmentation, rehabilitation, and assistive devices. Traditional exoskeletons, designed for strength enhancement and mobility assistance, often suffer from weight and comfort issues due to their rigid structures. Soft robotic wearables address these limitations by incorporating lightweight and flexible materials that conform to the human body (Zhu, Biswas, Dinulescu, Kastor, Hawkes, & Visell, 2022). One of the most well-known applications is soft robotic gloves, designed for stroke rehabilitation and grip assistance (Polygerinos, Wang, Galloway, Wood, & Walsh, 2015). These gloves use pneumatic artificial muscles (PAMs) or fluidic elastomer actuators (FEAs) to generate movement, mimicking the natural mechanics of human fingers. The force output of a PAM-based actuator can be estimated using the equation:

$$F = PA(1 - \frac{l}{l_0}) \tag{18}$$

where: F is the generated force, P is the applied pressure, A is the cross-sectional area of the actuator, l and l_0 are the current and initial lengths of the actuator.

Soft robotic exosuits are also being developed to assist individuals with muscular disorders or age-related mobility impairments. These systems integrate sensor-driven adaptive control, adjusting support levels in real-time based on the wearer's movement patterns (Jiang, Chen, Que, Liu, Wang, & Xu, 2017). Additionally, soft robotic wearables are being explored for athletic performance enhancement and military applications, where they provide fatigue reduction and injury prevention. Future advancements in wearable artificial intelligence (AI) and energy-efficient soft actuators are expected to further expand the potential of these systems. Soft robotics has emerged as a transformative technology with applications spanning medicine, industry, exploration, and human augmentation. By leveraging compliance, adaptability, and bio-inspired design, soft robots are overcoming the limitations of rigid robotic systems. As material science, actuation techniques, and AI-driven control continue to evolve, soft robotics is expected to redefine the boundaries of automation and human-robot interaction in the coming decades.

5. CHALLENGES AND LİMİTATİONS

Despite the significant advancements and promising applications of soft robotics, the field still faces several critical challenges that must be addressed for widespread adoption in real-world scenarios. These challenges stem primarily from the mechanical properties of soft materials, control complexities, and power management issues. The intrinsic compliance and deformability of soft robots, while advantageous in many applications, also introduce limitations related to durability, precision control, and energy efficiency (Lee et al., 2017; Yasa et al., 2023). This section explores these fundamental challenges and discusses potential solutions.

One of the primary limitations of soft robots is their limited durability and mechanical lifespan. Unlike rigid robots made from metals and high-strength polymers, soft robots rely on elastomers, hydrogels, and other deformable materials that are prone to wear, fatigue, and rupture over repeated use (Yongchang Zhang, Li, Quan, Li, Zhang, & Zhou, 2023). These materials exhibit time-dependent mechanical degradation, particularly under cyclic loading and environmental stressors such as temperature fluctuations, UV exposure, and humidity. The fatigue behavior of soft materials can be characterized using stress-strain relationships and fracture mechanics (J. Liu, Li, She, Blanchard, & Lin,

2024). The fatigue life N_f of a soft material under cyclic loading can be estimated using the S-N curve equation:

$$\sigma = \sigma_0 (N_f)^b \tag{19}$$

where: σ is the applied cyclic stress, σ_0 is the initial fatigue strength, N_f is the number of cycles to failure, b is a material-dependent fatigue exponent. To improve the durability of soft robots, researchers are developing self-healing polymers, reinforced elastomers, and composite materials with enhanced mechanical properties. For example, incorporating fiber-reinforced structures and layered architectures can enhance distribution of load and prevent catastrophic failure. Additionally, self-healing hydrogels and ionic elastomers allow robots to autonomously repair minor damages, extending their operational lifespan.

Another major concern is air-tightness and leakage in pneumatically and hydraulically actuated soft robots (Stano, Arleo, & Percoco, 2020). Over time, micro-cracks and punctures can lead to pressure loss, reducing actuation efficiency. Advanced fabrication techniques, such as multi-material 3D printing and nano-coating technologies, are being explored to address these issues.

Unlike rigid robots, which rely on well-defined kinematic models, soft robots exhibit highly nonlinear, continuum deformations that are difficult to model and control. Traditional robotic control approaches, such as PID control and rigid-body dynamics, do not directly apply to soft robotic systems due to their infinite degrees of freedom and hysteresis effects.

The deformation of soft actuators is typically governed by continuum mechanics and hyperelastic material models. One commonly used equation to describe soft robotic bending is the Euler-Bernoulli beam equation, shown as Eq. 15. Soft robots also suffer from hysteresis and viscoelastic effects, which cause lag in response time and unpredictable motion under dynamic loads (Gu, Gupta, Zhu, Zhu, & Zhu, 2017; Zou & Gu, 2018). The relationship between stress (σ) and strain (ϵ) in viscoelastic materials can be described using the Kelvin-Voigt model:

$$\sigma = E\epsilon + \eta \frac{d\epsilon}{dt} \tag{20}$$

where: E is the elastic modulus, η is the viscosity coefficient, $d\epsilon/dt$ represents the strain rate. To address these control challenges, researchers are exploring model-free control strategies, such as machine learning-based controllers and reinforcement learning (RL) (Bhagat et al., 2019; X. Liu, Onal, & Fu, 2023).

Instead of relying on explicit mathematical models, RL-based controllers update their control policies iteratively using the Q-learning algorithm:

$$Q(s,a) \leftarrow Q(s,a) + \alpha[r + \gamma max_{a'} Q(s',a') - Q(s,a)] \quad (21)$$

where: $Q(s,a)$ represents the expected reward for taking action a in state s, α is the learning rate, γ is the discount factor for future rewards.

Another promising approach is the use of sensor-based feedback control, where soft strain sensors and flexible capacitive sensors provide real-time deformation data. Kalman filtering and neural network-based estimators are increasingly being used to improve precision and reduce uncertainty in control (DongWook Kim, Park, & Park, 2021).

Energy efficiency is a critical challenge in soft robotics, particularly for untethered systems that rely on onboard power sources. Many soft robots use pneumatic, hydraulic, or dielectric elastomer actuators, which require external pumps, compressors, or high-voltage power supplies, limiting their portability and autonomy. For pneumatically actuated soft robots, the work done to expand an actuator follows the ideal gas law (Su et al., 2022):

$$W = P\Delta V \quad (22)$$

where: W is the work done by the actuator, P is the applied pressure, ΔV is the volume change of the actuator. Pneumatic systems often suffer from energy loss due to air leakage, heat dissipation, and compressor inefficiency. To improve energy efficiency, researchers are exploring low-pressure actuation systems, soft electrostatic actuators, and biologically inspired energy storage mechanisms, such as artificial muscles that use chemical energy conversion.

For dielectric elastomer actuators (DEAs), which require high-voltage operation, power optimization strategies are crucial (Gu, Zhu, et al., 2017; Gupta et al., 2019). The electrostatic energy stored in a DEA is given by:

$$U = \frac{1}{2} C V^2 \quad (23)$$

where: U is the stored energy, C is the capacitance of the elastomer, V is the applied voltage. Minimizing leakage currents and improving dielectric breakdown resistance are key strategies for enhancing the performance of DEAs in energy-efficient soft robots. Battery technology also presents challenges for untethered soft robots, as most flexible energy storage systems, such as thin-film lithium-ion batteries and supercapacitors, still have limited energy densities.

Recent research in energy harvesting, such as triboelectric nanogenerators (TENGs) and bio-inspired piezoelectric energy sources, aims to develop self-powered soft robotic systems that operate with minimal external energy input.

Despite their immense potential, soft robots face several critical challenges related to durability, control, and power management. Addressing these challenges requires interdisciplinary efforts in materials science, computational modeling, and energy-efficient system design. Advances in self-healing materials, machine learning-based control, and compact power sources are expected to drive the next generation of soft robotic systems toward practical, large-scale deployment. As research in this field continues, overcoming these limitations will pave the way for more reliable, intelligent, and autonomous soft robotic technologies.

6. FUTURE PERSPECTIVES AND RESEARCH DIRECTIONS

Soft robotics has the potential to redefine the landscape of automation, healthcare, and human-robot interaction by introducing systems that are safer, more adaptable, and capable of performing complex tasks in dynamic environments. However, to achieve widespread deployment and real-world applicability, several challenges must be overcome through advancements in materials science, fabrication techniques, computational modeling, and control strategies (Polygerinos et al., 2017). This section discusses the future potential of soft robotics, the role of emerging materials and fabrication technologies, and how soft robots will contribute to next-generation human-robot interaction (HRI).

The future of soft robotics is expected to be shaped by several key advancements, including increased autonomy, biointegration, and multifunctionality. Unlike traditional rigid robots, which are often constrained by pre-defined motion patterns, soft robots have the ability to self-adapt and morphologically evolve based on their interactions with the environment. This opens up possibilities for applications in adaptive automation, biomedical engineering, and exploratory robotics.

One of the most promising directions is the development of self-evolving soft robotic systems, which utilize machine learning and artificial intelligence (AI) to optimize their structure and control over time (Chin, Hellebrekers, & Majidi, 2020; Daekyum Kim et al., 2021). The control of such systems can be framed as an optimal decision-making problem, where the robot continuously updates its policy π to maximize cumulative rewards R:

$$\pi^* = argmax_\pi \mathbb{E}[\sum_{t=0}^{T} \gamma^t R_t] \quad (24)$$

where: π^* is the optimal control policy, γ is the discount factor for future rewards, R_t represents the reward at time step t. Future research will focus on developing soft robotic systems that learn and adapt their physical properties dynamically, optimizing energy efficiency and motion planning through data-driven techniques.

Another critical direction for soft robotics is its role in biohybrid robotics, where organic and synthetic components are integrated to create robots that function similarly to living organisms (Guix et al., 2021). Biohybrid robots could be used for regenerative medicine, environmental monitoring, and bio-sensing applications. These systems will require advancements in biocompatible actuators, biodegradable materials, and energy-efficient control strategies. The performance of soft robots heavily depends on the materials used in their construction. Future advancements in smart materials, programmable matter, and additive manufacturing will play a pivotal role in expanding the capabilities of soft robotic systems.

One major research focus is on self-healing and self-reconfigurable materials. Current elastomers and hydrogels used in soft robotics degrade over time due to repeated mechanical stress (Karimi, Alizadehyazdi, Jaeger, & Spenko, 2021; L. Wang & Iida, 2012). Self-healing materials based on dynamic covalent bonds or microvascular healing networks offer a potential solution. The self-healing process can be described by a diffusion-based healing model:

$$C(x,t) = C_0 e^{-Dt} \quad (25)$$

where: $C(x,t)$ is the concentration of healing agents over time, C_0 is the initial concentration, D is the diffusion coefficient.

Another emerging area is metamaterials and architected soft materials, which provide programmable mechanical responses. For example, auxetic metamaterials, which exhibit a negative Poisson's ratio, can be used to develop robotic structures that expand when stretched instead of contracting (Mark, Palagi, Qiu, & Fischer, 2016). This behavior enables extreme flexibility and adaptive stiffness modulation. The Poisson's ratio v is given by:

$$v = -\frac{d\epsilon_{trans}}{d\epsilon_{axial}} \quad (26)$$

where: ϵ_{trans} is the transverse strain, ϵ_{axial} is the axial strain.

Future fabrication techniques will also focus on multi-material 3D printing, soft lithography, and molecular self-assembly. These methods will enable the development of functionally graded soft robots, where stiffness, electrical conductivity, and responsiveness are spatially tuned to optimize performance.

Energy-efficient actuation technologies are also expected to advance significantly. Current soft actuators, such as dielectric elastomer actuators (DEAs) and ionic polymer-metal composites (IPMCs), require high voltages or continuous power input, limiting their practical applications. Future developments in electroactive polymers, hydrogel-based actuators, and biologically-inspired chemical actuators will lead to soft robots that can operate autonomously for extended durations with minimal energy consumption.

As robots become increasingly integrated into daily life, soft robotics is expected to play a critical role in reshaping human-robot interaction (HRI). Unlike traditional rigid robots, which can pose safety risks due to their inflexible structures, soft robots provide inherently safe interactions, making them ideal for collaborative workspaces, assistive devices, and personal robotics.

Soft robotic wearables are expected to revolutionize assistive technology for individuals with mobility impairments. Future soft exosuits will feature adaptive control algorithms that learn user movement patterns and adjust assistance levels accordingly (Shao, Wu, Chen, & Wu, 2019). The force output of these exosuits can be optimized using bio-inspired muscle models such as the Hill-type muscle model:

$$F = F_{max}(\frac{l}{l_0})(1 - v/v_{max}) \tag{26}$$

where: F_{max} is the maximum force, l is the current muscle length, l_0 is the optimal length, v is the contraction velocity, v_{max} is the maximum contraction velocity.

Soft robots will also enhance robotic companionship and caregiving. As the global population ages, socially assistive robots (SARs) based on soft robotics principles will provide physical and emotional support in elder care and rehabilitation (Sun, Effati, Naguib, & Nejat, 2022). Unlike traditional humanoid robots, soft SARs will leverage biomechanical intelligence and emotional expressiveness to create more natural, empathetic interactions.

In industrial and collaborative settings, soft robots will enable human-safe automation, reducing the need for protective barriers in human-robot

collaborative workspaces. Soft robotic manipulators, combined with real-time sensory feedback and machine learning-based adaptive control, will improve ergonomics, efficiency, and task execution safety.

Future research will focus on neuromorphic computing and artificial proprioception, allowing soft robots to sense and react to human touch, facial expressions, and speech cues more effectively. The integration of AI-driven behavioral modeling will further enable robots to predict and adapt to human actions, leading to a seamless and intuitive human-robot interaction experience.

Soft robotics is poised to drive the next wave of innovation in automation, healthcare, and human-robot collaboration. Future advancements in self-adaptive materials, energy-efficient actuation, AI-driven control, and neuromorphic sensing will unlock new capabilities, making soft robots more autonomous, durable, and seamlessly integrated into human environments. As interdisciplinary research continues to evolve, soft robotics will bridge the gap between biological and artificial systems, ultimately transforming how robots interact with the world.

7. CONCLUSION

Soft robotics has emerged as a transformative field that challenges traditional notions of robotic design, enabling flexible, adaptable, and bio-inspired robotic systems. By leveraging compliant materials, unconventional actuation mechanisms, and advanced fabrication techniques, soft robots have demonstrated significant potential across various domains, including healthcare, industrial automation, exploration, and human-robot interaction. This review has explored the fundamental principles, fabrication methods, control strategies, and applications of soft robotics while also addressing key challenges and future research directions. Despite its advancements, soft robotics still faces limitations related to durability, control precision, and energy efficiency. However, ongoing research in materials science, artificial intelligence, and energy-efficient actuation technologies is expected to drive further progress in the field.

Soft robotics has introduced a paradigm shift in robotics by prioritizing compliance, safety, and adaptability over traditional speed and precision constraints. Unlike rigid robots, which rely on well-defined kinematic models and rigid-body dynamics, soft robots exhibit highly deformable and non-linear behavior, making their modeling and control inherently complex. However, these challenges also provide opportunities for innovation, particularly in the areas of bio-inspired control strategies, reinforcement learning, and real-time sensory feedback integration.

The primary strengths of soft robotics lie in its ability to interact safely with humans and the environment, making it particularly useful for medical applications, assistive technologies, and human-robot collaboration. Additionally, the capability of soft robots to conform to irregular surfaces, navigate through confined spaces, and withstand mechanical shocks has made them ideal for exploration and search-and-rescue missions. However, the field still faces several limitations, particularly in terms of material durability, power efficiency, and actuation response time. Developing self-healing materials, energy-efficient actuators, and robust control strategies will be crucial for enhancing the practicality and reliability of soft robotic systems.

Despite these challenges, the interdisciplinary nature of soft robotics—combining elements of materials science, mechanical engineering, computational modeling, and artificial intelligence—ensures that continuous advancements will lead to more capable and intelligent soft robots in the future. The integration of smart materials, neuromorphic computing, and biologically inspired design principles will further push the boundaries of what soft robots can achieve, bringing them closer to real-world implementation.

The impact of soft robotics extends far beyond research laboratories, influencing a wide range of industrial, medical, and everyday applications. In the industrial sector, soft robotic grippers and manipulators are revolutionizing automation by enabling safe and adaptable object handling in manufacturing, food processing, and logistics. Unlike traditional robotic arms that require rigid pre-programmed control, soft robotic systems can adapt to different object shapes, sizes, and textures, reducing the complexity of automation and increasing operational flexibility. This adaptability has significant implications for collaborative robots (cobots), which are designed to work alongside human workers in shared environments without requiring safety barriers.

In healthcare, soft robotics is driving innovation in minimally invasive surgery, rehabilitation, and prosthetics. Soft robotic surgical tools, inspired by biological structures such as octopus tentacles and snake-like manipulators, are enabling surgeons to perform complex procedures with greater precision and reduced patient trauma. Similarly, soft exoskeletons and wearable robotic devices are enhancing mobility for individuals with neuromuscular disorders, allowing them to regain motor function through assistive robotic support. These developments mark a major step toward personalized and adaptive medical interventions, improving the quality of life for individuals with physical impairments.

Beyond industrial and medical applications, soft robotics is also influencing everyday life through consumer electronics, smart textiles, and human-assistive devices. Wearable soft robotic technologies, such as smart gloves, robotic clothing, and flexible haptic interfaces, are creating new possibilities in gaming, virtual reality (VR), and augmented reality (AR). Soft robots integrated into smart home systems may soon provide assistance in household tasks, enhancing convenience and accessibility for users with disabilities or elderly individuals.

Another critical area of impact is exploration and environmental monitoring, where soft robots are being used for underwater exploration, disaster response, and extraterrestrial missions. Unlike rigid rovers and drones, soft robots can mimic biological locomotion, allowing them to navigate harsh and unpredictable terrains, such as deep-sea environments or planetary surfaces. The development of self-sustaining, biohybrid soft robots capable of harvesting energy from their surroundings could further expand the role of soft robotics in environmental applications.

As research and technological advancements continue, soft robotics is expected to become an integral part of next-generation automation, healthcare, and daily human interaction. The seamless integration of adaptive intelligence, energy-efficient actuation, and biomimetic design will allow soft robots to transition from experimental prototypes to real-world solutions, transforming industries and redefining the boundaries of human-robot collaboration.

Soft robotics represents one of the most exciting frontiers in robotics, offering a fundamentally different approach to machine design and function. While significant challenges remain in terms of material durability, control complexity, and energy efficiency, ongoing interdisciplinary efforts are rapidly addressing these issues. As the field progresses, the fusion of artificial intelligence, soft materials, and bio-inspired engineering will unlock unprecedented possibilities, making soft robots more autonomous, intelligent, and seamlessly integrated into society. Ultimately, soft robotics has the potential to revolutionize the way humans interact with machines, paving the way for a future where robots are not only tools but also intuitive, adaptive, and life-enhancing companions.

REFERENCES

Ahmed, F., Waqas, M., Jawed, B., Soomro, A. M., Kumar, S., Hina, A., . . . Choi, K. H. (2022). Decade of bio-inspired soft robots: A review. *Smart Materials and Structures, 31*(7), 073002.

Albu-Schaffer, A., Eiberger, O., Grebenstein, M., Haddadin, S., Ott, C., Wimbock, T., . . . Hirzinger, G. (2008). Soft robotics. *IEEE Robotics & Automation Magazine, 15*(3), 20-30.

Ashuri, T., Armani, A., Jalilzadeh Hamidi, R., Reasnor, T., Ahmadi, S., & Iqbal, K. (2020). Biomedical soft robots: current status and perspective. *Biomedical Engineering Letters, 10*, 369-385.

Bell, M. A., Becker, K. P., & Wood, R. J. (2022). Injection molding of soft robots. *Advanced Materials Technologies, 7*(1), 2100605.

Best, C. M., Gillespie, M. T., Hyatt, P., Rupert, L., Sherrod, V., & Killpack, M. D. (2016). A new soft robot control method: Using model predictive control for a pneumatically actuated humanoid. *IEEE Robotics & Automation Magazine, 23*(3), 75-84.

Bhagat, S., Banerjee, H., Ho Tse, Z. T., & Ren, H. (2019). Deep reinforcement learning for soft, flexible robots: Brief review with impending challenges. *Robotics, 8*(1), 4.

Bira, N., Dhagat, P., & Davidson, J. R. (2020). A review of magnetic elastomers and their role in soft robotics. *Frontiers in Robotics and AI, 7*, 588391.

Bruder, D., Gillespie, B., Remy, C. D., & Vasudevan, R. (2019). Modeling and control of soft robots using the koopman operator and model predictive control. *arXiv preprint arXiv:1902.02827*.

Chin, K., Hellebrekers, T., & Majidi, C. (2020). Machine learning for soft robotic sensing and control. *Advanced Intelligent Systems, 2*(6), 1900171.

Cianchetti, M., Laschi, C., Menciassi, A., & Dario, P. (2018). Biomedical applications of soft robotics. *Nature Reviews Materials, 3*(6), 143-153.

Coyle, S., Majidi, C., LeDuc, P., & Hsia, K. J. (2018). Bio-inspired soft robotics: Material selection, actuation, and design. *Extreme Mechanics Letters, 22*, 51-59.

Crooks, W., Vukasin, G., O'Sullivan, M., Messner, W., & Rogers, C. (2016). Fin ray® effect inspired soft robotic gripper: From the robosoft grand challenge toward optimization. *Frontiers in Robotics and AI, 3*, 70.

Ding, L., Niu, L., Su, Y., Yang, H., Liu, G., Gao, H., & Deng, Z. (2022). Dynamic finite element modeling and simulation of soft robots. *Chinese journal of mechanical engineering, 35*(1), 24.

Duriez, C. (2013). *Control of elastic soft robots based on real-time finite element method.* Paper presented at the 2013 IEEE international conference on robotics and automation.

Ebrahimi, N., Bi, C., Cappelleri, D. J., Ciuti, G., Conn, A. T., Faivre, D., . . . Khalil, I. S. (2021). Magnetic actuation methods in bio/soft robotics. *Advanced Functional Materials, 31*(11), 2005137.

Fang, G., Matte, C.-D., Kwok, T.-H., & Wang, C. C. (2018). *Geometry-based direct simulation for multi-material soft robots.* Paper presented at the 2018 IEEE International Conference on Robotics and Automation (ICRA).

Gu, G.-Y., Gupta, U., Zhu, J., Zhu, L.-M., & Zhu, X. (2017). Modeling of viscoelastic electromechanical behavior in a soft dielectric elastomer actuator. *IEEE Transactions on Robotics, 33*(5), 1263-1271.

Gu, G.-Y., Zhu, J., Zhu, L.-M., & Zhu, X. (2017). A survey on dielectric elastomer actuators for soft robots. *Bioinspiration & biomimetics, 12*(1), 011003.

Guix, M., Mestre, R., Patiño, T., De Corato, M., Fuentes, J., Zarpellon, G., & Sánchez, S. (2021). Biohybrid soft robots with self-stimulating skeletons. *Science Robotics, 6*(53), eabe7577.

Gul, J. Z., Sajid, M., Rehman, M. M., Siddiqui, G. U., Shah, I., Kim, K.-H., . . . Choi, K. H. (2018). 3D printing for soft robotics–a review. *Science and technology of advanced materials, 19*(1), 243-262.

Gupta, U., Qin, L., Wang, Y., Godaba, H., & Zhu, J. (2019). Soft robots based on dielectric elastomer actuators: A review. *Smart Materials and Structures, 28*(10), 103002.

Hegde, C., Su, J., Tan, J. M. R., He, K., Chen, X., & Magdassi, S. (2023). Sensing in soft robotics. *ACS nano, 17*(16), 15277-15307.

Huang, X., Kumar, K., Jawed, M. K., Mohammadi Nasab, A., Ye, Z., Shan, W., & Majidi, C. (2019). Highly dynamic shape memory alloy actuator for fast moving soft robots. *Advanced Materials Technologies, 4*(4), 1800540.

Iida, F., & Laschi, C. (2011). Soft robotics: Challenges and perspectives. *Procedia Computer Science, 7*, 99-102.

Ishige, M., Umedachi, T., Taniguchi, T., & Kawahara, Y. (2019). Exploring behaviors of caterpillar-like soft robots with a central pattern generator-based controller and reinforcement learning. *Soft robotics, 6*(5), 579-594.

Jia, B., Liu, C., Zhang, Y., Tan, Y., Tian, X., Cui, Y., & Deng, Y. (2024). Light-Responsive Soft Robot Integrating Actuation and Function Based on Laser Cutting. *Micromachines, 15*(4), 534.

Jiang, Y., Chen, D., Que, J., Liu, Z., Wang, Z., & Xu, Y. (2017). *Soft robotic glove for hand rehabilitation based on a novel fabrication method.* Paper presented at the 2017 IEEE International Conference on Robotics and Biomimetics (ROBIO).

Jin, H., Dong, E., Xu, M., Liu, C., Alici, G., & Jie, Y. (2016). Soft and smart modular structures actuated by shape memory alloy (SMA) wires as tentacles of soft robots. *Smart Materials and Structures, 25*(8), 085026.

Joyee, E. B., & Pan, Y. (2019). Multi-material additive manufacturing of functional soft robot. *Procedia Manufacturing, 34*, 566-573.

Karimi, M. A., Alizadehyazdi, V., Jaeger, H. M., & Spenko, M. (2021). A self-reconfigurable variable-stiffness soft robot based on boundary-constrained modular units. *IEEE Transactions on Robotics, 38*(2), 810-821.

Kim, D., Kim, S.-H., Kim, T., Kang, B. B., Lee, M., Park, W., . . . Lee, H. (2021). Review of machine learning methods in soft robotics. *Plos one, 16*(2), e0246102.

Kim, D., Park, M., & Park, Y.-L. (2021). Probabilistic modeling and Bayesian filtering for improved state estimation for soft robots. *IEEE Transactions on Robotics, 37*(5), 1728-1741.

Kim, M. S., Heo, J. K., Rodrigue, H., Lee, H. T., Pané, S., Han, M. W., & Ahn, S. H. (2023). Shape memory alloy (SMA) actuators: The role of material, form, and scaling effects. *Advanced materials, 35*(33), 2208517.

Kim, S., Laschi, C., & Trimmer, B. (2013). Soft robotics: a bioinspired evolution in robotics. *Trends in biotechnology, 31*(5), 287-294.

Kim, Y., & Zhao, X. (2022). Magnetic soft materials and robots. *Chemical reviews, 122*(5), 5317-5364.

Kumar, A. (2018). Methods and materials for smart manufacturing: additive manufacturing, internet of things, flexible sensors and soft robotics. *Manufacturing Letters, 15*, 122-125.

Lee, C., Kim, M., Kim, Y. J., Hong, N., Ryu, S., Kim, H. J., & Kim, S. (2017). Soft robot review. *International Journal of Control, Automation and Systems, 15*, 3-15.

Liu, J., Li, W., She, Y., Blanchard, S., & Lin, S. (2024). Fatigue-Resistant Mechanoresponsive Color-Changing Hydrogels for Vision-Based Tactile Robots. *Advanced materials*, 2407925.

Liu, X., Onal, C. D., & Fu, J. (2023). Reinforcement learning of CPG-regulated locomotion controller for a soft snake robot. *IEEE Transactions on Robotics, 39*(5), 3382-3401.

Mark, A. G., Palagi, S., Qiu, T., & Fischer, P. (2016). *Auxetic metamaterial simplifies soft robot design.* Paper presented at the 2016 IEEE international conference on robotics and automation (ICRA).

Moseley, P., Florez, J. M., Sonar, H. A., Agarwal, G., Curtin, W., & Paik, J. (2016). Modeling, design, and development of soft pneumatic actuators with finite element method. *Advanced engineering materials, 18*(6), 978-988.

Naresh, C., Bose, P., & Rao, C. (2016). *Shape memory alloys: a state of art review*. Paper presented at the IOP conference series: materials science and engineering.

Natarajan, E., Hassan, C., Kit, A. C., Santhosh, M., Ramesh, S., & Sasikumar, R. (2021). Modeling of multiwall carbon nanotubes reinforced natural rubber for soft robotic applications–A comprehensive presentation. *Materials Today: Proceedings, 46*, 3251-3258.

Ng, C. S. X., & Lum, G. Z. (2023). Untethered soft robots for future planetary explorations? *Advanced Intelligent Systems, 5*(3), 2100106.

Olson, G., Hatton, R. L., Adams, J. A., & Mengüç, Y. (2020). An Euler–Bernoulli beam model for soft robot arms bent through self-stress and external loads. *International Journal of Solids and Structures, 207*, 113-131.

Polygerinos, P., Correll, N., Morin, S. A., Mosadegh, B., Onal, C. D., Petersen, K., . . . Shepherd, R. F. (2017). Soft robotics: Review of fluid-driven intrinsically soft devices; manufacturing, sensing, control, and applications in human-robot interaction. *Advanced engineering materials, 19*(12), 1700016.

Polygerinos, P., Wang, Z., Galloway, K. C., Wood, R. J., & Walsh, C. J. (2015). Soft robotic glove for combined assistance and at-home rehabilitation. *Robotics and Autonomous Systems, 73*, 135-143.

Schmitt, F., Piccin, O., Barbé, L., & Bayle, B. (2018). Soft robots manufacturing: A review. *Frontiers in Robotics and AI, 5*, 84.

Sebastian, A. (2025). Soft Robotics for Search and Rescue: Advancements, Challenges, and Future Directions. *arXiv preprint arXiv:2502.12373*.

Seok, S., Onal, C. D., Wood, R., Rus, D., & Kim, S. (2010). *Peristaltic locomotion with antagonistic actuators in soft robotics.* Paper presented at the 2010 IEEE international conference on robotics and automation.

Shao, Z., Wu, Q., Chen, B., & Wu, H. (2019). Force and deformation transmission characteristics of a compliant tendon–sheath actuation system based on Hill-type muscle model. *Proceedings of the Institution of Mechanical Engineers, Part H: Journal of Engineering in Medicine, 233*(7), 695-705.

Shih, B., Christianson, C., Gillespie, K., Lee, S., Mayeda, J., Huo, Z., & Tolley, M. T. (2019). Design considerations for 3D printed, soft, multimaterial resistive sensors for soft robotics. *Frontiers in Robotics and AI, 6*, 30.

Shintake, J., Cacucciolo, V., Floreano, D., & Shea, H. (2018). Soft robotic grippers. *Advanced materials, 30*(29), 1707035.

Silva, A., Fonseca, D., Neto, D. M., Babcinschi, M., & Neto, P. (2024). Integrated design and fabrication of pneumatic soft robot actuators in a single casting step. *Cyborg and Bionic Systems, 5*, 0137.

Spenko, M. (2023). Making contact: A review of robotic attachment mechanisms for extraterrestrial applications. *Advanced Intelligent Systems, 5*(3), 2100063.

Stano, G., Arleo, L., & Percoco, G. (2020). Additive manufacturing for soft robotics: design and fabrication of airtight, monolithic bending PneuNets with embedded air connectors. *Micromachines, 11*(5), 485.

Stano, G., & Percoco, G. (2021). Additive manufacturing aimed to soft robots fabrication: A review. *Extreme Mechanics Letters, 42*, 101079.

Su, H., Hou, X., Zhang, X., Qi, W., Cai, S., Xiong, X., & Guo, J. (2022). *Pneumatic soft robots: Challenges and benefits.* Paper presented at the Actuators.

Sun, Y.-C., Effati, M., Naguib, H. E., & Nejat, G. (2022). Softsar: The new softer side of socially assistive robots—Soft robotics with social human–robot interaction skills. *Sensors, 23*(1), 432.

Terrile, S., Argüelles, M., & Barrientos, A. (2021). Comparison of different technologies for soft robotics grippers. *Sensors, 21*(9), 3253.

Thuruthel, T. G., Shih, B., Laschi, C., & Tolley, M. T. (2019). Soft robot perception using embedded soft sensors and recurrent neural networks. *Science Robotics, 4*(26), eaav1488.

Trivedi, D., Rahn, C. D., Kier, W. M., & Walker, I. D. (2008). Soft robotics: Biological inspiration, state of the art, and future research. *Applied bionics and biomechanics, 5*(3), 99-117.

Walker, J., Zidek, T., Harbel, C., Yoon, S., Strickland, F. S., Kumar, S., & Shin, M. (2020). *Soft robotics: A review of recent developments of pneumatic soft actuators.* Paper presented at the Actuators.

Wallin, T., Pikul, J., & Shepherd, R. F. (2018). 3D printing of soft robotic systems. *Nature Reviews Materials, 3*(6), 84-100.

Wang, J., & Chortos, A. (2022). Control strategies for soft robot systems. *Advanced Intelligent Systems, 4*(5), 2100165.

Wang, L., & Iida, F. (2012). *Towards "soft" self-reconfigurable robots.* Paper presented at the 2012 4th IEEE RAS & EMBS International Conference on Biomedical Robotics and Biomechatronics (BioRob).

Wen, T., Hu, J., Zhang, J., Li, X., Kang, S., & Zhang, N. (2024). Design, performance analysis, and experiments of a soft robot for rescue. *Journal of Mechanisms and Robotics, 16*(7).

Whitesides, G. M. (2018). Soft robotics. *Angewandte Chemie International Edition, 57*(16), 4258-4273.

Xavier, M. S., Tawk, C. D., Zolfagharian, A., Pinskier, J., Howard, D., Young, T., . . . Bodaghi, M. (2022). Soft pneumatic actuators: A review of design, fabrication, modeling, sensing, control and applications. *IEEE Access, 10*, 59442-59485.

Yang, H. D., & Asbeck, A. T. (2018). *A new manufacturing process for soft robots and soft/rigid hybrid robots.* Paper presented at the 2018 IEEE/RSJ international conference on intelligent robots and systems (IROS).

Yap, Y. L., Sing, S. L., & Yeong, W. Y. (2020). A review of 3D printing processes and materials for soft robotics. *Rapid Prototyping Journal, 26*(8), 1345-1361.

Yasa, O., Toshimitsu, Y., Michelis, M. Y., Jones, L. S., Filippi, M., Buchner, T., & Katzschmann, R. K. (2023). An overview of soft robotics. *Annual Review of Control, Robotics, and Autonomous Systems, 6*(1), 1-29.

Youn, J.-H., Jeong, S. M., Hwang, G., Kim, H., Hyeon, K., Park, J., & Kyung, K.-U. (2020). Dielectric elastomer actuator for soft robotics applications and challenges. *Applied Sciences, 10*(2), 640.

Zhang, G., Li, S., Wu, Y., & Zhu, M. (2021). An investigation on the grasping position optimization-based control for industrial soft robot manipulator. *Machines, 9*(12), 363.

Zhang, Y., Li, P., Quan, J., Li, L., Zhang, G., & Zhou, D. (2023). Progress, challenges, and prospects of soft robotics for space applications. *Advanced Intelligent Systems, 5*(3), 2200071.

Zhang, Y., Wang, Z., Yang, Y., Chen, Q., Qian, X., Wu, Y., . . . Ji, Y. (2020). Seamless multimaterial 3D liquid-crystalline elastomer actuators for next-generation entirely soft robots. *Science advances, 6*(9), eaay8606.

Zhu, M., Biswas, S., Dinulescu, S. I., Kastor, N., Hawkes, E. W., & Visell, Y. (2022). Soft, wearable robotics and haptics: Technologies, trends, and emerging applications. *Proceedings of the IEEE, 110*(2), 246-272.

Zou, J., & Gu, G. (2018). High-precision tracking control of a soft dielectric elastomer actuator with inverse viscoelastic hysteresis compensation. *IEEE/ASME Transactions on Mechatronics, 24*(1), 36-44.